PARALLEL INTERFERENCE CANCELLATION MULTIUSER DETECTION: PERFORMANCE AND APPLICATIONS

A Dissertation

Presented to the Faculty of the Graduate School

of Cornell University

in Partial Fulfillment of the Requirements for the Degree of

Doctor of Philosophy

by

Donald Richard Brown

May 2000

PARALLEL INTERFERENCE CANCELLATION MULTIUSER DETECTION: PERFORMANCE AND APPLICATIONS

Donald Richard Brown, Ph.D.

Cornell University 2000

This dissertation considers the performance and applications of parallel interference cancellation (PIC) multiuser detectors for digital multiuser communication systems with nonorthogonal signaling. The majority of this dissertation focuses on wireless code division multiple access (CDMA) communication systems but we also consider the application of multiuser detection and PIC to digital subscriber loop communication systems here as well.

The first section of this dissertation analyzes the performance of parallel interference cancellation detectors in the K-user synchronous, nonorthogonal, binary communication scenario. We derive exact and approximate expressions for the bit error rate of the hard-PIC (HPIC) detector where the multiuser interference estimates are formed *after* hard decisions are performed on estimates of the interfering users signals. We compute expressions for the exact and approximate signal to interference plus noise ratio of the HPIC detector and present an analytical comparison to the successive interference cancellation (SIC) and matched filter (MF) detectors. We also analyze the performance of the linear-PIC (LPIC) detector where the multiuser interference estimates are formed *prior* to the hard decisions on estimates of the interfering users signals. We show that the HPIC detector is a better estimator of multiuser interference than the LPIC detector.

We derive an exact expression for the bit error rate of the LPIC detector and show that there exists a nontrivial class of operating conditions where the LPIC detector performs poorly. We present an analysis of the large-system case with random spreading sequences of length N that shows that the multistage LPIC detector does not converge to the decorrelating detector when $K/N > 0.17$.

In the middle section of this dissertation, we consider two distinct techniques for improving the performance of the HPIC detector. The first technique, called partial cancellation HPIC (PC-HPIC), attenuates each user's multiuser interference estimate by a individual scalar partial cancellation factor optimized under three different performance criteria. The second technique, called soft cancellation PIC (SC-PIC) replaces the $\mathrm{sgn}(\cdot)$ nonlinearity in the HPIC detector with a function that minimizes the Bayesian mean squared error of the interfering user's bit estimate. We present numerical results that suggest that both techniques yield significant performance improvements.

The final section of this dissertation considers the application of PIC multiuser detection to the IS–95 digital cellular downlink and to digital subscriber loops (DSLs). We show via analysis and numerical results with measured on-air data that PIC detection can significantly improve the fidelity of IS–95 downlink reception, especially in cases when the desired signal is received in the presence of strong out-of-cell multiuser interference. Our analysis of DSLs shows that PIC detection, as applied to the problem of crosstalk cancellation, does not provide any performance benefit in most cases. We demonstrate that more sophisticated multiuser detectors do have the potential to accurately cancel crosstalk and significantly improve the performance of DSLs.

BIOGRAPHICAL SKETCH

Donald Richard Brown III is an overall nice guy who's success can be largely attributed to an extraordinary run of good luck. He was born the son of Joyce and Donald Richard Brown Jr. on August 20, 1969 in Ridgeley, West Virginia, and has been called Rick by his family and friends ever since. As Rick grew up in the 1970's, the first true test of his luck came from the innocent influence of Evel Knievel, a flamboyant motorcycle stuntman whose stunts included a jump over a pool of sharks. Rick's desire to be just like Evel Knievel, his lack of sharks not withstanding, led to an unsuccessful attempt to ride a tricycle down a flight of brick stairs and resulted in several forehead stitches. Shortly after the bandages came off of his head, Rick learned how to ride a bicycle and began racing neighborhood children down the steep and bumpy hill behind his house. Luckily, he avoided serious injury but a spectacular crash led to the early loss of a front tooth. A new front tooth grew and Rick managed to avoid further facial injury for some time, but the skateboarding craze of the late 1970's led to two broken arms in a span of 3 months. Perhaps the luckiest thing that happened to Rick in the 1970's was that he never got the thing he wanted the most, a chemistry set. His parents, probably realizing that a chemistry set in the hands of their young Evel Knievel was not in their best interests, instead gave Rick a crystal radio kit and simple kit for experiments with electricity.

The 1980's tested Rick's luck in different ways. To the credit of his father who taught him Algebra II, Rick successfully completed four years of home-tutored high school in 1986 and, almost as an afterthought, applied to only one university: The University of Connecticut. Luckily, he was accepted. Rick decided to enroll in the Electrical Engineering program after careful thought that consisted

of approximately one hour of tinkering with a Radio Shack 555-timer kit. Rick worked part time while commuting to a branch campus and somehow managed to convince his supervisor in the bookkeeping office of the local nursing home to terminate his temporary position at $6.00 per hour and rehire him in a permanent position to create Lotus spreadsheets at $12.50 per hour. Luckily, Rick still didn't have enough money to pay for the entire four years of college so he decided to apply for a co-op job in his junior year and wound up working at General Electric for eight months. Despite the relatively tight job market in 1992 when he graduated with his BSEE, the contacts Rick made while on co-op led to an offer by General Electric in their prestigious Edison Engineering Program. Rick worked at General Electric for almost five years and, luckily, as part of the Edison Engineering Program, was required to take courses toward a Master of Science degree for the first two years. Rather than wasting the credits, Rick continued taking courses and decided to complete his Master of Science degree at The University of Connecticut while working full time at General Electric. It was during his final year there that he met Professor Lang Tong, a new assistant professor at The University of Connecticut who taught a course on Digital Communications. After sending two resumes to Qualcomm in 1995 that, luckily, were rejected, Rick completed his degree in January 1996 and talked with Professor Tong about perhaps pursuing a Doctoral degree.

One could certainly argue that 1996 was the luckiest year of Rick's life. In March, Rick became engaged to Jennifer M. Ramos and they were married in October. In August, as Rick was just beginning to think about the formidable process of applying to several schools for admission in September 1997, Rick received a call at work from Professor C. Richard Johnson Jr. from Cornell University, who also

has been called Rick since birth. Luckily, Professor Johnson was a friend of Professor Tong's and, even more remarkably, he was looking for a PhD student and had received a recommendation on Rick's behalf from Professor Tong. Rick met Professor Johnson in September and decided to apply only to Cornell. Despite his unremarkable GRE scores, he was accepted and began his studies at Cornell in January of 1997.

As Rick completes his studies at Cornell this spring, he recently accepted a position as an assistant professor at Worcester Polytechnic Institute to begin in the fall of 2000. His run of good luck appears to be far from over.

To my wife, my best friend, Jen.

ACKNOWLEDGEMENTS

There are so many people I want to thank, for without their help I would have never made it this far. These people are all largely responsible for much of the enjoyment and success I have experienced over the last three and one half years of my life at Cornell. In many ways, I am a little bit sad to see it end.

First, and most importantly, I want to thank Jen for her unconditional support and love. She has taught me by example the true meaning of hard work, dedication, and loyalty. She left her friends, family, and a job that she liked in Connecticut to start a new life with me in Ithaca that included a new and very difficult job at Corning. Despite the long hours she often worked, she was always willing to help me edit a paper or listen to a practice presentation. I am forever indebted to her.

Mom and Dad, thank you for taking the time to teach me so much before I ever went to a formal school. A large part of who I am today is due to the active role you took in my education and your consistent encouragement for me to do well in school.

I feel incredibly fortunate to have met Rick Johnson while considering schools in pursuit of my PhD. In addition to probably being the only academic advisor who has a place on the Wall of Fame at the Acme Oyster House in New Orleans, Rick and his family are probably the best friends that Jen and I made during our three and one half year stay in Ithaca. Rick has set an example as an advisor that I can only hope to emulate.

I would have never met Rick Johnson without the unselfish help of Professor Lang Tong who encouraged me to pursue my PhD at a "name brand" school. Although it would have been very easy for Lang to convince me to study under his supervision at The University of Connecticut, he instead facilitated my first

meeting with Rick Johnson at Cornell. I can never truly repay Lang, but I will always remember his example and I promise to do the same thing for an aspiring graduate student some day.

I am thankful to Professor Veeravalli and Professor Escobar for their time in reviewing this work and for their helpful comments. Their consistent willingness to meet with me and discuss many of the problems in this dissertation is greatly appreciated. I am also thankful for the valuable feedback from Stuart Sandberg of Aware regarding the results of Chapter 6 and from Laurence Mailaender of Lucent regarding several results in Chapter 2.

I want to thank Professor H. Vincent Poor and Professor Sergio Verdu of Princeton University for inviting me to work with them for the month of February 1999. In many ways, their insightful help and encouragement spawned my interest in parallel interference cancellation and planted the seeds that led to much of this dissertation. I am specifically grateful for Professor Poor's comments on Chapter 4 of this dissertation. I also am thankful for the logistical support provided by Stephanie Costantini who arranged my lodging and made my stay at Princeton quite comfortable.

I am grateful for the financial support of the National Science Foundation through grants MIP-9509011, ECS-9528363, ECS-9811297, and EEC-9872436. I want to also thank Applied Signal Technology for their financial support and especially John Treichler and Rich Gooch for inviting me to work with them at AST in April 1999. I also wish to thank Mariam Motamed, David Chou, and Reynold Wang for providing me with the tools and support to achieve my goals while I was at AST, and for providing me with the data and their feedback for several results in Chapter 5.

I am indebted to several people at General Electric for their support during my studies at Cornell including Paul Raymont who refused to let me resign in 1996 and convinced me to work part time for GE while at Cornell. I also want to thank Chris Fuselier for continuing this arrangement after Paul left, as well as the people with whom I interfaced over the years including Joe Krisciunas, Dan Dellavecchia, Tony Zupa, Ellen Edge, and Patrick Salas.

I wish to thank my graduate colleagues, including Tom, Raul, Phil, Jai, Wonzoo, Rick Martin, and Knox, who not only provided me with valuable help for several problems in this dissertation but who also gave me many hours of enjoyable company over lunch and other social occasions. I am specifically grateful for the help of fellow graduate student and GE employee Mehul Motani for his help on several results in Chapter 3 of this dissertation.

Finally, I wish to thank the friends I met at Cornell in their undergraduate years including Don, Andy, Scott, and David. Their encouragement during my first two semesters as a teaching assistant reinforced my desire to pursue an academic career. I am grateful to Don and Andy for their insight and discussion on many problems in multiuser communication systems as well as the time spent on the golf courses of Ithaca. Scott's enthusiasm for digital signal processing and his backup at Dragon Day in 1998 will never be forgotten. And finally, although we never caught anything much bigger than our lures, I greatly enjoyed the time I spent fishing and talking with David over the spring and summer of 1999.

TABLE OF CONTENTS

LIST OF TABLES

LIST OF FIGURES

CHAPTER 1

INTRODUCTION

"I can't understand why people are frightened by new ideas. I'm frightened of old ones."

– John Cage

1.1 Motivation

Two factors have spawned a great deal of the remarkable growth of telecommunications equipment and services over the last decade: the rapidly evolving media rich Internet and World Wide Web, and the explosion of demand for wireless access to voice and data services. Recently, the widespread deployment and advanced technology of second generation digital cellular systems has enabled a convergence of these applications to consumers around the world who are now just beginning to enjoy wireless access to email, the World Wide Web, and other information services. Third generation digital cellular systems, currently under development by the international standards bodies, promise even greater data rates and more extensive voice, data, and multimedia services towards the goal of ubiquitous access to any information service from anywhere on Earth.

Industry reports estimate that 273 million cellular handsets shipped to a worldwide subscriber base of 470 million users in 1999 and analysts currently predict that 900 million handsets will ship in 2005 to a worldwide subscriber base of 1.4 billion users. Currently, among the competing technologies fueling this growth, the most rapidly growing cellular technology is Code Division Multiple Access (CDMA), a multiple access communication method originally used for military

communications in the 1940's and adapted to cellular communication systems by Qualcomm in the 1980's (see [Vit95] for a good introduction to second generation CDMA cellular systems). The worldwide subscriber base for CDMA-based cellular phones was slightly over 50 million users at the end of 1999 and grew 118 percent from December 1998. Analysts predict that CDMA-based cellular phones will account for 31 percent of the worldwide cellular phone shipments in 2005, from a base of 13 percent in 1999.

The disproportionately large growth rate of CDMA cellular systems is, from the consumer perspective, due largely to improved sound quality, increased transmission reliability, improved battery life, and new services such as email and World Wide Web access. From the service providers' perspective, CDMA cellular systems are attractive because they are easier to plan and install than competing technologies and offer increased capacity while maintaining spectral compatibility with first generation analog cellular systems. These factors have also positioned CDMA as a likely technology to be used in worldwide standards for third generation digital cellular systems.

The exponential growth of CDMA digital cellular subscribers, in addition to the seemingly insatiable demand for access to bandwidth intensive applications and its penetration into the wireless market, has led to a dramatic increase in research in the area of improving the quality and efficiency of CDMA digital cellular communication systems. Unlike copper or fiber based communication systems where additional bandwidth can be added to existing systems by upgrading or installing additional cables, wireless and cellular communications systems have a fixed, finite amount of available bandwidth from which to serve their growing and increasingly sophisticated subscriber base. Coupled with the increasing performance of mi-

croprocessors and other integrated circuits, the three most promising technologies that will enable cellular systems to meet the future demands of subscribers are currently:

- antenna arrays and spatial diversity,
- source and channel coding, and
- multiuser detection.

This dissertation focuses primarily on the third enabling technology: multiuser detection. Multiuser detection refers to a class of algorithms in a communication receiver that "exploit the considerable structure of the multiuser interference in order to increase the efficiency with which channel resources are employed" [Ver98]. Prior to 1986, the conventional wisdom among researchers in CDMA cellular communication systems was that the multiuser interference observed in each user's received signal was well modeled by a Gaussian random process and that matched filter detection, which ignored the structure of the interference, was nearly optimum in this case. In 1986, Sergio Verdu developed the optimum (in the sense of minimum bit error rate) multiuser detector for CDMA communication systems by considering and exploiting the structure of the multiuser interference. Verdu's detector offered significantly improved performance with respect to the matched filter detector but, unfortunately, this dramatic performance improvement also came at the cost of an equally dramatic complexity increase. Since Verdu's groundbreaking result, the field of multiuser detection has become a vibrant area of research that remains active even today. The primary focus of the research in multiuser detection since 1986 has been the development of suboptimum multiuser detectors for CDMA systems that can be implemented with lower complexity than the optimum

detector while offering near optimum performance.

Within the field of multiuser detection, there exists a class of detectors called "decision-driven" multiuser detectors (see, for example, [Ver98, Ch. 7] and [HD98]) that offer good performance under a wide variety of operating conditions and have the feature of very low computational complexity. Decision-driven multiuser detectors use a heuristic concept in order to improve the quality of reception which can be stated in essence as follows: Given that the received signal is composed of three parts, the desired signal, the aggregate structured multiuser interference, and the unstructured channel noise, the decision-driven multiuser detector forms tentative decisions on the digital transmissions of all of the users and then uses these decisions to generate an estimate of some or all of the aggregate structured multiuser interference. This estimate is then subtracted from the received signal to form a new output from which new digital decisions are made. This idea is quite intuitive in that, if we assume that the aggregate multiuser interference was estimated perfectly, the output of this operation is composed only of the desired signal and the additive, unstructured channel noise. The multiuser interference is eliminated and the fidelity of the received signal is improved, resulting in improved bit error rates or increased system capacity.

This dissertation focuses on a particular realization of a decision-driven multiuser detector called the Parallel Interference Cancellation (PIC) detector. The first PIC receiver for CDMA communication systems was proposed by Varanasi and Aazhang in [VA90] and [VA91] where their PIC receiver was called a multistage detector. The multistage/PIC detector was shown to have close connections to Verdu's optimum detector and also to possess several desirable properties including the potential for near optimum performance, very low computational com-

plexity, and low decision latency. This combination of factors has led to an increase in research for various forms of PIC detection and several authors have even suggested recently that PIC detection is one of the most promising types of multiuser detection [BCW96]. In this dissertation, we present new analytical results exposing several aspects on the performance of two different types of PIC detection, we develop and test new approaches to improve the performance of PIC detection, and we investigate two practical, "real-world" applications for PIC detection.

The next section highlights the recent results in the literature regarding PIC detection relevant to this dissertation.

1.2 Literature Survey

A good introduction to CDMA cellular communication systems is [Vit95] and a good introduction to multiuser detection for CDMA communication systems is [Ver98]. In particular, Chapter 7 of [Ver98] presents a useful overview of decision directed multiuser detectors including successive interference cancellation, parallel interference cancellation, and decision feedback detectors.

1.2.1 Hard Parallel Interference Cancellation

Hard Parallel Interference Cancellation (HPIC), first called multistage detection and often just called parallel interference cancellation (PIC), was first described for asynchronous multiuser CDMA communication systems by Varanasi and Aazhang in [VA88] and [VA90] where the multistage detector was derived from an analysis of the optimum, joint maximum likelihood detector. The HPIC detector was independently proposed as an adaptive cochannel interference cancellation detector by

Kohno et al. in [KIHP90]. The multistage detector for synchronous systems was described in [VA91] and a bit error rate analysis was presented for the two-stage HPIC detector with a linear decorrelating detector front end. Extensions to the general multipath channel case were presented in [FA95].

The bit error rate performance of the HPIC detector has been considered in the aforementioned papers and by Hottinen et al. in [HHT95] via simulations of a multipath fading environment. Yoon et al. [YKI93] present a first order analysis of the bit error rate of the multistage HPIC detector that relies on an assumption that the decision statistics prior to the each stage's hard decision device are well modeled as independent Gaussian random variables. A more accurate bit error rate analysis of the HPIC detector in the K-user synchronous scenario, also under a Gaussian approximation on the multiuser interference, was derived by Divsalar and Simon in [DS94]. Divsalar and Simon recognized that the decisions at the output of the matched filter bank were in fact not independent of one another and proposed an approximate analysis in the case of random spreading sequences and random received phases that required numerical evaluation of explicitly defined one and two-dimensional definite integrals.

In Chapter 2 of this dissertation, we present a new *exact* analysis for the bit error rate and the signal to interference plus noise ratio (SINR) of the two-stage HPIC detector in the K-user synchronous case and explicitly describe methods for their computation. New approximate expressions for the bit error rate and SINR of the two-stage HPIC detector are also proposed. We present an analytical comparison of our approximate SINR expression to SINR expressions for the successive interference cancellation and matched filter detectors and show that the two-stage HPIC detector offers superior performance over a large class of operating

conditions.

1.2.2 Linear Parallel Interference Cancellation

Linear parallel interference cancellation (LPIC), also often called parallel interference cancellation (PIC), was first described by Kaul and Woerner in [KW94] and independently by Patel and Holtzman in [PH94] where the authors noted that linear multiuser interference estimates obviated the need for estimation of the user amplitudes, as required in HPIC detection. The paper by Patel and Holtzman is an often cited simulation comparison of the LPIC detector to a linear version of the successive interference cancellation (SIC) detector where the authors concluded that LPIC tended to perform better when the received user amplitudes were similar and that SIC tended to perform better when the received user amplitudes were disparate.

The two-stage LPIC detector and the approximate decorrelating detector can be shown to be equivalent linear detectors. An analysis of the approximate decorrelating detector was given by Mandayam and Verdu in [MV98a] where the authors derived an expression for the exact bit error rate and also proposed an approximate expression. Simulations in weakly correlated systems showed that the approximate decorrelating detector outperformed the matched filter detector in terms of bit error rate.

The multistage LPIC detector was compared via simulation to several other common multiuser detectors by Buehrer et al. in [BCW96]. The bit error rate of the multistage LPIC detector under an improved Gaussian approximation was studied by Buehrer and Woerner in [BW96]. The asymptotic multiuser efficiency of multistage LPIC detector was also studied by Buehrer and Woerner in [BW97].

Ghazi et al. showed analytically that, as the number of stages of the LPIC detector approaches infinity, the LPIC detector converges to the decorrelating detector [GMNK95] if the spectral radius of the signature waveform crosscorrelation matrix is less than two.

In Chapter 3 of this dissertation, we present new analytical results regarding the performance of the LPIC detector in the K-user synchronous scenario. We compare the performance of LPIC and HPIC detectors and show that the HPIC detector is a better estimator of multiuser interference. We present an exact bit error rate expression for the multistage LPIC detector and show via analysis and numerical examples that the LPIC detector can perform quite poorly in a large class of operating conditions. Our results also show that the multistage LPIC detector (which includes the approximate decorrelating detector if we fix the number of stages to two) can actually perform worse than the matched filter detector in several nontrivial cases.

1.2.3 Performance Adaptive Parallel Interference Cancellation

Techniques to improve the performance of the LPIC detector have received a lot of recent attention recently due to the fact that simulations (corroborated by the new analytical results presented in in Chapter 3 of this dissertation) have shown that the unmodified LPIC detector can exhibit poor performance in a large class of typical operating conditions. Correal et al. showed that the multistage LPIC detector's interference estimates were biased and proposed an ad-hoc partial cancellation factor in order to reduce this bias in [CBW97]. Correal et al. also demonstrated real time implementations of their partial cancellation LPIC detector in [CBW98] and

[CBW99]. Renucci et al. derived an implicit expression for the bit error rate optimum partial cancellation factors in [Ren98], [RW98a], and [RW98b]. Rasmussen et al. also derived a weighted, multistage LPIC detector with weights chosen to minimize the mean squared error at the output of the LPIC detector in [RGLM98]. Guo et al. demonstrated in [GRS+98] and [GRSL00] that this approach could yield precisely the linear MMSE detector in K stages, where K is the number of users in the system. Guo et al. also proposed a weighted multistage LPIC detector for long-coded CDMA systems with time invariant weights in [GRL99].

There has also been some recent work on the problem of improving the performance of the HPIC detector. Abrams et al. observed that attempting to completely cancel incorrect binary decisions leads to a doubling of the interference in the new decision statistic and proposed that the interference estimates should be multiplied by a scale factor such that the mean interference cancellation energy is minimized [AZJ95]. Divsalar and Simon took a different approach and proposed a detector that, in the two-stage case, formed a decision statistic from a weighted combination of the matched filter and the HPIC detector decision statistics in [DSR98]. Divsalar and Simon's work also extended to the multistage case and they demonstrated via simulation that significant performance gains with respect to the conventional HPIC detector were possible. Buehrer and Nicoloso commented on Divsalar and Simon's paper in [BN99] and cast their results in the context of the bias reduction results first presented by [CBW97] for the LPIC detector.

A great deal of research on the topic of improving the performance of decision-directed multiuser detectors doesn't fall into the category of LPIC or HPIC detection and instead has centered around the mapping function from the soft decision statistics at the output of the first stage to the interference estimates used for can-

cellation. The conventional HPIC detector with binary signaling uses the $\mathrm{sgn}(\cdot)$ operation and the conventional LPIC detector simply uses an identity mapping. In [ZB93] and [ZB98], Zhang and Brady examined PIC detection using multilevel quantizer, dead-zone nonlinearity, and linear clipper interference estimation functions. The linear clipper interference estimator was also considered for underwater acoustical channels by Brady and Catipovic in [BC94]. A sigmoidal interference estimator using the $\tanh(\cdot)$ function, justified by Bayesian minimum mean squared error arguments, was examined by Frey and Reinhardt in [FR97] and Gollamudi et al. in [GNHB98].

In Chapter 4 of this dissertation, we develop new methods to improve the performance of HPIC detection. We develop and analyze the performance of the HPIC detector in the K-user synchronous case using partial rather than full interference cancellation. Our approach differs from the approach in [DSR98] in two important ways. First, we propose that each user is assigned an individual partial cancellation factor rather than one partial cancellation factor for all users. Second, rather than an ad-hoc selection of partial cancellation factors, we derive expressions for optimum partial cancellation factors under three different performance criteria. It turns out that the partial cancellation factors that maximize the SINR of the HPIC detector are equivalent to the minimum mean interference cancellation energy scale factors derived in [AZJ95]. In this chapter we also derive an expression for the exact Bayesian MMSE interference estimator and show via a numerical example that the approximate expressions suggested in [FR97] and [GNHB98] can also be accurate. We present simulation results comparing the bit error rate and SINR performance of the improved PIC detectors in several operating scenarios. The results show that the improved performance PIC detectors exhibit significant

performance gains with respect to the HPIC and LPIC detectors in several cases.

1.2.4 Multiuser Detection for Eavesdropping in CDMA Systems

The uplink eavesdropping problem was considered by McKellips and Verdu in [MV98b] where it was shown that power-controlled cellular systems caused an eavesdropper to observe users at disparate powers which led to near-far problems with conventional, matched filter detection. McKellips and Verdu derived analytical expressions for the received power distribution at the eavesdropper and tested the performance of several multiuser detection schemes but did not investigate decision-directed interference cancellation detectors. McKellips and Verdu also considered cooperative eavesdropping syndicates in order to improve performance with respect to a single eavesdropper in [MV98c].

Golanbari and Ford considered successive interference cancellation for the IS–95 downlink in [GF99]. The authors recognized that the eavesdropper was likely to receive the downlink user transmissions at disparate amplitudes and that conventional, matched filter detection would not provide sufficient performance. The authors suggested using a decoder and reencoder in the interference cancellation loop in order to improve the reliability of interference cancellation.

In Chapter 5 of this dissertation, we consider optimum and suboptimum multiuser detection techniques for eavesdropping in the IS–95 downlink. We derive a new group-PIC (GPIC) detector that exploits the structure of the IS–95 downlink and we demonstrate that the GPIC detector can offer improved performance with respect to the conventional matched filter detector via simulation. We also test the GPIC detector with measured on-air IS–95 downlink data and show that

the GPIC detector can provide dramatically improved performance for weak base station eavesdropping.

1.2.5 Multiuser Detection for Digital Subscriber Loops

Digital subscriber loop (DSL) communication systems provide a technique to deliver broadband Internet access through existing twisted pair copper wires from telephone service providers to residential and business customers. Although not a wireless communication technique, DSLs share many common features with the wireless CDMA communication systems investigated in Chapters 2-5 of this dissertation. Good introductions to DSL technology can be found in [Rau99] and [SCS99].

DSL signals are carried between a telephone company and its customers on a group of copper cables that are bundled in close proximity. The unshielded nature of these cables leads to electromagnetic coupling and interference between the signals, resulting in the observation of a desired signal corrupted by structured multiuser interference and additive unstructured channel noise. Multiuser interference is typically called "crosstalk" in the DSL environment. Garth et al. recognized in [GHW99] that the problem of crosstalk mitigation for DSL systems is quite similar to that of multiuser interference cancellation for CDMA systems and suggested that, as Verdu did in 1986 for CDMA communication systems, researchers should discard the Gaussian assumption imposed on the crosstalk and begin to exploit its structure with sophisticated multiuser detection or crosstalk mitigation algorithms. Several authors including Cioffi et al. in [CCLS98] have stated that crosstalk is the limiting factor to achieving higher bandwidth efficiency and data transmission rates for DSL systems. Im and Werner [IW95] and Im and Shanbhag [IS98] pro-

posed crosstalk mitigation algorithms for use at the service provider's equipment that were essentially extensions of single user echo-cancellation techniques to the multiuser case. Cioffi et al. [CCLS98] and Cheong and Cioffi [CC99] investigated multiuser detection at the customer's equipment to mitigate crosstalk and also to show the potential for coexistence with home networking systems. They showed that large performance gains were possible using information theoretic arguments.

In Chapter 6 of this dissertation, we examine the DSL crosstalk environment and present a new first-order analysis of the relative amplitudes of the interfering users as a first step toward developing a model for the crosstalk that reflects its inherent structure. We then investigate several multiuser detection techniques including optimum and interference cancellation detectors for crosstalk mitigation in DSL communication systems.

1.3 Thesis Overview

This dissertation logically divides into three primary sections which can be described as:

- Performance analysis of PIC detection (Chapters 2-3)
- Algorithms for improved PIC detection (Chapter 4)
- Applications of PIC detection (Chapters 5-6)

The contents of these chapters are described in more detail below.

Chapter 2 of this dissertation presents an analysis of two performance measures for the hard parallel interference cancellation (HPIC) detector: bit error rate (BER) and signal to interference plus noise (SINR) ratio. To date, the majority of

the performance studies on the HPIC detector have relied on simulations or approximations on the multiuser interference but Chapter 2 presents a new *exact* analysis for both the bit error rate and the SINR of the two-stage HPIC detector. In addition to our exact expressions, we develop approximate expressions for the bit error rate and SINR of the two-stage HPIC detector that are simpler to evaluate and we demonstrate that these approximations are accurate in several cases. We also present an analytical SINR comparison between the two-stage HPIC, successive interference cancellation (SIC), and matched filter (MF) detectors that suggests that HPIC detection offers superior performance under a large class of operating conditions.

Chapter 3 of this dissertation presents a performance analysis for the linear parallel interference cancellation (LPIC) detector. We compare the performance of the two-stage HPIC and LPIC detectors and show that the two-stage HPIC detector is a better estimator of multiuser interference. We compare the multistage LPIC detector to the conventional matched filter detector and show that, somewhat surprisingly, the multistage LPIC detector's error probability may be worse than the matched filter detector under certain operating conditions. We develop asymptotic results exposing the behavior of the multistage LPIC detector as the number of stages goes to infinity and show that, in contrast to the matched filter detector, the LPIC detector can exhibit bit error rates greater than 1/2 for one or more users in a well defined class of operating conditions. We also examine the implications of our prior results for large CDMA communication system with random spreading sequences and show that the LPIC detector performs poorly when the ratio of the number of users to the system spreading gain exceeds 0.17.

Chapter 4 of this dissertation considers methods to improve the performance of the HPIC detector. Although much has been written recently on improving the performance of PIC detection, the vast majority of this work has focused on the LPIC detector. In this chapter, we focus on improving the performance of the HPIC detector, justified by the results in Chapter 3 which showed that the unmodified two-stage HPIC detector tends to perform better than the unmodified two-stage LPIC detector. We develop the partial cancellation HPIC (PC-HPIC) detector where the HPIC detector's interference cancellation estimates are scaled using "partial cancellation factors" in order to attenuate unreliable estimates. We also develop the soft cancellation PIC (SC-PIC) detector where the sgn(·) nonlinearity of the HPIC detector is replaced by an estimator minimizing the Bayesian mean squared error of the interference estimates. We demonstrate via analysis and simulations that both approaches can yield significant performance gains with respect to the (unmodified) full cancellation HPIC detector.

Chapter 5 of this dissertation applies PIC detection to the downlink of the IS–95 digital cellular communication system, a second generation CDMA digital cellular standard currently installed on 6 continents with over 50 million subscribers. The PIC detector is nearly unique among multiuser detectors in that its complexity is low enough to allow application to practical systems such as IS–95. We develop a reduced complexity optimum detector that exploits the structure of the IS–95 downlink, from which we derive a group-PIC (GPIC) detector. Simulations of an IS–95 downlink eavesdropping scenario suggest that the GPIC detector offers near-optimum performance in the cases considered and provides the largest benefit when the multiuser interference from neighboring cells is high. We also examine a snapshot of actual on-air data from an active IS–95 system and present results that

suggest that GPIC detection offers significant performance improvements when extracting weak signals in the presence of severe out-of-cell multiuser interference.

Chapter 6 of this dissertation diverges slightly from the prior chapters. Several authors have noted that the multiuser detection techniques developed for CDMA communication systems may also apply to digital subscriber loop (DSL) communication systems. DSL is a relatively new technology currently being deployed by telephone service providers across North America in order to deliver broadband Internet access through existing telephone wiring. The DSL signals are carried between the service provider and the home users on a group of copper cables that are bundled in close proximity. The unshielded nature of these cables leads to electromagnetic coupling and interference between the signals, resulting in the observation of a desired signal corrupted by structured multiuser interference and additive unstructured channel noise. Remarkably, the mathematical formulation for DSL systems is quite similar to that of CDMA systems and in this chapter we investigate the application of multiuser and PIC detection to DSL systems.

Chapter 7 of this dissertation summarizes the results presented in the prior chapters and concludes with a discussion of open areas of future research stemming from this work.

1.4 Thesis Contribution

The main contributions of this dissertation are listed as follows:

- Chapter 2
  - Exact and approximate expressions for computing the bit error rate of the two-stage HPIC detector under the K-user synchronous system

model.

  - Exact and approximate expressions for computing the signal to interference plus noise ratio (SINR) of the two-stage HPIC detector under the K-user synchronous system model.
  - An analytical SINR comparison between the two-stage HPIC, successive interference cancellation (SIC), and matched filter (MF) detectors showing that the two-stage HPIC detector provides superior SINR, transmit power efficiency, and system capacity performance over a large class of typical operating conditions.

- Chapter 3
  - A comparison between two-stage HPIC and LPIC detectors in the K-user synchronous case that showing that HPIC detection offers better interference estimation performance.
  - Simulations demonstrating the linkage between interference estimator performance and the bit error rate of LPIC and HPIC detectors.
  - An analytical comparison between the multistage LPIC and conventional matched filter detectors in the K-user synchronous case showing that there exists a class of operating scenarios where the LPIC detector performs worse than the matched filter detector.
  - An analysis of the multistage LPIC detector showing that, unlike the matched filter detector, there exists a class of operating conditions where the LPIC detector exhibits bit error rates greater than 1/2.
  - An analysis of the LPIC detector in the K-user synchronous case with random spreading sequences showing that, when the spreading gain (N)

and number of users (K) are both large, the two-stage LPIC detector has worse SINR performance than the matched filter detector when $K/N > 1/3$.

  - An analysis of the LPIC detector in the K-user synchronous case with random spreading sequences showing that, when the spreading gain (N) and number of users (K) are both large, the LPIC detector has a bit error rate of at least $1/2$ for at least one user in the CDMA communication system when $K/N > 0.17$.

- Chapter 4

  - Development and performance analysis of a performance adaptive two-stage HPIC detector in the K-user synchronous case using partial rather than full interference cancellation. Partial cancellation factors optimized under three different performance criteria are developed.

  - Development and performance testing of a two-stage soft-cancellation PIC detector in the K-user synchronous case using the Bayesian Minimum Mean Squared Error (BMMSE) estimator for the multiuser interference. Exact and approximate expressions are developed.

- Chapter 5

  - Development of a general system model for the IS–95 digital cellular downlink accounting for asynchronism and noncyclostationary cochannel interference from neighboring base stations.

  - Development of a reduced complexity optimum detector exploiting the structure of the multicell IS–95 digital cellular downlink.

  - Development of a group-PIC (GPIC) detector exploiting the structure of the multicell IS–95 digital cellular downlink.
  - Performance testing of the GPIC detector via simulations and and actual on-air measured data.

- Chapter 6
  - An analysis of near end crosstalker powers observed at the customer's modem in a discrete multitone, echo cancelled, asymmetric digital subscriber loop communication system.
  - Development of a simplified analytical model for crosstalk cancellation in a discrete multitone, echo cancelled, digital subscriber loop communication system.
  - Analysis and performance testing of several multiuser detectors, originally developed in the context of CDMA communication systems, for crosstalk cancellation in digital subscriber loop communication systems.

1.5 CDMA Communication System Model

Chapters 2-5 of this dissertation study PIC detection for CDMA cellular communication systems. In Chapter 5, we develop a system model specific to the IS–95 digital cellular downlink but in Chapters 2-4 we consider the general K-user CDMA communication system model shown in Figure 1.1 below.

The binary valued data stream from the k^{th} user is denoted as $\{b_n^{(k)}\}$. This data stream is spread by a unique signature sequence (also called the "code" in code division multiple access) and converted from discrete time to continuous-time

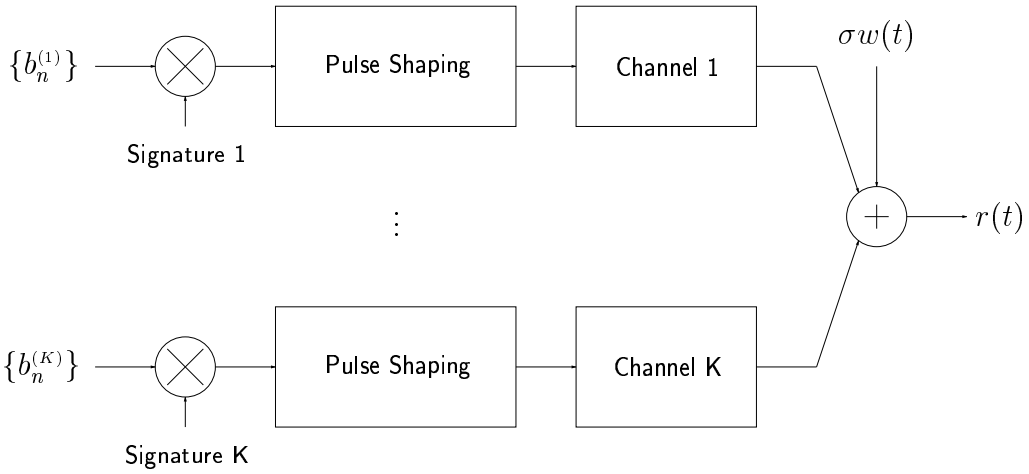

Figure 1.1: K-user CDMA communication system model.

via the pulse shaping operation. The channels account for multipath effects, asynchronism, and (complex) attenuation of the signal. The unstructured interference is modeled as an additive white Gaussian noise process denoted as $\sigma w(t)$ where $w(t)$ has zero mean and unit power spectral density. The continuous-time signal observed at the input of the receiver is denoted as $r(t)$.

In Chapters 2-4 of this dissertation, we assume that the users transmit *synchronously*, that the pulse shapes are such that they have support on $[0, T)$ where T is the duration of the baud interval, and that the channels are single-path. These assumptions are equivalent to the assumptions used to develop the basic K-user CDMA communication system model described in [Ver98]. Under these assumptions, we can write the received signal as

$$r(t) \;=\; \sum_{k=1}^{K} \sum_{n=-\infty}^{\infty} a_n^{(k)} b_n^{(k)} s_n^{(k)}(t - nT) + \sigma w(t)$$

where $a_n^{(k)}$ denotes the amplitude of the k^{th} user in the n^{th} baud interval and $s_n^{(k)}(t)$ denotes the unit energy signature waveform of the k^{th} user in the n^{th} baud interval. It has been shown [Ver98] that the baud-rate sampled vector output of a bank of

filters matched to the spreading waveforms of each user is a sufficient statistic for optimum demodulation. The matched filter bank is shown in Figure 1.2 where the continuous-time received signal $r(t)$ is filtered by a bank of K matched filters where the k^{th} matched filter computes the inner product of the received signal with the k^{th} user's spreading waveform.

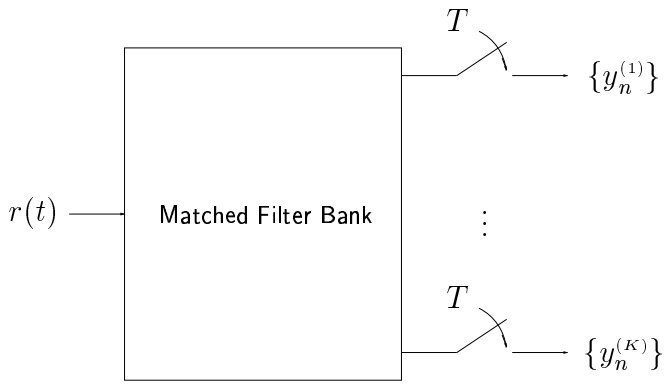

Figure 1.2: Matched filter detector for K-user CDMA communication system.

In Figure 1.2, each continuous-time matched filter output is sampled once per baud interval T and the k^{th} user's real valued, discrete-time output stream is denoted as $\{y_n^{(K)}\}$ where

$$\begin{aligned} y_n^{(k)} &\triangleq \int_{nT}^{(n+1)T} r(t)s_n^{(k)}(t-nT)\,dt \\ &= \sum_{\ell=1}^{K}\sum_{m=-\infty}^{\infty} a_m^{(\ell)}b_m^{(\ell)}\int_{nT}^{(n+1)T} s_n^{(k)}(t-nT)s_m^{(\ell)}(t-nT)\,dt \\ &\qquad +\sigma\int_{nT}^{(n+1)T} s_n^{(k)}(t-nT)w(t)\,dt. \end{aligned}$$

Since the imposed assumptions allow us to consider symbol-by-symbol detection and hence suppress the symbol index n, we can write the k^{th} user's matched filter

bank output as

$$y^{(k)} = a^{(k)}b^{(k)} + \sum_{\ell \neq k} \rho_{k\ell} a^{(\ell)} b^{(\ell)} + \sigma n^{(k)}$$

where

$$\rho_{k\ell} \triangleq \int_0^T s^{(k)}(t) s^{(\ell)}(t)\, dt$$

and

$$n^{(k)} \triangleq \int_0^T s^{(k)}(t) w(t)\, dt.$$

We can group the matched filter bank outputs into a K-dimensional vector and express the vector output of the matched filter bank as

$$\boldsymbol{y} = \boldsymbol{R}\boldsymbol{A}\boldsymbol{b} + \sigma \boldsymbol{n} \tag{1.1}$$

where $\boldsymbol{R} \in \mathbb{R}^{K \times K}$ is a symmetric matrix of user signature crosscorrelations such that $\boldsymbol{R}_{k\ell} = \rho_{k\ell}$. The signature waveforms are assumed to be normalized to unit energy such that $\boldsymbol{R}_{kk} = 1$ for all $k = 1, \ldots, K$ which implies that $|\boldsymbol{R}_{k\ell}| \leq 1$ for all $k \neq \ell$. The matrix $\boldsymbol{A} = \mathrm{diag}(a^{(1)}, \ldots, a^{(K)})$ is a $K \times K$ diagonal matrix of positive real amplitudes, $\boldsymbol{b} = [b^{(1)}, \ldots, b^{(K)}]^\top$ is a vector of i.i.d. equiprobable binary data symbols where $b^{(k)} \in \mathbb{B} = \{\pm 1\}$, and $\boldsymbol{n} = [n^{(1)}, \ldots, n^{(K)}]^\top$ represents the matched filtered, unit variance AWGN process where it can be shown that $\mathrm{E}[\boldsymbol{n}] = \boldsymbol{0}$ and $\mathrm{E}[\boldsymbol{n}\boldsymbol{n}^\top] = \boldsymbol{R}$. The channel noise and user symbols are assumed to be independent.

1.6 PIC Detection Framework

All of the PIC detectors considered in Chapters 2-4 of this dissertation operate exclusively on the vector of matched filter bank outputs given by (1.1). Moreover,

these PIC detectors all share a common structure, illustrated for the 3-user case in Figure 1.3 for a two-stage PIC detector. The structure of Figure 1.3 suggests that the two-stage PIC detector may be extended to K-users and/or multiple stages without any conceptual difficulty.

The essential feature of PIC detector X that distinguishes it from PIC detector Y is the choice of the interference estimator $f_{\mathsf{X}}^{(k)}(y^{(k)})$. The interference estimators for the PIC detectors considered in Chapters 2-4 of this dissertation are summarized in Table 1.1.

Table 1.1: Summary of PIC detectors.

X	$f_{\mathsf{X}}^{(k)}(y^{(k)})$
HPIC	$a^{(k)}\mathrm{sgn}(y^{(k)})$
LPIC	$y^{(k)}$
PC-HPIC	$g_k a^{(k)}\mathrm{sgn}(y^{(k)})$
SC-PIC	$a^{(k)}\tanh(y^{(k)}/\lambda)$

Extending Figure 1.3 to the K-user case, the output of the two-stage PIC detector X, prior to the hard decision device, may be written as

$$y_{\mathsf{X}}^{(k)} = a^{(k)}b^{(k)} + \underbrace{\sum_{\ell\neq k}\rho_{k\ell}\left[a^{(\ell)}b^{(\ell)} - f_{\mathsf{X}}^{(\ell)}(y^{(\ell)})\right]}_{\text{residual multiuser interference}} + \sigma n^{(k)}. \tag{1.2}$$

This expression suggests an important perspective on PIC detection that we will formalize in later chapters of this dissertation: $f_{\mathsf{X}}^{(\ell)}(y^{(\ell)})$ can be viewed as an estimator of $a^{(\ell)}b^{(\ell)}$ and the performance of PIC detector X is closely related to the performance of its estimator. If $f_{\mathsf{X}}^{(\ell)}(y^{(\ell)})$ is an accurate estimator of $a^{(\ell)}b^{(\ell)}$ then the residual multiuser interference term in (1.2) is small and the desired user's signal

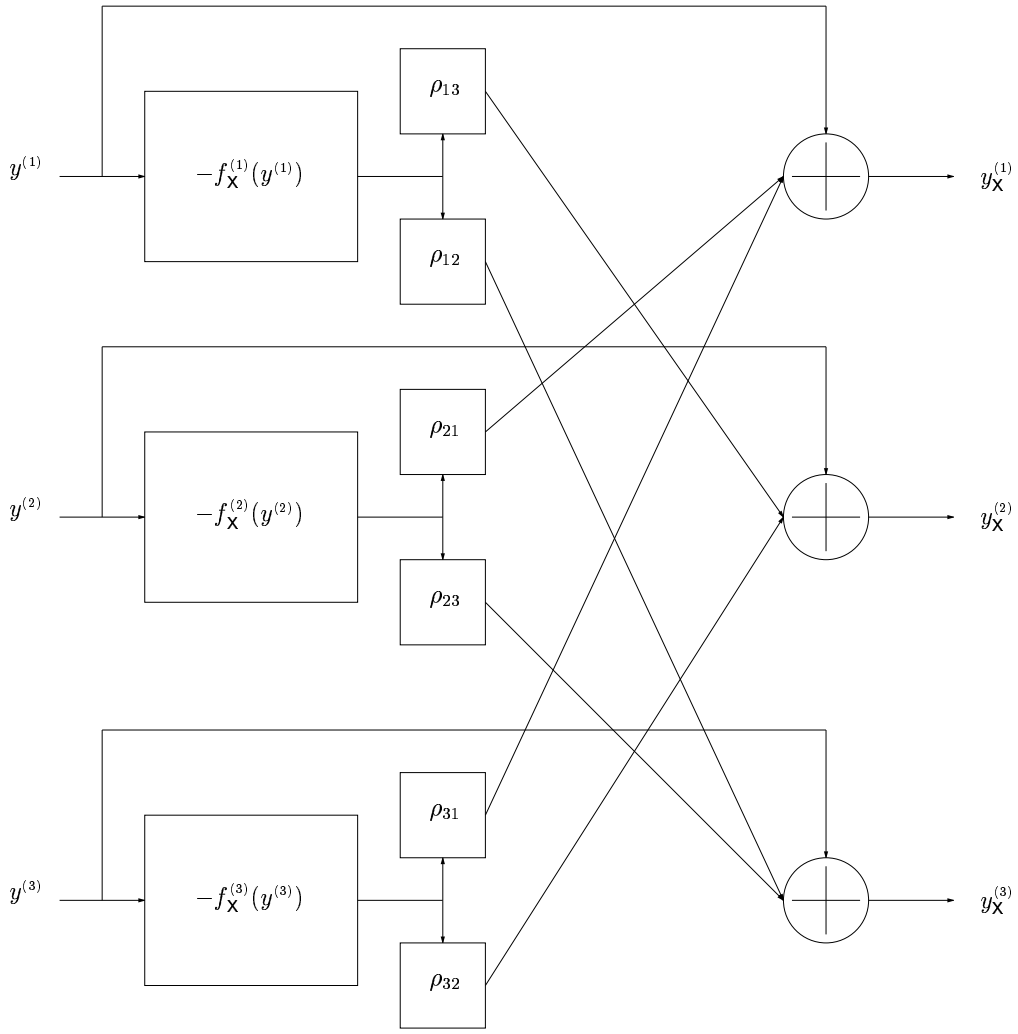

Figure 1.3: Two-stage PIC detector for 3-user CDMA communication system.

is impaired only by additive channel noise. On the other hand, if $f_{\mathsf{X}}^{(\ell)}(y^{(\ell)})$ is a particularly inaccurate estimator of $a^{(\ell)}b^{(\ell)}$, then the residual multiuser interference term in (1.2) may actually be larger than the interference term of the matched filter detector and performance may suffer.

Throughout this dissertation we will also find it convenient to group the outputs of the two-stage PIC detector into a K-dimensional vector as

$$\boldsymbol{y}_{\mathsf{X}} = \boldsymbol{y} - (\boldsymbol{R} - \boldsymbol{I})\boldsymbol{f}_{\mathsf{X}}(\boldsymbol{y}) \tag{1.3}$$

where $\boldsymbol{I}$ is the $K \times K$ identity matrix and $\boldsymbol{f}_{\mathsf{X}}(\boldsymbol{y}) = [f_{\mathsf{X}}^{(1)}(y^{(1)}), \ldots, f_{\mathsf{X}}^{(K)}(y^{(K)})]^{\top}$.

1.7 Table of Abbreviations

Table 1.2: Abbreviations used.

ADSL	Asymmetric Digital Subscriber Loop, [Rau99] and Chapter 6
BER	Bit error rate, [Pro95]
CDMA	Code Division Multiple Access, [Vit95]
DMT	Discrete MultiTone, [Rau99] and Chapter 6
DSL	Digital Subscriber Loop, [Rau99] and Chapter 6
EC	Echo Cancellation, [Rau99] and Chapter 6
FEXT	Far End CrossTalk, [Rau99] and Chapter 6
GPIC	Group Parallel Interference Cancellation, Chapter 5
HPIC	Hard Parallel Interference Cancellation, Chapters 2 and 4
IS–95	Mobile Station – Base Station Compatibility Standard for Dual-Mode Wideband Spread Spectrum Cellular Systems Interim Standard 95, [Tel95] and Chapter 5
JML	Joint Maximum Likelihood, [Ver98]
LPIC	Linear Parallel Interference Cancellation, Chapter 3
MAI	Multiple Access Interference, [Ver98]
MF	Matched Filter, [Ver98]
NEXT	Near End CrossTalk, [Rau99] and Chapter 6
PC-HPIC	Partial Cancellation Hard Parallel Interference Cancellation, Chapter 4
PIC	Parallel Interference Cancellation
SC-PIC	Soft Cancellation Parallel Interference Cancellation, Chapter 4
SIC	Successive Interference Cancellation, [Ver98] and Chapter 2
SIC2	Two-stage Successive Interference Cancellation, Chapter 6
SNR	Signal to Noise Ratio, [Pro95]
SINR	Signal to Interference plus Noise Ratio, [Ver98] and Chapter 2

CHAPTER 2

PERFORMANCE ANALYSIS OF HARD DECISION PARALLEL INTERFERENCE CANCELLATION

This chapter presents an analysis of two performance measures for the hard parallel interference cancellation (HPIC) detector: bit error rate (BER) and signal to interference plus noise ratio (SINR). Bit error rate, or, equivalently, probability of decision error, is a classical performance measure that has been analyzed for a variety of multiuser detectors including the matched filter (MF), decorrelating, and minimum mean squared error (MMSE) detectors [Ver98], to name just a few, and is often one of the most important performance measures for uncoded communication systems. To date, the majority of the performance studies on bit error rate of the HPIC detector have relied exclusively on approximations or simulations (see for instance [YKI93, HHT95, DS94]). The first section of this chapter presents an analytical study of the bit error rate of the two-stage HPIC detector. We show that exact computation of the bit error rate is indeed quite difficult even for a small number of users and is computationally infeasible for more than a handful of users. We suggest an approximation that yields a much simpler expression for the bit error rate of the HPIC detector and show that our approximation tends to be accurate in several cases.

The second section of this chapter presents an analysis of the SINR of the HPIC detector. SINR is an alternative performance measure that is often, but not always, closely related to the bit error rate performance of a multiuser detector. SINR can actually be a more relevant measure of performance than bit error rate when the detector's soft outputs are to be used by a channel decoder. In Section 2.2, we derive an exact expression for the SINR of the two-stage HPIC detector and, in order

to obtain useful analytical results, we also suggest an approximation that tends to yield accurate results under conditions when the matched filter bank outputs have reasonably low error probability. We extend these approximate SINR results to consider the implications on the power efficiency and theoretical system capacity of the two-stage HPIC detector. In the case when all users have equicorrelated signature waveforms, we show analytically that the HPIC detector outperforms the matched filter and successive interference cancellation (SIC) detectors in a large class of operating conditions.

2.1 Bit Error Rate Analysis

This section presents a bit error rate analysis for the two-stage HPIC detector as defined by (1.2) and Table 1.1. Our results differ from the bit error rate analysis in [VA91] where the authors calculated the exact bit error rate of the two-stage HPIC detector with a *decorrelating* first stage. The results in this chapter apply to the two-stage HPIC detector with a matched filter bank first stage. Moreover, the bit error rate analysis in [VA90], for the asynchronous case with matched filter bank first stage, is not quite correct since the authors' analysis implies that the matched filter bank decisions of users $2, \ldots, K$ are independent of the noise in user one's soft matched filter output. Our analysis shows that this is actually not a valid assumption and that the exact expression for the HPIC detector's bit error rate requires evaluation of several K-dimensional integrals of the K-dimensional joint Gaussian pdf. Unfortunately, these integrals do not reduce to closed form expressions except in degenerate cases and, in general, require numerical solution methods in even the $K = 2$ case. Since these results imply that computation of the

exact bit error rate of the HPIC detector is essentially an intractable problem for more than a handful of users, we pose a judicious approximation that allows us to derive a simpler expression for the approximate bit error rate of the HPIC detector that does not require integration. We verify the accuracy of this approximate bit error rate expression in a large class of operating conditions in the two-user case by direct comparison to the exact bit error rate expression. We also demonstrate the accuracy of the approximate bit error rate expression in the K-user case via simulation.

2.1.1 Exact Analysis

From (1.2) and Table 1.1, we can write the k^{th} user's two-stage HPIC detector output in the K-user synchronous case as

$$y_{\mathsf{HPIC}}^{(k)} = a^{(k)}b^{(k)} + \sum_{\ell \neq k} \rho_{k\ell}\left[a^{(\ell)}b^{(\ell)} - a^{(\ell)}\mathrm{sgn}(y^{(\ell)})\right] + \sigma n^{(k)}. \tag{2.1}$$

To compute the exact bit error rate of the two-stage HPIC detector, we denote without loss of generality user number one as the desired user. The bit error rate (or probability of decision error) of the HPIC detector for user one can then be written as

$$P_{\mathsf{HPIC}}^{(1)} = P(y_{\mathsf{HPIC}}^{(1)} > 0, b^{(1)} = -1) + P(y_{\mathsf{HPIC}}^{(1)} < 0, b^{(1)} = +1).$$

By the symmetry of the users' bits and channel noise, it can be shown that

$$P(y_{\mathsf{HPIC}}^{(1)} > 0, b^{(1)} = -1) = P(y_{\mathsf{HPIC}}^{(1)} < 0, b^{(1)} = +1)$$

hence

$$P_{\mathsf{HPIC}}^{(1)} = 2P(y_{\mathsf{HPIC}}^{(1)} > 0, b^{(1)} = -1).$$

Denoting $\bar{\boldsymbol{b}} = [b^{(2)}, \ldots, b^{(K)}]$ as the $(K-1)$-vector comprised of all users' bits except the desired user, we can write the desired probability as

$$\begin{aligned} P(y^{(1)}_{\mathsf{HPIC}} > 0, b^{(1)} = -1) &= \sum_{\bar{\boldsymbol{u}} \in \mathbb{B}^{K-1}} P\left(y^{(1)}_{\mathsf{HPIC}} > 0, b^{(1)} = -1, \bar{\boldsymbol{b}} = \bar{\boldsymbol{u}}\right) \\ &= \sum_{\bar{\boldsymbol{u}} \in \mathbb{B}^{K-1}} P\left(y^{(1)}_{\mathsf{HPIC}} > 0 \,|\, b^{(1)} = -1, \bar{\boldsymbol{b}} = \bar{\boldsymbol{u}}\right) P\left(b^{(1)} = -1, \bar{\boldsymbol{b}} = \bar{\boldsymbol{u}}\right) \\ &= \frac{1}{2^K} \sum_{\bar{\boldsymbol{u}} \in \mathbb{B}^{K-1}} P\left(y^{(1)}_{\mathsf{HPIC}} > 0 \,|\, \boldsymbol{b} = \left[-1, \bar{\boldsymbol{u}}^\top\right]^\top\right) \end{aligned}$$

where $\mathbb{B} = \{\pm 1\}$ and where we have used the assumption that all of the users' bits are equiprobable and independent of each other. If we condition $y^{(1)}_{\mathsf{HPIC}}$ on $\boldsymbol{b} = \left[-1, \bar{\boldsymbol{u}}^\top\right]^\top$ and assume that $\boldsymbol{A}$, $\boldsymbol{R}$, and σ are fixed and known, then the key step in order to evaluate the bit error rate of the two-stage HPIC detector is to view $y^{(1)}_{\mathsf{HPIC}}$ as a function that maps the realizations of the random variables $\{n^{(k)}\}_{k=1}^K$ to a point in $\mathbb{R}$. Although (2.1) conditioned on $\boldsymbol{b}$ appears to be a function of only one random variable, $n^{(k)}$, (2.1) is also a function of the matched filter outputs $\{y^{(\ell)}\}_{\ell \neq k}$. Since $y^{(\ell)}$ conditioned on $\boldsymbol{b}$ is a function of the random variable $n^{(\ell)}$, then $y^{(k)}_{\mathsf{HPIC}}$ is actually function of the K correlated Gaussian random variables $\{n^{(\ell)}\}_{\ell=1}^K$. In this context, it can be shown that $y^{(1)}_{\mathsf{HPIC}}$ is a measurable mapping [Bil95] from $\mathbb{R}^K$ to $\mathbb{R}$ implying that there exists a set $\Omega(\bar{\boldsymbol{u}}) \subset \mathbb{R}^K$ such that

$$y^{(1)}_{\mathsf{HPIC}} > 0 \text{ and } \boldsymbol{b} = \left[-1, \bar{\boldsymbol{u}}^\top\right]^\top \quad \Leftrightarrow \quad \boldsymbol{n} \in \Omega(\bar{\boldsymbol{u}}).$$

This then implies that the bit error rate of the two-stage HPIC detector can be computed via

$$\begin{aligned} P^{(1)}_{\mathsf{HPIC}} &= \frac{1}{2^{K-1}} \sum_{\bar{\boldsymbol{u}} \in \mathbb{B}^{K-1}} P\left(\boldsymbol{n} \in \Omega(\bar{\boldsymbol{u}})\right) \\ &= \frac{1}{2^{K-1}} \sum_{\bar{\boldsymbol{u}} \in \mathbb{B}^{K-1}} \int_{\boldsymbol{\omega} \in \Omega(\bar{\boldsymbol{u}})} f(\boldsymbol{\omega})\, d\boldsymbol{\omega} \end{aligned} \tag{2.2}$$

where f is the joint Gaussian pdf of the K-dimensional channel noise vector $\boldsymbol{n}$ with zero mean and covariance matrix $\boldsymbol{R}$.

Although (2.2) is an exact expression for the bit error rate of the two-stage HPIC detector, evaluation of (2.2) is not straightforward since the set $\Omega(\bar{\boldsymbol{u}})$ is not given in an explicit form. To construct the set $\Omega(\bar{\boldsymbol{u}})$ explicitly in the synchronous K-user case, we denote $d^{(k)} = \mathrm{sgn}(y^{(k)})$ and $\bar{\boldsymbol{d}} = [d^{(2)}, \ldots, d^{(K)}]$. Since $d^{(k)}$ is the decision generated by the matched filter bank for user k then it can be shown that

$$\begin{aligned} d^{(k)} = +1 \text{ and } \boldsymbol{b} = \left[-1, \bar{\boldsymbol{u}}^\top\right]^\top &\Leftrightarrow y^{(k)} > 0 \text{ and } \boldsymbol{b} = \left[-1, \bar{\boldsymbol{u}}^\top\right]^\top \\ &\Leftrightarrow -\rho_{k1} a^{(1)} + \sum_{\ell=2}^{K} \rho_{k\ell} a^{(\ell)} u^{(\ell)} + \sigma n^{(k)} > 0 \qquad (2.3) \\ &\Leftrightarrow n^{(k)} > \frac{\rho_{k1} a^{(1)} - \sum_{\ell=2}^{K} \rho_{k\ell} a^{(\ell)} u^{(\ell)}}{\sigma} \end{aligned}$$

and that

$$\begin{aligned} d^{(k)} = -1 \text{ and } \boldsymbol{b} = \left[-1, \bar{\boldsymbol{u}}^\top\right]^\top &\Leftrightarrow y^{(k)} < 0 \text{ and } \boldsymbol{b} = \left[-1, \bar{\boldsymbol{u}}^\top\right]^\top \\ &\Leftrightarrow -\rho_{k1} a^{(1)} + \sum_{\ell=2}^{K} \rho_{k\ell} a^{(\ell)} u^{(\ell)} + \sigma n^{(k)} < 0 \qquad (2.4) \\ &\Leftrightarrow n^{(k)} < \frac{\rho_{k1} a^{(1)} - \sum_{\ell=2}^{K} \rho_{k\ell} a^{(\ell)} u^{(\ell)}}{\sigma}. \end{aligned}$$

These results can be combined to write

$$\bar{\boldsymbol{d}} = \bar{\boldsymbol{v}} \text{ and } \boldsymbol{b} = [-1, \bar{\boldsymbol{u}}^\top]^\top \quad \Leftrightarrow \quad \bar{\boldsymbol{n}} \in S(\bar{\boldsymbol{u}}, \bar{\boldsymbol{v}}) \qquad (2.5)$$

where $S(\bar{\boldsymbol{u}}, \bar{\boldsymbol{v}})$ is a rectangular subset of $\mathbb{R}^{K-1}$. Observe that the events $\bar{\boldsymbol{d}} = \bar{\boldsymbol{v}}$, for all $\bar{\boldsymbol{v}} \in \mathbb{B}^{K-1}$, satisfy the requirements (unconditionally or conditioned on $\boldsymbol{b}$) to form a partition of the probability space since these events are mutually exclusive in that

$$P\left(\bar{\boldsymbol{d}} = \bar{\boldsymbol{v}}, \bar{\boldsymbol{d}} = \bar{\boldsymbol{v}}' \,|\, \boldsymbol{b} = \left[-1, \bar{\boldsymbol{u}}^\top\right]^\top\right) \;=\; 0 \qquad \forall \bar{\boldsymbol{v}} \neq \bar{\boldsymbol{v}}'$$

and exhaustive in that

$$\sum_{\bar{\boldsymbol{v}} \in \mathbb{B}^{K-1}} P\left(\bar{\boldsymbol{d}} = \bar{\boldsymbol{v}} \,|\, \boldsymbol{b} = \left[-1, \bar{\boldsymbol{u}}^\top\right]^\top\right) \;=\; 1.$$

Application of the total probability theorem then allows us to write

$$P\left(y_{\mathsf{HPIC}}^{(1)} > 0 \,|\, \boldsymbol{b} = \left[-1, \bar{\boldsymbol{u}}^{\top}\right]^{\top}\right) = \sum_{\bar{\boldsymbol{v}} \in \mathbb{B}^{K-1}} P\left(y_{\mathsf{HPIC}}^{(1)} > 0,\, \bar{\boldsymbol{d}} = \bar{\boldsymbol{v}} \,|\, \boldsymbol{b} = \left[-1, \bar{\boldsymbol{u}}^{\top}\right]^{\top}\right) \quad (2.6)$$

and (2.1) and (2.5) imply that

$$\left\{ \begin{array}{l} \bar{\boldsymbol{d}} = \bar{\boldsymbol{v}}, \\ \boldsymbol{b} = \left[-1, \bar{\boldsymbol{u}}^{\top}\right]^{\top}, \text{ and} \\ y_{\mathsf{HPIC}}^{(1)} > 0 \end{array} \right\} \Leftrightarrow \left\{ \begin{array}{l} \bar{\boldsymbol{n}} \in S(\bar{\boldsymbol{u}}, \bar{\boldsymbol{v}}), \text{ and} \\ n^{(1)} > \frac{a^{(1)} - \sum_{k=2}^{K} \rho_{1k} a^{(k)} [u^{(k)} - v^{(k)}]}{\sigma} \end{array} \right\} \quad (2.7)$$

$$\Leftrightarrow \boldsymbol{n} \in \Omega(\bar{\boldsymbol{u}}, \bar{\boldsymbol{v}})$$

where $\Omega(\bar{\boldsymbol{u}}, \bar{\boldsymbol{v}})$ is a rectangular subset of $\mathbb{R}^K$ explicitly defined by (2.3), (2.4), (2.5), and (2.7). The exhaustive property of $\bar{\boldsymbol{d}}$ implies that

$$\Omega(\bar{\boldsymbol{u}}) \;=\; \bigcup_{\bar{\boldsymbol{v}} \in \mathbb{B}^{K-1}} \Omega(\bar{\boldsymbol{u}}, \bar{\boldsymbol{v}})$$

and the mutually exclusive property of $\bar{\boldsymbol{d}}$ implies that

$$\Omega(\bar{\boldsymbol{u}}, \bar{\boldsymbol{v}}) \bigcap \Omega(\bar{\boldsymbol{u}}, \bar{\boldsymbol{v}}') \;=\; \emptyset \qquad \forall \bar{\boldsymbol{v}} \neq \bar{\boldsymbol{v}}'.$$

This then implies that $\{\Omega(\bar{\boldsymbol{u}}, \bar{\boldsymbol{v}})\}_{\bar{\boldsymbol{v}} \in \mathbb{B}^{K-1}}$ specifies a convenient partition of the set $\Omega(\bar{\boldsymbol{u}})$. Hence, the K-dimensional integral in (2.2) over the complicated set $\Omega(\bar{\boldsymbol{u}})$ can be conveniently expressed as a sum of 2^{K-1} integrals over the K-dimensional rectangular regions specified by the partition $\{\Omega(\bar{\boldsymbol{u}}, \bar{\boldsymbol{v}})\}_{\bar{\boldsymbol{v}} \in \mathbb{B}^{K-1}}$ such that

$$P_{\mathsf{HPIC}}^{(1)} \;=\; \frac{1}{2^{K-1}} \sum_{\bar{\boldsymbol{u}} \in \mathbb{B}^{K-1}} \sum_{\bar{\boldsymbol{v}} \in \mathbb{B}^{K-1}} \int_{\boldsymbol{\omega} \in \Omega(\bar{\boldsymbol{u}}, \bar{\boldsymbol{v}})} f(\boldsymbol{\omega})\, d\boldsymbol{\omega}. \quad (2.8)$$

Combined with (2.3), (2.4), (2.5), and (2.7), this last expression yields an explicit method for calculation of the bit error rate of the K-user, two-stage HPIC detector. The integration regions $\Omega(\bar{\boldsymbol{u}}, \bar{\boldsymbol{v}})$ are explicitly derived for the two-user case in Table 4.1 of Chapter 4. Unfortunately, the integrals in (2.8) do not simplify

to a form where the K-dimensional integration of the joint Gaussian pdf can be avoided except in trivial cases (e.g., $\boldsymbol{R} = \boldsymbol{I}$). This implies that computation of the bit error rate of the HPIC detector requires the numerical evaluation of 2^{2K-2} integrals over K-dimensional rectangular regions, a computationally prohibitive task for K more than a handful of users. A reasonable approximation for the bit error rate of the two-stage HPIC detector requiring no integration is developed in the next section.

2.1.2 Approximate Analysis

In this section we pose an approximation for the bit error rate of the two-stage HPIC detector of (2.1). This approximation eliminates the integration required in the exact K-user bit error rate expression (2.8) and is shown to be reasonably accurate in several cases.

Using the notation of the prior section, we can apply Bayes' rule to (2.6) to write

$$P\left(y_{\mathsf{HPIC}}^{(1)} > 0,\, \bar{\boldsymbol{d}} = \bar{\boldsymbol{v}} \,|\, \boldsymbol{b} = \left[-1, \bar{\boldsymbol{u}}^{\top}\right]^{\top}\right) = P\left(y_{\mathsf{HPIC}}^{(1)} > 0 \,|\, \bar{\boldsymbol{d}} = \bar{\boldsymbol{v}},\, \boldsymbol{b} = \left[-1, \bar{\boldsymbol{u}}^{\top}\right]^{\top}\right) \cdot P\left(\bar{\boldsymbol{d}} = \bar{\boldsymbol{v}} \,|\, \boldsymbol{b} = \left[-1, \bar{\boldsymbol{u}}^{\top}\right]^{\top}\right).$$

If we assume that $\bar{\boldsymbol{n}}$ is approximately independent of $n^{(1)}$ then this implies that conditioning on $\bar{\boldsymbol{d}} = \bar{\boldsymbol{v}}$ does not imply anything about $n^{(1)}$ and we can pose the first approximation as

$$P\left(y_{\mathsf{HPIC}}^{(1)} > 0 \,|\, \bar{\boldsymbol{d}} = \bar{\boldsymbol{v}},\, \boldsymbol{b} = \left[-1, \bar{\boldsymbol{u}}^{\top}\right]^{\top}\right) \approx Q\left(\frac{a^{(1)} - \sum_{k=2}^{K} \rho_{1k} a^{(k)} [u^{(k)} - v^{(k)}]}{\sigma}\right)$$

where $Q(x) \stackrel{\Delta}{=} \int_x^{\infty} e^{-t^2/2}\, dt$. To form the second approximation, we first note that

$$P\left(\bar{\boldsymbol{d}} = \bar{\boldsymbol{v}} \,|\, \boldsymbol{b} = \left[-1, \bar{\boldsymbol{u}}^{\top}\right]^{\top}\right) = P\left(d^{(2)} = v^{(2)}, \ldots, d^{(K)} = v^{(K)} \,|\, \boldsymbol{b} = \left[-1, \bar{\boldsymbol{u}}^{\top}\right]^{\top}\right).$$

If we assume that $n^{(k)}$ is approximately independent of $n^{(\ell)}$ for all $k \neq \ell$ then this implies that, conditioned on $\boldsymbol{b}$, the matched filter decision $d^{(k)}$ is approximately independent of $d^{(\ell)}$ for all $k \neq \ell$ and we can pose the second approximation as

$$P\left(\bar{\boldsymbol{d}} = \bar{\boldsymbol{v}} \,|\, \boldsymbol{b} = \left[-1, \bar{\boldsymbol{u}}^{\top}\right]^{\top}\right) \approx \prod_{k=2}^{K} P\left(d^{(k)} = v^{(k)} \,|\, \boldsymbol{b} = \left[-1, \bar{\boldsymbol{u}}^{\top}\right]^{\top}\right).$$

We note that each of the probabilities in the product can be expressed as a single Q function. In light of the exact bit error rate results in the prior section, these results imply that the bit error rate of the two-stage HPIC detector may be approximated as

$$P_{\mathsf{HPIC}}^{(1)} \approx \frac{1}{2^{K-1}} \sum_{\bar{\boldsymbol{u}} \in \mathbb{B}^{K-1}} \sum_{\bar{\boldsymbol{v}} \in \mathbb{B}^{K-1}} Q\left(\frac{x_{\mathsf{HPIC}}(\bar{\boldsymbol{u}}, \bar{\boldsymbol{v}})}{\sigma}\right) \prod_{k=2}^{K} Q\left(\frac{x_{\mathsf{MF}}(\bar{\boldsymbol{u}}, v^{(k)})}{\sigma}\right) \quad (2.9)$$

where

$$x_{\mathsf{HPIC}}(\bar{\boldsymbol{u}}, \bar{\boldsymbol{v}}) = a^{(1)} - \sum_{k=2}^{K} \rho_{1k} a^{(k)} [u^{(k)} - v^{(k)}]$$

and

$$x_{\mathsf{MF}}(\bar{\boldsymbol{u}}, v^{(k)}) = \begin{cases} -\rho_{k1} a^{(1)} + \sum_{\ell=2}^{K} \rho_{k\ell} a^{(\ell)} u^{(\ell)} & \text{if } v^{(k)} = -1 \\ \rho_{k1} a^{(1)} - \sum_{\ell=2}^{K} \rho_{k\ell} a^{(\ell)} u^{(\ell)} & \text{if } v^{(k)} = +1 \end{cases}.$$

Figures 2.1, 2.2, and 2.3 plot the exact (2.8) and approximate (2.9) bit error rates of the two-stage HPIC detector in the two-user synchronous scenario for the cases when the user signature waveform crosscorrelation is $\rho = 0.2$, $\rho = 0.5$, and $\rho = 0.8$. The approximations appear to be accurate in a large class of operating conditions but the ratio of approximate to exact bit error rate is also plotted in each case to indicate the regions in SNR-space where (2.9) has lower accuracy. These results suggest that (2.9) tends to estimate the bit error rate conservatively (the approximate bit error rate is greater than the exact bit error rate) over most of the two-user SNR-space.

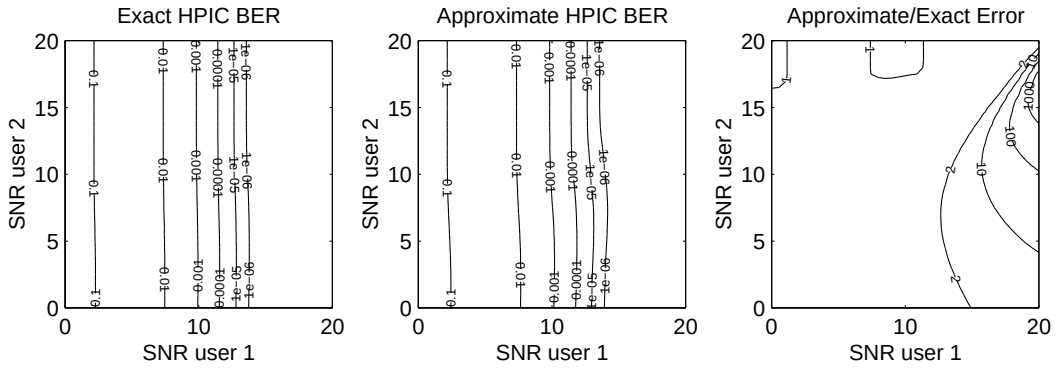

Figure 2.1: Exact and approximate bit error rates for user one at the output of the two-stage HPIC detector with two users and $\rho = 0.2$.

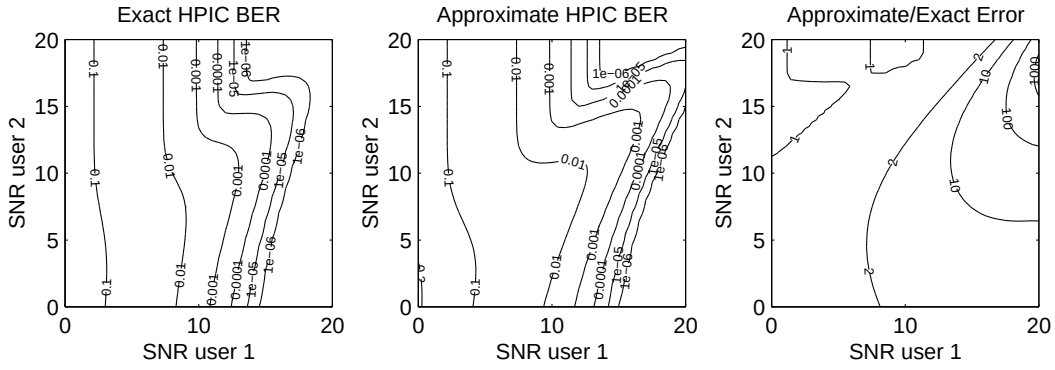

Figure 2.2: Exact and approximate bit error rates for user one at the output of the two-stage HPIC detector with two users and $\rho = 0.5$.

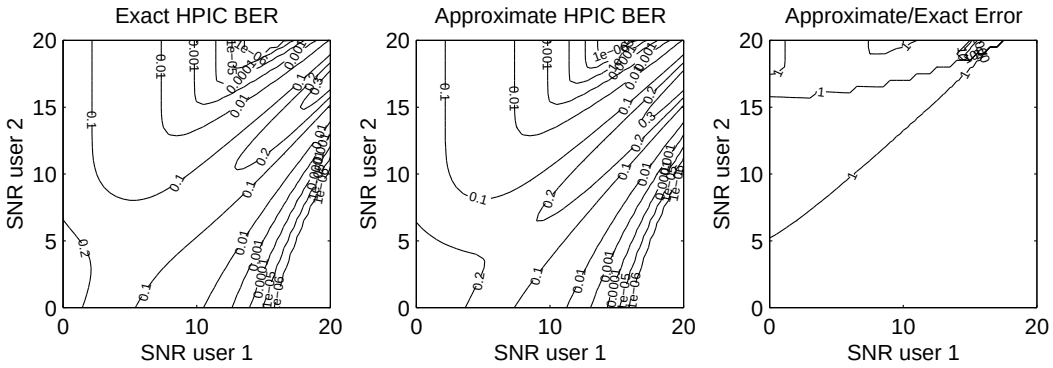

Figure 2.3: Exact and approximate bit error rates for user one at the output of the two-stage HPIC detector with two users and $\rho = 0.8$.

Figure 2.4 shows a comparison of the approximate bit error rate expression (2.9) to simulation results for the two-stage HPIC detector in the K-user synchronous scenario for the case with random, binary spreading sequences of length $N = 32$. The approximate bit error rate expression appears to be reasonably accurate in most cases and, as was seen in the two-user case, it appears to estimate the bit error rate conservatively (the approximate bit error rate is greater than the simulated bit error rate) in the cases considered.

We conclude this section by noting that even the approximate bit error rate expression (2.9) is not of a form that allows us to answer questions such as, "For a bit error rate performance requirement $P_{\mathsf{HPIC}}^{(1)}$, what is the minimum value of $a^{(1)}$ necessary to satisfy this requirement?". The next section of this chapter considers the signal to interference plus noise ratio (SINR) performance of the two-stage HPIC detector where it turns out that we will be able to answer just such a question.

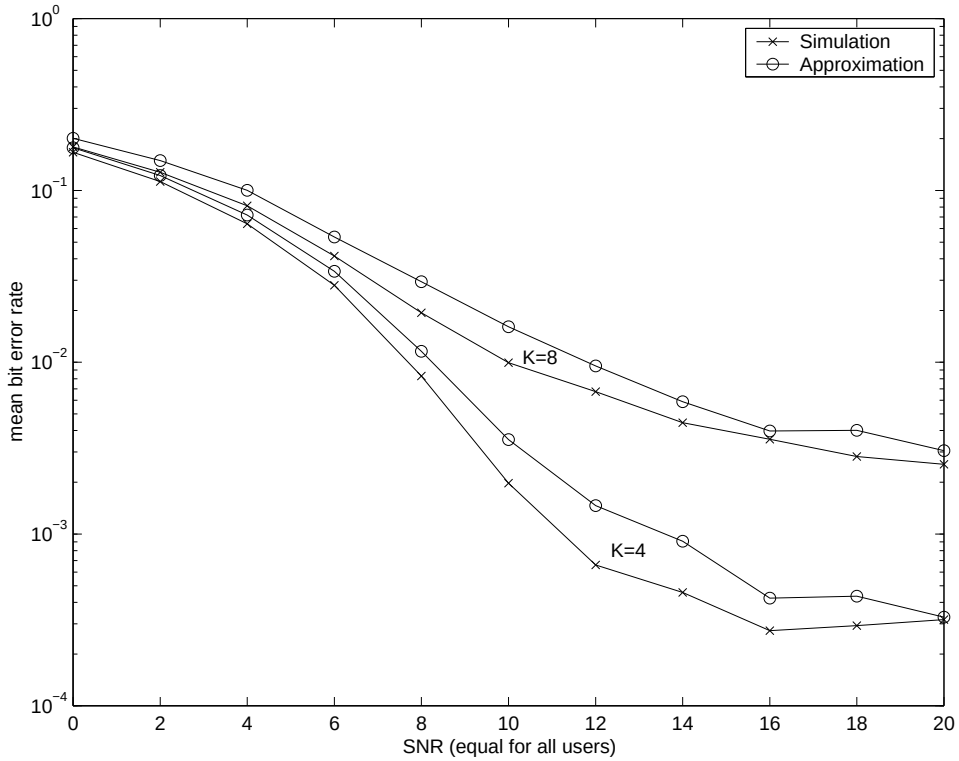

Figure 2.4: Simulated and approximate HPIC bit error rates for $K = 4$ and $K = 8$ users with random spreading sequences of length $N = 32$.

2.2 SINR Analysis

In this section, we study the signal to interference plus noise ratio (SINR) performance of the two-stage HPIC detector and its implications on required transmit powers and theoretical system capacity. We present an exact expression for the SINR of the two-stage HPIC detector in the K-user synchronous case and, although the exact SINR expression is in fact simpler that the exact bit error rate expressions of the prior section, we suggest a simplifying approximation that holds in typical operating scenarios when the error probability of the matched filter detector is reasonably low. Using this result, we consider the case when each user in the CDMA communication system has a particular SINR requirement and derive a general expression for the minimum transmit powers necessary to satisfy these requirements. Note that, in a nonorthogonal multiuser system such as CDMA, increasing one user's transmit power to meet their SINR requirement also has the effect of increasing the interference seen by the other users in the system, hence lowering their SINR. The approximations used in this section allow the required transmit powers to be computed via a set of simultaneous linear equations.

As a first step towards understanding the SINR performance of HPIC, we derive closed form expressions for the total required transmit power and theoretical system capacity of the two-stage HPIC detector in the equicorrelated case where all users have identical signature waveform crosscorrelations. These expressions are analytically compared to the results for the successive interference cancellation (SIC) and matched filter (MF) detectors derived in [LE99] under identical assumptions. We provide analytical proofs showing that, in the cases considered, the two-stage HPIC detector requires less total transmit power and has greater theoretical system capacity than the SIC or MF detectors. Numerical results verifying

the analysis are also presented.

2.2.1 Exact SINR of Two-Stage HPIC

The notation $\mathrm{SINR}_{\mathsf{X}}^{(k)}$ denotes the SINR of the k^{th} user's output of multiuser detector $\mathsf{X} \in \{\mathsf{HPIC}, \mathsf{LPIC}, \mathsf{MF}, \mathsf{SIC}\}$ defined as

$$\mathrm{SINR}_{\mathsf{X}}^{(k)} \triangleq \frac{\mathrm{E}[y_{\mathsf{X}}^{(k)} \mid b^{(k)}]^2}{\mathrm{var}[y_{\mathsf{X}}^{(k)} \mid b^{(k)}]} \tag{2.10}$$

where $y_{\mathsf{X}}^{(k)}$ denotes the k^{th} user's soft output from multiuser detector X prior to hard decision. We can then compute the SINR of the HPIC detector as

$$\mathrm{SINR}_{\mathsf{HPIC}}^{(k)} = \frac{\left(a^{(k)}b^{(k)} + \sum_{\ell \neq k} \rho_{k\ell} a^{(\ell)} \Psi_\ell\right)^2}{\sum_{\ell \neq k} \sum_{m \neq k} \rho_{k\ell}\rho_{km} a^{(\ell)} a^{(m)} \Omega_{\ell m} + 2\sigma \sum_{\ell \neq k} \rho_{k\ell} a^{(\ell)} \Phi_{\ell k} + \sigma^2} \tag{2.11}$$

where we have used the assumption that the users' bits and noise are independent and zero mean and where

$$\begin{aligned}
\Psi_\ell &\triangleq \mathrm{E}[\epsilon^{(\ell)} \mid b^{(k)}], \\
\Omega_{\ell m} &\triangleq \mathrm{E}[\epsilon^{(\ell)}\epsilon^{(m)} \mid b^{(k)}] - \mathrm{E}[\epsilon^{(\ell)} \mid b^{(k)}]\mathrm{E}[\epsilon^{(m)} \mid b^{(k)}], \text{ and} \\
\Phi_{\ell k} &\triangleq \mathrm{E}[\epsilon^{(\ell)} n^{(k)} \mid b^{(k)}]
\end{aligned}$$

with $\epsilon^{(\ell)} \triangleq b^{(\ell)} - \mathrm{sgn}(y^{(\ell)})$ for notational convenience. Exact expressions for Ψ, Ω, and Φ are presented in the following analysis.

- Ψ_ℓ for $\ell \neq k$

  Recall that $\Psi_\ell = \mathrm{E}[b^{(\ell)} - \mathrm{sgn}(y^{(\ell)}) \mid b^{(k)}]$. The assumptions that the users' bits are independent and zero mean imply that $\Psi_\ell = -\mathrm{E}[\mathrm{sgn}(y^{(\ell)}) \mid b^{(k)}]$. Condi-

tioning temporarily on all of the users' bits, we can write

$$\begin{aligned}\mathrm{E}[\mathrm{sgn}(y^{(\ell)}) \,|\, \boldsymbol{b}] &= P(y^{(\ell)} > 0 \,|\, \boldsymbol{b}) - P(y^{(\ell)} < 0 \,|\, \boldsymbol{b}) \\ &= Q\left(\frac{-\boldsymbol{r}_\ell^\top \boldsymbol{A}\boldsymbol{b}}{\sigma}\right) - \left(1 - Q\left(\frac{-\boldsymbol{r}_\ell^\top \boldsymbol{A}\boldsymbol{b}}{\sigma}\right)\right) \\ &= 1 - 2Q\left(\frac{\boldsymbol{r}_\ell^\top \boldsymbol{A}\boldsymbol{b}}{\sigma}\right)\end{aligned} \tag{2.12}$$

where $\boldsymbol{r}_\ell^\top$ is the ℓ^{th} row of the signature cross correlation matrix $\boldsymbol{R}$ and where we have used the facts that $y^{(\ell)} = \boldsymbol{r}_\ell^\top \boldsymbol{A}\boldsymbol{b} + \sigma n^{(\ell)}$ and $Q(x) + Q(-x) = 1$. To remove the conditioning on $\boldsymbol{b}$, first denote $\mathcal{B}^{(k)}$ as the set of cardinality 2^{K-1} of all possible, equiprobable, binary K-vectors with the k^{th} user's bit fixed to the known value $b^{(k)}$. Then it follows that

$$\begin{aligned}\mathrm{E}[\mathrm{sgn}(y^{(\ell)}) \,|\, b^{(k)}] &= \frac{1}{2^{K-1}} \sum_{\boldsymbol{b} \in \mathcal{B}^{(k)}} \left(1 - 2Q\left(\frac{\boldsymbol{r}_\ell^\top \boldsymbol{A}\boldsymbol{b}}{\sigma}\right)\right) \\ &= 1 - \frac{1}{2^{K-2}} \sum_{\boldsymbol{b} \in \mathcal{B}^{(k)}} Q\left(\frac{\boldsymbol{r}_\ell^\top \boldsymbol{A}\boldsymbol{b}}{\sigma}\right)\end{aligned}$$

and Ψ_ℓ follows directly as its negative.

- $\Omega_{\ell m}$ for $(\ell \neq k) \neq (m \neq k)$

  Recall that

$$\begin{aligned}\Omega_{\ell m} &= \mathrm{E}[(b^{(\ell)} - \mathrm{sgn}(y^{(\ell)}))(b^{(m)} - \mathrm{sgn}(y^{(m)})) \,|\, b^{(k)}] - \Psi_\ell \Psi_m \\ &= \mathrm{E}[b^{(\ell)} b^{(m)} \,|\, b^{(k)}] - \mathrm{E}[b^{(\ell)} \mathrm{sgn}(y^{(m)}) \,|\, b^{(k)}] - \mathrm{E}[b^{(m)} \mathrm{sgn}(y^{(\ell)}) \,|\, b^{(k)}] \\ &\quad + \mathrm{E}[\mathrm{sgn}(y^{(\ell)}) \mathrm{sgn}(y^{(m)}) \,|\, b^{(k)}] - \Psi_\ell \Psi_m.\end{aligned}$$

  We will derive expressions for each element of $\Omega_{\ell m}$ in the following analysis.

  - The assumptions that the users' bits are assumed independent and zero mean imply that $\mathrm{E}[b^{(\ell)} b^{(m)} \,|\, b^{(k)}] = 0$.

– To compute $\mathrm{E}[b^{(\ell)}\mathrm{sgn}(y^{(m)}) \,|\, b^{(k)}]$, we can temporarily condition on $\boldsymbol{b}$ and use (2.12) to write

$$\mathrm{E}[b^{(\ell)}\mathrm{sgn}(y^{(m)}) \,|\, \boldsymbol{b}] \;=\; b^{(\ell)} \left[1 - 2Q\left(\frac{\boldsymbol{r}_m^\top \boldsymbol{A}\boldsymbol{b}}{\sigma}\right)\right].$$

Removing the conditioning on $\boldsymbol{b}$, we can write

$$\begin{aligned}\mathrm{E}[b^{(\ell)}\mathrm{sgn}(y^{(m)}) \,|\, b^{(k)}] &= \frac{1}{2^{K-1}} \sum_{\boldsymbol{b}\in\mathcal{B}^{(k)}} b^{(\ell)} \left[1 - 2Q\left(\frac{\boldsymbol{r}_m^\top \boldsymbol{A}\boldsymbol{b}}{\sigma}\right)\right] \\ &= \frac{-1}{2^{K-2}} \sum_{\boldsymbol{b}\in\mathcal{B}^{(k)}} b^{(\ell)} Q\left(\frac{\boldsymbol{r}_m^\top \boldsymbol{A}\boldsymbol{b}}{\sigma}\right).\end{aligned}$$

An expression for $\mathrm{E}[b^{(m)}\mathrm{sgn}(y^{(\ell)}) \,|\, b^{(k)}]$ can be derived similarly.

– To compute $\mathrm{E}[\mathrm{sgn}(y^{(\ell)})\mathrm{sgn}(y^{(m)}) \,|\, b^{(k)}]$ we can temporarily condition on all of the users' bits to write

$$\begin{aligned}\mathrm{E}[\mathrm{sgn}(y^{(\ell)})\mathrm{sgn}(y^{(m)}) \,|\, \boldsymbol{b}] \;=\; &+P(\{y^{(\ell)} > 0\} \cap \{y^{(m)} > 0\} \,|\, \boldsymbol{b}) \\ &+P(\{y^{(\ell)} < 0\} \cap \{y^{(m)} < 0\} \,|\, \boldsymbol{b}) \\ &-P(\{y^{(\ell)} > 0\} \cap \{y^{(m)} < 0\} \,|\, \boldsymbol{b}) \\ &-P(\{y^{(\ell)} < 0\} \cap \{y^{(m)} > 0\} \,|\, \boldsymbol{b}).\end{aligned}$$

Using the notation of [AS72, pp. 936], where

$$L(h,k,\rho) \;\triangleq\; \int_h^\infty \int_k^\infty g(x,y,\rho)\, dy\, dx$$

where $g(x,y,\rho)$ is the bivariate Gaussian pdf parameterized by ρ, it can

be shown that

$$\begin{aligned}
\mathrm{E}[\mathrm{sgn}(y^{(\ell)})\mathrm{sgn}(y^{(m)}) \,|\, \boldsymbol{b}] &= +L\left(\frac{-\boldsymbol{r}_\ell^\top \boldsymbol{A}\boldsymbol{b}}{\sigma}, \frac{-\boldsymbol{r}_m^\top \boldsymbol{A}\boldsymbol{b}}{\sigma}, \rho_{\ell m}\right) \\
&\quad +L\left(\frac{\boldsymbol{r}_\ell^\top \boldsymbol{A}\boldsymbol{b}}{\sigma}, \frac{\boldsymbol{r}_m^\top \boldsymbol{A}\boldsymbol{b}}{\sigma}, \rho_{\ell m}\right) \\
&\quad -L\left(\frac{-\boldsymbol{r}_\ell^\top \boldsymbol{A}\boldsymbol{b}}{\sigma}, \frac{\boldsymbol{r}_m^\top \boldsymbol{A}\boldsymbol{b}}{\sigma}, -\rho_{\ell m}\right) \\
&\quad -L\left(\frac{\boldsymbol{r}_\ell^\top \boldsymbol{A}\boldsymbol{b}}{\sigma}, \frac{-\boldsymbol{r}_m^\top \boldsymbol{A}\boldsymbol{b}}{\sigma}, -\rho_{\ell m}\right) \\
&\triangleq M\left(\frac{\boldsymbol{r}_\ell^\top \boldsymbol{A}\boldsymbol{b}}{\sigma}, \frac{\boldsymbol{r}_m^\top \boldsymbol{A}\boldsymbol{b}}{\sigma}, \rho_{\ell m}\right).
\end{aligned}$$

Removing the conditioning on $\boldsymbol{b}$, we can write

$$\mathrm{E}[\mathrm{sgn}(y^{(\ell)})\mathrm{sgn}(y^{(m)}) \,|\, b^{(k)}] = \frac{1}{2^{K-1}} \sum_{\boldsymbol{b}\in\mathcal{B}^{(k)}} M\left(\frac{\boldsymbol{r}_\ell^\top \boldsymbol{A}\boldsymbol{b}}{\sigma}, \frac{\boldsymbol{r}_m^\top \boldsymbol{A}\boldsymbol{b}}{\sigma}, \rho_{\ell m}\right)$$

These results can be combined to yield an exact expression for $\Omega_{\ell m}$. Note that there is no closed form expression for $L(h, k, \rho)$ except in special cases. Computation of $\mathrm{E}[\mathrm{sgn}(y^{(\ell)})\mathrm{sgn}(y^{(m)}) \,|\, b^{(k)}]$ will, in general, require numerical integration of several two dimensional integrals.

- $\Omega_{\ell\ell}$ for $\ell \neq k$

  The results of the prior case for $\Omega_{\ell m}$ can be applied directly to this case, recognizing that $\mathrm{E}[(b^{(\ell)})^2 \,|\, b^{(k)}] = \mathrm{E}[(\mathrm{sgn}(y^{(\ell)}))^2 \,|\, b^{(k)}] = 1$. We can then write

$$\Omega_{\ell\ell} = 2 + \frac{1}{2^{K-3}} \sum_{\boldsymbol{b}\in\mathcal{B}^{(k)}} b^{(\ell)} Q\left(\frac{\boldsymbol{r}_\ell^\top \boldsymbol{A}\boldsymbol{b}}{\sigma}\right) - \Psi_\ell^2.$$

- $\Phi_{\ell k}$ for $\ell \neq k$

  In order to derive an exact expression for $\Phi_{\ell k}$ we will state a useful result first. Suppose that u and v are unit variance, zero mean, Gaussian random

variables and that $E[uv] = \rho$. Then

$$\mathrm{E}[u\mathrm{sgn}(t+v) \,|\, t] = \int_{-\infty}^{\infty}\int_{-\infty}^{\infty} u\mathrm{sgn}(t+v)\frac{1}{2\pi\sqrt{1-\rho^2}}\exp\left[-\frac{1}{2\sigma^2(1-\rho^2)}(u^2-2\rho uv+v^2)\right] du\, dv$$

and it can be shown via the substitution $w = \frac{u-\rho v}{\sqrt{1-\rho^2}}$ and subsequent integration that

$$\mathrm{E}[u\mathrm{sgn}(t+v) \,|\, t] \;=\; \frac{2\rho}{\sqrt{2\pi}}\exp\left(\frac{-t^2}{2}\right). \tag{2.13}$$

Recall that $\Phi_{\ell k} = \mathrm{E}[(b^{(\ell)} - \mathrm{sgn}(y^{(\ell)}))n^{(k)} \,|\, b^{(k)}]$. Since the users' bits and channel noise are assumed independent and zero mean, $\mathrm{E}[b^{(\ell)}n^{(k)}] = 0$ and $\Phi_{\ell k} = -\mathrm{E}[\mathrm{sgn}(y^{(\ell)})n^{(k)} \,|\, b^{(k)}]$. Conditioning temporarily on all of the users' bits, and recognizing that $\mathrm{sgn}(y^{(\ell)}) = \mathrm{sgn}(y^{(\ell)}/\sigma)$ for $\sigma \neq 0$, we can use (2.13) to write

$$\mathrm{E}[\mathrm{sgn}(y^{(\ell)})n^{(k)} \,|\, \boldsymbol{b}] \;=\; \frac{2\rho_{\ell k}}{\sqrt{2\pi}}\exp\left(\frac{-\left(\frac{-\boldsymbol{r}_\ell^\top \boldsymbol{A}\boldsymbol{b}}{\sigma}\right)^2}{2}\right).$$

The conditioning on $\boldsymbol{b}$ is removed as before to write

$$\mathrm{E}[\mathrm{sgn}(y^{(\ell)})n^{(k)} \,|\, b^{(k)}] \;=\; \frac{\rho_{\ell k}}{\sqrt{2\pi}2^{K-2}}\sum_{\boldsymbol{b}\in\mathcal{B}^{(k)}}\exp\left(\frac{-(\boldsymbol{r}_\ell^\top \boldsymbol{A}\boldsymbol{b})^2}{2\sigma^2}\right)$$

and $\Phi_{\ell k}$ follows directly as its negative.

These results combined with (2.11) yield an expression for the exact SINR of the two-stage HPIC detector. Although this expression is simpler to compute than the corresponding exact bit error rate of the two-stage HPIC detector, the exact SINR expression is still unwieldy and difficult to analyze. In the next section we develop an approximate expression for the SINR of the two-stage HPIC detector that tends to be accurate in typical operating conditions and leads to analytical comparisons with the SIC and MF detectors.

2.2.2 Approximate SINR of Two-Stage HPIC

To facilitate an analysis of the two-stage HPIC detector that exposes its behavior in typical operating scenarios, we will impose the following "normal-operating" assumptions also imposed in [LE99] and indirectly in [Ver98, pp. 378]:

1. Assume that $\epsilon^{(\ell)}$ is approximately independent of $b^{(k)}$ for all $\ell \neq k$, or in other words that an error in the decision of the matched filter output for user ℓ is independent of the bit transmitted by user k.

2. Assume that $\epsilon^{(\ell)}$ is approximately independent of $\epsilon^{(m)}$ for all $\ell \neq m$, or in other words that matched filter decision errors for user ℓ are independent of matched filter decision errors for user m.

3. Assume that $\epsilon^{(\ell)}$ is approximately independent of $n^{(k)}$ for all $\ell \neq k$, or in other words that matched filter decision errors for user ℓ are independent of the Gaussian channel noise in the k^{th} user's soft matched filter output.

These assumptions are well justified unless the error probabilities at the output of the matched filter detector are high. They imply that

$$\begin{aligned} \Psi_\ell &\approx 0 \quad \forall \ell \neq k \\ \Omega_{\ell m} &\approx 0 \quad \forall (\ell \neq k) \neq (m \neq k) \\ \Phi_{\ell k} &\approx 0 \quad \forall \ell \neq k. \end{aligned}$$

The remaining term requiring calculation is $\Omega_{\ell\ell}$ which can be derived as

$$\begin{aligned} \Omega_{\ell\ell} &= \mathrm{E}[(\epsilon^{(\ell)})^2 \mid b^{(k)}] - \mathrm{E}[\epsilon^{(\ell)} \mid b^{(k)}]^2 \\ &\approx \mathrm{E}[(\epsilon^{(\ell)})^2] - 0 = 4P_{\mathsf{MF}}^{(\ell)} \end{aligned}$$

where $P_{\mathsf{MF}}^{(\ell)} = P(b^{(\ell)} \neq \mathrm{sgn}(y^{(\ell)}))$ is the probability of error of the ℓ^{th} user's matched filter output and where the imposed assumptions were used in the approximation. Under these approximations, the SINR of the HPIC detector may then be written as

$$\mathrm{SINR}_{\mathsf{HPIC}}^{(k)} = \frac{\alpha^{(k)}}{\sum_{\ell \neq k} r_{k\ell}\alpha^{(\ell)} 4P_{\mathsf{MF}}^{(\ell)} + 1} \tag{2.14}$$

where $\alpha^{(k)} = (a^{(k)}/\sigma)^2$ is the normalized power (or SNR) of the k^{th} user and $r_{k\ell} = \rho_{k\ell}^2$ is the squared crosscorrelation of the k^{th} and ℓ^{th} users' signature waveforms.

Figures 2.5, 2.6, and 2.7, plot the exact (2.11) and approximate (2.14) SINRs (in dB) of the two-stage HPIC detector in the two-user synchronous scenario for the cases where $\rho = 0.2$, $\rho = 0.5$, and $\rho = 0.8$ respectively. The approximations appear to be accurate in a large class of operating conditions when ρ is small. The ratio of approximate to exact bit error rate is also plotted in each case to indicate the regions in SNR-space where the approximations have lower accuracy. As expected, the approximations are less accurate in this case as ρ approaches one.

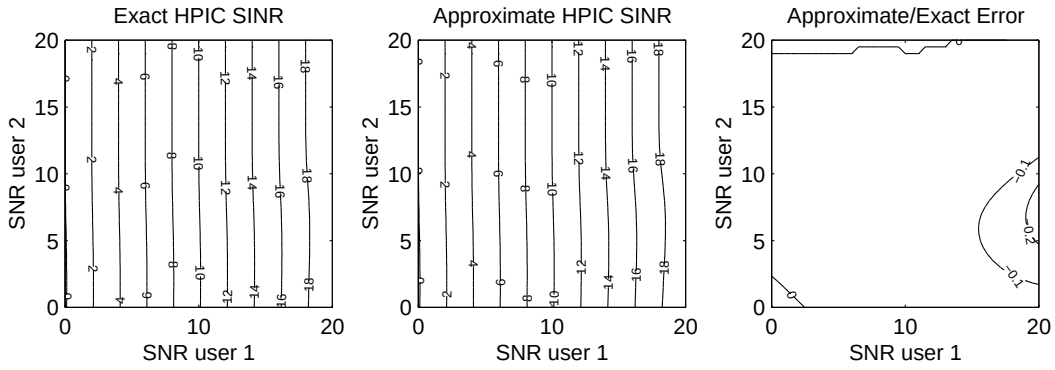

Figure 2.5: Exact and approximate SINR (in dB) for user one at the output of the two-stage HPIC detector with two users and $\rho = 0.2$.

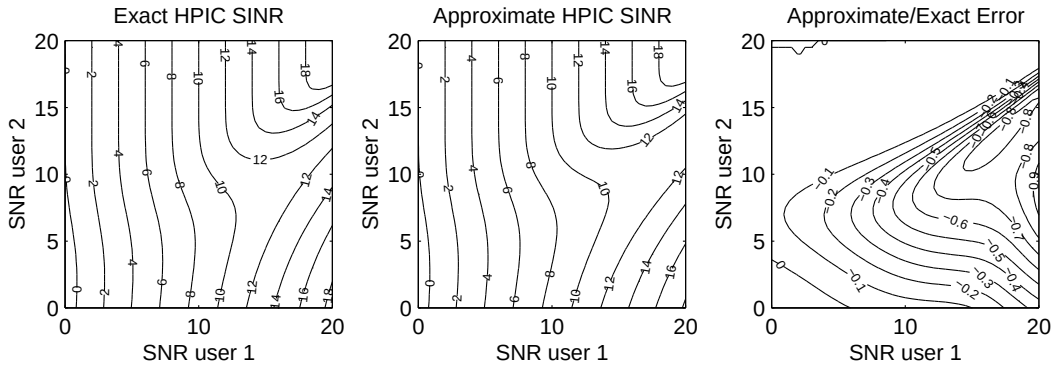

Figure 2.6: Exact and approximate SINR (in dB) for user one at the output of the two-stage HPIC detector with two users and $\rho = 0.5$.

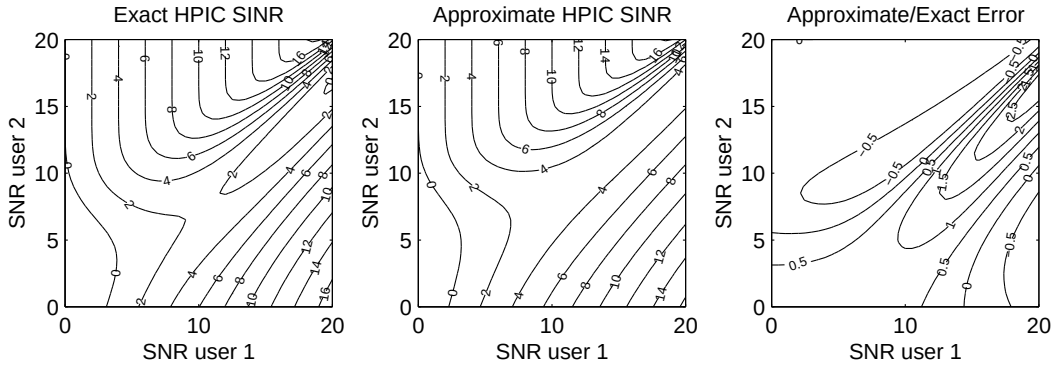

Figure 2.7: Exact and approximate SINR (in dB) for user one at the output of the two-stage HPIC detector with two users and $\rho = 0.8$.

2.2.3 Power Efficiency

In this section, we use the result of (2.14) to calculate the normalized power required by each user in the system in order to meet a particular SINR requirement. If we define the normalized power vector $\boldsymbol{\alpha} = [\alpha^{(1)}, \ldots, \alpha^{(K)}]^\top$ then (2.14) implies that

$$\begin{aligned} \boldsymbol{\alpha} &= [4\boldsymbol{S}(\boldsymbol{\Gamma} - \boldsymbol{I})\boldsymbol{P}]\boldsymbol{\alpha} + \boldsymbol{S}\boldsymbol{e} \\ &= [\boldsymbol{I} - 4\boldsymbol{S}(\boldsymbol{\Gamma} - \boldsymbol{I})\boldsymbol{P}]^{-1}\boldsymbol{S}\boldsymbol{e} \end{aligned} \tag{2.15}$$

where $\boldsymbol{S}$ is a diagonal matrix with the $\ell\ell^{th}$ element equal to the output SINR requirement for user ℓ, $\boldsymbol{P}$ is a diagonal matrix with the $\ell\ell^{th}$ element equal to $P_{\mathsf{MF}}^{(\ell)}$, $\boldsymbol{\Gamma}$ is a matrix of squared signature crosscorrelations given as

$$\boldsymbol{\Gamma} = \begin{bmatrix} r_{11} & \cdots & r_{1K} \\ \vdots & \ddots & \vdots \\ r_{K1} & \cdots & r_{KK} \end{bmatrix}$$

where $r_{\ell\ell} = 1$ for all ℓ, and $\boldsymbol{e}$ is a K-vector with all elements equal to one. If the inverse exists in (2.15) then there is a unique solution for the normalized user powers given $\boldsymbol{S}$, $\boldsymbol{\Gamma}$, and $\boldsymbol{P}$. Also note that when the interference cancellation is perfect (i.e., when $\boldsymbol{P} = \boldsymbol{0}$) then $\boldsymbol{\alpha} = \boldsymbol{S}\boldsymbol{e}$ or, in other words, each user's normalized power (SNR) is equal to their output SINR requirement. This is intuitively satisfying since perfect cancellation implies that there is no residual multiuser interference in the outputs of the two-stage HPIC detector and that Gaussian noise is the only channel impairment.

Proposition 1. *Under the following assumptions:*

1. *The squared user crosscorrelations are all identical, i.e., $r_{k\ell} = r$ for all $k \neq \ell$,*

2. *The user output SINR requirements are all identical, i.e., $\boldsymbol{S} = s\boldsymbol{I}$, and*

3. The decision error probabilities are all identical, i.e., $\boldsymbol{P} = p\boldsymbol{I}$,

then the total transmit power required for two-stage HPIC detection may be written as

$$\boldsymbol{e}^\top \boldsymbol{\alpha} \;=\; \frac{Ks}{1 - 4rsp(K-1)} \tag{2.16}$$

Proof. Under the assumptions of the proposition, we can rewrite (2.15) as

$$\boldsymbol{\alpha} \;=\; s\underbrace{[\boldsymbol{I} - 4sp\boldsymbol{\Lambda}]}_{\boldsymbol{\Delta}}{}^{-1}\boldsymbol{e} \tag{2.17}$$

where $\boldsymbol{\Lambda}$ is defined such that its diagonal elements are all equal to zero and its off-diagonal elements are all equal to r. The inverse in this last expression can be computed explicitly since $\boldsymbol{\Delta}$ has explicit solutions to its eigenvalues and eigenvectors. Denoting $x = -4rsp$, it can be shown that the diagonal elements of $\boldsymbol{\Delta}^{-1}$ are all identical and equal to $\frac{x(2-K)-1}{x^2(K-1)+x(2-K)-1}$ and that the off-diagonal elements of $\boldsymbol{\Delta}^{-1}$ are all identical and equal to $\frac{x}{x^2(K-1)+x(2-K)-1}$. It then follows directly that

$$\alpha^{(k)} = \frac{s(x(2-K) - 1 + (K-1)x)}{x^2(K-1) + x(2-K) - 1}.$$

Recognizing that the numerator and denominator have the common factor $x - 1$, we can simplify this last expression to write

$$\alpha^{(k)} = \frac{s}{(K-1)x + 1}$$

hence the total normalized power required for the HPIC detector is given in (2.16) after the substitution $x = -4rsp$. □

The following remarks expose some of the intuitive properties of (2.16):

- The cases of perfect cancellation ($p = 0$) or orthogonal transmission ($r = 0$) are identical and lead to a total normalized power requirement of Ks.

- For fixed K, nonzero crosscorrelation or nonzero error probabilities lead to a penalty term in the denominator of (2.16) that increases in the total power required.

2.2.4 System Capacity

A theoretical measure of system capacity, denoted as K_{max}, can be defined as the operating point at which the required power is infinite, or equivalently, when the denominator of (2.16) equals zero. In this case, we can state that, for the HPIC detector,

$$K_{max} = \frac{1}{4rsp} + 1 \tag{2.18}$$

which implies that the system capacity is approximately inversely proportional to the product of the squared signature crosscorrelations r, the required output SINR s, and the error probability p of the MF first stage.

2.2.5 Comparison to MF and SIC Multiuser Detectors

Using the two-stage HPIC SINR results derived in the prior section and the SINR results on SIC and MF multiuser detectors from [LE99], we can form Table 2.1 to compare the total power required ($\boldsymbol{e}^\top\boldsymbol{\alpha}$) and system capacity ($K_{max}$) of the HPIC, SIC, and MF detectors for a given SINR requirement under the assumptions of Proposition 1. We note that the expressions for total power and system capacity for the SIC detector are simplified but equivalent to the expressions presented in [LE99].

Comparison of the HPIC and MF detectors is straightforward. A system using HPIC detection requires less total transmit power $\boldsymbol{e}^\top\boldsymbol{\alpha}$ and has a higher K_{max}

Table 2.1: Summary of multiuser detector total power and system capacity results under the assumptions of Proposition 1 for $\theta \stackrel{\Delta}{=} \frac{1+rs}{1+4rsp}$.

Detector	$\boldsymbol{e}^\top \boldsymbol{\alpha}$	K_{max}
MF	$\frac{Ks}{1-rs(K-1)}$	$\frac{1}{rs}+1$
SIC	$\frac{\theta^K-1}{r(1-4p\theta^K)}$	$\frac{-\log(4p)}{\log\theta}$
HPIC	$\frac{Ks}{1-4rsp(K-1)}$	$\frac{1}{4rsp}+1$

than a system with MF detection when $p < 0.25$ for any admissible values of K, r, and s. Conversely, for $p > 0.25$, a system using MF detection requires lower total transmit power and has a higher K_{max} than HPIC for any K, r, and s. Since an error probability $p > 0.25$ describes an unusual operating region where communication has very low reliability, we can say roughly that the HPIC detector is uniformly superior to the MF detector in terms of SINR, total required power, and system capacity in the equicorrelated case.

We compare HPIC and SIC detectors in the following propositions.

Proposition 2. *Under the same assumptions as Proposition 1 and $K \geq 2$, HPIC detection requires less total transmit power than SIC detection when $0 \leq p < 0.25$ and $rs > 0$.*

Proof. To show that HPIC requires less total power than SIC we will show that

$$\frac{Ks}{1-4rsp(K-1)} < \frac{\theta^K-1}{r(1-4p\theta^K)}$$

for $\theta \stackrel{\Delta}{=} \frac{1+rs}{1+4rsp}$. For notational convenience we define

$$q = 4p$$

$$\lambda = rs$$

and we also assume that all parameters are such that both denominators are positive in order for this comparison to make any sense. In this case we can cross multiply the expressions to get the following equivalent expression

$$K\lambda(1-q\theta^K) \quad < \quad (\theta^K-1)(1-q\lambda(K-1))$$

for $\theta = \frac{1+\lambda}{1+q\lambda}$ and collection of like terms yields

$$K\lambda(1-q)+1+q\lambda \quad < \quad \theta^K(1+q\lambda). \tag{2.19}$$

It can be shown that (2.19) holds for $K=2$ under the assumptions of the proposition. To show that (2.19) also holds for arbitrary K we will use an inductive proof. Assume that (2.19) holds for some value of $K-1$. Then we will show that it also holds for K. The hypothesis of the induction implies that

$$(K-1)\lambda(1-q)+1+q\lambda \quad < \quad \theta^{K-1}(1+q\lambda)$$

for a particular value of $K-1$. Multiplying both sides by θ, the hypothesis implies that

$$\theta[(K-1)\lambda(1-q)+1+q\lambda] \quad < \quad \theta^K(1+q\lambda).$$

This last expression, combined with (2.19), implies that it is sufficient to show that

$$K\lambda(1-q)+1+q\lambda \quad < \quad \theta[(K-1)\lambda(1-q)+1+q\lambda]$$

in order to prove the claim. Using the fact that $\theta(1+q\lambda)=1+\lambda$ we can write an equivalent expression

$$K\lambda(1-q)+1+q\lambda-1-\lambda \quad < \quad \theta(K-1)\lambda(1-q)$$

and simplifying

$$K\lambda(1-q)-\lambda(1-q) \quad < \quad \theta(K-1)\lambda(1-q)$$

which leads to the common positive factor $\lambda(1-q)$ hence

$$(K-1) \quad < \quad \theta(K-1)$$

which holds for $\theta > 1$ and $K \geq 2$. But $\theta > 1$ is equivalent to $0 \leq q < 1$ or, equivalently, $0 \leq p < 0.25$ hence (2.19) is true for K under the hypothesis that it is true for $K-1$. Since (2.19) can be shown explicitly true for $K = 2$ the claim is proven inductively. □

Proposition 3. *Under the same assumptions as Proposition 1 and $K \geq 2$, HPIC has greater K_{max} than SIC when $0 < p < 0.25$ and $rs > 0$.*

Proof. To prove this proposition, we first note that when $p = 0$ the denominator of both the HPIC and SIC total power expressions can never go to zero as K increases, hence both algorithms have theoretically infinite capacity when the MF decision error probability is zero. In order to prove that K_{max} is greater for HPIC than SIC when $0 < p < 0.25$, we wish to show under our previously established notation that

$$\frac{1}{q\lambda} + 1 > \frac{-\log q}{\log \theta}.$$

Since $q\lambda > 0$ and $\log\theta > 0$ we can express this inequality equivalently as

$$q\lambda \log q > (1+q\lambda)\log\frac{1+q\lambda}{1+\lambda}$$

where we have substituted $\theta = \frac{1+\lambda}{1+q\lambda}$. Defining

$$h(\lambda, q) = q\lambda \log q - (1+q\lambda)\log\frac{1+q\lambda}{1+\lambda}$$

then it is equivalent to prove that $h(\lambda, q) > 0$ for all $\lambda > 0$ and $0 < q < 1$. To show this, we note that

$$\lim_{q \downarrow 0} h(\lambda, q) = 0 - \log\frac{1}{1+\lambda} = \log(1+\lambda) > 0 \tag{2.20}$$

and that

$$\lim_{q \uparrow 1} h(\lambda, q) \quad = \quad 0. \tag{2.21}$$

Since $h(q, \lambda)$ is continuous in q on the open interval $0 < q < 1$ for $\lambda > 0$, we can compute its partial derivative in this region as

$$\frac{\partial}{\partial q} h(\lambda, q) \quad = \quad \lambda \log \frac{q + q\lambda}{1 + q\lambda} < 0$$

where the inequality follows directly from the the assumptions $0 < q < 1$ and $\lambda > 0$. This implies that $h(\lambda, q)$ is monotonically decreasing on the open interval $0 < q < 1$ and this fact combined with (2.20) and (2.21) implies that $h(\lambda, q) > 0$ on the open interval $0 < q < 1$. □

Intuitively, HPIC detection tends to outperform both SIC and MF detection in the $0 \leq p < 0.25$ interval because the decisions from the first stage are reliable enough such that cancellation is beneficial to the final decision statistics at the output of the second stage. The first user in a SIC detector is actually decided via MF detection and their decision statistic is subject to the interference of all of the other users. The second user's decision statistic is subject to $K - 1$ interference terms and so forth. Unlike SIC detection, HPIC detection attempts to cancel *all* of the multiple access interference *for each user*. When the interference estimates are reliable ($0 \leq p < 0.25$), and the operating conditions satisfy the approximations used to derive (2.14) and the assumptions of Proposition 1, the results of this analysis imply that better performance can be achieved by canceling all of the multiple access interference in parallel rather than successively.

2.2.6 Numerical Results

Although the prior section analytically showed that HPIC detection requires less total transmit power and provides greater theoretical system capacity than SIC and MF detection, this section presents numerical examples that demonstrate that the actual performance difference may be quite significant. Figure 2.8 plots the total normalized power from Table 2.1 for HPIC, SIC, and MF detectors as a function of K for several values of p. Note that the MF power requirements do not change as a function of decision error probability since there is no interference cancellation. These results show that HPIC detection may require several orders of magnitude less power than the SIC and MF detectors in the cases considered.

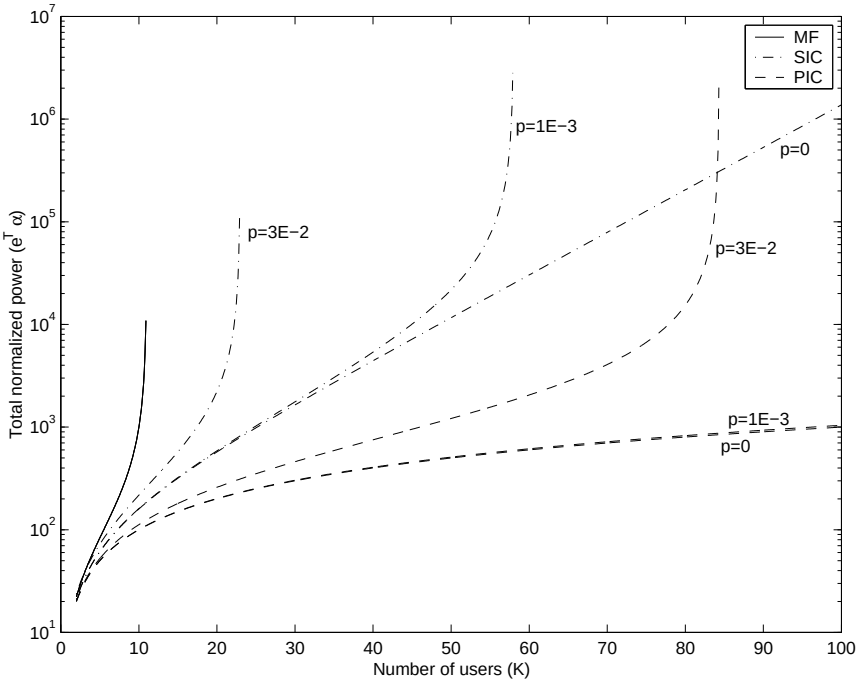

Figure 2.8: Normalized total power required for HPIC, SIC, and MF detection to meet the SINR requirement $s = 10$ for $r = 0.01$.

Figure 2.9 plots the theoretical system capacity expressions from Table 2.1 for

HPIC, SIC, and MF detectors as a function of p for two values of s. These results show that HPIC may offer several orders of magnitude greater theoretical system capacity than the SIC and MF detectors in the cases considered.

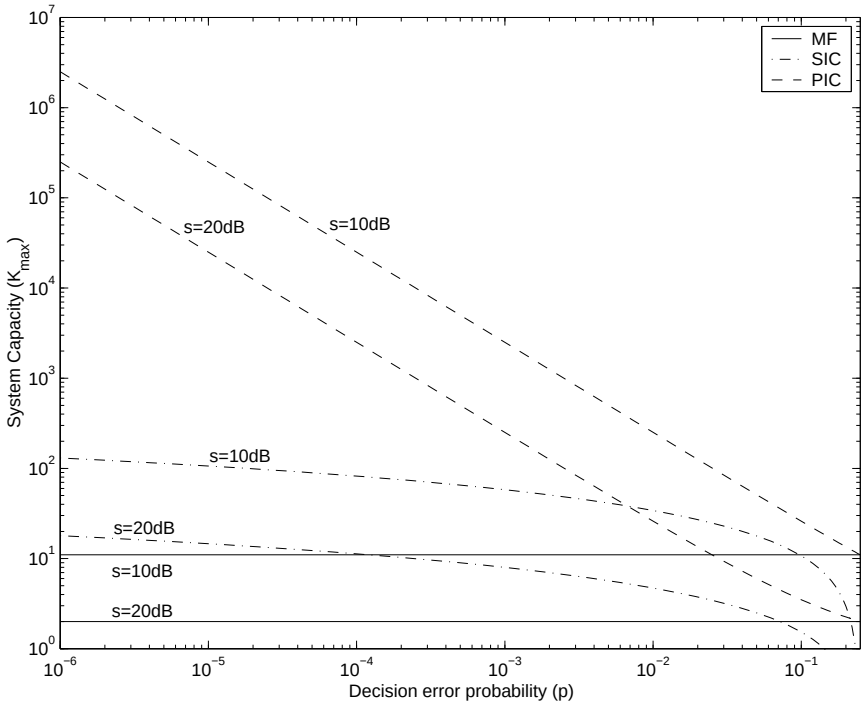

Figure 2.9: Theoretical system capacity for HPIC, SIC, and MF detection to meet the SINR requirements $s = 10$dB and $s = 20$dB for $r = 0.01$.

2.3 Conclusions

In this section we analyzed two important performance measures of the HPIC detector: bit error rate and SINR. We showed that computing the exact bit error rate of the HPIC detector is difficult even for a small number of users and computationally infeasible for a system with more than a handful of users. An approximate expression for the bit error rate of the HPIC detector was derived

that shows promise with low computational complexity and good accuracy in a variety of operating conditions.

We also derived an exact expression for the SINR of the HPIC detector and derived an approximate expression to facilitate analytical results. We examined the implications of the SINR results on power efficiency and theoretical system capacity. In the case where all users have the same SINR requirement and where the signature correlations are identical between all users, we showed analytically that HPIC outperforms SIC and MF detection in terms of power efficiency and theoretical system capacity. Numerical results suggest that the performance differences may be significant.

CHAPTER 3

PERFORMANCE ANALYSIS OF LINEAR PARALLEL INTERFERENCE CANCELLATION

3.1 Introduction

This chapter[1] analyzes the behavior of the LPIC detector in the synchronous K-user CDMA communication scenario as described in in Section 1.5. From (1.2) and Table 1.1, we can write the k^{th} user's two-stage LPIC detector output in the K-user synchronous case as

$$y_{\mathsf{LPIC}}^{(k)} = a^{(k)}b^{(k)} + \sum_{\ell \neq k} \rho_{k\ell}[a^{(\ell)}b^{(\ell)} - y^{(\ell)}] + \sigma n^{(k)}. \tag{3.1}$$

From (1.3), we can group the two-stage LPIC detector's outputs into a K-vector to write

$$\boldsymbol{y}_{\mathsf{LPIC}} = \boldsymbol{y} - (\boldsymbol{R} - \boldsymbol{I})\boldsymbol{y}.$$

We note that under this notation it is evident that the two-stage LPIC detector is equivalent to the *approximate decorrelator* [Ver98] which has received some attention in the literature recently [MV98a] due to its low computational complexity and good performance under certain operating conditions. Hence the analytical results in [MV98a] apply here to the two-stage LPIC detector.

In this chapter we also consider LPIC detectors with M stages of interference

[1]The results presented in this chapter are due in large part to a collaborative effort with Mehul Motani, a fellow graduate student at Cornell University, Professor Venu Veeravalli of Cornell University, and Professor H. Vincent Poor of Princeton University, and have been submitted for publication to IEEE Transactions on Information Theory.

cancellation which may be compactly expressed in matrix notation as

$$\boldsymbol{y}_{\mathsf{LPIC}}(m+1) = \boldsymbol{y} - (\boldsymbol{R} - \boldsymbol{I})\boldsymbol{y}_{\mathsf{LPIC}}(m) \qquad m = 0, 1, \ldots, M-1 \quad (3.2a)$$

$$\boldsymbol{y}_{\mathsf{LPIC}}(0) = \boldsymbol{y} \quad (3.2b)$$

where $M = 1$ specifies the two-stage[2] LPIC detector and $M = 0$ specifies the MF detector. In contrast to the HPIC detector of Chapter 2, we note that the LPIC detector is in fact a linear detector for any number of stages of interference cancellation in the sense that the LPIC detector's soft outputs can be expressed as a linear combination of the original matched filter outputs $\boldsymbol{y}$. Unlike the majority of linear detectors, including the decorrelating and MMSE detectors, implementation of the LPIC detector does not require a matrix inversion and hence the LPIC detector is attractive due to its relatively low complexity.

The goal of this chapter is to develop a better understanding of the behavior and performance of the LPIC detector. Other authors have noted limitations in LPIC performance including the original paper by Kaul and Woerner [KW94] where the authors noticed that there existed conditions where interference cancellation actually degraded system performance. Since then, several authors have proposed various improvements to the LPIC detector including [CBW97], [RW98a], and [BN99]. We do not propose to fix the LPIC detector in this chapter but rather to understand it better so that we can bound the operating regions where the LPIC detector exhibits good or bad performance. In that spirit, this chapter is presented as a collection of related analytical results that compare the LPIC detector to the HPIC and MF detectors as well as expose the asymptotic behavior

[2]In this chapter, we will consistently use the symbol M to describe the number of stages of interference cancellation. Under this notation, $M + 1$ describes the actual number of detector stages in the sense that $M = 1$ describes the two-stage LPIC detector.

of the LPIC detector as the number of stages of interference cancellation (M) approaches infinity.

The remainder of this chapter is organized as follows. Section 3.2 compares the performance of the two-stage HPIC and LPIC detectors in order to gain a better understanding of the significant performance differences between these detector observed by several authors. Section 3.3 compares the LPIC detector with M stages of interference cancellation to the conventional matched filter detector and shows that the LPIC detector's error probability may be worse than the matched filter under certain operating conditions. Section 3.4 analyzes operating conditions that lead to the LPIC detector exhibiting an error probability greater than 0.5. Section 3.5 develops asymptotic results on the behavior of the LPIC detector as the number of interference cancellation stages $M \to \infty$. Section 3.6 examines the implications of the results in the prior sections for a CDMA communication system with random spreading sequences in the "large-system" scenario where the number of users K and the spreading gain N both approach infinity but the ratio K/N is kept constant.

3.2 LPIC vs. HPIC Performance Comparison

This section presents an analytical performance comparison between the two-stage HPIC and LPIC detectors. The results in this section are motivated by simulation studies (e.g., [BN99]) which have shown that the two-stage HPIC detector can significantly outperform the two-stage LPIC detector in terms of error probability under a variety of operating conditions. Unfortunately, the results of Chapter 2 suggest that direct analysis of the two-stage HPIC detector's error probability is

difficult in general since the exact HPIC error probability expressions involve K-dimensional numerical integration of the joint Gaussian probability distribution function. Rather than comparing the error probabilities of the two-stage HPIC and LPIC detector directly, we choose to instead compare the performance of their interference estimators with the intuition that better interference estimates would tend to yield better error probability performance.

Recall that, under the K-user synchronous system model, the two-stage LPIC and HPIC detector outputs for the k^{th} user from (1.2) and Table 1.1 may be written explicitly as

$$\begin{aligned} y_{\mathsf{LPIC}}^{(k)} &= a^{(k)}b^{(k)} + \sum_{\ell \neq k} \rho_{k\ell} \underbrace{\left[a^{(\ell)}b^{(\ell)} - y^{(\ell)}\right]}_{\triangleq -e_{\mathsf{LPIC}}^{(\ell)}} + \sigma n^{(k)} \\ y_{\mathsf{HPIC}}^{(k)} &= a^{(k)}b^{(k)} + \sum_{\ell \neq k} \rho_{k\ell} \underbrace{\left[a^{(\ell)}b^{(\ell)} - a^{(\ell)}\mathrm{sgn}(y^{(\ell)})\right]}_{\triangleq -e_{\mathsf{HPIC}}^{(\ell)}} + \sigma n^{(k)} \end{aligned}$$

Comparison of these expressions reveals that the fundamental difference between the two-stage HPIC and LPIC detectors is in the multiple access interference estimates. Intuitively, one would expect better estimates to generally lead to better error probability performance hence we will examine the bias and mean squared error (MSE) of the HPIC and LPIC estimators in the following analytical development.

3.2.1 LPIC Interference Estimator Performance

We can calculate the bias of the two-stage LPIC detector's multiple access interference estimator (for the ℓ^{th} user) as

$$\begin{aligned} \text{bias}^{(\ell)}_{\mathsf{LPIC}} &= \mathrm{E}[e^{(\ell)}_{\mathsf{LPIC}} \mid b^{(\ell)}] \\ &= \mathrm{E}\left[\sum_{k\neq\ell} \rho_{\ell k} a^{(k)} b^{(k)} + \sigma n^{(\ell)}\right] \\ &= 0 \end{aligned}$$

since $\mathrm{E}[b^{(k)}] = 0$ and $\mathrm{E}[n^{(k)}] = 0$ for all k. This shows that the matched filter outputs are conditionally unbiased estimators for the product of the ℓ^{th} user's bit and amplitude. We note that it has been observed in [CBW97] that this unbiasedness property does not extend to additional stages of the LPIC detector and that later stages of the LPIC detector might exhibit significant bias in the multiple access interference estimates.

The MSE of the ℓ^{th} user's LPIC multiple access interference estimator can be calculated as

$$\begin{aligned} \text{MSE}^{(\ell)}_{\mathsf{LPIC}} &= \mathrm{E}\left[(e^{(\ell)}_{\mathsf{LPIC}})^2 \mid b^{(\ell)}\right] \\ &= \mathrm{E}\left[\left(\sum_{k\neq\ell} \rho_{\ell k} a^{(k)} b^{(k)} + \sigma n^{(\ell)}\right)^2\right] \\ &= \sum_{k\neq\ell} \left(a^{(k)}\rho_{\ell k}\right)^2 + \sigma^2 \end{aligned} \tag{3.3}$$

where we have used the facts that $\mathrm{E}[\boldsymbol{b}\boldsymbol{b}^\top] = \boldsymbol{I}$, $\mathrm{E}[\boldsymbol{b}\boldsymbol{n}^\top] = \boldsymbol{0}$, and $\mathrm{E}[\boldsymbol{n}\boldsymbol{n}^\top] = \boldsymbol{R}$.

3.2.2 HPIC Interference Estimator Performance

The bias of the ℓ^{th} user's multiple access interference estimator for the HPIC detector can be calculated as

$$\begin{aligned}
\text{bias}^{(\ell)}_{\mathsf{HPIC}} &= \mathrm{E}[e^{(\ell)}_{\mathsf{HPIC}} \mid b^{(\ell)}] \\
&= 0 \cdot P(\text{sgn}(y^{(\ell)}) = b^{(\ell)}) - 2a^{(\ell)}b^{(\ell)} \cdot P(\text{sgn}(y^{(\ell)}) \neq b^{(\ell)}) \\
&= -2a^{(\ell)}b^{(\ell)} P(\text{sgn}(y^{(\ell)}) \neq b^{(\ell)})
\end{aligned}$$

where $P(\text{sgn}(y^{(\ell)}) \neq b^{(\ell)}) = P^{(\ell)}_{\mathsf{MF}}$ is the matched filter detector's probability of bit error for user ℓ given by the expression in [Ver98] as

$$P(\text{sgn}(y^{(\ell)}) \neq b^{(\ell)}) = \frac{1}{2^{K-1}} \sum_{\substack{b^{(\ell)}=1 \\ b^{(k)} \in \{\pm 1\} \ \forall k \neq \ell}} Q\left(\frac{a^{(\ell)}b^{(\ell)} + \sum_{k \neq \ell} \rho_{\ell k} a^{(k)} b^{(k)}}{\sigma}\right)$$

where $Q(x) \triangleq \int_x^\infty e^{-t^2/2}\, dt$. We observe that the ℓ^{th} user's HPIC multiple access interference estimator is biased unless $P(\text{sgn}(y^{(\ell)}) \neq b^{(\ell)}) = 0$.

The MSE of the ℓ^{th} user's HPIC multiple access interference estimator can be calculated as

$$\begin{aligned}
\text{MSE}^{(\ell)}_{\mathsf{HPIC}} &= \mathrm{E}\left[(e^{(\ell)}_{\mathsf{HPIC}})^2 \mid b^{(\ell)}\right] \\
&= (a^{(\ell)})^2 \mathrm{E}\left[|\text{sgn}(y^{(\ell)}) - b^{(\ell)}|^2\right] \\
&= (a^{(\ell)})^2 [0 \cdot P(\text{sgn}(y^{(\ell)}) = b^{(\ell)}) + 4 \cdot P(\text{sgn}(y^{(\ell)}) \neq b^{(\ell)})] \\
&= (a^{(\ell)})^2 4 P(\text{sgn}(y^{(\ell)}) \neq b^{(\ell)}).
\end{aligned} \tag{3.4}$$

We note that both the bias and MSE of the HPIC multiple access interference estimator are proportional to the probability of bit error from the first (matched filter) stage.

3.2.3 LPIC vs. HPIC Performance Comparison

An exact analytical comparison of $\mathrm{MSE}^{(\ell)}_{\mathsf{LPIC}}$ and $\mathrm{MSE}^{(\ell)}_{\mathsf{HPIC}}$ is difficult due to the sum of Q functions involved in the evaluation of (3.4). An explanation for the significant performance difference between the HPIC and LPIC detector seen in the simulation results of [BN99] is possible if we resort to a Gaussian approximation for the multiple access interference (e.g., see [Pur77]). Even though this approximation is not valid under all circumstances (see [PV97]), its use in this case provides some insight into the relative performance of the HPIC and LPIC multiple access interference estimators in the absence of more exact methods. Moreover, the result presented in the following proposition is shown in Section 3.6.1 to be asymptotically exact in the case of large CDMA systems with random spreading sequences.

Under the Gaussian approximation assumption, the multiple access interference is assumed to be well-modeled as a Gaussian random variable and the probability of bit error for user ℓ can be written as

$$P(\mathrm{sgn}(y^{(\ell)}) \neq b^{(\ell)}) \approx Q\left(\frac{a^{(\ell)}}{\sqrt{\sum_{k\neq\ell}\left(a^{(\ell)}\rho_{\ell k}\right)^2+\sigma^2}}\right) = Q\left(\frac{a^{(\ell)}}{\sqrt{\mathrm{MSE}^{(\ell)}_{\mathsf{LPIC}}}}\right)$$

hence

$$\mathrm{MSE}^{(\ell)}_{\mathsf{HPIC}} \approx \mathrm{AMSE}^{(\ell)}_{\mathsf{HPIC}} = 4(a^{(\ell)})^2 Q\left(\frac{a^{(\ell)}}{\sqrt{\mathrm{MSE}^{(\ell)}_{\mathsf{LPIC}}}}\right) \tag{3.5}$$

where $\mathrm{AMSE}^{(\ell)}_{\mathsf{HPIC}}$ denotes the *approximate* MSE of the ℓ^{th} user's interference estimate with the HPIC detector. With this development we can prove the following proposition.

Proposition 4. *For arbitrary* $\boldsymbol{R}$, σ, $\boldsymbol{A}$, K, *and* ℓ, $MSE^{(\ell)}_{\mathsf{LPIC}} > AMSE^{(\ell)}_{\mathsf{HPIC}}$.

Proof. Let $x = a^{(\ell)}/\sqrt{\mathrm{MSE}^{(\ell)}_{\mathsf{LPIC}}}$. Then $x > 0$ since $a^{(\ell)} > 0$ and $\mathrm{MSE}^{(\ell)}_{\mathsf{LPIC}} > 0$. An

upper bound on the Q function for $x > 0$ is given in [Ver98] where

$$Q(x) < \frac{1}{\sqrt{2\pi}x} \exp\left(-\frac{x^2}{2}\right).$$

Then

$$\mathrm{AMSE}_{\mathsf{HPIC}}^{(\ell)} < 4a^{(\ell)} \sqrt{\frac{\mathrm{MSE}_{\mathsf{LPIC}}^{(\ell)}}{2\pi}} \exp\left(-\frac{x^2}{2}\right)$$

hence it suffices to show

$$\frac{4x}{\sqrt{2\pi}} \exp\left(-\frac{x^2}{2}\right) < 1$$

for $x > 0$ in order to prove the proposition. Since both sides of the inequality are positive we can take the natural logarithm to write

$$\ln(x) + \ln\left(\frac{4}{2\pi}\right) - \frac{x^2}{2} < 0$$

but $\ln(x) < x - 1$ for all $x > 0$ hence

$$\ln(x) + \ln\left(\frac{4}{2\pi}\right) - \frac{x^2}{2} < x - 1 + \ln\left(\frac{4}{2\pi}\right) - \frac{x^2}{2}. \tag{3.6}$$

The discriminant of this quadratic equation is given by

$$1 - 4\left[\frac{1}{2} - \frac{1}{2}\ln\left(\frac{4}{2\pi}\right)\right] = -1 + 2\ln\left(\frac{4}{2\pi}\right)$$

which is strictly less than zero, hence the quadratic equation in (3.6) has no real roots. This implies that (3.6) is either always less than zero or greater than zero. Inspection of (3.6) shows that it is always less than zero, hence $\mathrm{MSE}_{\mathsf{LPIC}}^{(\ell)} > \mathrm{AMSE}_{\mathsf{HPIC}}^{(\ell)}$. □

As a numerical example of the interference estimator performance, consider a multiuser communication system with $K = 6$ equipower, equicorrelated users such that $\rho_{k\ell} = \rho$ for all $k \neq \ell$. The exact and approximate interference estimator MSE

performance for the two-stage LPIC and HPIC detector is shown in Figure 3.1 over a range of typical SNR values for several values of ρ. Note that the approximate HPIC interference estimator MSE ($\mathrm{AMSE}^{(k)}_{\mathsf{HPIC}}$) is quite accurate in all of the cases shown and is nearly indistinguishable from the exact HPIC interference estimator MSE ($\mathrm{MSE}^{(k)}_{\mathsf{HPIC}}$) in the cases where $\rho = 0.2$ and $\rho = 0.5$. Moreover, these cases demonstrate the superiority of the HPIC interference estimator in terms of MSE and give some feeling for its relative performance with respect to the LPIC interference estimator.

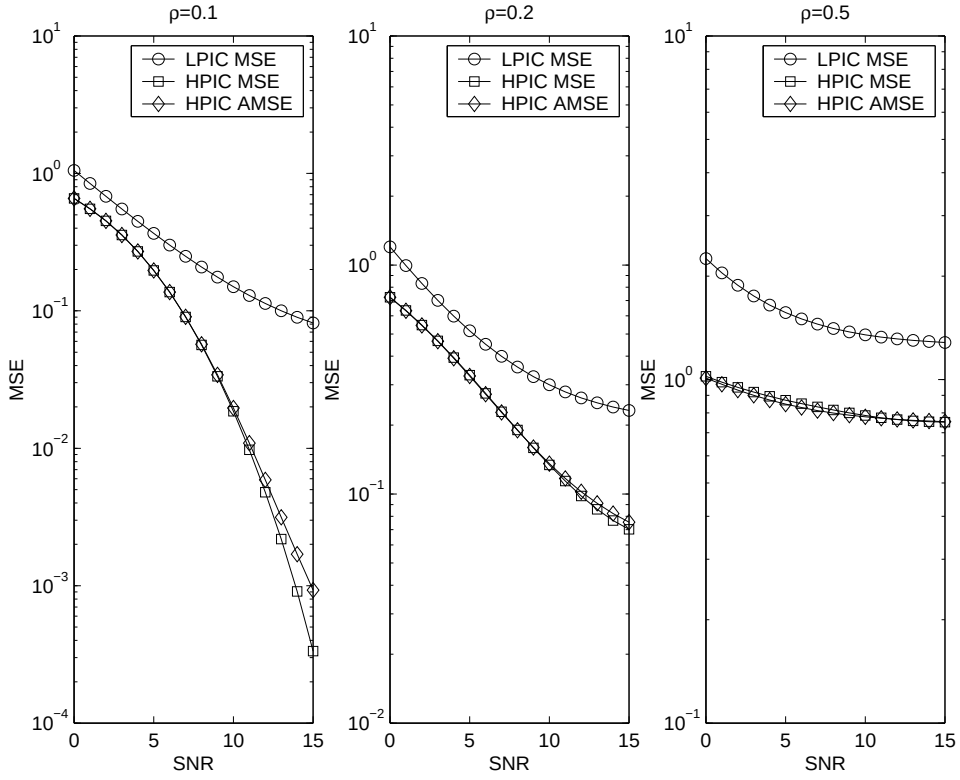

Figure 3.1: MSE of two-stage LPIC and HPIC estimators for 6 equipower, equicorrelated users.

3.3 Comparison to the Matched Filter Detector

The goal of this section is to show that the matched filter detector outperforms the multistage LPIC detector at any stage in terms of error probability when the desired user's amplitude exceeds a finite threshold. Analogous results comparing the matched filter to the linear decorrelating and MMSE detectors have recently been obtained by Moustakides and Poor in [MP99]. Here, we use a similar method of proof for the LPIC detector. We denote the error probability for the k^{th} user of the LPIC detector with M stages of interference cancellation and MF detector as $P_{\mathsf{LPIC}}^{(k)}(M)$ and $P_{\mathsf{MF}}^{(k)}$ respectively.

Proposition 5. *For arbitrary fixed desired user k, LPIC detector with $M > 0$ stages of interference cancellation, correlation matrix $\boldsymbol{R} \neq \boldsymbol{I}$, noise standard deviation $\sigma > 0$, and interfering user amplitudes $a^{(\ell)}$ $\forall \ell \neq k$, there exists an amplitude threshold $a^* < \infty$ such that $P_{\mathsf{LPIC}}^{(k)}(M) > P_{\mathsf{MF}}^{(k)}$ for $a^{(k)} > a^*$.*

Proof. For nonzero noise power, the probability of a decision error for the k^{th} user of an arbitrary linear detector F can be expressed as

$$P_{\mathsf{F}}^{(k)} = \frac{1}{2^{K-1}} \sum_{\boldsymbol{b} \in \mathcal{B}_k} Q\left(\frac{\boldsymbol{f}^{(k)\top} \boldsymbol{R} \boldsymbol{A} \boldsymbol{b}}{\sigma \sqrt{\boldsymbol{f}^{(k)\top} \boldsymbol{R} \boldsymbol{f}^{(k)}}} \right)$$

where $\mathcal{B}_k$ is the set of all possible bit vectors such that $b^{(k)} = +1$ and $b^{(\ell)} \in \{\pm 1\}$ for all $\ell \neq k$ and $\boldsymbol{f}^{(k)} \in \mathbb{R}^{K \times 1}$ denotes the effective linear operation on the matched filter bank outputs to form the decision statistic for user k. The matched filter detector is given as $\boldsymbol{f}^{(k)} = \boldsymbol{e}_k$. The LPIC detector's output after M stages of interference cancellation can be written as

$$\boldsymbol{y}_{\mathsf{LPIC}}(M) = \sum_{m=0}^{M} (\boldsymbol{I} - \boldsymbol{R})^m \boldsymbol{y} = \boldsymbol{L}(M) \boldsymbol{y}$$

hence $\boldsymbol{f}^{(k)} = \boldsymbol{L}(M)\boldsymbol{e}_k$. Since $Q(x)$ is a monotonically decreasing function in x,

$$\frac{\boldsymbol{e}_k^\top \boldsymbol{L}(M)\boldsymbol{R}\boldsymbol{A}\boldsymbol{b}}{\sigma\sqrt{\boldsymbol{e}_k^\top \boldsymbol{L}(M)\boldsymbol{R}\boldsymbol{L}(M)\boldsymbol{e}_k}} < \frac{\boldsymbol{e}_k^\top \boldsymbol{R}\boldsymbol{A}\boldsymbol{b}}{\sigma\sqrt{\boldsymbol{e}_k^\top \boldsymbol{R}\boldsymbol{e}_k}} \quad \forall \boldsymbol{b} \in \mathcal{B}_k \tag{3.7}$$

implies that $P_{\mathsf{LPIC}}^{(k)}(M) > P_{\mathsf{MF}}^{(k)}$. We note that this is a sufficient but not necessary condition and the converse is not necessarily true. Observing that $\boldsymbol{e}_k^\top \boldsymbol{R}\boldsymbol{e}_k = 1$, $\boldsymbol{A}\boldsymbol{e}_k = a^{(k)}\boldsymbol{e}_k$, and denoting $\boldsymbol{d} = \boldsymbol{b} - \boldsymbol{e}_k$ we can rewrite (3.7) as

$$a^{(k)}\boldsymbol{e}_k^\top \boldsymbol{L}(M)\boldsymbol{R}\boldsymbol{e}_k + \boldsymbol{e}_k^\top \boldsymbol{L}(M)\boldsymbol{R}\boldsymbol{A}\boldsymbol{d} < \sqrt{\boldsymbol{e}_k^\top \boldsymbol{L}(M)\boldsymbol{R}\boldsymbol{L}(M)\boldsymbol{e}_k}\left(a^{(k)} + \boldsymbol{e}_k^\top \boldsymbol{R}\boldsymbol{A}\boldsymbol{d}\right) \tag{3.8}$$

for all $\boldsymbol{d} \in \mathcal{D}_k$ where $\mathcal{D}_k$ is the set of all vectors such that the k^{th} element $d^{(k)} = 0$ and $d^{(\ell)} \in \{\pm 1\}$ for all $\ell \neq k$. Using the Schwarz inequality and the fact that $\boldsymbol{R}$ is nonnegative definite, we note that

$$\begin{aligned}
\boldsymbol{e}_k^\top \boldsymbol{L}(M)\boldsymbol{R}\boldsymbol{e}_k &= \boldsymbol{e}_k^\top \boldsymbol{L}(M)\boldsymbol{R}^{1/2}\boldsymbol{R}^{1/2}\boldsymbol{e}_k \\
&\leq \sqrt{\boldsymbol{e}_k^\top \boldsymbol{L}(M)\boldsymbol{R}\boldsymbol{L}(M)\boldsymbol{e}_k}\sqrt{\boldsymbol{e}_k^\top \boldsymbol{R}\boldsymbol{e}_k} \\
&= \sqrt{\boldsymbol{e}_k^\top \boldsymbol{L}(M)\boldsymbol{R}\boldsymbol{L}(M)\boldsymbol{e}_k}
\end{aligned}$$

with equality if and only if $\boldsymbol{L}(M) = \alpha\boldsymbol{I}$ or if and only if $\boldsymbol{R} = \boldsymbol{I}$. In the case where $\boldsymbol{R} = \boldsymbol{I}$ the users' signatures are all mutually orthogonal and the LPIC detector is identical to the matched filter detector. Since our proposition assumes that $\boldsymbol{R} \neq \boldsymbol{I}$ we can rearrange the terms in (3.8) to write

$$a^{(k)} > \frac{\left[\boldsymbol{e}_k^\top \boldsymbol{L}(m)\boldsymbol{R}\boldsymbol{A} - \sqrt{\boldsymbol{e}_k^\top \boldsymbol{L}(M)\boldsymbol{R}\boldsymbol{L}(M)\boldsymbol{e}_k}\boldsymbol{e}_k^\top \boldsymbol{R}\boldsymbol{A}\right]\boldsymbol{d}}{\sqrt{\boldsymbol{e}_k^\top \boldsymbol{L}(M)\boldsymbol{R}\boldsymbol{L}(M)\boldsymbol{e}_k} - \boldsymbol{e}_k^\top \boldsymbol{L}(M)\boldsymbol{R}\boldsymbol{e}_k} \quad \forall \boldsymbol{d} \in \mathcal{D}_k$$

hence the threshold

$$a^* = \max_{\boldsymbol{d}\in\mathcal{D}_k} \frac{\left[\boldsymbol{e}_k^\top \boldsymbol{L}(m)\boldsymbol{R}\boldsymbol{A} - \sqrt{\boldsymbol{e}_k^\top \boldsymbol{L}(M)\boldsymbol{R}\boldsymbol{L}(M)\boldsymbol{e}_k}\boldsymbol{e}_k^\top \boldsymbol{R}\boldsymbol{A}\right]\boldsymbol{d}}{\sqrt{\boldsymbol{e}_k^\top \boldsymbol{L}(M)\boldsymbol{R}\boldsymbol{L}(M)\boldsymbol{e}_k} - \boldsymbol{e}_k^\top \boldsymbol{L}(M)\boldsymbol{R}\boldsymbol{e}_k}$$

will satisfy the requirements. We can remove $\boldsymbol{d}$ from this expression by exploiting the binary nature of its elements to maximize the right hand side of the inequality

by setting

$$d^{(\ell)} = \mathrm{sgn}\left(\left[\boldsymbol{e}_k^\top \boldsymbol{L}(M)\boldsymbol{R}\boldsymbol{A} - \sqrt{\boldsymbol{e}_k^\top \boldsymbol{L}(M)\boldsymbol{R}\boldsymbol{L}(M)\boldsymbol{e}_k}\,\boldsymbol{e}_k^\top \boldsymbol{R}\boldsymbol{A}\right]\boldsymbol{e}_\ell\right) \quad \forall \ell \neq k$$

from which it follows directly that

$$a^* = \frac{a^{(\ell)}\left|\sqrt{\boldsymbol{e}_k^\top \boldsymbol{L}(M)\boldsymbol{R}\boldsymbol{L}(M)\boldsymbol{e}_k}\,\boldsymbol{e}_k^\top \boldsymbol{R}\boldsymbol{e}_\ell - \boldsymbol{e}_k^\top \boldsymbol{L}(M)\boldsymbol{R}\boldsymbol{e}_\ell\right|}{\sqrt{\boldsymbol{e}_k^\top \boldsymbol{L}(M)\boldsymbol{R}\boldsymbol{L}(M)\boldsymbol{e}_k} - \boldsymbol{e}_k^\top \boldsymbol{L}(M)\boldsymbol{R}\boldsymbol{e}_k} < \infty \tag{3.9}$$

and that $P_{\mathsf{LPIC}}^{(k)}(M) > P_{\mathsf{MF}}^{(k)}$ for $a^{(k)} > a^*$. □

We note that the existence of the amplitude threshold $a^* < \infty$ does not rely on the structure of the LPIC detector and the above analysis applies to any linear detector that is not a function of the user amplitudes including the decorrelating detector. Computation of the threshold a^* is dependent on the particular linear detector. We also note that a^* is not a necessary threshold but sufficient and is quite likely to be loose in the sense that values of $a^{(k)}$ significantly less than a^* may also cause the LPIC detector to exhibit a higher probability of bit error than the matched filter detector.

As a numerical example, consider the two-stage ($M = 1$) LPIC detector where $\boldsymbol{L}(M) = 2\boldsymbol{I} - \boldsymbol{R}$. The communication system has $K = 3$ users with $a^{(k)}/\sigma = 4$ for $k = 2, \ldots, K$. The normalized user correlation matrix is given by

$$\boldsymbol{R} = \frac{1}{4}\begin{bmatrix} 4 & 2 & 1 \\ 2 & 4 & 1 \\ 1 & 1 & 4 \end{bmatrix}.$$

Computation of (3.9) under these conditions yields $a^* \approx 4.69$ and a plot of the error probabilities shows that the actual crossover point occurs at $a^{(1)} \approx 2.25$.

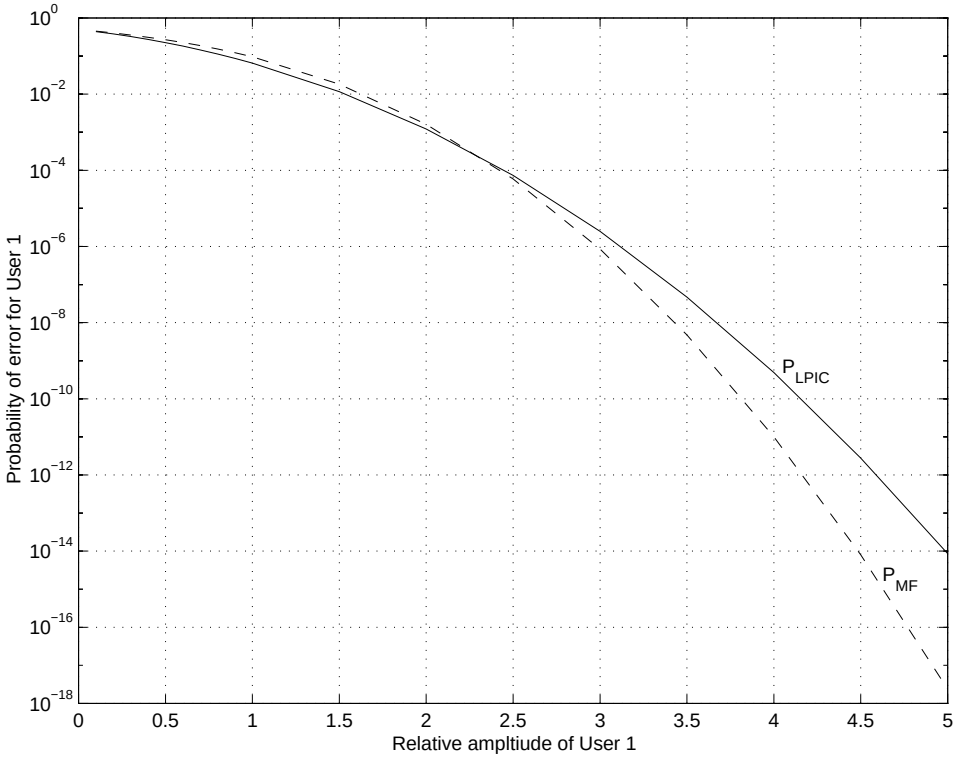

Figure 3.2: Example of error probabilities $P_{\mathsf{LPIC}}^{(1)}(M)$ and $P_{\mathsf{MF}}^{(1)}$ for a two-stage LPIC detector ($M = 1$) and $K = 3$ equipower users.

3.4 LPIC Misperformance

This section shows the existence of operating conditions where the LPIC detector exhibits a probability of error $P_{\mathsf{LPIC}}^{(k)}(M) > 0.5$.[3] This behavior is in contrast to the matched filter detector which never exhibits a probability of error greater than 0.5 under any operating conditions within the scope of the K-user, synchronous, binary system model. We make this claim more precise with the following proposition.

Proposition 6. *For an arbitrary fixed desired user k in a system with $K > 2$ users, an LPIC detector with $M > 0$ stages of interference cancellation where M is odd, and equal amplitude users such that $\boldsymbol{A} = a\boldsymbol{I}$ and $\frac{a}{\sigma} > 0$, there exists $\boldsymbol{R}$ such that $P_{\mathsf{LPIC}}^{(k)}(M) > 0.5$.*

Proof. Applying the assumptions of the proposition to the left hand side of (3.7) we can write the argument of the Q function for the LPIC detector's error probability expression as

$$\frac{\boldsymbol{e}_k^\top \boldsymbol{L}(M)\boldsymbol{R}\boldsymbol{A}\boldsymbol{b}}{\sigma\sqrt{\boldsymbol{e}_k^\top \boldsymbol{L}(M)\boldsymbol{R}\boldsymbol{L}(M)\boldsymbol{e}_k}} = \underbrace{\frac{a\boldsymbol{e}_k^\top \boldsymbol{L}(M)\boldsymbol{R}\boldsymbol{e}_k}{\sigma\sqrt{\boldsymbol{e}_k^\top \boldsymbol{L}(M)\boldsymbol{R}\boldsymbol{L}(M)\boldsymbol{e}_k}}}_{\alpha_k} + \underbrace{\frac{a\boldsymbol{e}_k^\top \boldsymbol{L}(M)\boldsymbol{R}\boldsymbol{d}}{\sigma\sqrt{\boldsymbol{e}_k^\top \boldsymbol{L}(M)\boldsymbol{R}\boldsymbol{L}(M)\boldsymbol{e}_k}}}_{\beta_k(\boldsymbol{d})}$$

hence

$$P_{\mathsf{LPIC}}^{(k)}(M) = \frac{1}{2^{K-1}} \sum_{\boldsymbol{d}\in\mathcal{D}_k} Q\left(\alpha_k + \beta_k(\boldsymbol{d})\right). \tag{3.10}$$

Recognizing that $\boldsymbol{d} \in \mathcal{D}_k$ implies that $-\boldsymbol{d} \in \mathcal{D}_k$ and that $\beta_k(-\boldsymbol{d}) = -\beta_k(\boldsymbol{d})$ we can rewrite (3.10) as

$$P_{\mathsf{LPIC}}^{(k)}(M) = \frac{1}{2^K} \sum_{\boldsymbol{d}\in\mathcal{D}_k} Q\left(\alpha_k + \beta_k(\boldsymbol{d})\right) + Q\left(\alpha_k - \beta_k(\boldsymbol{d})\right).$$

[3] We note that if the detector is aware of the fact that its binary decisions have error probability greater than 0.5 then a simple sign change on the decisions would yield an error probability of less than 0.5. In this context, this section describes the operating regions where this misperformance occurs so as to alert the detector when such a bit-flipping strategy might be beneficial.

Suppose temporarily that $\alpha_k < 0$. Since $Q(x)$ is monotonically decreasing in x then

$$Q\left(\alpha_k + \beta_k(\boldsymbol{d})\right) + Q\left(\alpha_k - \beta_k(\boldsymbol{d})\right) > Q\left(\beta_k(\boldsymbol{d})\right) + Q\left(-\beta_k(\boldsymbol{d})\right) = 1$$

and it follows directly that

$$\frac{1}{2^K} \sum_{\boldsymbol{d} \in \mathcal{D}_k} Q\left(\alpha_k + \beta_k(\boldsymbol{d})\right) + Q\left(\alpha_k - \beta_k(\boldsymbol{d})\right) > \frac{1}{2^K} \sum_{\boldsymbol{d} \in \mathcal{D}_k} 1 = \frac{2^{K-1}}{2^K} = \frac{1}{2}.$$

Hence it is sufficient to show that there exists $\boldsymbol{R}$ such that $\alpha_k < 0$. Since $a/\sigma > 0$ and $\sqrt{\boldsymbol{e}_k^\top \boldsymbol{L}(M)\boldsymbol{R}\boldsymbol{L}(M)\boldsymbol{e}_k} > 0$ then $P_{\mathsf{LPIC}}^{(k)}(M) > 0.5$ if and only if there exists $\boldsymbol{R}$ such that $\boldsymbol{e}_k^\top \boldsymbol{L}(M)\boldsymbol{R}\boldsymbol{e}_k < 0$. We note that for the matched filter detector $\boldsymbol{L}(M) = \boldsymbol{I}$ hence $\alpha_k = a/\sigma > 0$ for all $\boldsymbol{R}$. This justifies our earlier claim that the matched filter detector cannot have an error probability greater than 0.5.

Returning to the LPIC detector, we wish to show that there exists $\boldsymbol{R}$ such that $\boldsymbol{e}_k^\top \boldsymbol{L}(M)\boldsymbol{R}\boldsymbol{e}_k < 0$. To show this, recall that the multistage LPIC detector may be written as

$$\boldsymbol{L}(M) = \sum_{m=0}^{M} (\boldsymbol{I} - \boldsymbol{R})^m.$$

Let $\boldsymbol{I} - \boldsymbol{R} = \boldsymbol{V}\boldsymbol{\Lambda}\boldsymbol{V}^{-1}$ where $\boldsymbol{V}$ is a matrix with columns representing the eigenvectors of $(\boldsymbol{I} - \boldsymbol{R})$ and $\boldsymbol{\Lambda}$ is a diagonal matrix of corresponding eigenvalues. Then

$$\boldsymbol{L}(M) = \boldsymbol{V} \left[\sum_{m=0}^{M} \boldsymbol{\Lambda}^m \right] \boldsymbol{V}^{-1}.$$

It can be shown that each eigenvector of $(\boldsymbol{I} - \boldsymbol{R})$ is also an eigenvector of $\boldsymbol{R}$ and that if λ is an eigenvalue of $(\boldsymbol{I} - \boldsymbol{R})$ then $1 - \lambda$ is an eigenvalue of $\boldsymbol{R}$. Using these

facts, we can write

$$\begin{aligned}
\boldsymbol{L}(M)\boldsymbol{R} &= \boldsymbol{V}\left[\sum_{m=0}^{M}\boldsymbol{\Lambda}^m\right](\boldsymbol{I}-\boldsymbol{\Lambda})\boldsymbol{V}^{-1} \\
&= \boldsymbol{V}\left[\sum_{m=0}^{M}\boldsymbol{\Lambda}^m - \sum_{m=0}^{M}\boldsymbol{\Lambda}^{m+1}\right]\boldsymbol{V}^{-1} \\
&= \boldsymbol{V}\left[\boldsymbol{I}-\boldsymbol{\Lambda}^{M+1}\right]\boldsymbol{V}^{-1} \\
&= \boldsymbol{I}-\boldsymbol{V}\boldsymbol{\Lambda}^{M+1}\boldsymbol{V}^{-1}
\end{aligned}$$

hence

$$\boldsymbol{e}_k^\top \boldsymbol{L}(M)\boldsymbol{R}\boldsymbol{e}_k = 1 - \boldsymbol{e}_k^\top \boldsymbol{V}\boldsymbol{\Lambda}^{M+1}\boldsymbol{V}^{-1}\boldsymbol{e}_k. \tag{3.11}$$

In order to prove the existence of an $\boldsymbol{R}$ such that (3.11) is less than zero we will constrain the remaining analysis to the equicorrelated case where $\rho_{k\ell} = \rho$ for all $k \neq \ell$. In this case it can be shown that $\boldsymbol{I}-\boldsymbol{R}$ has one eigenvalue equal to $(1-K)\rho$ and $K-1$ eigenvalues equal to ρ. Furthermore, it can be shown that $\boldsymbol{V}$ can be written in the form

$$\boldsymbol{V} = \begin{bmatrix} \boldsymbol{v}_1 & \boldsymbol{v}_2 & \dots & \boldsymbol{v}_K \end{bmatrix}$$

where the normalized eigenvectors are given by

$$\begin{aligned}
\boldsymbol{v}_1 &= \frac{1}{\sqrt{K}}\begin{bmatrix} 1 & 1 & 1 & 1 & \dots & 1 \end{bmatrix}^\top \\
\boldsymbol{v}_2 &= \frac{1}{\sqrt{2}}\begin{bmatrix} 1 & -1 & 0 & 0 & \dots & 0 \end{bmatrix}^\top \\
\boldsymbol{v}_3 &= \frac{1}{\sqrt{6}}\begin{bmatrix} 1 & 1 & -2 & 0 & \dots & 0 \end{bmatrix}^\top \\
&\vdots \\
\boldsymbol{v}_K &= \frac{1}{\sqrt{(K-1)+(K-1)^2}}\begin{bmatrix} 1 & 1 & 1 & 1 & \dots & -(K-1) \end{bmatrix}^\top
\end{aligned}$$

where $\boldsymbol{v}_1$ is the eigenvector corresponding to the unique eigenvalue. We have used the normalized eigenvectors so that $\boldsymbol{V}^{-1} = \boldsymbol{V}^\top$. Using the fact that in the

equicorrelated, equipower case $\boldsymbol{e}_k^\top \boldsymbol{V}\boldsymbol{\Lambda}^{M+1}\boldsymbol{V}^{-1}\boldsymbol{e}_k$ does not depend on the choice of k, we can set $k = K$ and explicitly evaluate (3.11) to write

$$1 - \boldsymbol{e}_K^\top \boldsymbol{V}\boldsymbol{\Lambda}^{M+1}\boldsymbol{V}^{-1}\boldsymbol{e}_K = 1 - \left(\frac{(1-K)^{M+1}\rho^{M+1}}{K} + \frac{(K-1)^2\rho^{M+1}}{(K-1)+(K-1)^2} \right).$$

Under our assumption that M is odd then $(1-K)^{M+1} = (K-1)^{M+1}$ and we can simplify this expression to write the following condition

$$\left(\frac{K}{(K-1)^{M+1} + (K-1)} \right)^{\frac{1}{M+1}} < \rho \leq 1 \qquad \forall M \text{ odd.} \tag{3.12}$$

Satisfying this condition leads to an autocorrelation matrix $\boldsymbol{R}$ which causes the LPIC detector with M stages of interference cancellation to exhibit an error probability of greater than 0.5. □

We note that when $K = 2$, the lower bound on ρ is computed to be 1 for any value of M, hence no admissible choice of ρ will lead to an error probability greater than 0.5 at any stage in the two-user equipower scenario. On the other hand, when $K > 2$ then the lower bound is strictly less than one for all odd values of M and is decreasing in M. The common case of the two-stage LPIC detector ($M = 1$) leads to the following condition on ρ

$$\frac{1}{\sqrt{K-1}} < \rho \leq 1.$$

In the limit, as $M \to \infty$ (through all odd values of M) it can be shown that the condition on ρ is

$$\frac{1}{K-1} < \rho \leq 1.$$

We note that this condition is equivalent to $\boldsymbol{R}$ having an eigenvalue greater than 2 in the equicorrelated case. The fact that the bound is decreasing in M implies

that the performance of the LPIC detector may become worse at later stages when compared to earlier stages. In fact, if

$$\frac{1}{K-1} < \rho < \frac{1}{\sqrt{K-1}}$$

then the two-stage LPIC detector will not exhibit a probability of error greater than 0.5 but eventually, for M large enough and odd, the multistage LPIC detector will exhibit a probability of error greater than 0.5.

As a numerical example, consider a communication system with $K = 8$ equipower, equicorrelated users where $a/\sigma = 10$ and $\rho = 0.25$. Figure 3.3 shows the error probability for any user k versus M, the number of interference cancellation stages. Note that $P_{\mathsf{LPIC}}^{(k)}(M) > 0.5$ for all odd values of $M \geq 3$. Moreover, note that, at even values of M, the LPIC detector exhibits poor error probability performance with respect to the matched filter detector in this example, yet the error probability does not exceed 0.4 for any even value of M. This example suggests that the error probabilities for odd and even values of M converge to a pair of respective fixed points symmetric around 0.5 as $M \to \infty$. A rigorous proof of this conjecture is left as an open problem.

Figure 3.4 shows the minimum values of ρ versus M such that $P_{\mathsf{LPIC}}^{(k)}(M) > 0.5$. Examination of Figure 3.4 or calculation of (3.12) shows that values of ρ satisfying $0.3780 < \rho \leq 1$ when $M = 1$ and $K = 8$ lead to an LPIC detector error probability of greater than 0.5. This agrees with the results shown in Figure 3.3 where $\rho = 0.25$ and the error probability of the two-stage LPIC detector is less than 0.5. When $M = 3$, Figure 3.4 shows that values of ρ satisfying $0.2401 < \rho \leq 1$ when $M = 3$ and $K = 8$ will lead to an LPIC detector error probability of greater than 0.5, also agreeing with the results shown in Figure 3.3.

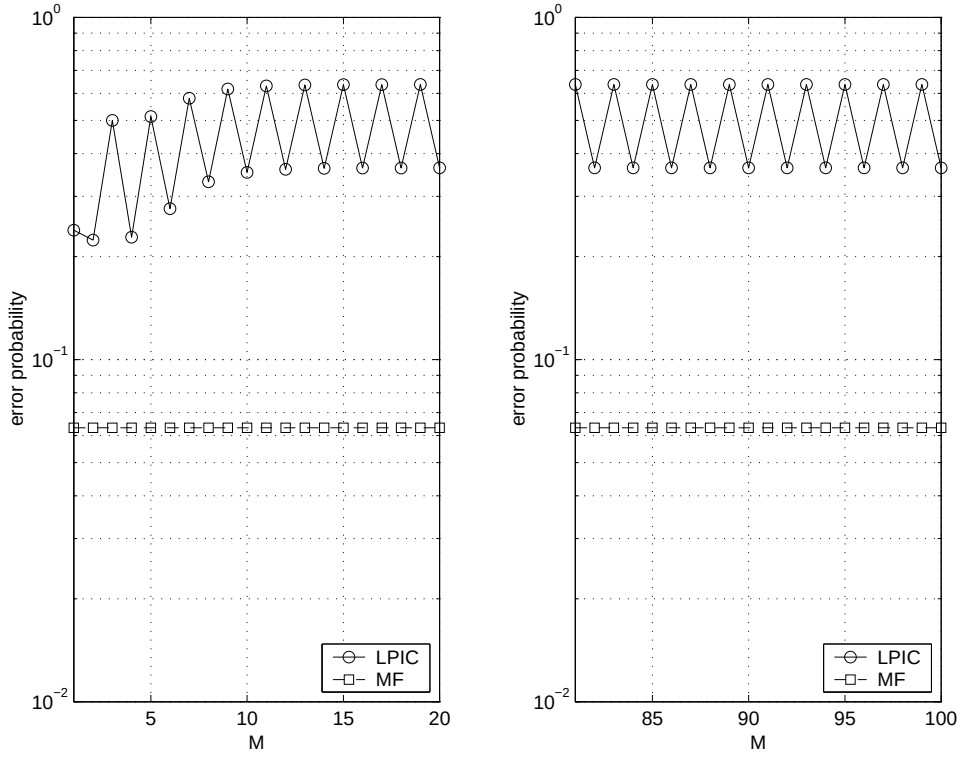

Figure 3.3: Example of error probabilities $P_{\mathsf{LPIC}}^{(k)}(M)$ and $P_{\mathsf{MF}}^{(k)}$ for an LPIC detector with M stages of interference cancellation in an equicorrelated, equipower communication system with $K = 8$ users.

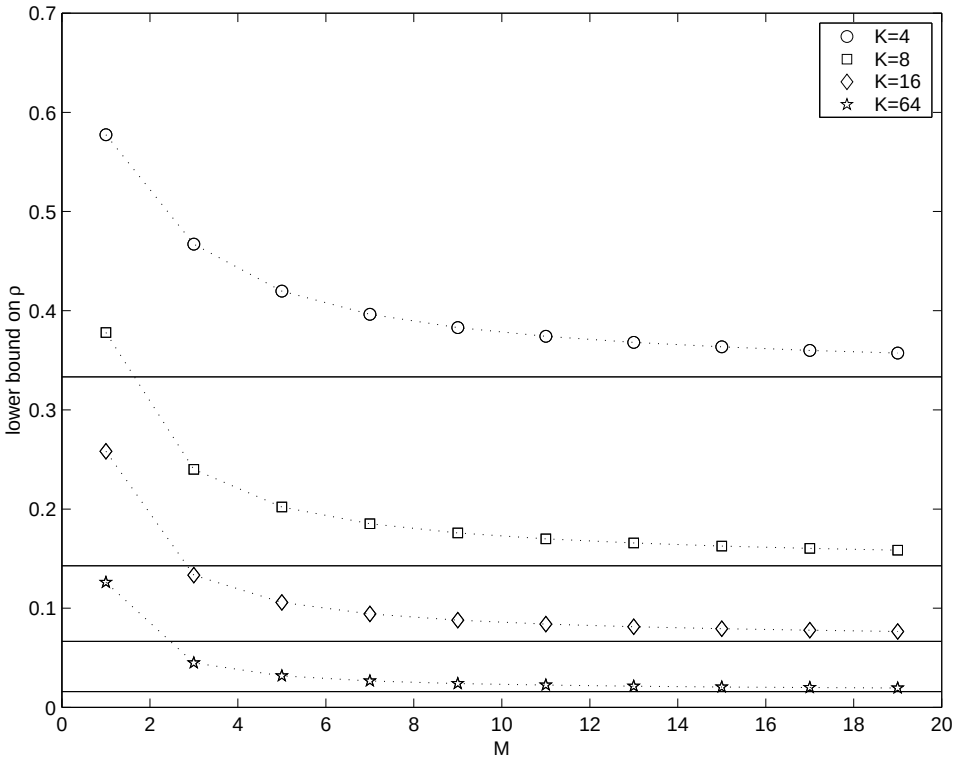

Figure 3.4: Correlation lower bound (3.12) of an LPIC detector with M stages of interference cancellation for odd values of M.

3.5 LPIC Asymptotic Behavior for Large M

This section analyzes the behavior of the LPIC detector in the asymptotic case where the number of interference cancellation stages M goes to infinity. It has been shown in [GMNK95] that the multistage LPIC detector converges to the decorrelating detector as $M \to \infty$ when the spectral radius of the signature crosscorrelation matrix $\rho(\boldsymbol{R})$ is less than 2. This section analyzes the asymptotic behavior of the LPIC detector when $\rho(\boldsymbol{R}) > 2$.

Recall that the multistage LPIC detector may be expressed as

$$\boldsymbol{L}(M) = \sum_{m=0}^{M} (\boldsymbol{I} - \boldsymbol{R})^m.$$

Let $\rho(\boldsymbol{R})$ represent the spectral radius of the signature crosscorrelation matrix $\boldsymbol{R}$ where $\rho(\boldsymbol{R}) \stackrel{\Delta}{=} \max_k |\gamma_k|$ and where the $\{\gamma_k\}$ is the set of eigenvalues of $\boldsymbol{R}$. Note that $\gamma_k = 1 - \lambda_k$ where $\{\lambda_k\}$ is the set of eigenvalues of $(\boldsymbol{I} - \boldsymbol{R})$ under the notation established in Section 3.4. It was shown in [GMNK95] that

$$\boldsymbol{L}(\infty) = \sum_{m=0}^{\infty} (\boldsymbol{I} - \boldsymbol{R})^m = \boldsymbol{R}^{-1}$$

if $\boldsymbol{R}$ is nonsingular and if $\rho(\boldsymbol{R}) < 2$. If $\rho(\boldsymbol{R}) > 2$ then there exists at least one $|\lambda_k| > 1$ and it is clear that $\boldsymbol{L}(M)$ does not converge to $\boldsymbol{R}^{-1}$ as $M \to \infty$. The following proposition analyzes the error probability of the LPIC detector when $\rho(\boldsymbol{R}) > 2$ as $M \to \infty$.

Proposition 7. *Let $P_{\mathsf{LPIC}}^{(k)}(M)$ be the error probability of an LPIC detector with M stages of interference cancellation for the k^{th} user. Given $\boldsymbol{R}$ such that $\rho(\boldsymbol{R}) > 2$, there exists M^* and k such that $P_{\mathsf{LPIC}}^{(k)}(M) > 0.5$ for all odd integer values of $M \geq M^*$.*

Proof. The proof of the proposition relies on the result in Proposition 6, which states that

$$P_{\mathsf{LPIC}}^{(k)}(M) > 0.5 \Leftrightarrow \boldsymbol{e}_k^\top \boldsymbol{L}(M)\boldsymbol{R}\boldsymbol{e}_k < 0.$$

Hence it suffices to show that given $\boldsymbol{R}$ such that $\rho(\boldsymbol{R}) > 2$, there exists k and M such that $\boldsymbol{e}_k^\top \boldsymbol{L}(M)\boldsymbol{R}\boldsymbol{e}_k < 0$.

Since $\boldsymbol{R}$ is symmetric, it can be decomposed as $\boldsymbol{R} = \boldsymbol{V}\boldsymbol{\Gamma}\boldsymbol{V}^\top$, where $\boldsymbol{V}$ is an orthogonal matrix consisting of the eigenvectors of $\boldsymbol{R}$ and $\boldsymbol{\Gamma}$ is the diagonal matrix containing the eigenvalues of $\boldsymbol{R}$. Moreover, since $\boldsymbol{L}(M)\boldsymbol{R}$ is a polynomial in $\boldsymbol{R}$, it has the decomposition

$$\boldsymbol{L}(M)\boldsymbol{R} = \boldsymbol{V} f(\boldsymbol{\Gamma})\boldsymbol{V}^\top$$

where $f(\boldsymbol{\Gamma}) = \mathrm{diag}(f(\gamma_1), \ldots, f(\gamma_K))$ and $f(\gamma_k) = \gamma_k \sum_{m=0}^{M}(1-\gamma_k)^m$. Letting $\boldsymbol{V} = [\boldsymbol{v}_1 \ \cdots \ \boldsymbol{v}_K]$, we can also write

$$\boldsymbol{L}(M)\boldsymbol{R} = \sum_{k=1}^{K} \boldsymbol{v}_k \boldsymbol{v}_k^\top f(\gamma_k).$$

Let $\mathcal{X} = \{\ell \in \{1, 2, \ldots, K\} : \gamma_\ell > 2\}$. Then we can write

$$\boldsymbol{e}_k^\top \boldsymbol{L}(M)\boldsymbol{R}\boldsymbol{e}_k = \sum_{\ell \in \mathcal{X}} \boldsymbol{e}_k^\top \boldsymbol{v}_\ell \boldsymbol{v}_\ell^\top \boldsymbol{e}_k f(\gamma_\ell) + \sum_{\ell \notin \mathcal{X}} \boldsymbol{e}_k^\top \boldsymbol{v}_\ell \boldsymbol{v}_\ell^\top \boldsymbol{e}_k f(\gamma_\ell).$$

It can be shown that $0 < f(\gamma_\ell) \leq \gamma_\ell$ for any M if $0 < \gamma_\ell \leq 2$. This fact combined with the property that all of the elements of $\boldsymbol{V}$ are finite implies that the second summation can be upper bounded by a finite constant C that does not depend on M or k. Hence we can write

$$\boldsymbol{e}_k^\top \boldsymbol{L}(M)\boldsymbol{R}\boldsymbol{e}_k < \sum_{\ell \in \mathcal{X}} \boldsymbol{e}_k^\top \boldsymbol{v}_\ell \boldsymbol{v}_\ell^\top \boldsymbol{e}_k f(\gamma_\ell) + C.$$

It can be shown that $f(\gamma_\ell) < 0$ when $\gamma_\ell > 2$ and M is odd. Moreover, $f(\gamma_\ell)$ is unbounded from below as $M \to \infty$ when $\gamma_\ell > 2$ and M is odd. This implies that

there exists M^* such that

$$\sum_{\ell \in \mathcal{X}} \boldsymbol{e}_k^\top \boldsymbol{v}_\ell \boldsymbol{v}_\ell^\top \boldsymbol{e}_k f(\gamma_\ell) < -C$$

since each eigenvector $\boldsymbol{v}_\ell$ can not have all zero elements and we can choose k such that $\boldsymbol{e}_k^\top \boldsymbol{v}_\ell \neq 0$ for at least one $\ell \in \mathcal{X}$. This implies that

$$\boldsymbol{e}_k^\top \boldsymbol{L}(M^*) \boldsymbol{R} \boldsymbol{e}_k < 0.$$

Finally, for any odd $M \geq M^*$,

$$\boldsymbol{e}_k^\top \boldsymbol{L}(M) \boldsymbol{R} \boldsymbol{e}_k \leq \boldsymbol{e}_k^\top \boldsymbol{L}(M^*) \boldsymbol{R} \boldsymbol{e}_k < 0.$$

□

The previous proposition indicates that if $\rho(\boldsymbol{R}) > 2$, there exists at least one user whose probability of error will exceed 0.5. It is tempting to think that if $\rho(\boldsymbol{R}) > 2$, all users will exhibit error probabilities greater than 0.5 for sufficiently large M. The following example indicates otherwise.

Suppose we have $K = 5$ users and a signature crosscorrelation matrix $\boldsymbol{R}$ which satisfies

$$\boldsymbol{R} = \frac{1}{11} \begin{bmatrix} 11 & -1 & -1 & -1 & 3 \\ -1 & 11 & 7 & 7 & 7 \\ -1 & 7 & 11 & 7 & 7 \\ -1 & 7 & 7 & 11 & 7 \\ 3 & 7 & 7 & 7 & 11 \end{bmatrix}. \tag{3.13}$$

The spectral radius of $\boldsymbol{R}$ is given by its largest eigenvalue which is computed to be $\rho(\boldsymbol{R}) = 32/11 = \gamma_1 > 2$ and it can be verified that all other eigenvalues of $\boldsymbol{R}$ are in

the open interval $(0, 2)$. The unit-norm eigenvector associated with the maximum eigenvalue is given as

$$\boldsymbol{v}_1^\top = \frac{1}{2}\begin{bmatrix} 0 & 1 & 1 & 1 & 1 \end{bmatrix}^\top.$$

Examination of the quantity $\boldsymbol{e}_k \boldsymbol{L}(M)\boldsymbol{R}\boldsymbol{e}_k$ for user $k = 1$ reveals that

$$\boldsymbol{e}_1^\top \boldsymbol{L}(M)\boldsymbol{R}\boldsymbol{e}_1 = 0 \cdot f(32/11) + \sum_{\ell=2}^{K} \boldsymbol{e}_1^\top \boldsymbol{v}_\ell \boldsymbol{v}_\ell^\top \boldsymbol{e}_1 f(\gamma_\ell) > 0 \Rightarrow P_{\mathsf{LPIC}}^{(1)}(M) < 0.5$$

since $f(\gamma_\ell) > 0$ for $\ell = 2, \ldots, K$ and any value of M. The key to this example is that the eigenvector associated with the maximum eigenvalue has a zero in a fortuitous location for the user $k = 1$. All other users $k \neq 1$ would exhibit misperformance. In any case, this example confirms our claim that not every user will necessarily exhibit an error probability greater than 0.5 when $\rho(\boldsymbol{R}) > 2$ since there is no guarantee that the eigenvector associated with the maximum eigenvalue has all nonzero entries for general $\boldsymbol{R}$.

The prior example leads to the following proposition. The proof is similar to that of Proposition 7.

Proposition 8. *Suppose $\boldsymbol{R}$ satisfies $\rho(\boldsymbol{R}) > 2$ and has an eigenvector, associated with an eigenvalue greater than two, with all nonzero entries. Then there exists M^* such that for all k, $P_{\mathsf{LPIC}}^{(k)}(M) > 0.5$ for all odd integer values of $M \geq M^*$.*

Recall that even though $P_{\mathsf{LPIC}}^{(k)}(M) > 0.5$ for odd values of M, $P_{\mathsf{LPIC}}^{(k)}(M)$ may be less than 0.5 for even values of M as shown in Figure 3.3.

Proposition 8 leads to the natural question, "When does $\boldsymbol{R}$ have an eigenvector with nonzero entries which is associated with an eigenvalue greater than two?" We have not been able to classify all such correlation matrices, but Perron's Theorem [HJ94, pp. 500] and its extensions identify a large class of such matrices. The theorem states that

Theorem 1. *Perron's Theorem. If* $\boldsymbol{A}$ *is an* $n \times n$ *matrix with positive entries, then*

1. $\rho(\boldsymbol{A}) > 0$ *and is a simple (multiplicity one) eigenvalue of* $\boldsymbol{A}$.

2. *The eigenvector associated with* $\lambda = \rho(\boldsymbol{A})$ *has positive entries.*

Although Perron's Theorem may be generalized from the class of all positive matrices to particular classes of nonnegative matrices [HJ94, pp. 508, 516], it does not extend to the case of signature crosscorrelation matrices with negative elements. This implies that the class of signature crosscorrelation matrices with two or more negative elements (since signature cross correlation matrices are symmetric and all elements on the diagonal are equal to one) are not covered by Perron's Theorem or its extensions. One example of just such a signature crosscorrelation matrix was given in (3.13). On the other hand, the implications of Perron's Theorem are stronger than necessary and simulations suggest that it is actually fairly difficult to find valid signature crosscorrelation matrices with an eigenvalue greater than two and an associated eigenvector with one or more elements equal to zero. The simulations presented in the next section (see Figure 3.8) suggest that the LPIC misperformance results described in this section extend to all users even in the case of random signature sequences.

3.6 Random Signature Sequences: Large-System Analysis

This section considers the implications of the general results developed in the prior sections to a CDMA communication system where the elements of $\boldsymbol{R}$ are random

and change at each bit interval. More precisely, given a CDMA communication system with spreading gain N, this section considers the case where the signature crosscorrelation matrix can be written as

$$\boldsymbol{R} = \frac{1}{N}\boldsymbol{S}^{\top}\boldsymbol{S} \tag{3.14}$$

where $\boldsymbol{S} \in \mathbb{B}^{N\times K}$ and the k^{th} column of $\boldsymbol{S}$ is denoted by $\boldsymbol{s}_k$ and represents the k^{th} user's binary random spreading sequence. All elements of $\boldsymbol{S}$ are independent and randomly chosen with equal probabilities. To obtain analytical results, we will focus on the "large-system" case described in [VS99] where the spreading gain (N) and the number of users (K) both approach infinity but their ratio $\beta = K/N$ converges to a fixed constant.

3.6.1 Performance Comparison

Since Proposition 4 holds for arbitrary $\boldsymbol{R}$ then it also holds for $\boldsymbol{R}$ described by (3.14). It turns out that the large-system random spreading sequences case allows us to reconsider Proposition 4 without the use of the Gaussian approximation to achieve an *exact* comparison of the MSE of the interference estimates for the two-stage LPIC and HPIC detector.

In the large-system case it was shown in [Ver98, pp. 116] that the average error probability for the matched filter detector with random spreading sequences can be written without approximation as

$$\mathrm{E}[P(\mathrm{sgn}(y^{(\ell)}) \neq b^{(\ell)})] = \mathrm{E}[P_{\mathsf{MF}}^{(\ell)}] = Q\left(\frac{a^{(\ell)}}{\sqrt{\sigma^2 + \beta\bar{a}^2}}\right)$$

where

$$\bar{a}^2 \;=\; \lim_{K\to\infty}\frac{1}{K}\sum_{k\neq\ell}(a^{(k)})^2. \tag{3.15}$$

This result in combination with (3.4) allows us to express the average interference estimate MSE for the ℓ^{th} user of the two-stage HPIC detector as

$$\mathrm{E}[\mathrm{MSE}^{(\ell)}_{\mathsf{HPIC}}] = 4(a^{(\ell)})^2 Q\left(\frac{a^{(\ell)}}{\sqrt{\sigma^2+\beta\bar{a}^2}}\right).$$

It is also possible to calculate the average interference estimate MSE of the ℓ^{th} user of the two-stage LPIC detector in the large-system random spreading sequences case without approximation as

$$\begin{aligned}
\mathrm{E}[\mathrm{MSE}^{(\ell)}_{\mathsf{LPIC}}] &= E\left[(e^{(\ell)}_{\mathsf{LPIC}})^2 \mid b^{(\ell)}\right] \\
&= E\left[\left(\sum_{k\neq\ell} \boldsymbol{s}_\ell^\top \boldsymbol{s}_k a^{(k)} b^{(k)} + \sigma n^{(\ell)}\right)^2\right] \\
&= \sigma^2 + \beta \lim_{K\to\infty} \frac{1}{K}\sum_{k\neq\ell} (a^{(k)})^2 \\
&= \sigma^2 + \beta\bar{a}^2
\end{aligned}$$

where we have used the property that

$$\mathrm{E}[\boldsymbol{s}_\ell^\top \boldsymbol{s}_k \boldsymbol{s}_\ell^\top \boldsymbol{s}_j] \;=\; \begin{cases} 1/N & \text{if } k=j \\ 0 & \text{otherwise} \end{cases}.$$

Hence, in the large-system random spreading sequences case, we can write the *exact* expression

$$\mathrm{E}[\mathrm{MSE}^{(\ell)}_{\mathsf{HPIC}}] = 4(a^{(\ell)})^2 Q\left(\frac{a^{(\ell)}}{\sqrt{\mathrm{E}[\mathrm{MSE}^{(\ell)}_{\mathsf{LPIC}}]}}\right)$$

which leads to the following proposition.

Proposition 9. *For random* $\boldsymbol{R}$ *given by (3.14), arbitrary fixed* σ, $\boldsymbol{A}$, *and* ℓ, $E[MSE^{(\ell)}_{\mathsf{LPIC}}] > E[MSE^{(\ell)}_{\mathsf{HPIC}}]$ *asymptotically as* $K\to\infty$, $N\to\infty$, *and* $K/N\to\beta$.

Proof. The proof follows that of Proposition 4. □

Figure 3.5 plots the analytically determined interference estimator MSE's of the LPIC and HPIC detectors for several values of β in the large-system case with random spreading sequences. This figure verifies the proposition and shows that the HPIC detector's interference estimates have lower MSE than the LPIC detector at any point in SNR-space for any value of β. The performance difference between the LPIC and HPIC detectors is several orders of magnitude for small values of β.

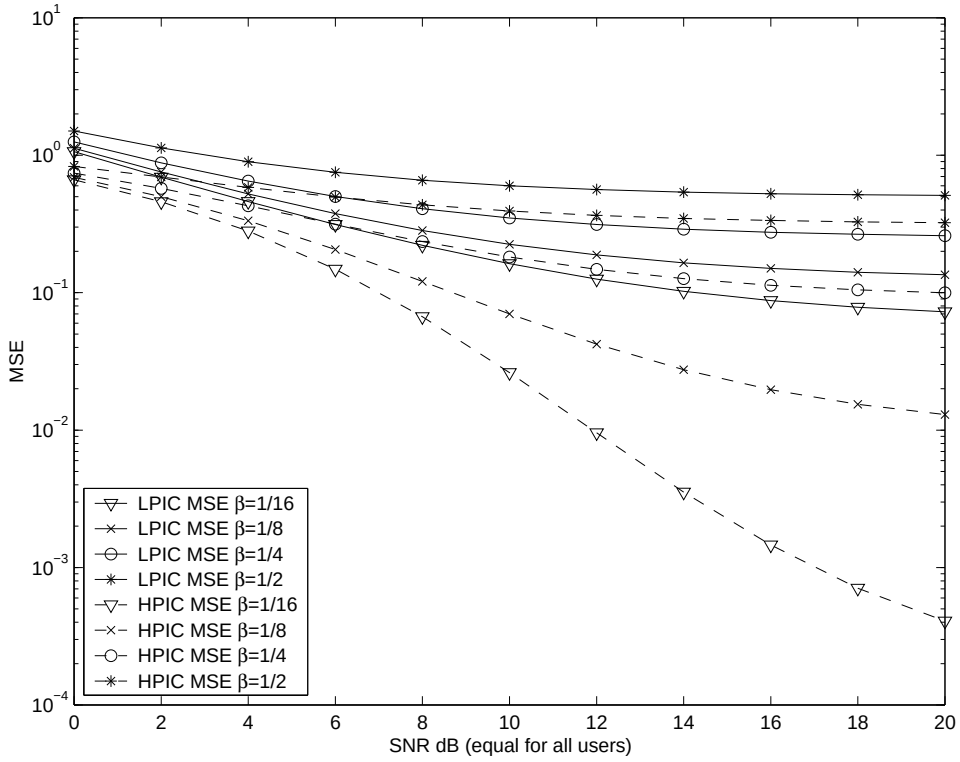

Figure 3.5: MSE of two-stage LPIC and HPIC detector interference estimators in a large system with random spreading.

We also compare the error probability performance of the two-stage HPIC and LPIC detectors in Figure 3.6. This figure shows a simulation of two-stage LPIC and HPIC detector error probabilities in a large system ($N = 256$) with random spreading sequences for several values of β. The HPIC detector outperforms the

LPIC detector at all points in the simulation. This result adds credence to our intuition that better interference estimates tend to lead to better PIC detector output (e.g., BER or SINR) performance.

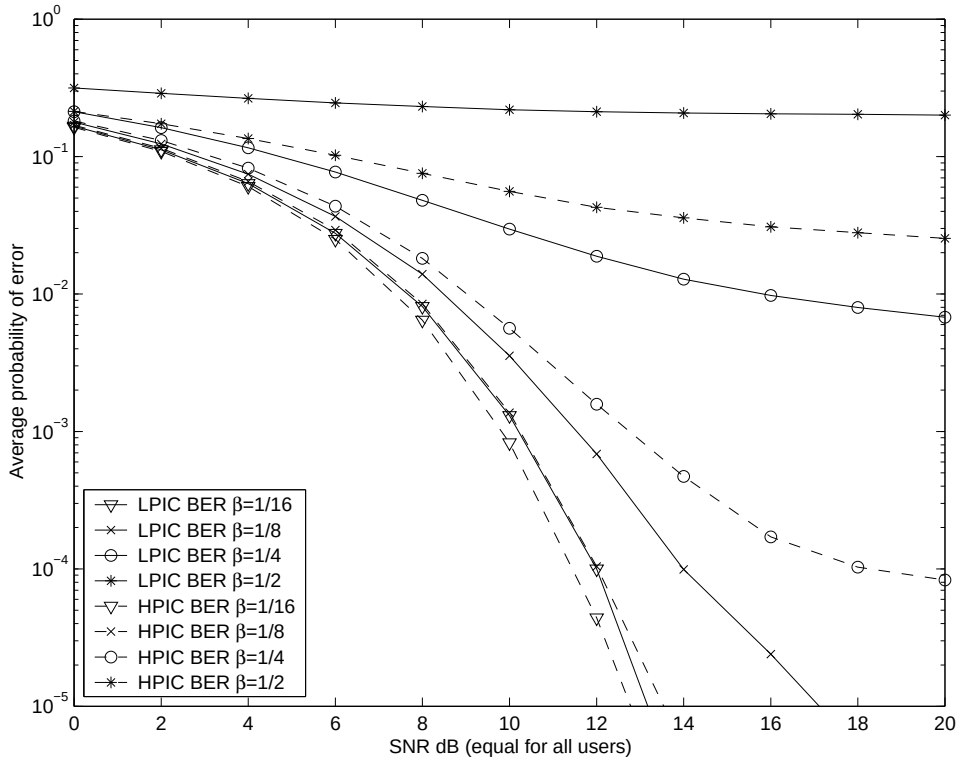

Figure 3.6: Bit error rate of two-stage LPIC and HPIC detectors in a large system with random spreading.

In summary, Proposition 9 and the simulation results of Figure 3.6 suggest that the two-stage HPIC detector is not only uniformly superior to the two-stage LPIC detector in terms of interference estimator performance but may also be superior to the two-stage LPIC detector in terms of *error probability* for large CDMA systems with synchronous users and random spreading sequences.

3.6.2 Comparison to the Matched Filter Detector

Direct interpretation of Proposition 5 in the large-system case with random spreading sequences is difficult since, unlike the matched filter, an exact expression for the LPIC detector's average probability of error $\mathrm{E}[P_{\mathsf{LPIC}}^{(\ell)}(M)]$ is difficult to obtain even in the two-stage ($M = 1$) case. Rather than directly comparing the error probabilities of the MF and LPIC detectors, we can instead compare their output SINRs using the SINR definition of Chapter 2 in (2.10). In this case, the expectations in (2.10) are averaged over the transmitted data, noise, and random signature sequences.

We note that the MF detector's error probability in the large-system case with random spreading sequences is a function only of its SINR where

$$\mathrm{E}[P_{\mathsf{MF}}^{(\ell)}] = Q\left(\sqrt{\frac{(a^{(\ell)})^2}{\sigma^2 + \beta\bar{a}^2}}\right) = Q\left(\sqrt{\mathrm{SINR}_{\mathsf{MF}}^{(\ell)}}\right) \tag{3.16}$$

as shown in [Ver98, pp. 116 and 281] with $\bar{a}^2$ as defined in (3.15). For an expression of the form in (3.16) to also apply to the multistage LPIC detector it is necessary to show that the LPIC detector's decision statistic after M stages of interference cancellation can be modeled by a Gaussian random variable in the large-system, random spreading sequences scenario. Although numerical evidence suggests that this may indeed be the case, a rigorous proof of this property appears to be difficult and remains an open problem. We proceed with the SINR analysis but caution the reader that these results do not directly lead to any conclusions about the relative bit error rates of the LPIC and MF detectors. Moreover, we justify the choice of SINR as a useful performance measure by noting that SINR is a more relevant measure of performance than bit error rate if the multiuser detector's outputs are to be used by a decoder.

The asymptotic SINR of the approximate decorrelator for a large CDMA system with random spreading sequences is given in [Ver98, pp. 281] as

$$\mathrm{SINR}_{\mathsf{AD}}^{(\ell)} = \mathrm{SINR}_{\mathsf{LPIC}}^{(\ell)}(1) = \frac{(a^{(\ell)}(1-\beta))^2}{\sigma^2(1-\beta+\beta^2)+\bar{a}^2(\beta^2+\beta^3)}$$

where we have used the fact that the two-stage ($M = 1$) LPIC detector is equivalent to the approximate decorrelator. Comparison of $\mathrm{SINR}_{\mathsf{LPIC}}^{(\ell)}(1)$ to $\mathrm{SINR}_{\mathsf{MF}}^{(\ell)}$ reveals that $(a^{(\ell)})^2$ can be factored out of both expressions and that there is no a^* threshold behavior as seen in Proposition 5. Instead, the relationship between $\mathrm{SINR}_{\mathsf{LPIC}}^{(\ell)}(1)$ and $\mathrm{SINR}_{\mathsf{MF}}^{(\ell)}$ depends on β and the ratio of mean interference to noise power $\bar{a}^2/\sigma^2$. The region in $(\bar{a}^2/\sigma^2, \beta)$ space where the MF detector outperforms the two-stage LPIC detector in terms of asymptotic SINR in the large-system random spreading sequences case is shown in Figure 3.7. Note that the MF detector outperforms the two-stage LPIC detector for almost all values of β when $\bar{a}^2/\sigma^2$ is small since the multiple access interference estimates are unreliable in this region. Inspection of the asymptotic SINR expressions for large $\bar{a}^2/\sigma^2$ also yields the somewhat surprising result that the MF detector outperforms the two-stage LPIC detector in terms of asymptotic SINR for all $\beta > 1/3$.

Calculation of the asymptotic SINR of the multistage LPIC detector for arbitrary $M > 1$ is more complicated and appears to require computation of the moments of the random eigenvalues of $\boldsymbol{R}$ from the distribution given in [VS99]. An analytical comparison of the MF and multistage LPIC detectors' asymptotic SINRs remains an open problem.

3.6.3 LPIC Misperformance and Asymptotic Results

Proposition 6 does not have direct application in the case when the signature crosscorrelation matrix $\boldsymbol{R}$ is random since Proposition 6 involves selection of some

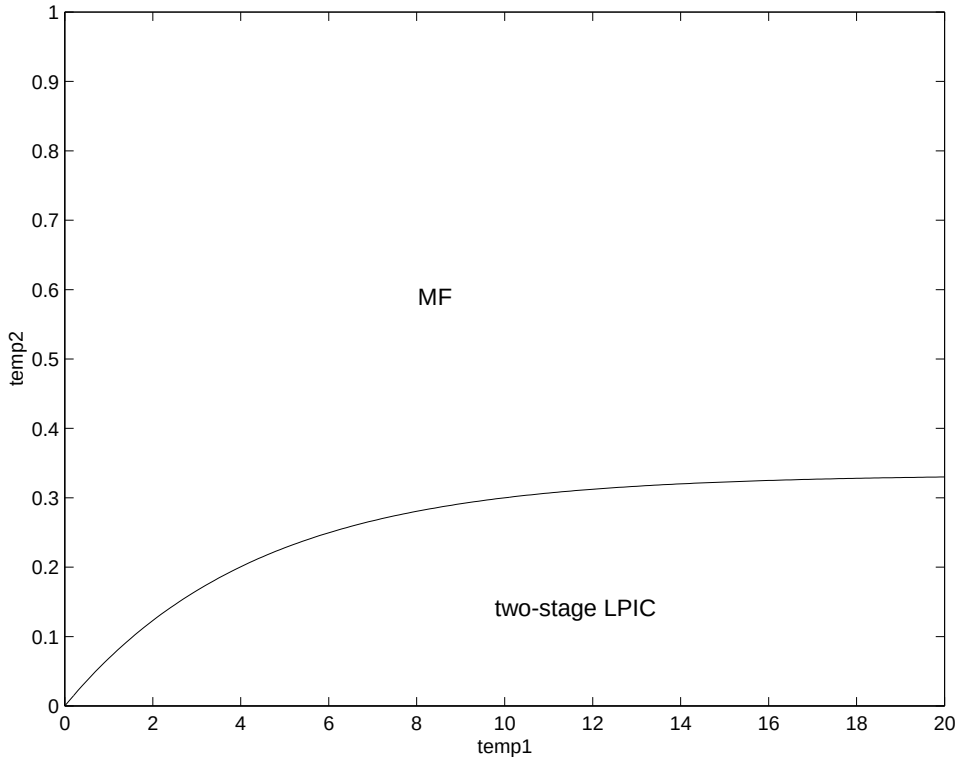

Figure 3.7: $\mathrm{SINR}_{\mathsf{LPIC}}^{(\ell)}(1) < \mathrm{SINR}_{\mathsf{MF}}^{(\ell)}$ in the region marked "MF" and $\mathrm{SINR}_{\mathsf{LPIC}}^{(\ell)}(1) > \mathrm{SINR}_{\mathsf{MF}}^{(\ell)}$ in the region marked "two-stage LPIC" for the large-system scenario with random spreading sequences.

particular $\boldsymbol{R}$ to show misperformance of the LPIC detector. However, Proposition 7 does have a meaningful interpretation due to the following theorem by Bai and Yin [BY93].

Theorem 2. *(Bai and Yin). Let $\boldsymbol{S}$ be a $N \times K$ matrix of independent and identically distributed (i.i.d.) random variables with zero mean and unit variance. Let $\boldsymbol{R} = \frac{1}{N}\boldsymbol{S}^{\top}\boldsymbol{S}$. If $E|S_{11}|^4 < \infty$, then, as $K \to \infty, N \to \infty, \frac{K}{N} \to \beta \in (0,1)$, the largest eigenvalue of $\boldsymbol{R}$ converges to $\left(1+\sqrt{\beta}\right)^2$ with probability one. The minimum eigenvalue converges to $\left(1-\sqrt{\beta}\right)^2$ with probability one.*

This theorem indicates that the largest eigenvalue of $\boldsymbol{R}$, defined as $\gamma_{max} = \rho(\boldsymbol{R})$ with $\boldsymbol{R}$ as defined in (3.14), converges asymptotically to a deterministic value

$$\gamma_{max} \to \left(1+\sqrt{\beta}\right)^2 \tag{3.17}$$

as K and N both go to infinity and $K/N \to \beta$. Recall that Proposition 7 considered the case where $\rho(\boldsymbol{R}) > 2$. Manipulation of (3.17) yields

$$\left(1+\sqrt{\beta}\right)^2 > 2 \Rightarrow \beta > \left(\sqrt{2}-1\right)^2 \approx 0.17.$$

This implies that for $K/N > 0.17$, $\rho(\boldsymbol{R}) > 2$ almost surely. In this case, Proposition 7 implies that at least one user will have probability of error greater than 0.5 almost surely in each bit interval. To be precise, we note that the misperforming user may be different for each realization of $\boldsymbol{R}$ so this result does not necessarily imply that the average error probability (over all possible realizations of $\boldsymbol{R}$) is necessarily greater than 0.5 for one or more users. The numerical example presented in Figure 3.8 suggests that all users may indeed have an average error probability greater than 0.5 as $M \to \infty$, but a rigorous proof of this conjecture is left as an open problem since it appears to require knowledge of the asymptotic structure of the eigenvectors of $\boldsymbol{R}$.

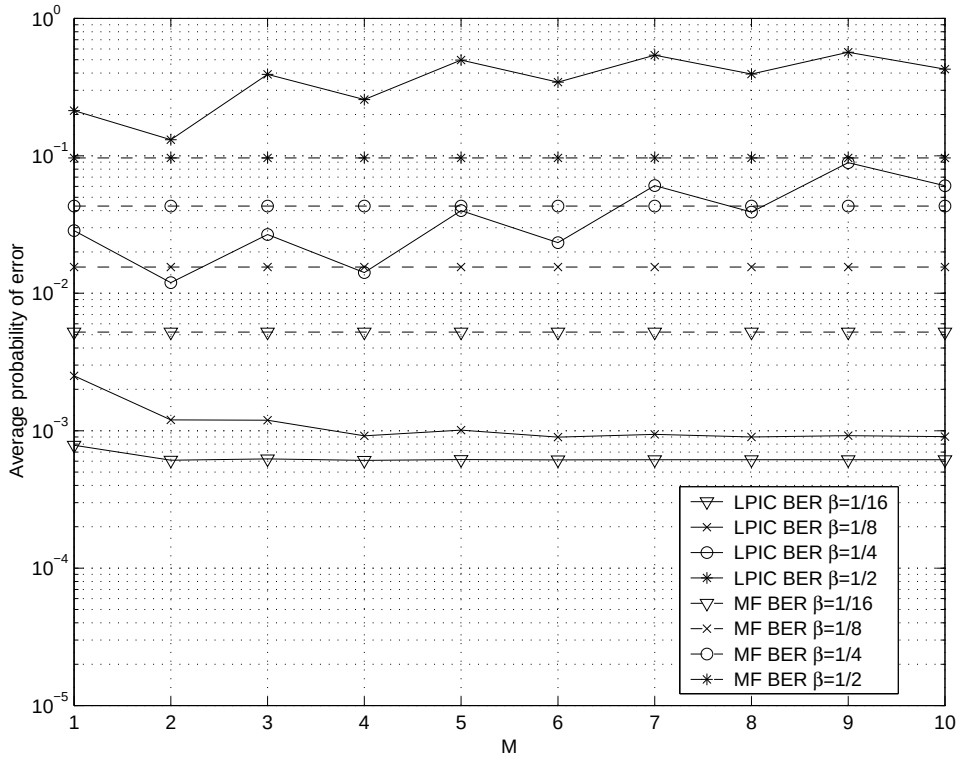

Figure 3.8: CDMA system with spreading gain $N = 256$ and random spreading sequences error probability versus number of LPIC interference cancellation stages M. All users have unit amplitude and the noise standard deviation is $\sigma = 0.3$. The single user bound is $\approx 4.29 \cdot 10^{-4}$ in this case.

3.7 Conclusions

This chapter examined several performance aspects of the multistage LPIC detector. We presented analytical evidence that supports the recent simulation evidence of other authors (e.g., [BN99]) suggesting that Varanasi and Aazhang's HPIC detector may outperform the LPIC detector in a large class of common operating scenarios. The LPIC detector was also shown to exhibit a worse error probability than the matched filter detector in the case where the desired user has sufficiently high amplitude. We showed that, unlike the matched filter detector, the LPIC detector may exhibit an output error probability greater than 0.5 for binary signaling under certain operating conditions. Asymptotic results were presented that describe bounds on the good-performance regions of the LPIC detector in terms of the eigenvalues of the signature crosscorrelation matrix as the number of interference cancellation stages (M) approaches infinity.

The implications of the prior results were studied in the last section for CDMA communication systems with large bandwidth, a large number of users, and random spreading sequences. We showed the somewhat surprising result that the two-stage LPIC detector exhibits worse asymptotic output SINR performance than the MF detector when $K/N > 1/3$ for any choice of desired user amplitude and interference or noise powers. We also showed the asymptotic result that application of the multistage LPIC detector to a CDMA system with $K/N > 0.17$ will not yield the decorrelating detector as $M \to \infty$ and that at least one user will exhibit an error probability worse than 0.5 in each bit interval.

CHAPTER 4

PERFORMANCE ADAPTIVE PARALLEL INTERFERENCE CANCELLATION

The prior chapters of this dissertation analyzed the two most common implementations of parallel interference cancellation: LPIC and HPIC. The common thread to both of these schemes, as well as the original work by Varanasi and Aazhang [VA90, VA91], Yoon, Kohno, and Imai [YKI92], and Kawabe et al [KKKF93], is that the PIC detector attempts to completely cancel the interference caused by all other users in order to form its output decision statistic. As has been suggested recently in [DSR98], full cancellation may not always be the best philosophy. Rather, when the interference estimates are unreliable, it may be better to not attempt to cancel any multiple access interference or perhaps to cancel only a portion of the interference. Divsalar and Simon's paper [DSR98] proposed an improved PIC detector with an output decision statistic (in the two-stage case) formed from a linear combination of the full cancellation HPIC and matched filter detectors' output decision statistics. A single weighting factor was chosen to specify the proportion of the linear combination and was selected in an ad-hoc manner to reflect the expected accuracy of the HPIC detector's interference estimator. Divsalar and Simon showed via simulation that, even with an ad-hoc choice of weighting factor, their improved PIC detector offered significant performance improvements with respect to the "brute force", or full cancellation, HPIC detector in several cases.

Other than the work by Divsalar and Simon, the majority of the recent research on improving the performance of PIC detection has focused on the LPIC detector [BW96, BN99, CBW97, CBW98, RW98a, XWLNT99, GRL99] due to its linear nature and the ability to obtain analytical results. Recently, an improved

version of the LPIC detector was proposed that converges to the linear MMSE detector in K stages [GRSL00]. Unfortunately, since each stage requires K^2 multiplications and there are K such stages, the number of multiplications required by this algorithm is on the order of K^3. This complexity is equivalent (in order) to the complexity of performing a $K \times K$ matrix inversion for direct computation of the linear MMSE detector. More importantly, the key disadvantage of focusing on improving the performance of the LPIC detector is that the ultimate performance of any improved LPIC algorithm is limited by the fact that it is linear. It is evident from the simulation results presented in [BCW96] that even the full cancellation HPIC detector often outperforms the linear MMSE detector in terms of bit error rate in a variety of scenarios. An improved performance nonlinear PIC detector, as sought in this chapter, potentially offers even greater performance improvements.

This chapter focuses on the problem of improving the performance of the two-stage HPIC detector through two distinct approaches. The first approach, developed in Section 4.1, proposes a scaling or attenuation of the hard decisions from the matched filter bank first stage in order to attenuate unreliable bit estimates. This idea is similar to that proposed by Divsalar and Simon in [DSR98] for the two-stage case, but with two improvements. The first improvement is that we suggest assigning an *individual* partial cancellation factor to each user rather than assigning one partial cancellation factor to all users. We show via a two-user example that assigning one partial cancellation factor to all users can be significantly suboptimum with respect to the individual partial cancellation factor approach. Our second improvement is that we consider analytical methods for computing *optimum* partial cancellation factors for three different performance criteria. We show that calculation of the partial cancellation factors to minimize the exact

or approximate bit error rate of this detector is difficult and numerical methods must be used to optimize the partial cancellation factors under these criteria (perhaps justifying the ad-hoc partial cancellation factor selection in [DSR98]). We also consider partial cancellation factor optimization under the SINR criterion and show that, unlike the bit error rate optimizations, a simple expression for the SINR maximizing partial cancellation factors can be obtained even in the general K-user case. We compare the performance of each of these methods in the two-user case to illustrate their relative performance gains with respect to the full cancellation HPIC detector.

Section 4.2 develops the second performance adaptive approach. We propose to improve the quality of the interference estimates from the matched filter bank outputs by forming estimates of the interfering users' bits that minimize the Bayesian MSE. This approach differs fundamentally from the first approach in that, rather than optimizing some performance measure at the output of the PIC detector, we instead optimize the performance of the interference estimates that are used to generate the output of the PIC detector. As discussed in the prior chapters of this dissertation, the intuition behind this approach is that if the interference estimates are high quality, then the performance at the output of the PIC detector will also tend to be good. An approximate version of this estimator is also proposed in this chapter that has low computational complexity in the general K-user case and simulation results are presented that suggest that this approach can offer very good performance.

4.1 Partial Cancellation HPIC

This section proposes a new performance adaptive detector called the partial cancellation hard parallel interference cancellation (PC-HPIC) detector in order to improve the performance of the standard HPIC detector described in Chapter 2. The motivation behind PC-HPIC is developed by showing that there exists a set of operating conditions where HPIC actually performs worse than the MF detector in terms of bit error rate. Intuitively, the poor performance of the HPIC detector is due to the fact that the HPIC detector attempts to cancel all of the multiple access interference even when the interfering users' bit estimates are unreliable. When the HPIC detector attempts to cancel a binary interference term with an incorrect bit estimate, the interference is doubled rather than canceled. If this happens often enough, the performance of the HPIC detector can actually be significantly worse than the MF detector. The PC-HPIC detector addresses this problem by considering the reliability of the hard bit estimates used in the interference cancellation. If the estimates are unreliable, the PC-HPIC detector only attempts to cancel a portion of the multiple access interference to avoid the problem of interference doubling.

From (1.2) and Table 1.1, we can write the k^{th} user's two-stage PC-HPIC detector output in the K-user synchronous case as

$$y^{(k)}_{\mathsf{PC-HPIC}} \;=\; a^{(k)}b^{(k)} + \sum_{\ell \neq k} \rho_{k\ell} a^{(\ell)} [b^{(\ell)} - g_\ell \mathrm{sgn}(y^{(\ell)})] + \sigma n^{(k)}. \tag{4.1}$$

From (1.3), we can group the two-stage PC-HPIC detector's outputs into a K-vector to write

$$\boldsymbol{y}_{\mathsf{PC-HPIC}} \;=\; \boldsymbol{y} - (\boldsymbol{R} - \boldsymbol{I})\boldsymbol{A}\boldsymbol{G}\mathrm{sgn}(\boldsymbol{y})$$

where $\boldsymbol{G} = \mathrm{diag}(g_1, \ldots, g_K)$. These expressions are quite similar to the HPIC

detector in (2.1) except for the real scalar terms $\{g_\ell\}_{\ell=1}^K$ which denote the partial cancellation or weighting factors. These partial cancellation factors are chosen in order to mitigate the performance degradation due to interference doubling from unreliable interfering bit estimates. In the case when $\boldsymbol{G} = \boldsymbol{I}$ it is clear that the PC-HPIC detector is equivalent to the full cancellation HPIC detector. In the case when $\boldsymbol{G} = \boldsymbol{0}$ it is clear that the PC-HPIC detector is equivalent to the conventional MF detector.

The key ideas behind PC-HPIC are illustrated in this section by considering the two-user synchronous CDMA system model. The two-user synchronous case allows a graphical analysis that provides a visual intuition of the PC-HPIC detector without the complexity inherent in the K-user problem and allows us to demonstrate that significant performance gains can be realized by the PC-HPIC detector with respect to the full cancellation HPIC detector. Chapter 2 presented exact and approximate bit error rate expressions for the full cancellation HPIC detector and we extend these results to provide equivalent expressions for the bit error rate of the PC-HPIC detector in this section. As was seen in Chapter 2, computation of the bit error rate of the full cancellation HPIC detector can be difficult for the $K > 2$ case and we show in this section that, unfortunately, bit error rate computations are no simpler for the PC-HPIC detector. We will show that this leads to difficulties in computing the optimum partial cancellation factors under either the exact or approximate bit error rate criteria even in the two-user case and makes these approaches practically infeasible for K much larger than two. On the other hand, Chapter 2 also presents a relatively simple closed form expression for the approximate SINR of the full cancellation HPIC detector. We take advantage of that result in this section by extending the SINR results to the PC-HPIC

detector and computing the optimum partial cancellation factors that maximize the output SINR of the PC-HPIC detector. It turns out that the expressions for the SINR maximizing partial cancellation factors are relatively simple and extend easily to the K-user case.

4.1.1 Exact Bit Error Rate of Two-User HPIC

In the two-user synchronous case, the matched filter bank soft outputs can be written as

$$\begin{aligned} y^{(1)} &= a^{(1)}b^{(1)} + \rho a^{(2)}b^{(2)} + \sigma n^{(1)} \\ y^{(2)} &= a^{(2)}b^{(2)} + \rho a^{(1)}b^{(1)} + \sigma n^{(2)}. \end{aligned}$$

The HPIC multiuser detector forms a decision statistic for user one with the expression

$$y^{(1)}_{\mathsf{HPIC}} = a^{(1)}b^{(1)} + \rho a^{(2)}[b^{(2)} - \mathrm{sgn}(y^{(2)})] + \sigma n^{(1)}.$$

In the two-user scenario, the uncoded bit error rate of the MF detector [Ver98] for user one can be written as

$$P^{(1)}_{\mathsf{MF}} = \frac{1}{2}Q\left(\frac{a^{(1)} + \rho a^{(2)}}{\sigma}\right) + \frac{1}{2}Q\left(\frac{a^{(1)} - \rho a^{(2)}}{\sigma}\right). \tag{4.2}$$

To calculate the exact uncoded bit error rate of the HPIC detector in the two-user case, we use the analysis of Chapter 2 to write (2.8) as

$$P^{(1)}_{\mathsf{HPIC}} = \frac{1}{2}\sum_{u\in\{\pm 1\}}\sum_{v\in\{\pm 1\}}\int_{\boldsymbol{\omega}\in\Omega(u,v)} f(\boldsymbol{\omega})\, d\boldsymbol{\omega}. \tag{4.3}$$

where the integration is 2-dimensional[1] in this case. Recall that, conditioned on $\bar{\boldsymbol{b}} = [-1, u]^\top$, the joint event $\mathrm{sgn}(y^{(2)}) = v$ and $y^{(1)}_{\mathsf{HPIC}} > 0$ occurs if and only if

[1]It is actually possible in this case to write (4.3) as a 1-dimensional integral of a function composed as a product of an exponential and a Q function for efficient calculation in Matlab, but this is still technically a 2-dimensional integral.

$\boldsymbol{n} = [n^{(1)}, n^{(2)}]^\top \in \Omega(u, v)$. Using (2.3), (2.4), (2.5), and (2.7), the rectangular regions $\Omega(u, v)$ are explicitly given in Table 4.1.

Table 4.1: Regions of $\boldsymbol{n}$-space such that HPIC makes a decision error for user one given $b^{(1)} = -1$.

u	v	$\Omega(u, v)$
-1	-1	$\left(\frac{a^{(1)}}{\sigma}, \infty\right) \times \left(-\infty, \frac{\rho a^{(1)} + a^{(2)}}{\sigma}\right)$
-1	+1	$\left(\frac{a^{(1)} + 2\rho a^{(2)}}{\sigma}, \infty\right) \times \left(\frac{\rho a^{(1)} + a^{(2)}}{\sigma}, \infty\right)$
+1	-1	$\left(\frac{a^{(1)} - 2\rho a^{(2)}}{\sigma}, \infty\right) \times \left(-\infty, \frac{\rho a^{(1)} - a^{(2)}}{\sigma}\right)$
+1	+1	$\left(\frac{a^{(1)}}{\sigma}, \infty\right) \times \left(\frac{\rho a^{(1)} - a^{(2)}}{\sigma}, \infty\right)$

Figure 4.1 plots the analytical bit error rates of the MF and HPIC detectors for user one for the case when $\rho = 0.2$. The third subplot shows the ratio of the MF bit error rate to the HPIC bit error rate where the HPIC detector has a lower bit error rate than the MF detector over regions of the SNR-space with contours greater than one. Figures 4.2 and 4.3 also show the cases when $\rho = 0.5$ and $\rho = 0.8$ respectively. The symmetry of the two-user problem implies that the bit error rate plots for user two can be seen by simply swapping the axis labels.

These figures show that the HPIC detector tends to perform well in regions of SNR-space where user two has higher SNR than user one since, in this region, user two's matched filter output produces reliable estimates of user two's bits and interference cancellation is accurate with high probability. On the other hand, the MF detector tends to perform well in regions of SNR-space where user one has higher SNR than user two. In fact, it is visibly evident in Figures 4.2 and 4.3 that the MF detector has a lower bit error rate for user one than the HPIC detector in the "southeast" corner of the SNR-space. The exact regions of SNR-space where the MF detector outperforms the HPIC detector are plotted for $\rho = 0.2$, $\rho = 0.5$,

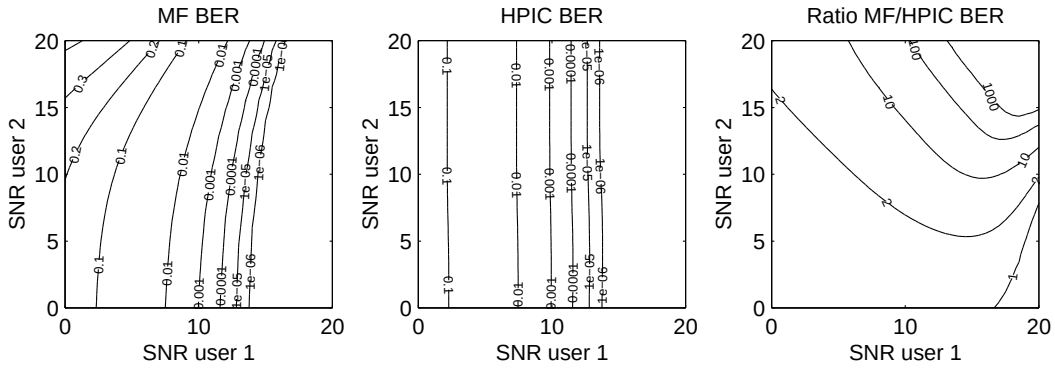

Figure 4.1: MF and two-stage HPIC bit error rates for user one two users and $\rho = 0.2$.

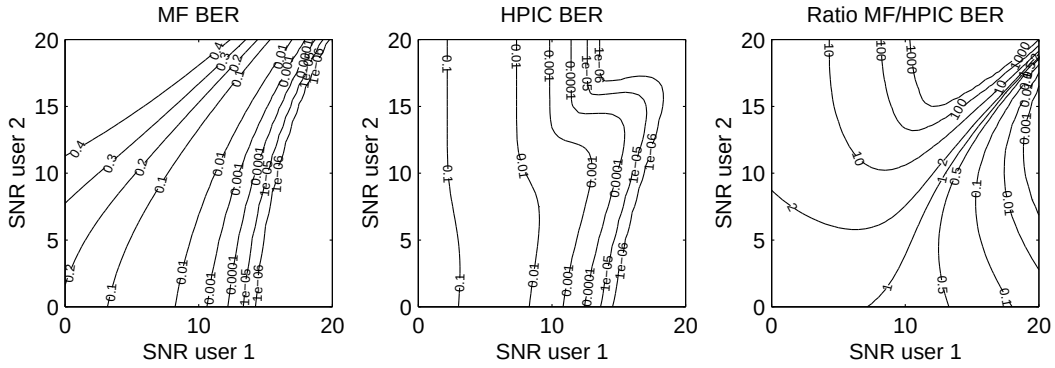

Figure 4.2: MF and two-stage HPIC bit error rates for user one two users and $\rho = 0.5$.

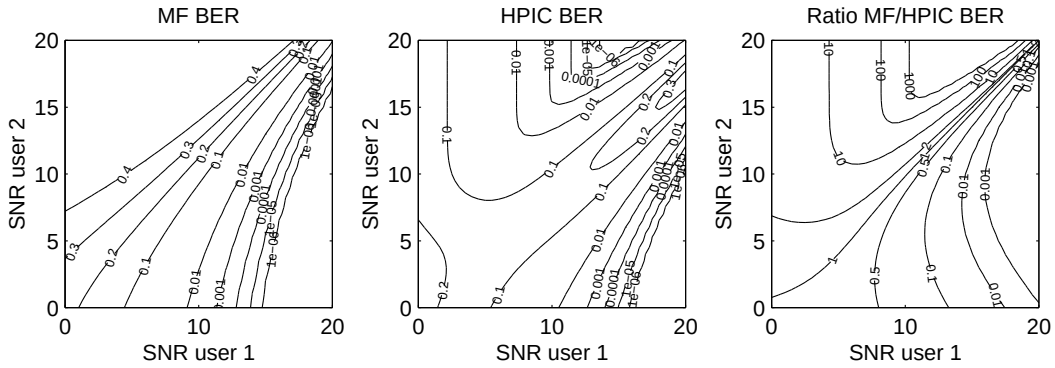

Figure 4.3: MF and two-stage HPIC bit error rates for user one two users and $\rho = 0.8$.

and $\rho = 0.8$ in Figure 4.4. In this figure, the MF detector has a lower bit error rate in the regions "southeast" of the equiBER boundaries and HPIC has a lower bit error rate in the regions "northwest" of the boundaries. Intuitively, the "southeast" area of the plot represents a region where user one is received at high SNR and at an amplitude much higher than user two. In this region, the MF detector's output for user one is fairly reliable but the MF detector's output for user two is unreliable due to the large amount of interference from user one. When the HPIC detector attempts to cancel the interference from user two, the unreliable estimate of user two's bit too often leads to a doubling of the interference rather than a cancellation. The end result is that the performance of the HPIC detector is worse for user one in the "southeast" regions of the SNR-space when compared to the MF detector.

4.1.2 Two-User Partial Cancellation Factor Analysis

A simple solution to the problem of poor the HPIC detector performance seen in the "southeast" corners of the SNR-space of Figures 4.2-4.3 would be to turn off the

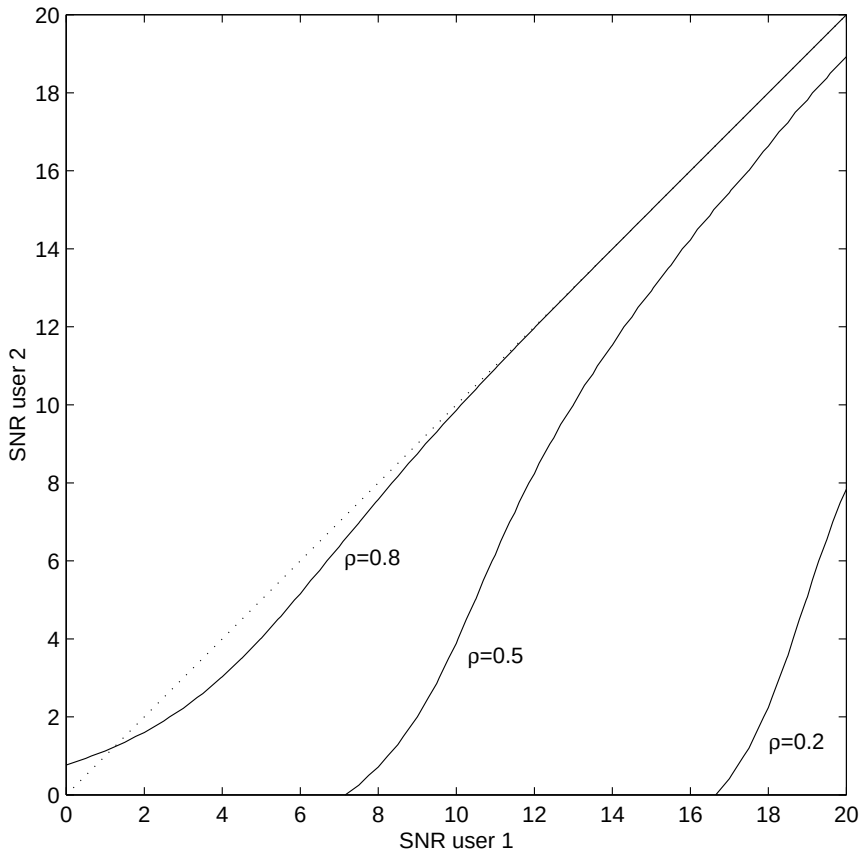

Figure 4.4: EquiBER curves for HPIC and MF detectors for signature crosscorrelation coefficients $\rho = 0.2$, $\rho = 0.5$, and $\rho = 0.8$. The MF detector has lower bit error rate in the "southeast" regions and HPIC has lower bit error rate in "northwest" regions of the plot. The equal power operating condition ($a^{(1)} = a^{(2)}$) is shown by the dotted line.

interference cancellation when operating in the appropriate "southeast" region of the SNR-space. In this case, turning off the interference cancellation would result in the HPIC detector reconfiguring itself into the MF detector and performance would improve accordingly. This reconfigurable HPIC/MF detector would require some rule based on the parameters $a^{(1)}$, $a^{(2)}$, ρ, and σ in order to know when to turn on/off the interference cancellation. Note that, unlike the full cancellation HPIC detector, this detector requires knowledge of the noise power.

A more sophisticated approach to mitigating the problem of interference doubling in the HPIC detector is the PC-HPIC detector. In the two-user synchronous case, the PC-HPIC detector forms a soft decision statistic from the expression

$$y^{(1)}_{\mathsf{PC-HPIC}} = a^{(1)}b^{(1)} + \rho a^{(2)}(b^{(2)} - g\mathrm{sgn}(y^{(2)})) + \sigma n^{(1)}$$

where g is a real valued parameter, called the partial cancellation factor, chosen to minimize the bit error rate. Clearly, setting $g = 1$ results in the full cancellation HPIC detector and setting $g = 0$ results in the MF detector, hence, if g is chosen wisely, the bit error rate of this new detector should be no worse than either the MF or full cancellation HPIC detectors.

Exact Bit Error Rate Optimization

To calculate the exact bit error rate of the PC-HPIC detector in the two-user case, Table 4.2 shows the regions in $\boldsymbol{n}$-space that result in a decision error for user one conditioned on the transmitted symbols, as was described for the full cancellation HPIC detector in Table 4.1. Note that the regions of integration remain rectangular but are now a function of the partial cancellation factor g. Given g, the error probability for user one is then given by (4.3) with rectangular integration regions $\Omega(u, v)$ from Table 4.2.

Table 4.2: Regions of $\boldsymbol{n}$-space such that PC-HPIC, parameterized by the partial cancellation factor g, makes a decision error for user one given $b^{(1)} = -1$.

u	v	$\Omega(u,v)$
-1	-1	$\left(\frac{a^{(1)}+(1-g)\rho a^{(2)}}{\sigma}, \infty\right) \times \left(-\infty, \frac{\rho a^{(1)}+a^{(2)}}{\sigma}\right)$
-1	+1	$\left(\frac{a^{(1)}+(1+g)\rho a^{(2)}}{\sigma}, \infty\right) \times \left(\frac{\rho a^{(1)}+a^{(2)}}{\sigma}, \infty\right)$
+1	-1	$\left(\frac{a^{(1)}-(1+g)\rho a^{(2)}}{\sigma}, \infty\right) \times \left(-\infty, \frac{\rho a^{(1)}-a^{(2)}}{\sigma}\right)$
+1	+1	$\left(\frac{a^{(1)}-(1-g)\rho a^{(2)}}{\sigma}, \infty\right) \times \left(\frac{\rho a^{(1)}-a^{(2)}}{\sigma}, \infty\right)$

The problem here is not to compute the bit error rate of the PC-HPIC detector but rather to compute the value of g that minimizes it. To compute this value of g, we first define

$$\begin{aligned} h_L(w,t) &\triangleq \int_{-\infty}^{t} \frac{1}{2\pi\sqrt{1-\rho^2}} \exp\left(-\frac{x^2-2\rho xw+w^2}{2(1-\rho^2)}\right) dx \\ &= \frac{1}{\sqrt{2\pi}} \exp\left(-\frac{w^2}{2}\right) \int_{-\infty}^{t} \frac{1}{\sqrt{2\pi}\sqrt{1-\rho^2}} \exp\left(-\frac{(x-\rho w)^2}{2(1-\rho^2)}\right) dx \\ &= \frac{1}{\sqrt{2\pi}} \exp\left(-\frac{w^2}{2}\right) Q\left(\frac{\rho w - t}{\sqrt{1-\rho^2}}\right) \end{aligned}$$

and similarly

$$\begin{aligned} h_R(w,t) &\triangleq \int_{t}^{\infty} \frac{1}{2\pi\sqrt{1-\rho^2}} \exp\left(-\frac{x^2-2\rho xw+w^2}{2(1-\rho^2)}\right) dx \\ &= \frac{1}{\sqrt{2\pi}} \exp\left(-\frac{w^2}{2}\right) Q\left(\frac{t-\rho w}{\sqrt{1-\rho^2}}\right). \end{aligned}$$

Then the exact bit error rate of the PC-HPIC detector for user one can be written from (4.3) and Table 4.2 as

$$P_{\mathsf{HPIC}}^{(1)} = \frac{1}{2}\left[\int_{f_1(g)}^{\infty} h_L(w,t_1)\,dy + \int_{f_2(g)}^{\infty} h_R(w,t_1)\,dy + \int_{f_3(g)}^{\infty} h_L(w,t_2)\,dy + \int_{f_4(g)}^{\infty} h_R(w,t_2)\,dy\right]$$

where

$$\begin{aligned} f_1(g) &= \frac{a^{(1)} + (1-g)\rho a^{(2)}}{\sigma}, \\ f_2(g) &= \frac{a^{(1)} + (1+g)\rho a^{(2)}}{\sigma}, \\ f_3(g) &= \frac{a^{(1)} - (1+g)\rho a^{(2)}}{\sigma}, \\ f_4(g) &= \frac{a^{(1)} - (1-g)\rho a^{(2)}}{\sigma}, \\ t_1 &= \frac{\rho a^{(1)} + a^{(2)}}{\sigma}, \text{ and} \\ t_2 &= \frac{\rho a^{(1)} - a^{(2)}}{\sigma}. \end{aligned}$$

Proceeding toward the analytical solution to the optimum value of g, the derivative of $P^{(1)}_{\mathsf{HPIC}}$ with respect to g can be computed as

$$\frac{\partial}{\partial g} P^{(1)}_{\mathsf{HPIC}} = \frac{\rho a^{(2)}}{2\sigma} \left[h_L(f_1(g), t_1) - h_R(f_2(g), t_1) + h_L(f_3(g), t_2) - h_R(f_4(g), t_2) \right]$$

using Theorem 6.1.7 of [Str95, pp.213]. Hence the value of g that minimizes the bit error rate is also the value of g that solves the equation

$$h_L(f_1(g), t_1) + h_L(f_3(g), t_2) = h_R(f_2(g), t_1) + h_R(f_4(g), t_2),$$

or explicitly, after substitution and cancellation of common factors,

$$\begin{aligned} &\exp\left(\frac{-\rho a^{(1)} a^{(2)} + g[\rho a^{(1)} a^{(2)} + (\rho a^{(2)})]^2}{\sigma^2}\right) Q\left(\frac{[(1-g)\rho^2 - 1]a^{(2)}}{\sigma\sqrt{1-\rho^2}}\right) + \\ &\exp\left(\frac{\rho a^{(1)} a^{(2)} + g[\rho a^{(1)} a^{(2)} - (\rho a^{(2)})]^2}{\sigma^2}\right) Q\left(\frac{[-(1+g)\rho^2 + 1]a^{(2)}}{\sigma\sqrt{1-\rho^2}}\right) = \\ &\quad \exp\left(\frac{-\rho a^{(1)} a^{(2)} - g[\rho a^{(1)} a^{(2)} + (\rho a^{(2)})]^2}{\sigma^2}\right) Q\left(\frac{[-(1+g)\rho^2 + 1]a^{(2)}}{\sigma\sqrt{1-\rho^2}}\right) + \\ &\quad \exp\left(\frac{\rho a^{(1)} a^{(2)} - g[\rho a^{(1)} a^{(2)} - (\rho a^{(2)})]^2}{\sigma^2}\right) Q\left(\frac{[(1-g)\rho^2 - 1]a^{(2)}}{\sigma\sqrt{1-\rho^2}}\right). \end{aligned}$$

Unfortunately, there does not appear to be a closed form solution for g to solve this last equation hence we must resort to numerical methods for a solution. Figure 4.5

shows the numerically derived optimum values for g at each point in the SNR-space for the cases when $\rho = 0.2$, $\rho = 0.5$ and $\rho = 0.8$.

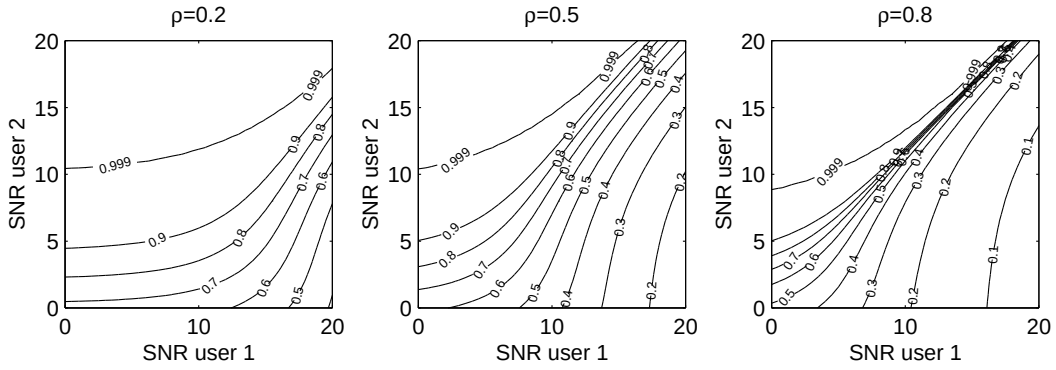

Figure 4.5: Bit error rate optimum PC-HPIC partial cancellation factor g.

Consistent with the results shown in Figure 4.4, the optimum cancellation factor in each case is close to one when the users' SNRs are in the "northwest" corner of the SNR-space and is much smaller than one when the user SNRs are in the "southeast" corner of the SNR-space. By the symmetry of the two-user case, the same results can be easily stated for user two by simply swapping the axis labels. This result illustrates a significant weakness in the approach used in [DSR98] where all users are assigned the same partial cancellation factor. As an example of a case where it is clearly suboptimum to apply an identical partial cancellation factor to all users, suppose that user one's SNR is 10dB, user two's SNR is 15dB, and that $\rho = 0.5$. In this case, the minimum bit error rate for user one is achieved if the cancellation factor is set to $g \approx 1$ in this case. On the other hand, the value of g that minimizes the bit error rate for user two, seen by simply swapping the SNR axis labels, is $g \approx 0.38$ in this case. Assigning a single partial cancellation factor to both users in this case would degrade the performance of one or both users.

The results also suggest that, at values of ρ closer to 1, the optimum partial

cancellation factor can be quite sensitive to the users' SNRs. The third subplot of Figure 4.5 shows that the partial cancellation factor contours are closely spaced in the "northeast" corner, indicating that the optimum partial cancellation factor is highly sensitive to small perturbations in this region. For example, in the case where user two's SNR is 20dB, if user one's SNR is 16dB the optimum cancellation factor is $g \approx 1$ but if user one's SNR is 18dB then the optimum cancellation factor is $g \approx 0.4$. This implies that ad-hoc selection of partial cancellation factors, as in [DSR98], may lead to poor performance in the case when the users are received at disparate powers.

Approximate Bit Error Rate Optimization

The second approach to computing the optimum partial cancellation factor g posed in this section is to select g to minimize the approximate bit error rate (2.9) of the PC-HPIC detector. Since it was shown to be quite difficult in the last section to calculate the optimum value of g in order to minimize the exact bit error rate of the PC-HPIC detector, we hope that minimizing the approximate bit error rate expression will yield a simpler solution. In the two-user case, we can modify (2.9), originally posed for the full cancellation HPIC detector, to account for the partial cancellation factor inherent in the PC-HPIC detector to write

$$P^{(1)}_{\mathsf{PC-HPIC}} \approx \frac{1}{2} \sum_{u\in\{\pm 1\}} \sum_{v\in\{\pm 1\}} Q\left(\frac{a^{(1)} - \rho a^{(2)}[u - gv]}{\sigma}\right) Q\left(\frac{v[\rho a^{(1)} - a^{(2)}u]}{\sigma}\right). \quad (4.4)$$

Theorem 6.1.7 of [Str95, pp.213] implies that

$$\frac{\partial}{\partial g} Q(f(g)) \;=\; -\frac{\partial}{\partial g} f(g) \frac{1}{\sqrt{2\pi}} \exp\left(-\frac{1}{2}(f(g))^2\right)$$

hence the value of g that minimizes (4.4) is the value of g that solves

$$\sum_{u\in\{\pm 1\}} \sum_{v\in\{\pm 1\}} \frac{\rho a^{(2)} v}{\sqrt{2\pi}\sigma} \exp\left(\frac{-\left(a^{(1)} - \rho a^{(2)}[u - gv]\right)^2}{2\sigma^2}\right) Q\left(\frac{v[\rho a^{(1)} - a^{(2)}u]}{\sigma}\right) = 0.$$

Although it is possible to further simplify this last expression by canceling some common factors, there appears to be no analytical solution for g in this case and we must resort again to numerical methods for a solution. Figure 4.6 shows the numerically derived values for g that minimize the approximate bit error rate expression at each point in the SNR-space for the cases when $\rho = 0.2$, $\rho = 0.5$ and $\rho = 0.8$.

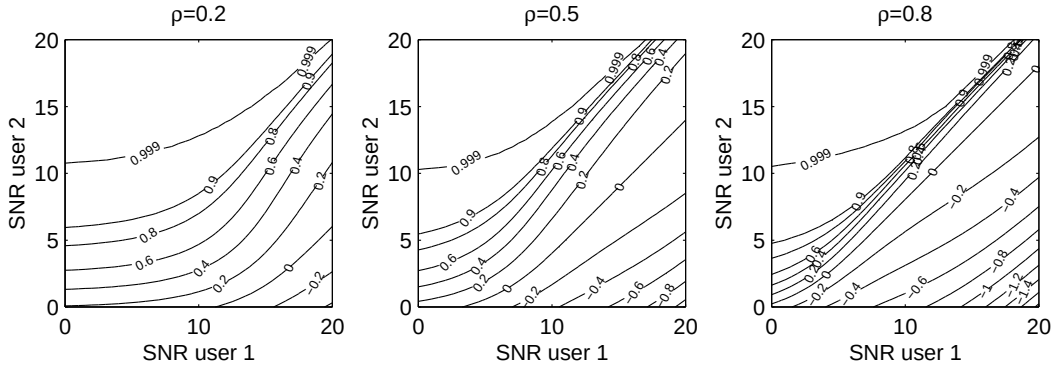

Figure 4.6: Approximate bit error rate optimum partial cancellation factor g.

Figure 4.6 shows that, when the approximate expression is used for the bit error rate of the PC-HPIC detector, the optimum value of g is computed to be negative in some cases, especially in the "southeast" corner of the plots for the cases where $\rho = 0.5$ and $\rho = 0.8$. This is in contrast to the optimum values of g numerically determined for the exact PC-HPIC bit error rate expression which appear to always lie in the interval $[0, 1]$.

Approximate SINR Optimization

The third approach to computing the optimum partial cancellation factors posed in this section is to select partial cancellation factors which maximize the output SINR of the PC-HPIC detector. Unlike the two prior cases, we will show that,

under the"normal-operating" assumptions described in Section 2.2.2 that are well justified unless the error probabilities at the output of the matched filter detector are high, we can write a very simple closed form solution for the optimum partial cancellation factor that maximizes the output SINR of the PC-HPIC detector.

The first step in the analysis is to modify the SINR expression (2.11), originally posed for the full cancellation HPIC detector, to account for the partial cancellation factor inherent in the PC-HPIC detector. In the two-user case with user one designated as the desired user, (2.11) can be written as

$$\mathrm{SINR}^{(1)}_{\mathsf{PC-HPIC}} = \frac{\left(a^{(1)}b^{(1)} + \rho a^{(2)}\Psi_2\right)^2}{(\rho a^{(2)})^2\Omega_{22} + 2\sigma\rho a^{(2)}\Phi_{21} + \sigma^2}$$

where

$$\begin{aligned}
\Psi_2 &\triangleq \mathrm{E}[\epsilon^{(2)} \,|\, b^{(1)}], \\
\Omega_{22} &\triangleq \mathrm{E}[(\epsilon^{(\ell)})^2 \,|\, b^{(1)}] - \Psi_2^2, \text{ and} \\
\Phi_{21} &\triangleq \mathrm{E}[\epsilon^{(2)} n^{(1)} \,|\, b^{(1)}]
\end{aligned}$$

with $\epsilon^{(2)} \triangleq b^{(2)} - g\mathrm{sgn}(y^{(2)})$. Note that (2.11) holds here with the modification that $\epsilon^{(2)}$ accounts for the partial cancellation factor of the PC-HPIC detector. We assume that the error probabilities of the matched filter bank are sufficiently low such that the three independence assumptions discussed in Section 2.2.2 hold. As in the case with the full cancellation HPIC detector, the independence assumptions imply here that $\Psi_2 \approx 0$ and $\Phi_{21} \approx 0$ for the PC-HPIC detector. The remaining term requiring calculation is Ω_{22} which, using the assumptions and the prior approximation on Ψ_2, can be derived as

$$\begin{aligned}
\Omega_{22} &\approx \mathrm{E}[(\epsilon^{(2)})^2] - 0 \\
&\approx (1+g)^2 P^{(2)}_{\mathsf{MF}} + (1-g)^2(1 - P^{(2)}_{\mathsf{MF}}) \\
&\approx 1 + (4P^{(2)}_{\mathsf{MF}} - 2)g + g^2
\end{aligned}$$

where $P_{\mathsf{MF}}^{(2)} = P(b^{(2)} \neq \mathrm{sgn}(y^{(2)}))$ denotes the probability of error of user two's matched filter output. Note that this last expression is consistent with both the full cancellation HPIC results when $g = 1$ and the MF results when $g = 0$. Under these approximations, user one's SINR at the output of the PC-HPIC detector may then be written as

$$\mathrm{SINR}_{\mathsf{PC-HPIC}}^{(1)} = \frac{\alpha^{(1)}}{r\alpha^{(2)}[1 + (4P_{\mathsf{MF}}^{(2)} - 2)g + g^2] + 1} \tag{4.5}$$

where $\alpha^{(k)} = (a^{(k)}/\sigma)^2$ is the normalized power (or SNR) of the k^{th} user and $r = \rho^2$ is the squared crosscorrelation of the users' signature waveforms.

It is now straightforward to find the value of g that maximizes (4.5). We can use the trick that the value of g that maximizes the SINR is equivalent to the value of g that minimizes the inverse of the SINR, or specifically

$$g = \arg\min_x \left\{ r\frac{\alpha^{(2)}}{\alpha^{(1)}}[1 + (4P_{\mathsf{MF}}^{(\ell)} - 2)x + x^2] + \frac{1}{\alpha^{(1)}} \right\}. \tag{4.6}$$

Taking the derivative with respect to x and setting it equal to zero, we can explicitly write the SINR maximizing value of the partial cancellation factor as

$$g = 1 - 2P_{\mathsf{MF}}^{(2)}.$$

This expression is intuitive in the sense that if user two's matched filter error probability is zero, then $g = 1$ and full cancellation is performed. On the other hand, if the user two's matched filter error probability is poor, say $1/2$, then $g = 0$ and no cancellation is performed. This expression even makes sense in the unusual case when the user two's matched filter error probability is equal to one where, due to the binary nature of the user's symbols, the matched filter always makes decisions that are the opposite sign of the correct decision. In this case, $g = -1$ which implies that the PC-HPIC detector will perform full cancellation of the

negative of the matched filter decision. But this is equivalent to performing full cancellation with the correct decision.

We also note that (4.6) is identical to the "optimum amplitude estimate" derived in the context of a "feedback cancellation CDMA receiver" in [AZJ95]. In [AZJ95], the authors analyzed a detector with similar structure to the HPIC detector and derived an amplitude estimate for each user that minimizes the mean squared value of the cancellation residue, defined under the notation of this chapter as $\mathrm{E}[(b^{(2)} - g\mathrm{sgn}(y^{(2)}))^2]$. Their results imply that the SINR maximizing partial cancellation factors also minimize the cancellation residue power, which also follows intuitively from (4.5).

Figure 4.7 plots the approximate SINR maximizing values of g in the two-user case at each point in the SNR-space for the cases when $\rho = 0.2$, $\rho = 0.5$ and $\rho = 0.8$. The plots assume that the bit error rate of the MF detector is given by the uncoded MF detector bit error rate in (4.2) with variables swapped between users one and two to represent user two's bit error rate. The results are intuitively satisfying since little or no cancellation is specified in the "southeast" corners of the plots and approximately full cancellation is specified in the "northwest" corners of the plots, as expected.

Unlike the two prior cases where we showed that computation of the partial cancellation factors that minimize the exact or approximate bit error rate expressions was difficult even in the two-user case and we did not attempt to compute partial cancellation factors when $K > 2$, the SINR maximizing partial cancellation factor analysis does in fact extend quite easily to the $K > 2$ case. Using the independence assumptions to state that $\Omega_{k\ell} \approx 0$ for all $k \neq \ell$ and $\ell \neq 1$ and $m \neq 1$, we

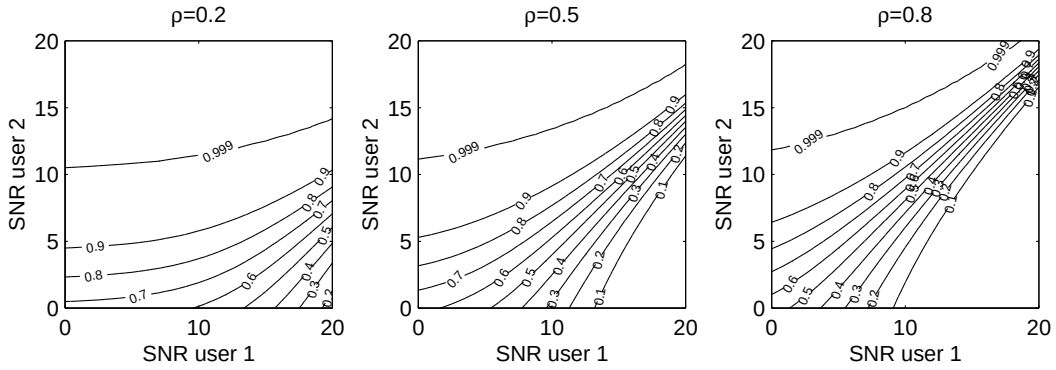

Figure 4.7: Approximate SINR optimum partial cancellation factor g.

can extend (4.5) to the general K-user case to write

$$\text{SINR}^{(1)}_{\text{PC}-\text{HPIC}} \;=\; \frac{\alpha^{(1)}}{\sum\limits_{k=2}^{K} r_{1k}\alpha^{(k)}[1+(4P^{(k)}_{\text{MF}}-2)g_k+g_k^2]+1} \tag{4.7}$$

where $r_{1k} = \rho^2_{1k}$ denotes the squared crosscorrelation of user one and user k's signature waveforms. It can be shown that the values of $\{g_k\}_{k=1}^K$ that maximize (4.7) are equivalent to the values of $\{g_k\}_{k=1}^K$ that minimize the summation in the denominator. Moreover, it is evident that each g_k multiplies only one element in the summation, hence the values of $\{g_k\}_{k=1}^K$ may be chosen *independently* in order to minimize the summation in the denominator. These facts lead to the SINR maximizing value of the k^{th} user's partial cancellation factor as

$$g_k \;=\; 1-2P^{(k)}_{\text{MF}}. \tag{4.8}$$

An important feature of the SINR maximizing partial cancellation factors is that their values are independent of the user for which the SINR is maximized. Hence, the set of partial cancellation factors that maximizes the SINR for user one also maximizes the SINR for all other users in the system. But the primary advantage of this SINR maximizing approach is that, if the receiver can form good estimates

of the bit error rates at the output of the matched filter bank, computation of the optimum partial cancellation factors is straightforward in this case for an *arbitrary number of users*. This is in contrast to the results in the prior sections where we showed that computing the exact or approximate bit error rate minimizing partial cancellation factors was quite difficult even in the two-user case.

In the next section, we examine the performance of the PC-HPIC detector with partial cancellation factors chosen according to each of the three methods presented here.

4.1.3 PC-HPIC Performance Comparison

Rather than directly plotting the bit error rates of the PC-HPIC detector with partial cancellation factors chosen from the three methods presented in the prior section, in this section we instead plot the bit error rate performance *gain* of the PC-HPIC detector with respect to the full cancellation HPIC detector in Figures 4.8, 4.9, and 4.10 for the cases when $\rho = 0.2$, $\rho = 0.5$ and $\rho = 0.8$, respectively. A value of x on these contour plots denotes a point in SNR-space where the PC-HPIC detector has a bit error rate x times *less* than the full cancellation HPIC detector.

These results show that, as expected, the PC-HPIC detector does not provide any real performance gain over the full cancellation HPIC detector in the "northwest" corner of the SNR-space but that PC-HPIC can provide significant performance gains in regions on the "east" side of the SNR-space. The PC-HPIC detectors with partial cancellation factors chosen via minimization of the exact bit error rate expression and maximization of the approximate SINR expression remarkably yield similar performance despite large gaps in the complexity of can-

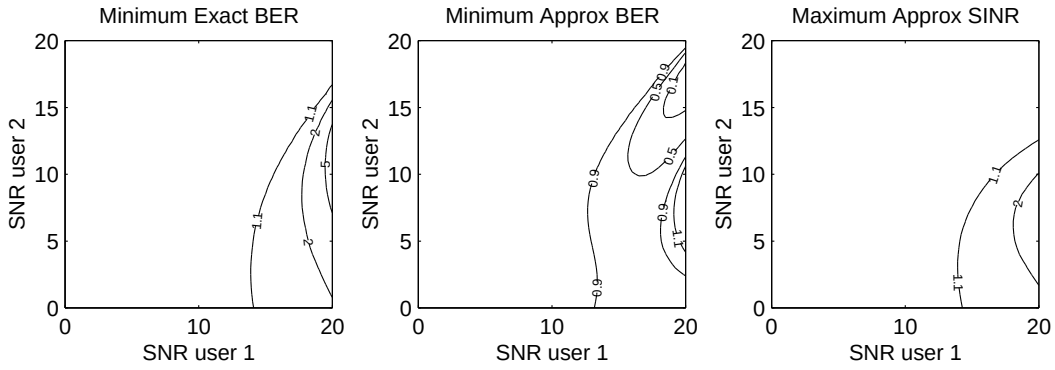

Figure 4.8: PC-HPIC bit error rate performance gains for user one with respect to the full cancellation HPIC detector for the two-user case when $\rho = 0.2$

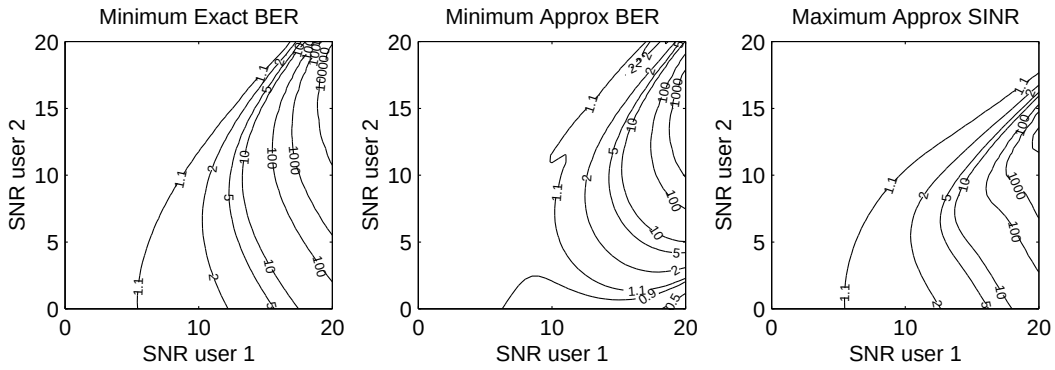

Figure 4.9: PC-HPIC bit error rate performance gains for user one with respect to the full cancellation HPIC detector for the two-user case when $\rho = 0.5$

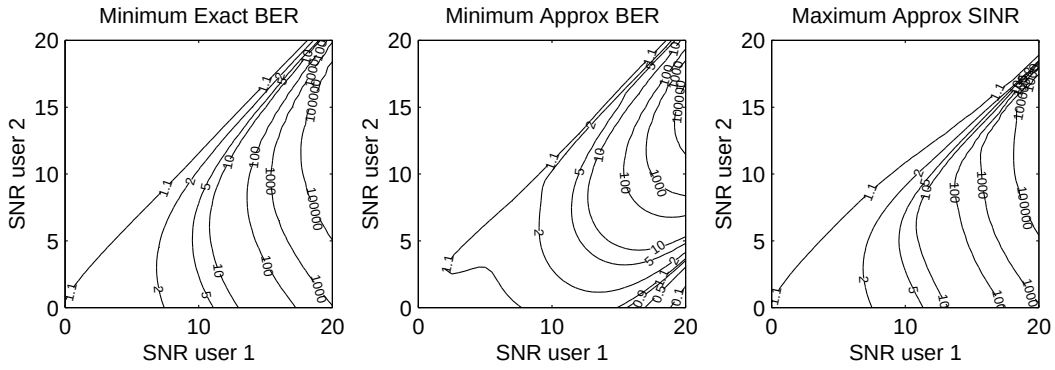

Figure 4.10: PC-HPIC bit error rate performance gains for user one with respect to the full cancellation HPIC detector for the two-user case when $\rho = 0.8$

cellation factor computation. Despite the approximations imposed in the SINR maximizing partial cancellation factors, these results show that the PC-HPIC detector with SINR maximizing partial cancellation factors tends to yield equal or better performance than the full cancellation HPIC detector at all tested points in the SNR-space. On the other hand, the PC-HPIC detector with partial cancellation factors selected via minimization of the approximate bit error rate criterion do not always lead to improved performance as can be seen in Figure 4.8 where there are contours with value below one indicating a degradation in bit error rate performance.

We also note that the PC-HPIC detector with partial cancellation factors selected via maximization of the approximate SINR criterion does not provide any tangible performance gain in the two-user, equal power case. In Figures 4.9 and 4.10, it is evident that both the minimum exact BER and minimum approximate BER PC-HPIC detectors yield significant performance gains on the equal power line ($\text{SNR}^{(1)} = \text{SNR}^{(2)}$) in the high-SNR "northeast" corner of the SNR-space. The maximum approximate SINR PC-HPIC detector does not provide any

performance gain in this region. Moreover, the maximum approximate SINR PC-HPIC detector yields only marginal performance gains (less than a factor of 2) at any point on the equal power line in the cases considered.

4.2 Soft Cancellation PIC

As first discussed in [VA91] with regards to the multistage detector, the HPIC detector has the desirable property that, given a desired user of arbitrary index k, if the bit estimates of the interfering users $\ell \neq k$ are equal to the optimum joint maximum likelihood (JML) estimates then it can be shown that the HPIC detector yields the JML estimate for the desired user. This result suggests that there is a linkage between the quality of the estimates used for interference cancellation and the output performance (e.g., BER or SINR) of the PIC detector. Further reinforcing this intuition, Section 3.6.1 of this dissertation analyzed the mean squared error (MSE) of the interference estimators for the unmodified two-stage HPIC and LPIC detectors. Simulations suggested that interference estimates with lower MSE result in better bit error rate performance for PIC detection.

In this section, we take this idea a step further. Specifically, we consider consider the case when the ℓ^{th} user's interference estimate is generated by the Bayesian minimum mean squared error (BMMSE) [Kay93] estimator given the observation $y^{(\ell)}$. The problem is to find a closed form expression for the nonlinear function, or estimator, yielding the BMMSE estimates. We call the particular performance adaptive PIC detector the soft cancellation parallel interference cancellation (SC-PIC) detector. From (1.2), we can write the decision statistic of the SC-PIC

detector as

$$y^{(k)}_{\mathsf{SC-PIC}} = a^{(k)}b^{(k)} + \sum_{\ell \neq k} \rho_{k\ell}\left[a^{(\ell)}b^{(\ell)} - f^{(\ell)}_{\mathsf{SC-PIC}}(y^{(\ell)})\right] + \sigma n^{(k)}$$

where $f^{(\ell)}_{\mathsf{SC-PIC}}(y^{(\ell)})$ is the nonlinear Bayesian MMSE estimator of $a^{(\ell)}b^{(\ell)}$ given the observation $y^{(\ell)}$. The Bayesian MMSE estimator is derived in the following section followed by a discussion on performance analysis and simulation results.

4.2.1 Bayesian MMSE Interference Estimation

Given the soft matched filter output of the ℓ^{th} user, denoted as $y^{(\ell)}$, as an observation for $a^{(\ell)}b^{(\ell)}$, the optimum estimator for $a^{(\ell)}b^{(\ell)}$ in terms of minimizing the Bayesian MSE [Kay93, pp. 313] is the mean of the posterior pdf of $a^{(\ell)}b^{(\ell)}$, given as

$$\begin{aligned} f^{(\ell)}_{\mathsf{SC-PIC}}(y^{(\ell)}) &= E\left[a^{(\ell)}b^{(\ell)} \,|\, y^{(\ell)}\right] \\ &= a^{(\ell)}E\left[b^{(\ell)} \,|\, y^{(\ell)}\right] \end{aligned}$$

since $a^{(\ell)}$ is assumed constant and known. We can write

$$\begin{aligned} E\left[b^{(\ell)} \,|\, y^{(\ell)}\right] &= \int b g(b \,|\, y^{(\ell)})\, db \\ &= (-1)P(b=-1 \,|\, y^{(\ell)}) + (+1)P(b=+1 \,|\, y^{(\ell)}) \\ &= (-1)\frac{\frac{1}{2}g(y^{(\ell)} \,|\, b^{(\ell)}=-1)}{f(y^{(\ell)})} + (+1)\frac{\frac{1}{2}g(y^{(\ell)} \,|\, b^{(\ell)}=+1)}{f(y^{(\ell)})} \end{aligned}$$

where $g(y^{(\ell)} \,|\, b^{(\ell)})$ is the conditional pdf of the ℓ^{th} user's matched filter observation given the ℓ^{th} user's bit and where the last equality is a result of the application of Bayes' rule. In the synchronous, K-user case,

$$g(y^{(\ell)} \,|\, b^{(\ell)}=-1) = \frac{1}{2^{K-1}}\frac{1}{\sqrt{2\pi}\sigma}\sum_{\boldsymbol{u}\in\mathcal{B}^-}\exp\left(\frac{-(y^{(\ell)} - \boldsymbol{r}_\ell^\top \boldsymbol{A}\boldsymbol{u})^2}{2\sigma^2}\right)$$

and

$$g(y^{(\ell)} \mid b^{(\ell)} = +1) = \frac{1}{2^{K-1}} \frac{1}{\sqrt{2\pi}\sigma} \sum_{\boldsymbol{u} \in \mathcal{B}^+} \exp\left(\frac{-(y^{(\ell)} - \boldsymbol{r}_\ell^\top \boldsymbol{A}\boldsymbol{u})^2}{2\sigma^2} \right)$$

where $\mathcal{B}^-$ ($\mathcal{B}^+$) is the set of cardinality 2^{K-1} of all possible binary vectors $\boldsymbol{b}$ such that $b^{(\ell)} = -1$ ($b^{(\ell)} = +1$) and where $\boldsymbol{r}_\ell^\top$ is the ℓ^{th} row of the signature correlation matrix $\boldsymbol{R}$. The unconditional pdf of $y^{(\ell)}$ can also be written as

$$g(y^{(\ell)}) = \frac{1}{2^K} \frac{1}{\sqrt{2\pi}\sigma} \sum_{\boldsymbol{u} \in \mathbb{B}^K} \exp\left(\frac{-(y^{(\ell)} - \boldsymbol{r}_\ell^\top \boldsymbol{A}\boldsymbol{u})^2}{2\sigma^2} \right)$$

where $\mathbb{B}^K = \{\pm 1\}^K$ is the set of cardinality 2^K of all possible binary K-vectors. Hence, the exact expression for the Bayesian MMSE estimator of $b^{(\ell)}$ can be written as

$$\begin{aligned} f^{(\ell)}_{\mathsf{SC-PIC}}(y^{(\ell)}) &= a^{(\ell)} \frac{\sum_{\boldsymbol{u} \in \mathcal{B}^+} \exp\left(\frac{-(y^{(\ell)} - \boldsymbol{r}_\ell^\top \boldsymbol{A}\boldsymbol{u})^2}{2\sigma^2} \right) - \sum_{\boldsymbol{u} \in \mathcal{B}^-} \exp\left(\frac{-(y^{(\ell)} - \boldsymbol{r}_\ell^t op \boldsymbol{A}\boldsymbol{u})^2}{2\sigma^2} \right)}{\sum_{\boldsymbol{u} \in \mathbb{B}^K} \exp\left(\frac{-(y^{(\ell)} - \boldsymbol{r}_\ell^\top \boldsymbol{A}\boldsymbol{u})^2}{2\sigma^2} \right)} \\ &= a^{(\ell)} \frac{\sum_{\boldsymbol{u} \in \mathbb{B}^K} u^{(\ell)} \exp\left(\frac{-(y^{(\ell)} - \boldsymbol{r}_\ell^\top \boldsymbol{A}\boldsymbol{u})^2}{2\sigma^2} \right)}{\sum_{\boldsymbol{u} \in \mathbb{B}^K} \exp\left(\frac{-(y^{(\ell)} - \boldsymbol{r}_\ell^\top \boldsymbol{A}\boldsymbol{u})^2}{2\sigma^2} \right)}. \end{aligned} \tag{4.9}$$

This last expression shows that a fundamental difference between SC-PIC and PC-HPIC is that the SC-PIC interference estimates in (4.9) use the soft decision statistic $y^{(\ell)}$ whereas PC-HPIC interference estimates in (4.1) use the hard decision statistic $\mathrm{sgn}(y^{(\ell)})$. Specifically, the PC-HPIC detector forms interference estimates based on a linear scaling of the observation $\mathrm{sgn}(y^{(\ell)})$ where the linear scale factor (also called the partial cancellation factor) reflects the average reliability of the decision statistic computed from the operating conditions $a^{(1)}$, $a^{(2)}$, ρ, and σ. The information in the soft decision statistic $y^{(\ell)}$ is not used. Like the PC-HPIC detector, the SC-PIC detector forms scaled interference estimates based on the averaged reliability information available from the assumed known quantities $a^{(1)}$, $a^{(2)}$, ρ, and σ, but SC-PIC explicitly uses the soft observation $y^{(\ell)}$ rather than $\mathrm{sgn}(y^{(\ell)})$.

Unfortunately, the complexity of the estimator given in (4.9) is quite high since the detector must compute 2^K values *for each user* to calculate the numerator and denominator. This prevents direct application to systems with more than a handful of users. One simplified approach would be to impose a Gaussian approximation on the multiple access interference in the matched filter detector's output. Specifically, the matched filter detector's output for the ℓ^{th} user can be written as

$$\begin{aligned} y^{(\ell)} &= a^{(\ell)}b^{(\ell)} + \sum_{k\neq\ell} \rho_{\ell k} a^{(k)} b^{(k)} + \sigma n^{(\ell)} \\ &= a^{(\ell)}b^{(\ell)} + I^{(\ell)} \end{aligned}$$

and the Gaussian approximation implies that $I^{(\ell)} \sim \mathcal{N}(0, \sigma^2_{I^{(\ell)}})$ where

$$\sigma^2_{I^{(\ell)}} = \sum_{k\neq\ell} (\rho_{\ell k} a^{(k)})^2 + \sigma^2.$$

Using the Gaussian approximation, the prior analysis can be repeated to yield the estimator minimizing the Bayesian MSE as

$$\hat{b}^{(\ell)}_{\mathsf{BMMSE}} = \tanh\left(\frac{a^{(\ell)} y^{(\ell)}}{\sigma^2_{I^{(\ell)}}}\right). \tag{4.10}$$

Although the Gaussian approximation has been shown to be a tool of questionable merit (see [PV97]) for analysis of the bit error rate of most multiuser detectors, in this case the Gaussian approximation is applied as a soft cancellation heuristic in order to avoid the complexity of calculating the exact soft cancellation function given in (4.9). A simulated example of the approximate Bayesian MMSE estimator's performance with respect to the exact Bayesian MMSE estimator for the case of 8 equal power users at 10dB SNR in a system with binary random spreading sequences of length 16 is shown in Figure 4.11. This figure suggests that the performance penalty incurred by the approximate BMMSE estimator can be quite small in most cases.

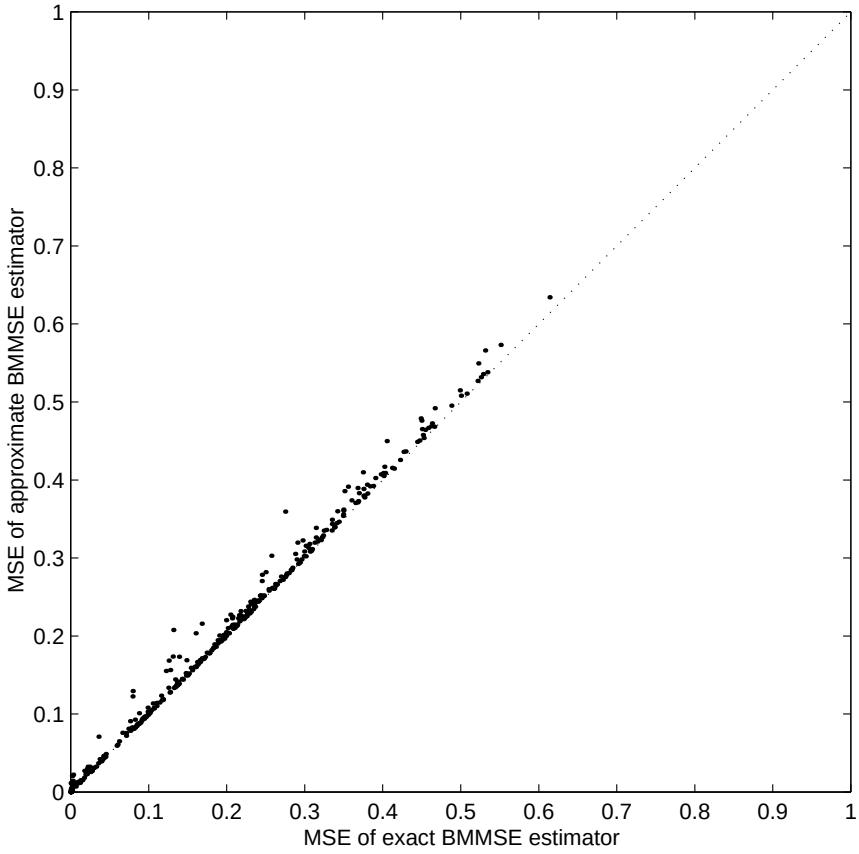

Figure 4.11: Comparison of exact (4.9) and approximate (4.10) BMMSE estimators.

Another nice feature of the approximate Bayesian MMSE estimator is that, at least in the case when the signature sequences are fixed and the channel is fixed or slowly time varying, the term $\sigma_{I^{(\ell)}}$ could be estimated at the receiver without explicit knowledge of all of the user amplitudes and signature crosscorrelation factors since $\sigma_{I^{(\ell)}}$ is simply the variance of the k^{th} user's matched filter output conditioned on $b^{(k)}$.

4.2.2 SC-PIC Performance

Analytical bit error rate results for the SC-PIC detector are difficult to obtain even in the two-user approximate BMMSE case since computation of bit error rate requires two-dimensional integration of the joint Gaussian pdf over complicated nonrectangular regions. As in [DSR98], we must resort to simulations to demonstrate the performance of the SC-PIC detector. Moreover, since the simulations are accurate only for bit error rates greater than 10^{-7}, it would be misleading to plot the performance gain (as a ratio of bit error rates) of the SC-PIC detector with respect to the full cancellation HPIC detector as done in the prior sections for the PC-HPIC detector. Instead, we plot the bit error rate contours (for values greater than 10^{-6}) of the SC-PIC, PC-HPIC, and full cancellation HPIC detectors directly for comparison.

Figures 4.12, 4.13, and 4.14 compare the simulated bit error rate performance of the SC-PIC detector in the two-user case when $\rho = 0.2$, $\rho = 0.5$, and $\rho = 0.8$, respectively. The exact Bayesian MMSE estimates (4.9) were used in this case since the two-user problem is not prohibitively complex. The SC-PIC bit error rate figures are presented next to the bit error rate results for the PC-HPIC detector with exact bit error rate minimizing partial cancellation factors and the

full cancellation HPIC detector for comparison.

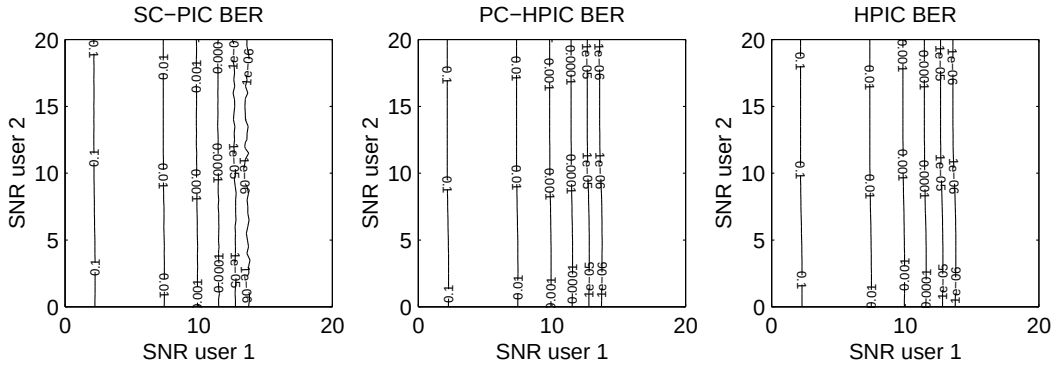

Figure 4.12: Bit error rate of user one comparison of SC-PIC, PC-HPIC (minimum exact BER), and full cancellation HPIC detectors when $\rho = 0.2$.

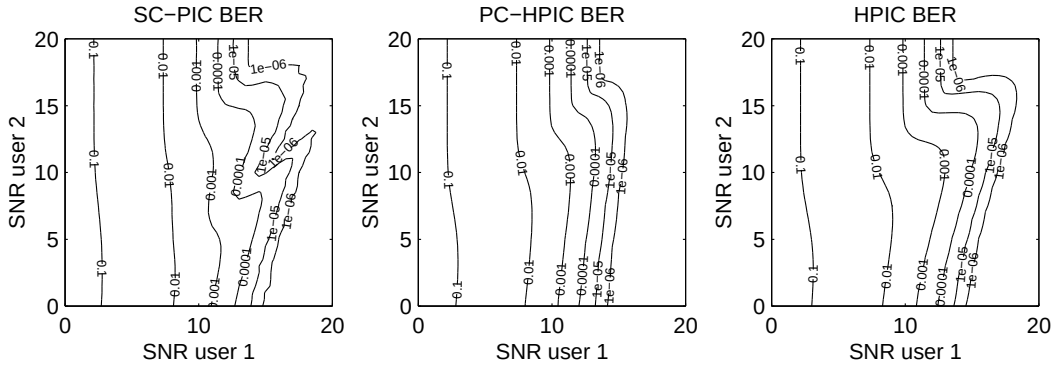

Figure 4.13: Bit error rate of user one comparison of SC-PIC, PC-HPIC (minimum exact BER), and full cancellation HPIC detectors when $\rho = 0.5$.

These results suggest that the HPIC, PC-HPIC, and SC-PIC detectors all perform approximately the same in the $\rho = 0.2$ case and performance differences are more significant for higher values of ρ. Figures 4.15 and 4.16 show the regions in SNR-space where the SC-PIC detector performs better or worse than the PC-HPIC and full cancellation HPIC detectors for the cases when $\rho = 0.5$ and $\rho = 0.8$.

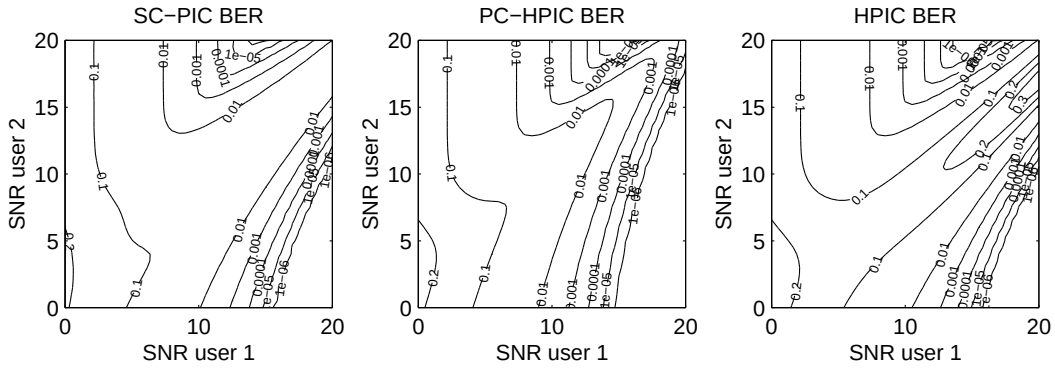

Figure 4.14: Bit error rate of user one comparison of SC-PIC, PC-HPIC (minimum exact BER), and full cancellation HPIC detectors when $\rho = 0.8$.

Due to the fact that the SC-PIC bit error rates were generated by simulations, the plots show several distinct regions:

- Regions marked "SC-PIC" are regions where SC-PIC has better (lower) bit error rate performance than the PIC detector to which it is compared.
- Regions marked "PC-HPIC" are regions where PC-HPIC has better (lower) bit error rate performance than SC-PIC.
- Regions marked "HPIC" are regions where HPIC has better (lower) bit error rate performance than SC-PIC.
- Regions with light shading are regions where the SC-PIC bit error rate simulation data is inconclusive and we are unable to say that one algorithm outperforms another with reasonable confidence.
- Regions with dark shading are regions where SC-PIC and the PIC detector to which it is compared both exhibit good performance with bit error rates less than 10^{-5}. In these regions, the simulation data is also inconclusive in

terms of ranking the performance of the algorithms.

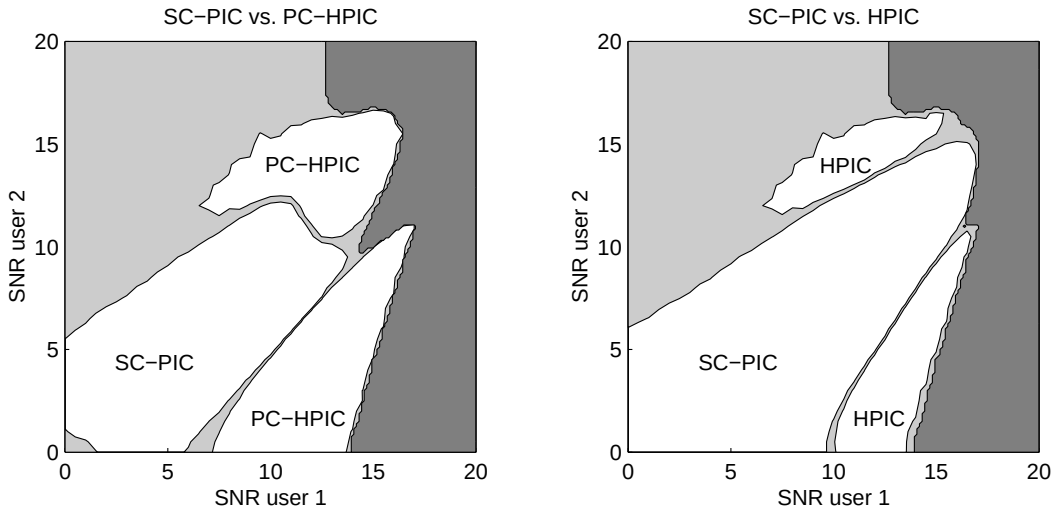

Figure 4.15: Bit error rate comparison between SC-PIC and PC-HPIC (minimum exact BER) and SC-PIC and full cancellation HPIC detector when $\rho = 0.5$.

The figures show that, unlike the minimum exact bit error rate PC-HPIC detector, the SC-PIC detector actually can perform worse than the full cancellation HPIC detector in some regions of the two-user SNR space. The SC-PIC detector tends to offer better performance in the case where both users SNRs are similar and when their SNRs are relatively low. The reason for this may be due to the fact that minimizing the Bayesian MSE of the multiple access interference estimates is an inaccurate proxy for optimizing the bit error rate in the two-user case when both users have high SNR. Large regions of SNR space are marked as inconclusive either due to the fact that the regions exhibit very low bit error rates that are difficult to accurately estimate via simulation or due to the fact that both of the detectors' bit error rates may be quite close in these regions.

In the two-user case, the result that the SC-PIC detector performs even better

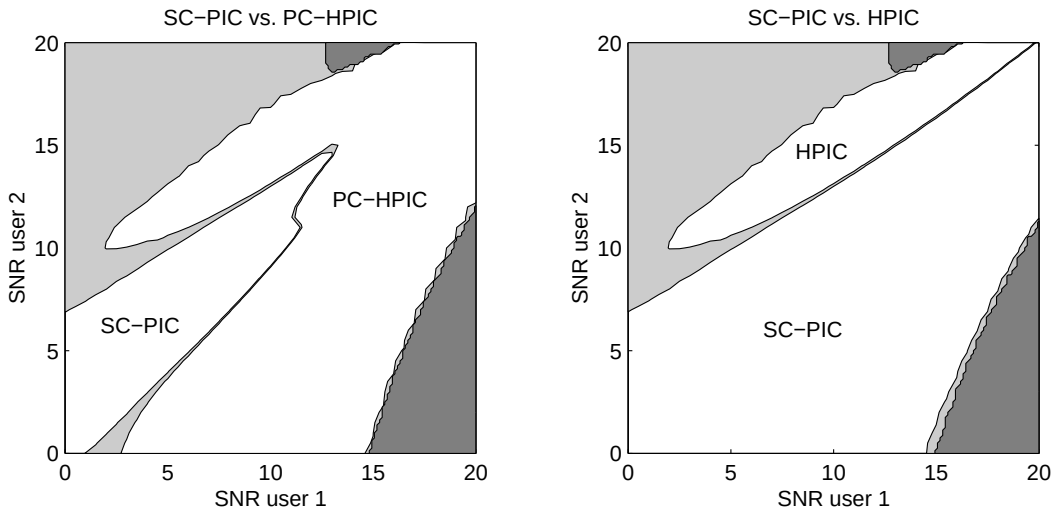

Figure 4.16: Bit error rate comparison between SC-PIC and PC-HPIC (minimum exact BER) and SC-PIC and full cancellation HPIC detector when $\rho = 0.8$.

in terms of bit error rate than the bit error rate optimized PC-HPIC detector in some regions of SNR-space may seem counterintuitive at first but it actually illustrates the important difference between the SC-PIC and PC-HPIC approaches to improving HPIC performance. The interference estimates in the PC-HPIC detector are constrained to the form $g_\ell \text{sgn}(y^{(\ell)})$ and g_ℓ is optimized based on knowledge of the user amplitudes, signature crosscorrelations, and noise power. These quantities are all fixed and do give a measure of the *average* reliability of the interfering user's bit estimate, but the PC-HPIC detector does not use the soft matched filter output which gives a measure of the *instantaneous* reliability of the bit estimate. These results suggest that the functional constraint imposed on the interfering bit estimates of the PC-HPIC detector, although certainly leading to improved performance with respect to the full cancellation HPIC detector and better performance in some cases than the SC-PIC detector, may not lead to the best possible performance. A better approach would be to write the interference estimates in the form

$f(y^{(\ell)})$ where f is an estimator selected to optimize some performance measure. The SC-PIC detector selects f such that the Bayesian MSE of the interference estimate is optimized. More sophisticated choices for f such as an f that minimizes the output bit error rate of the PIC detector remain an open problem.

Figures 4.17 and 4.18 show the simulated mean bit error rates and SINR, respectively, of several detectors in the case of 8 equipower users in a system with random binary spreading sequences of length 32. The SC-PIC detector uses the approximate Bayesian MMSE estimates (4.10) and the PC-HPIC detector uses the SINR maximizing partial cancellation factors (4.8) in these simulations. Figure 4.17 shows that the Divsalar [DSR98], PC-HPIC, and SC-PIC detectors can all improve the BER performance of the HPIC detector but that the Divsalar scheme is sensitive to the ad-hoc choice of partial cancellation factor. Figure 4.18 shows that the Divsalar detectors can actually exhibit worse SINR performance than the full cancellation HPIC detector and that only the PC-HPIC and SC-PIC detectors improve the SINR performance of HPIC detection in this case. This may be an important consideration if the multiuser detector outputs are to be used by a channel decoder. Unlike the PC-HPIC approach where an optimum individual partial cancellation factor is computed for each user at each new bit interval due to the changing signature crosscorrelations, the Divsalar detectors in these simulations use a single, fixed, ad-hoc partial cancellation factor for all users irrespective of the signature crosscorrelations. The PC-HPIC detector performs somewhat better than the HPIC detector in terms of BER and SINR but actually exhibits worse BER performance than one of the Divsalar detectors, perhaps due to the evidence seen in the two-user case where the SINR maximizing PC-HPIC detector does not offer much BER performance gain when users are received with

equal power. The SC-PIC detector, even with the approximate Bayesian MMSE interference estimates, is uniformly superior to the other detectors in both BER and SINR in the cases considered.

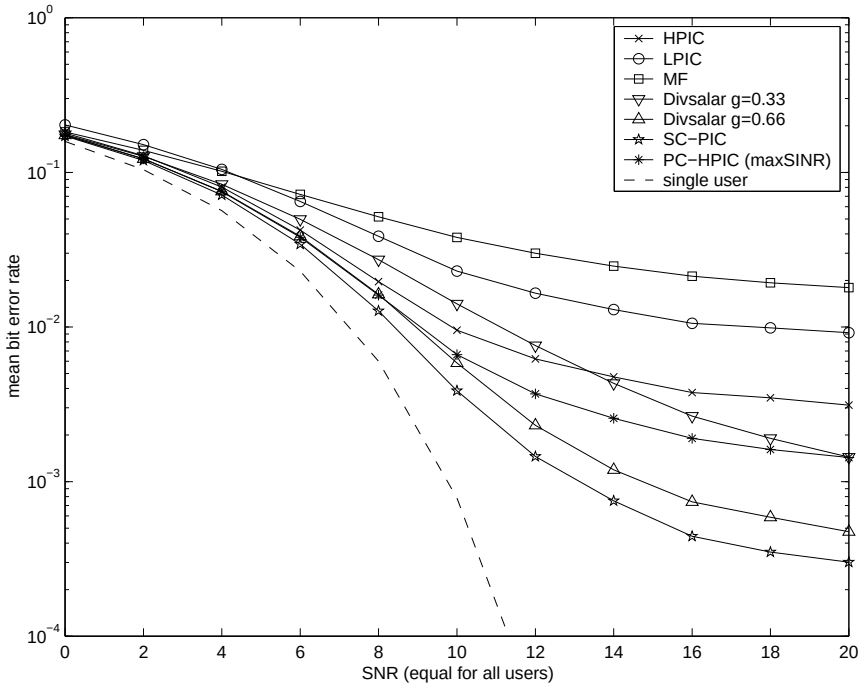

Figure 4.17: Mean bit error rate for various multiuser detectors in a scenario with 8 equipower users with length-32 random spreading sequences.

Figures 4.19 and 4.20 show the simulated mean bit error rates and SINR, respectively, of the same detectors in the case of $K \in \{2, \ldots, 12\}$ equipower users in a system with random binary spreading sequences of length 16. The SC-PIC detector uses the approximate Bayesian MMSE estimates (4.10) and the PC-HPIC detector uses the SINR maximizing partial cancellation factors (4.8) in these simulations. In both figures, the LPIC detector shows particularly poor performance as the number of users increases, consistent with the results of Chapter 3. Also, in both figures, the SC-PIC detector shows uniformly superior BER and SINR perfor-

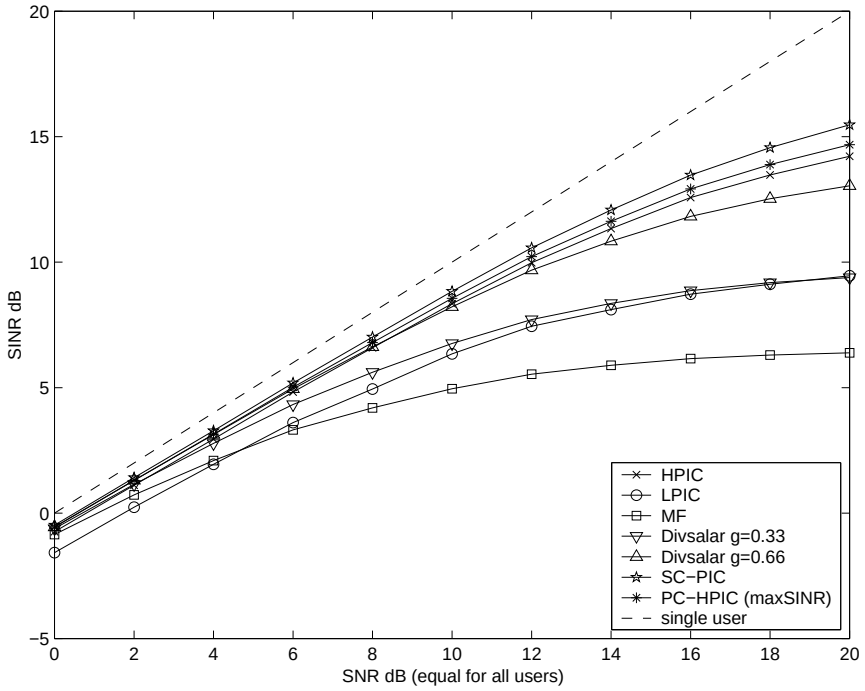

Figure 4.18: Mean SINR for various multiuser detectors in a scenario with 8 equipower users with length-32 random spreading sequences.

mance with respect to all of the other detectors in the cases considered, consistent with the results in Figures 4.17 and 4.18. In Figure 4.19, the SC-PIC, PC-HPIC, and Divsalar ($g = 0.66$) detectors all yield BER performance improvements with respect to the LPIC, HPIC, and MF detectors, except in the case when $K = 2$ where, somewhat surprisingly, the LPIC detector outperforms all but the SC-PIC detector. The Divsalar detector with $g = 0.66$ actually outperforms the PC-HPIC detector in terms of BER over the range of users considered, perhaps due to the reasons explained for Figures 4.17 and 4.18. In Figure 4.20, the PC-HPIC detector exhibits better SINR performance than either Divsalar detector as well as the full cancellation HPIC detector. The Divsalar detectors exhibit worse SINR performance than the full cancellation HPIC detector for small values of K.

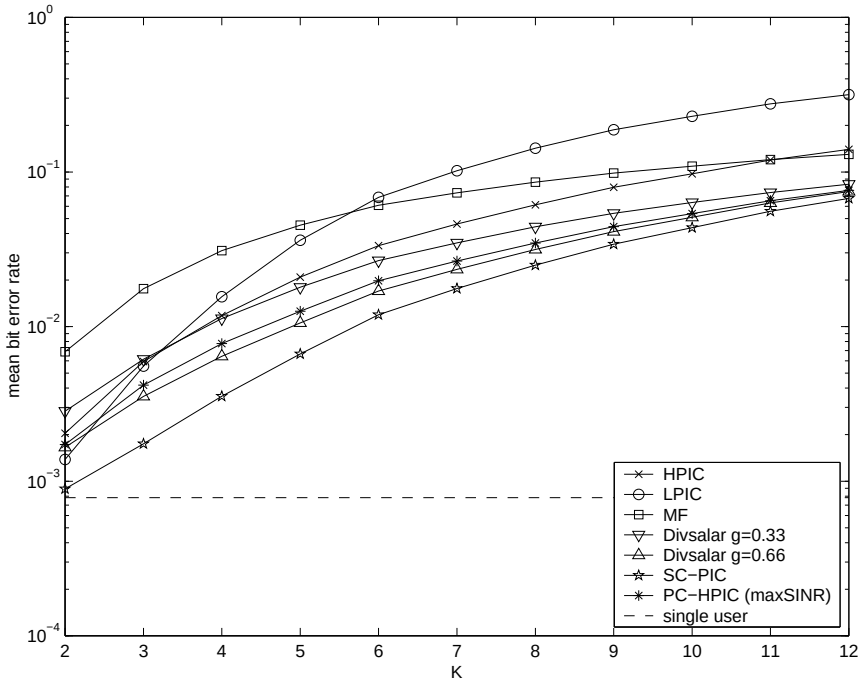

Figure 4.19: Mean bit error rate for various multiuser detectors in a scenario with K equipower users at 10dB SNR with length-16 random spreading sequences.

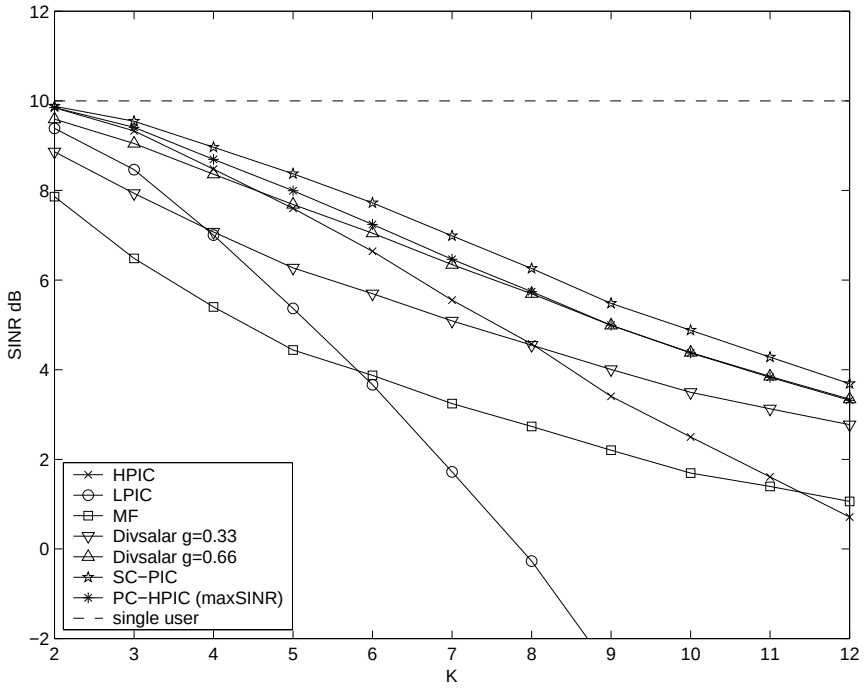

Figure 4.20: Mean SINR for various multiuser detectors in a scenario with K equipower users at 10dB SNR with length-16 random spreading sequences.

4.3 Conclusions

In this chapter we proposed two new approaches to improve the performance of PIC detection. Unlike the majority of the recent work on improved PIC performance that has focused on the LPIC detector, we considered nonlinear schemes that potentially offer superior performance to linear detectors. The results showed that the techniques did indeed, in most cases, yield improved bit error rate performance with respect to the HPIC, LPIC, and MF detectors. The PC-HPIC detector with SINR maximizing partial cancellation factors and the approximate Bayesian MMSE version of the SC-PIC detector appear to have the most promise in CDMA systems with more than two users due to their relatively low complexity and potential for high performance. The complexity of calculating the bit error rate minimizing PC-HPIC partial cancellation factors prevents its consideration in most practical cases and ad-hoc cancellation factors currently remain a computationally feasible, albeit suboptimum, alternative.

CHAPTER 5

APPLICATIONS OF MULTIUSER DETECTION: EAVESDROPPING IN THE IS–95 DOWNLINK

5.1 Introduction

IS–95 [Tel95] is a worldwide standard for Code Division Multiple Access (CDMA) digital cellular communication systems with over 50 million subscribers and installed systems in 6 continents. A mobile user in an IS–95 system typically demodulates the downlink transmission from their base station with a matched filter receiver and coherent multipath combining. Since 1986 when Verdu derived the optimum multiuser detector [Ver86] for CDMA communication systems and showed that multiuser detection receivers may significantly outperform the matched filter, there has been a great deal of research on suboptimum multiuser detection techniques for CDMA. Unfortunately, the majority of these multiuser detection receivers have been regarded as too complex for cost-effective implementation in IS–95 receivers.

In this chapter[1] we attempt to bridge the gap between multiuser detection receivers and the IS–95 downlink. In the context of a multi-cell environment, the IS–95 downlink presents a unique challenge not often considered in the multiuser detection literature: non-cyclostationary cochannel interference from neighboring base stations. This feature of the IS–95 downlink precludes the use of linear mul-

[1]The theoretical results presented in this chapter appeared in part in [BJP99] and are due to a collaborative effort with Professors H. Vincent Poor and Sergio Verdu of Princeton University during my visit to their department in February, 1999. The on-air data results presented in this chapter are due to a collaborative effort with Rich Gooch, Mariam Motamed, and David Chou of Applied Signal Technology in Sunnyvale, CA, during my visit to AST in April 1999.

tiuser detectors that use subspace tracking or adaptive gradient descent algorithms since the interference subspace changes at each symbol interval. Moreover, common linear multiuser detectors such as the decorrelating and MMSE detectors are also likely to be too complex for the IS–95 downlink since the non-cyclostationary cochannel interference forces the receiver to recompute linear transforms at every symbol interval.

The first goal of this chapter is to understand optimum multiuser detection in the context of the IS–95 downlink. Although the optimum detector is often too complex for implementation in realistic systems, its role is still important in order to determine the relative performance of suboptimum multiuser detectors. We find that the structure of the IS–95 downlink allows the optimum detector to be posed in a computationally efficient form with complexity exponentially less than a brute-force implementation.

The second goal of this chapter is to propose a computationally efficient nonlinear multiuser detector for the IS–95 downlink called the Group Parallel Interference Cancellation (GPIC) detector. The GPIC detector is derived from examination of properties of the reduced complexity optimum detector and also exploits the structure in the IS–95 downlink. Simulations of an IS–95 downlink eavesdropping scenario suggest that the GPIC detector offers near-optimum performance in the cases considered and provides the largest benefit when the desired signal is received in the presence of strong cochannel interference. We also examine a snapshot of actual on-air data from an active IS–95 system and present results that suggest that GPIC detection offers significant performance improvements when extracting weak signals in the presence of severe cochannel interference.

This balance of this chapter is organized as follows. In Section 5.2 we de-

velop a concise model with mild simplifying assumptions for the IS–95 downlink that includes the effects of the time and phase asynchronous, nonorthogonal, and non-cyclostationary transmissions of a B base station communication system. In Section 5.3 we use this model to examine the optimum (joint maximum likelihood) detector in the IS–95 downlink context. In Section 5.4 we examine the structure of the IS–95 downlink model to develop a reduced complexity optimum detector that has exponentially less complexity than the brute-force optimum detector. In Section 5.5 we develop the suboptimum GPIC detector with computational complexity similar to conventional matched filter detection. In Section 5.6 we examine the performance of the GPIC detector relative to the conventional matched filter and optimum detectors via simulation and show that the GPIC detector exhibits near-optimum performance in the cases we examined. Finally, in Section 5.7 we apply the GPIC detector to an on-air snapshot of data from an active IS–95 system to examine the potential for performance improvements in an eavesdropping scenario.

5.2 IS–95 Downlink System Model

Consider the simplified IS–95 downlink system model depicted in Figure 5.1 where B cellular base stations each transmit digital information to their local users. We denote $b \in 1, \ldots, B$ as the base station index and we denote K_b as the number of data streams simultaneously transmitted by the b^{th} base station, not including the pilot transmission. We note that K_b is typically greater than the actual number of physical users in the cell since the IS–95 standard specifies that each base station must transmit additional data streams for call setup, paging, and overhead infor-

mation. For the purposes of this chapter, we will henceforth refer to each of these data streams as a "user" even if the data stream is an overhead channel and not actually allocated to a particular user in the cell. The total number of users in the system is then $K = \sum_{b=1}^{B} K_b$.

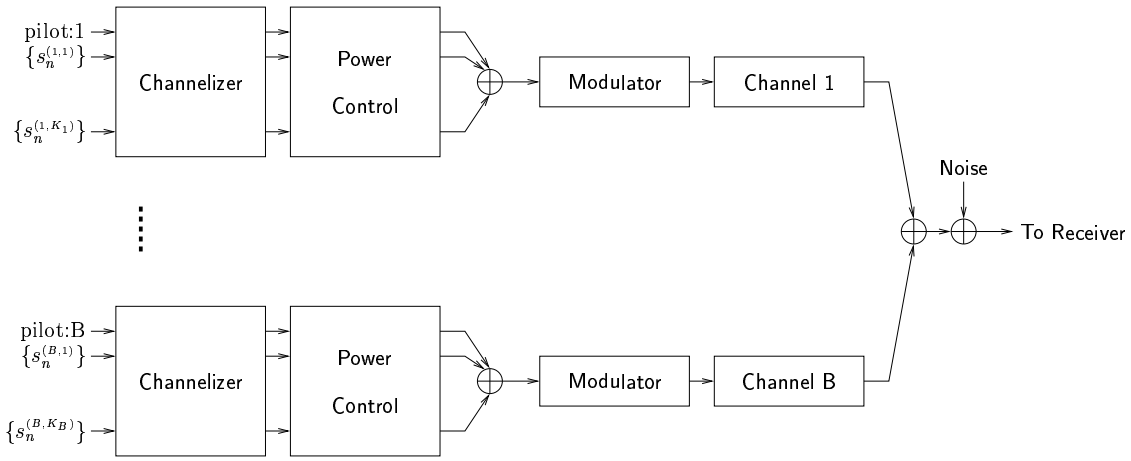

Figure 5.1: IS–95 digital cellular downlink system model.

In general, an IS–95 downlink receiver in the cell system observes each base station's aggregate transmission through an individual propagation channel (including multipath, delay, and attenuation) summed and corrupted by additive channel noise. In this model, we consider only the portion of the IS–95 system "inside the coders" in the sense that the transmitted symbols at the input to the channelization block are from the output of the repetition and convolutional coders as specified by the IS–95 standard. Although an actual IS–95 downlink receiver would also be required to perform decoding and descrambling operations on its received data stream, we limit the scope of this chapter to the problem of detecting the coded symbols. To facilitate the analytical development in the following sections, we also make the following simplifying assumptions which may be relaxed or eliminated at the expense of greater notational complexity:

- We ignore the soft-handoff feature of IS–95 where two base stations may be transmitting identical bit streams to a single user.

- We assume the user population remains fixed over the receiver's observation interval. This implies that users do not enter or leave the system, users are not handed off between cells, and that voice activity switching does not occur during the observation interval.

- We ignore base station antenna sectorization.

The details of the IS–95 standard as it relates to the elements in Figure 5.1 may be summarized as follows:

- Channelizer: Spreads and orthogonalizes the coded binary input symbols by assigning a unique length-64 Walsh code to each user and linearly modulating the input symbols with the this code. Each user's Walsh code remains fixed for the duration of the connection. The Walsh-0 code is always assigned to the base station's pilot signal which transmits a constant stream of binary symbols equal to $+1$. The remaining 63 Walsh codes are assigned as needed to the users in the cell as well as overhead and paging channels.

- Power Control: Sets the gain on each user's transmission to provide no more than an acceptable transmission quality to each user in order to not generate excessive cochannel interference in neighboring cells.

- Modulator: Multiplies the aggregate base station transmission by a complex pseudonoise (PN) code for base station discrimination and performs base-band filtering and RF conversion. The PN-code has elements from the set $\{1+j, 1-j, -1+j, -1-j\}$ and has a period of 2^{15} chips. Each base station

uses the same PN-code but is distinguished by a unique, fixed PN-phase. Baseband filtering is specified by a FIR model in the IS–95 standard.

The channel noise is modeled as an additive, white, complex Gaussian random process denoted by $\sigma w(t)$ where $E(w(t)) = 0$ and $E(\mathrm{Re}(w(t))^2) = E(\mathrm{Im}(w(t))^2) = 1/2$. The real and imaginary parts are uncorrelated and also assumed to be independent of the base station transmissions.

Indexing the users by a two dimensional index (base station, user number), we denote the $(b,k)^{th}$ user's positive real amplitude and coded binary symbols at symbol index n as $a_n^{(b,k)}$ and $s_n^{(b,k)}$ respectively[2]. Also denote the unit-energy combined impulse response of the $(b,k)^{th}$ user's channelization code, PN-code, baseband pulse shaping, and propagation channel at symbol index n as $c_n^{(b,k)}(t)$. Note that $c_n^{(b,k)}(t)$ includes any inherent propagation delay and asynchronicity between base stations and is assumed to be FIR. Let ϕ_b denote the received phase of the transmission from the b^{th} base station. The baseband signal observed at the receiver may then be written as

$$r(t) = \sum_{b=1}^{B} e^{j\phi_b} \sum_{n=-L}^{L} \left[a_n^{(b,0)} c_n^{(b,0)}(t-nT) + \sum_{k=1}^{K_b} s_n^{(b,k)} a_n^{(b,k)} c_n^{(b,k)}(t-nT) \right] + \sigma w(t).$$

where we have separated the terms corresponding to the non-data-bearing pilots with the superscript notation $(b,0)$. Note that, in general, $c_n^{(b,k)}(t) \neq c_m^{(b,k)}(t)$ for $n \neq m$ even if the propagation channel is time invariant since the IS–95 PN-code changes at each symbol interval.

In order to represent the observation $r(t)$ compactly, we establish the following vector notation. If $x_n^{(b,k)}$ represents a (possibly complex) scalar quantity corre-

[2]In contrast to the prior chapters where the symbol b was used to represent binary user symbols, this chapter uses b to denote the base station index. As a consequence, we use the symbol s to denote the binary user symbols in this chapter.

sponding to the b^{th} base station's k^{th} user at symbol index n we can construct the vectors

$$\begin{aligned} \boldsymbol{x}_n^{[b]} &= \left[x_n^{(b,1)}, \ldots, x_n^{(b,K_b)}\right]^\top, \\ \boldsymbol{x}^{[b]} &= \left[\boldsymbol{x}_{-L}^{[b]\top}, \ldots, \boldsymbol{x}_L^{[b]\top}\right]^\top, \text{ and} \\ \boldsymbol{x} &= \left[\boldsymbol{x}^{[1]\top}, \ldots, \boldsymbol{x}^{[B]\top}\right]^\top. \end{aligned}$$

The superscripts $\boldsymbol{x}^\top$, $\boldsymbol{x}^*$ and $\boldsymbol{x}^H$ denote transpose, complex conjugate, and complex conjugate transpose, respectively. Define $\boldsymbol{s}$, $\boldsymbol{a}$, and $\boldsymbol{c}(t)$ according to this notation. Let $\boldsymbol{A} = \text{diag}(\boldsymbol{a})$ represent the $K(2L+1) \times K(2L+1)$ dimensional diagonal amplitude matrix and let

$$\boldsymbol{\Phi} = \text{diag}(\underbrace{e^{j\phi_1}, \ldots, e^{j\phi_1}}_{K_1 \text{ terms}}, \ldots, \underbrace{e^{j\phi_B}, \ldots, e^{j\phi_B}}_{K_B \text{ terms}})$$

be the $K(2L+1) \times K(2L+1)$ dimensional diagonal matrix of transmission phases. Then we can write the continuous time observation as

$$\begin{aligned} r(t) &= \underbrace{\sum_{b=1}^{B} e^{j\phi_b} \sum_{n=-L}^{L} a_n^{(b,0)} c_n^{(b,0)}(t-nT)}_{\text{pilots}} + \underbrace{\boldsymbol{c}^\top(t)\boldsymbol{\Phi}\boldsymbol{A}\boldsymbol{s}}_{\text{users}} + \underbrace{\sigma w(t)}_{AWGN} \\ &= p(t) + \boldsymbol{c}^\top(t)\boldsymbol{\Phi}\boldsymbol{A}\boldsymbol{s} + \sigma w(t) \end{aligned} \tag{5.1}$$

where pilots are denoted as $p(t)$ for notational convenience.

5.3 Optimum Detector

In this section we examine optimum (joint maximum likelihood) detection in the context of our IS–95 downlink system model. In a single-cell scenario with single-path channels, the receiver observes the transmission of K synchronous, orthogonal signals in the presence of independent AWGN and it is easy to show that the optimum detector is equivalent to the conventional single-user matched filter detector.

However, when additional cells are considered, the receiver observes nonorthogonal cochannel interference from the other cells and the optimum detector is not the matched filter detector.

We assume that the receiver is able to acquire the pilot (and hence the PN-phase) of each base station $b \in \{1, \ldots, B\}$ perhaps via correlation with the known periodic PN-code of length 2^{15}. This then allows the receiver to estimate the impulse response of the propagation channel and transmission phase for each base station. For each base station, the receiver can then construct a bank of 63 matched filters, one matched filter for each of the non-pilot Walsh codes, in order to determine which users (or equivalently, which Walsh codes) are active in each cell. Since the receiver now knows the active Walsh codes, the PN-phase, the propagation channels, and the baseband pulse-shaping, we can construct the set of $c_n^{(b,k)}(t)$ for the set of users in each cell. Finally, the receiver can then generate amplitude estimates for each user and the pilots through a variety of methods. For the purposes of the remaining analytical development, we assume that all of these estimates are perfect and that the only unknowns in (5.1) are $\boldsymbol{s}$ and $\sigma w(t)$.

Let $\mathcal{I}$ represent a compact interval in time containing the support of $r(t)$ and let $\mathcal{U}$ represent the set of cardinality $2^{K(2L+1)}$ containing all admissible binary symbol vectors of length $K(2L+1)$. Then the decision rule for jointly optimum estimates [Ver98] is given by

$$\hat{\boldsymbol{s}} = \arg\max_{\boldsymbol{u}\in\mathcal{U}} \exp\left(-\frac{1}{\sigma^2}\int_{\mathcal{I}} |r(t) - p(t) - \boldsymbol{c}^\top(t)\boldsymbol{\Phi}\boldsymbol{A}\boldsymbol{u}|^2 dt\right).$$

Manipulation of the term inside the exponent yields the expression for optimum decisions on the IS–95 downlink as

$$\hat{\boldsymbol{s}} = \arg\max_{\boldsymbol{u}\in\mathcal{U}} \underbrace{2\mathrm{Re}[\boldsymbol{u}^\top \boldsymbol{A}\boldsymbol{\Phi}^H(\boldsymbol{y} - \boldsymbol{p})] - \boldsymbol{u}^\top \boldsymbol{A}\boldsymbol{\Phi}^H \boldsymbol{R}\boldsymbol{\Phi}\boldsymbol{A}\boldsymbol{u}}_{\Omega(\boldsymbol{u})}$$

where $\boldsymbol{y} = \int_{\mathcal{I}} \boldsymbol{c}^*(t) r(t)\, dt$ represents the $K(2L+1)$-vector of matched filter outputs, $\boldsymbol{p} = \int_{\mathcal{I}} \boldsymbol{c}^*(t) p(t)\, dt$ represents the $K(2L+1)$-vector of matched filter outputs for the pilot portion of the received signal, and $\boldsymbol{R} = \int_{\mathcal{I}} \boldsymbol{c}^*(t) \boldsymbol{c}^\top(t)\, dt$ represents the $K(2L+1) \times K(2L+1)$ dimensional user signature correlation matrix. The brute-force solution to this problem requires the evaluation of $2^{K(2L+1)}$ different hypotheses to find the maximum. Several authors have noted that $\boldsymbol{R}$ exhibits a banded structure and have used this fact to achieve complexity reduction using Viterbi-style dynamic programming algorithms [Ver98]. Although a good idea in practice, we will not consider Viterbi-style dynamic programming algorithms in this chapter in order to clarify the development of the IS–95 structure based complexity reduction. The reduced complexity optimum detector developed in the next section does not prevent the use of Viterbi-style dynamic programming algorithms and both ideas can be combined to achieve even greater complexity reduction.

5.4 Reduced Complexity Optimum Detector

In this section we exploit the structure of the IS–95 downlink in order to propose an *optimum* detector requiring significantly less complexity than the brute-force approach. The intuitive idea behind the reduced complexity optimum detector is to use the fact that the $K_b + 1$ synchronous user plus pilot transmissions from base station b are mutually orthogonal at every symbol index if the propagation channel from the b^{th} base station to the receiver is single-path. This will allow us to "decouple" the decisions of one base station's users to achieve the desired complexity reduction while retaining optimality. Note that this technique can also be applied in the multi-path channel case but since users within a cell are no longer

orthogonal there will be some loss of optimality.

The signature correlation matrix $\boldsymbol{R}$ has dimensions $K(2L+1)\times K(2L+1)$ and exhibits the structure

$$\boldsymbol{R} = \int_{\mathcal{I}} \begin{bmatrix} \boldsymbol{c}^{[1]*}(t) \\ \vdots \\ \boldsymbol{c}^{[B]*}(t) \end{bmatrix} \begin{bmatrix} \boldsymbol{c}^{[1]\top}(t) & \cdots & \boldsymbol{c}^{[B]\top}(t) \end{bmatrix} dt = \begin{bmatrix} \boldsymbol{R}^{[1,1]} & \ldots & \boldsymbol{R}^{[1,B]} \\ \vdots & \ddots & \vdots \\ \boldsymbol{R}^{[B,1]} & \ldots & \boldsymbol{R}^{[B,B]} \end{bmatrix}$$

where $\boldsymbol{R}^{[b,b']}$ has dimension $K_b(2L+1)\times K_{b'}(2L+1)$. The submatrices $\boldsymbol{R}^{[b,b']}$ have the structure

$$\boldsymbol{R}^{[b,b']} = \begin{bmatrix} \boldsymbol{R}^{[b,b']}_{-L,-L} & \ldots & \boldsymbol{R}^{[b,b']}_{-L,L} \\ \vdots & \ddots & \vdots \\ \boldsymbol{R}^{[b,b']}_{L,-L} & \ldots & \boldsymbol{R}^{[b,b']}_{L,L} \end{bmatrix}$$

where

$$\boldsymbol{R}^{[b,b']}_{n,n'} = \int_{\mathcal{I}} \boldsymbol{c}^{[b]*}_{n}(t)\boldsymbol{c}^{[b']\top}_{n'}(t)\,dt = \boldsymbol{R}^{[b',b]H}_{n',n}.$$

At this point we require the propagation channels to be single-path in order to proceed with the complexity reduction. This assumption, combined with the facts that

1. the IS–95 pulse shaping filters approximately satisfy the Nyquist pulse criterion and

2. each user in a given cell is assigned a unique Walsh code orthogonal to all other users in the same cell,

implies that the downlink transmissions in each cell do not interfere with the other downlink transmissions in the same cell and that the downlink transmissions in each cell are received without any intersymbol interference. In this case, the IS–95

downlink signature correlation matrix exhibits two special properties that lead to the reduced complexity optimum detector:

- The group-orthonormality of the signature sequences of each base-station at symbol index n implies that $\boldsymbol{R}_{n,n}^{[b,b]} = \boldsymbol{I}$.
- The lack of intersymbol interference implies that $\boldsymbol{R}_{n,n'}^{[b,b]} = \boldsymbol{0}$ for $n \neq n'$.

The combination of these two properties implies that $\boldsymbol{R}^{[b,b]} = \boldsymbol{I}$ for $b = 1, \ldots, B$. Let $\boldsymbol{X} = \boldsymbol{A}\boldsymbol{\Phi}^H \boldsymbol{R} \boldsymbol{\Phi} \boldsymbol{A}$ and note that since $\boldsymbol{R}$ is a Hermitian matrix then $\boldsymbol{X}$ is also Hermitian. Moreover, since $\boldsymbol{\Phi}$ and $\boldsymbol{A}$ are diagonal, $\boldsymbol{X}$ shares the same IS–95 structure properties as $\boldsymbol{R}$ except that $\boldsymbol{X}^{[b,b]} = (\boldsymbol{A}^{[b,b]})^2$. It turns out that this difference will not matter in the maximization of $\Omega(\boldsymbol{u})$. Using our previously developed notation, we can write

$$\Omega(\boldsymbol{u}) \;=\; 2\mathrm{Re}[\boldsymbol{u}^\top \boldsymbol{A}\boldsymbol{\Phi}^H(\boldsymbol{y} - \boldsymbol{p})] - \boldsymbol{u}^\top \boldsymbol{X}\boldsymbol{u}. \tag{5.2}$$

First, since $\boldsymbol{A}$ and $\boldsymbol{\Phi}$ are diagonal, we can isolate the symbols from the first[3] base station to write

$$2\mathrm{Re}[\boldsymbol{u}^\top \boldsymbol{A}\boldsymbol{\Phi}^H(\boldsymbol{y} - \boldsymbol{p})] \;=\; \boldsymbol{u}^{[1]\top} 2\mathrm{Re}[\boldsymbol{A}^{[1]}\boldsymbol{\Phi}^{[1]H}(\boldsymbol{y}^{[1]} - \boldsymbol{p}^{[1]})] + \bar{\boldsymbol{u}}^\top 2\mathrm{Re}[\bar{\boldsymbol{A}}\bar{\boldsymbol{\Phi}}^H(\bar{\boldsymbol{y}} - \bar{\boldsymbol{p}})] \tag{5.3}$$

where vectors with an overbar are $(K - K_1)(2L+1) \times 1$ dimensional with elements from all base stations except $b = 1$ and matrices with an overbar are $(K - K_1)(2L+1) \times (K - K_1)(2L+1)$ dimensional with corresponding elements.

The quadratic term in (5.2) may be rewritten as

$$\boldsymbol{u}^\top \boldsymbol{X}\boldsymbol{u} = \sum_{b=1}^{B} \sum_{b'=1}^{B} \boldsymbol{u}^{[b]\top} \boldsymbol{X}^{[b,b']} \boldsymbol{u}^{[b']}.$$

[3]In order to achieve the maximum complexity reduction we assume without loss of generality that $K_1 = \max_b K_b$.

The binary nature of $\boldsymbol{u}$ and the fact that $\boldsymbol{X}^{[b,b]}$ is diagonal implies that

$$\begin{aligned}\boldsymbol{u}^{[b]\top}\boldsymbol{X}^{[b,b]}\boldsymbol{u}^{[b]} &= \mathbf{1}^{\top}(\boldsymbol{A}^{[b,b]})^2\mathbf{1} \\ &= \alpha_b\end{aligned}$$

where α_b is a real positive constant that does not depend on $\boldsymbol{u}$. Denoting $\alpha = \sum_{b=1}^{B}\alpha_b$ then

$$\boldsymbol{u}^{\top}\boldsymbol{X}\boldsymbol{u} = \alpha + \sum_{b=1}^{B}\sum_{b'\neq b}\boldsymbol{u}^{[b]\top}\boldsymbol{X}^{[b,b']}\boldsymbol{u}^{[b']}.$$

Again, we isolate the symbols from the first base station to write

$$\boldsymbol{u}^{\top}\boldsymbol{X}\boldsymbol{u} = \alpha + \sum_{b=2}^{B}\boldsymbol{u}^{[b]\top}\boldsymbol{X}^{[b,1]}\boldsymbol{u}^{[1]} + \sum_{b=2}^{B}\boldsymbol{u}^{[1]\top}\boldsymbol{X}^{[1,b]}\boldsymbol{u}^{[b]} + \underbrace{\sum_{b=2}^{B}\sum_{\substack{b'\neq b\\ b'\neq 1}}\boldsymbol{u}^{[b]\top}\boldsymbol{X}^{[b,b']}\boldsymbol{u}^{[b']}}_{G(\bar{\boldsymbol{u}})}.$$

Since $\boldsymbol{X}$ is a Hermitian matrix then $\boldsymbol{X}^{[b,1]H} = \boldsymbol{X}^{[1,b]}$ and we can write

$$\boldsymbol{u}^{\top}\boldsymbol{X}\boldsymbol{u} = \alpha + \sum_{b=2}^{B}\boldsymbol{u}^{[1]\top}2\mathrm{Re}\left(\boldsymbol{X}^{[1,b]}\boldsymbol{u}^{[b]}\right) + G(\bar{\boldsymbol{u}}). \tag{5.4}$$

Finally, we plug (5.3) and (5.4) back into (5.2) and collect terms to write

$$\begin{aligned}\Omega(\boldsymbol{u}) = \boldsymbol{u}^{[1]\top}&\underbrace{2\mathrm{Re}\left[\boldsymbol{A}^{[1]}\boldsymbol{\Phi}^{[1]H}(\boldsymbol{y}^{[1]}-\boldsymbol{p}^{[1]}) - \sum_{b=2}^{B}\boldsymbol{X}^{[1,b]}\boldsymbol{u}^{[b]}\right]}_{F(\bar{\boldsymbol{u}})} \\ &+ \bar{\boldsymbol{u}}^{\top}2\mathrm{Re}[\bar{\boldsymbol{A}}\bar{\boldsymbol{\Phi}}^{H}(\bar{\boldsymbol{y}}-\bar{\boldsymbol{p}})] - \alpha - G(\bar{\boldsymbol{u}}).\end{aligned} \tag{5.5}$$

Observe that (5.5) is maximized when $\boldsymbol{u} = \left[\mathrm{sgn}(\bar{\boldsymbol{v}})^{\top}, \bar{\boldsymbol{v}}\right]^{\top}$ where

$$\bar{\boldsymbol{v}} = \arg\max_{\bar{\boldsymbol{u}}\in\mathbb{B}^{K-K_1}}\Omega\left(\left[\mathrm{sgn}(F(\bar{\boldsymbol{u}}))^{\top}, \bar{\boldsymbol{u}}^{\top}\right]^{\top}\right)$$

The key difference between the reduced complexity and brute-force optimum detectors is that the reduced complexity algorithm requires the evaluation of

$2^{(K-K_1)(2L+1)}$ hypotheses in order to maximize $\Omega(\boldsymbol{u})$ whereas the brute-force optimum detector requires the evaluation of $2^{K(2L+1)}$ hypotheses. For an eavesdropper in a cell system with two or three significant base stations, this complexity reduction can be significant.

This prior analysis can also be easily applied to the synchronous CDMA case where sequence detection is not necessary and the brute-force optimum detector requires the evaluation of Ω for 2^K hypotheses. In this case, the reduced complexity optimum detector requires the evaluation of Ω for 2^{K-K_1} hypotheses.

5.5 Group Parallel Interference Cancellation Detector

Although the IS–95 downlink has a structure which lends itself to reduced complexity optimum detection, it is often the case that the reduced complexity optimum detector is too computationally expensive to implement even with Viterbi-style dynamic programming algorithms. In this section we pose a suboptimum detector called the Group Parallel Interference Cancellation detector (GPIC) that also takes advantage of the orthogonality between user transmissions from the same base station in the IS–95 downlink. Two observations regarding (5.5) will be useful in the development of the GPIC detector:

- Suppose the receiver has perfect knowledge of $\bar{\boldsymbol{s}}$, the symbols transmitted from base stations $2, \ldots, B$. Then, as we showed, $\hat{\boldsymbol{s}}^{[1]} = \text{sgn}(F(\bar{\boldsymbol{s}}))$ is the optimum estimate for the symbols from base station 1. The orthogonality of the users in base station 1 results in single user error probability with low computational complexity.

- Denote the joint maximum likelihood (JML) estimate of $\boldsymbol{s}$ as

$$\hat{\boldsymbol{s}}_{\mathsf{JML}} = [\hat{\boldsymbol{s}}_{\mathsf{JML}}^{[1]\top}, \hat{\bar{\boldsymbol{s}}}_{\mathsf{JML}}^{\top}]^{\top}$$

  and suppose the receiver has perfect knowledge of $\hat{\bar{\boldsymbol{s}}}_{\mathsf{JML}}$. In this case, we showed that $\hat{\boldsymbol{s}}^{[1]} = \mathrm{sgn}(F(\hat{\bar{\boldsymbol{s}}}_{\mathsf{JML}}))$ is the JML estimate for the symbols from base station 1. The orthogonality of the users in base station 1 results in JML error probability with low computational complexity.

Unfortunately, realistic receivers do not have access to the actual symbols or JML estimates in general, but we are compelled to ask the following question: What if the receiver formed some low-complexity estimate $\hat{\bar{\boldsymbol{s}}}$ of $\bar{\boldsymbol{s}}$ and we let $\hat{\boldsymbol{s}}^{[1]} = \mathrm{sgn}(F(\hat{\bar{\boldsymbol{s}}}))$? In fact, consider the lowest complexity estimate of $\bar{\boldsymbol{s}}$: conventional matched filter estimates where $\hat{\bar{\boldsymbol{s}}}_{\mathsf{MF}} = \mathrm{sgn}(\mathrm{Re}(\bar{\boldsymbol{\Phi}}^{H}\bar{\boldsymbol{y}}))$. Then

$$\begin{aligned}\hat{\boldsymbol{s}}^{[1]} &= \mathrm{sgn}(F(\hat{\bar{\boldsymbol{s}}}_{\mathsf{MF}})) \\ &= \mathrm{sgn}\left(\mathrm{Re}\left[\boldsymbol{A}^{[1]}\boldsymbol{\Phi}^{[1]H}(\boldsymbol{y}^{[1]} - \boldsymbol{p}^{[1]}) - \sum_{b=2}^{B}\boldsymbol{X}^{[1,b]}\hat{\boldsymbol{s}}_{\mathsf{MF}}^{[b]}\right]\right)\end{aligned}$$

but since $\boldsymbol{X}^{[1,b]} = \boldsymbol{A}^{[1]}\boldsymbol{\Phi}^{[1]H}\boldsymbol{R}^{[1,b]}\boldsymbol{\Phi}^{[b]}\boldsymbol{A}^{[b]}$ then

$$\hat{\boldsymbol{s}}^{[1]} = \mathrm{sgn}\left\{\mathrm{Re}\left[\boldsymbol{\Phi}^{[1]H}\left((\boldsymbol{y}^{[1]} - \boldsymbol{p}^{[1]}) - \sum_{b=2}^{B}\boldsymbol{R}^{[1,b]}\boldsymbol{\Phi}^{[b]}\boldsymbol{A}^{[b]}\hat{\boldsymbol{s}}_{\mathsf{MF}}^{[b]}\right)\right]\right\} \tag{5.6}$$

where we have factored out the common $\boldsymbol{A}^{[1]}$ term since it does not affect the sign operation. It is evident from this last expression that a receiver using (5.6) forms decisions by subtracting the estimated cochannel interference $b \neq 1$ from the matched filter inputs (minus the known pilot terms) corresponding to the users in cell 1. When this operation is performed on all of the base stations it is called parallel interference cancellation and since the interference cancellation is performed over groups of users we coin the name Group Parallel Interference Cancellation

for this receiver. If the receiver forms a bank of matched filter estimates for all base stations then we can extend this idea to write the following expression for the GPIC detector of base station b as

$$\hat{\boldsymbol{s}}^{[b]} = \text{sgn}\left\{\text{Re}\left[\boldsymbol{\Phi}^{[b]H}\left((\boldsymbol{y}^{[b]}-\boldsymbol{p}^{[b]})-\sum_{b'\neq b}\boldsymbol{R}^{[b,b']}\boldsymbol{\Phi}^{[b']}\boldsymbol{A}^{[b']}\hat{\boldsymbol{s}}_{\mathsf{MF}}^{[b']}\right)\right]\right\}$$

where $\hat{\boldsymbol{s}}^{[b']} = \text{sgn}(\text{Re}(\bar{\boldsymbol{\Phi}}^{[b']H}\boldsymbol{y}^{[b']}))$. Some algebraic manipulation yields a simple expression for the GPIC receiver for all base stations as

$$\hat{\boldsymbol{s}}_{\mathsf{GPIC}} = \text{sgn}\left[\text{Re}\left(\boldsymbol{\Phi}^{H}(\boldsymbol{y}-\boldsymbol{p})+\left(\boldsymbol{I}-\boldsymbol{\Phi}^{H}\boldsymbol{R}\boldsymbol{\Phi}\right)\boldsymbol{A}\hat{\boldsymbol{s}}_{\mathsf{MF}}\right)\right].$$

We note that although it is certainly possible to perform GPIC detection in batch where all $K(2L+1)$ symbols are first estimated with the conventional matched filter detector and stored prior to calculation of the GPIC symbol estimates, it is also possible to implement the GPIC receiver with detection delay proportional to K. This feature is in contrast to the previously considered optimum detectors where detection cannot occur until all of $r(t)$ is observed.

In the following sections we examine the performance of the GPIC detector using simulated data and actual on-air data gathered with an omnidirectional antenna in an active IS–95 system.

5.6 Simulation Results

In this section we compare the performance of the GPIC detector to the optimum detector and conventional matched filter detector via simulation. We examine an eavesdropping scenario where the receiver is positioned on the dashed line in the simple cellular system shown in Figure 5.2 with $B = 2$ base stations, $K_1 = 2$ and $K_2 = 2$ users in each cell, and 5 bits in each user's transmission ($L = 2$). The users

are represented by small circles and the eavesdropping receiver is represented by a small square with an antenna symbol. We evaluate the quality of reception from both base stations as the receiver moves on the dashed line from point a to point b.

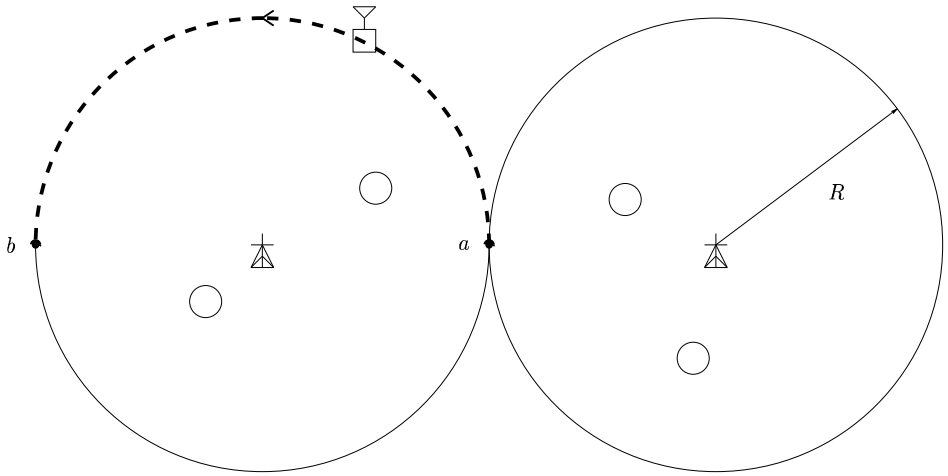

Figure 5.2: Simple two base station IS–95 cellular system with circular cells of radius R and centered base stations.

The propagation channels between the base stations and the eavesdropping receiver are assumed to be single path with random received phases uniformly distributed in $[0, 2\pi)$. Asynchronism offsets are also assumed to be uniformly distributed. User powers, phases and delays are assumed to be time invariant over the 5-bit transmissions. We assume the user positions to be uniformly distributed within the cell. This assumption combined with IS–95 downlink power control implies that the user amplitudes observed at the eavesdropper are also random with the distribution derived in Section 5.9 under similar path-loss modeling assumptions as the uplink study in [MV98c].

Figure 5.3 shows the bit error rate of the conventional matched filter (denoted

by "MF"), optimum (denoted by "OPT"), and GPIC (denoted by "GPIC") for a user in the first cell, averaged over the user positions, delays, phases, amplitudes, and PN-codes. Note that in this simulation, the distance to the desired base station is fixed and the cochannel interference is decreasing as we move the eavesdropper away from base station 2. Figure 5.4 shows the results of the same simulation for a user in the second cell. In this case the eavesdropper is moving away from the desired base station and remaining at a fixed distance from the interfering base station.

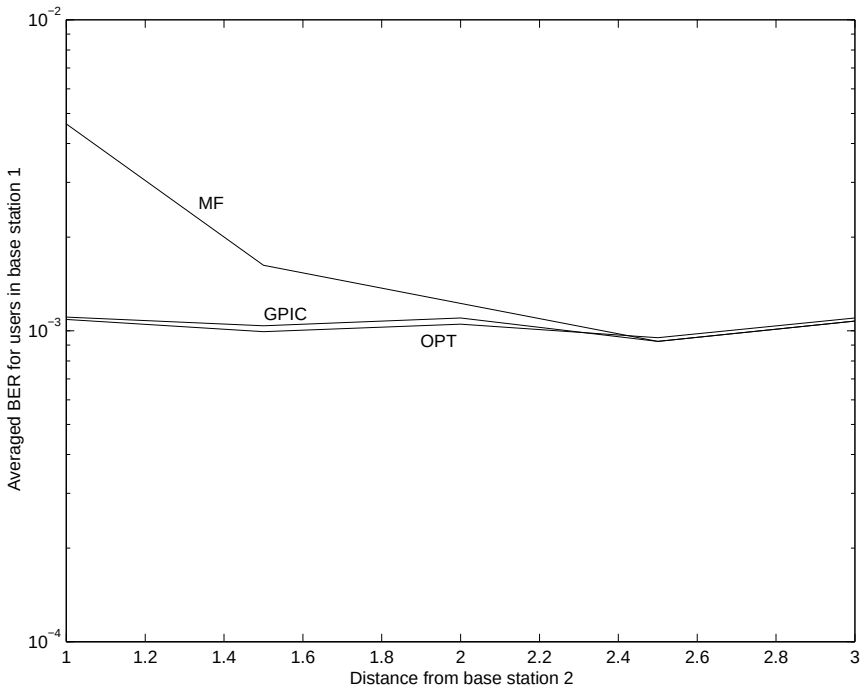

Figure 5.3: Averaged eavesdropping bit error rate for a user in cell 1. Single user error probability is 10^{-3} irrespective of distance to base station 2.

As expected, Figure 5.3 shows that the conventional matched filter detector performs well when the eavesdropper is listening to base station 1 in a position distant from base station 2. However, because of its near-far susceptibility, the matched

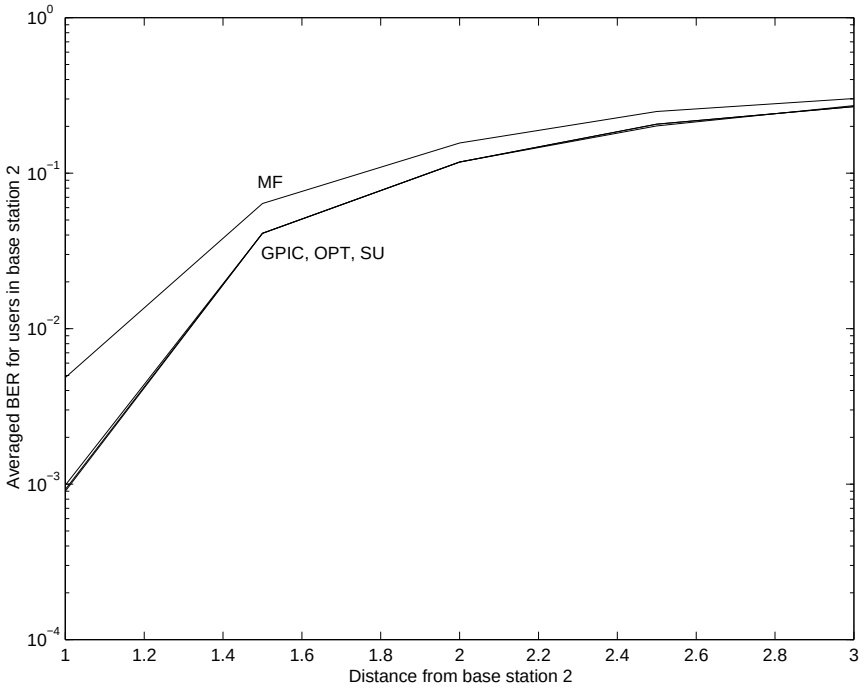

Figure 5.4: Averaged eavesdropping bit error rates for users in cell 2. Single user error probability is denoted by "SU" and is indistinguishable from the optimum and GPIC detectors.

filter detector performs poorly when the eavesdropper is positioned close to strong interference. The GPIC detector does not suffer from this problem and actually exhibits performance indistinguishable from the optimum detector in these examples. This simulation suggests that the GPIC detector may offer near-optimum eavesdropping performance over a wide range of cochannel interference powers with the most benefit in operating scenarios with severe cochannel interference.

5.7 On-Air Data

This section tests the performance of the GPIC eavesdropper on one snapshot of actual on-air measured data from an IS–95 cellular system. One 45.6ms snapshot of measured data was gathered from an IS–95 downlink system with an omnidirectional antenna. The received waveform was sampled at twice the chip rate to yield a data file with 112000 samples corresponding to 875 (coded) symbol periods. The results of a base station pilot survey are shown in Figure 5.5. Note that phase offset does not affect this plot since all correlations are displayed in magnitude. The correlations were taken over an entire period of the PN-sequence.

Throughout this section, base station 1 denotes the base station with the strongest pilot as seen at PN-offset 20000 in Figure 5.5. Base station 2 denotes the second strongest base station at PN-offset 62500. The power of the pilot from base station 1 is approximately 11dB higher than the pilot from base station 2 hence the eavesdropper is probably positioned very close to base station 1 and relatively distant from base station 2. The remaining base stations seen in Figure 5.5 are ignored in the following development for clarity.

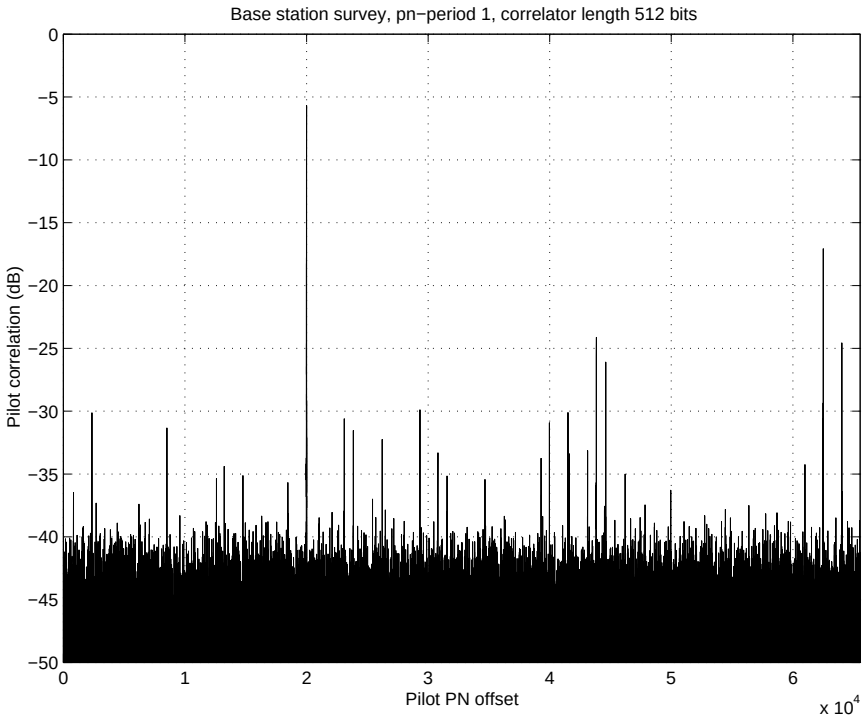

Figure 5.5: Base station pilot survey for IS–95 on-air data.

5.7.1 Conventional Matched Filter Detection

In this section we qualitatively examine the soft outputs of conventional matched filter detection for base stations 1 and 2. The matched filters are obtained by estimating the impulse response of the combined propagation channel and pulse shaping filters via pilot correlation and convolving this impulse response with the appropriate combined Walsh and PN-codes for each active user in the system. Although Rake detection is not used, the matched filter receiver considered in this section automatically includes coherent multipath combining since it incorporates the estimated impulse response of the propagation channel.

Suppressing the soft outputs of the inactive channels for clarity, Figure 5.6 shows the histogram frequency of the matched filter outputs for the active Walsh channels of base station 1. Figure 5.6 clearly shows that the eye is open for all of the active channels and implies that one could expect that hard decisions on the coded symbols of these channels would have low probability of error. In addition to the strong pilot channel at Walsh code 0, there is a strong paging channel at Walsh code 1, a relatively weak sync channel at Walsh code 32, and two traffic channels of disparate power at Walsh codes 12 and 63. Matched filter detection appears to be adequate for downlink reception of this base station.

Figure 5.7 shows the histogram frequency of the matched filter outputs for the active Walsh channels of base station 2. Figure 5.7 clearly shows that, unlike the transmissions from base station 1, all of the channels from base station 2 are highly corrupted by interference (including cochannel interference from base station 1, other base stations, and "unstructured" noise sources). The eye is closed for all Walsh channels, implying that hard decisions on these coded symbols are likely to have very high error rates.

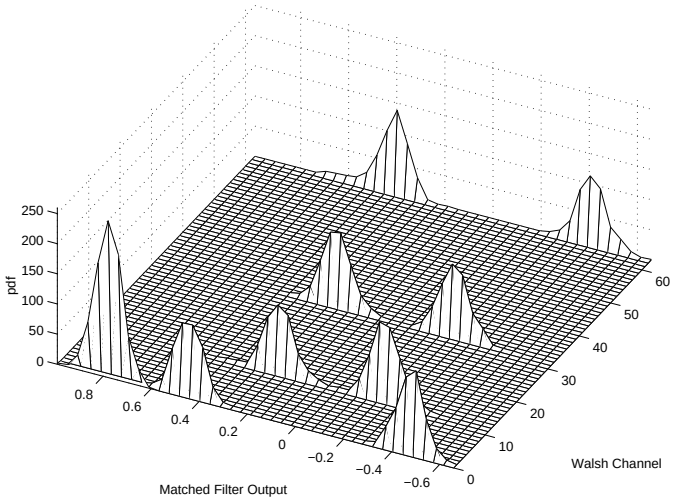

Figure 5.6: Histograms of MF outputs by Walsh channel for base station 1.

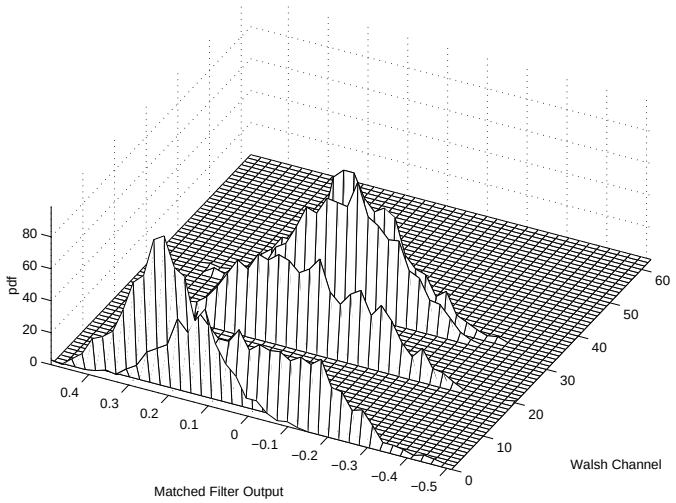

Figure 5.7: Histograms of MF outputs by Walsh channel for base station 2.

5.7.2 GPIC Detection

In this section we qualitatively examine the soft outputs of the GPIC detector for base stations 1 and 2. The matched filter outputs generated in the prior subsection are passed through a hard decision device and then respread by the combined impulse response of the appropriate Walsh codes, PN-codes, and estimated pulse-shaping and propagation channel impulse responses. The waveforms are then scaled and rotated according to each user's estimated amplitude and phase.

Figure 5.8 shows the histogram of the matched filter outputs by Walsh channel of base station 1 after subtraction of the estimated interference from base station 2. There is little noticeable change from the results in Figure 5.6 since the cochannel interference from base station 2 is very small with respect to the transmission of base station 1 and interference cancellation has little effect.

Figure 5.9 shows the histogram of the matched filter outputs by Walsh channel of base station 2 after subtraction of the estimated interference from base station 1. The performance improvement is significant with respect to the conventional matched filter results in Figure 5.7. The error probability in channels 1 and 20 appears to be much lower and channels 32 and 34 are beginning to exhibit troughs in the middle of the pdf indicating improved error rates. The pilot channel is also significantly cleaner.

The results in this section agree with the simulation results in Section 5.6 and imply that the GPIC detector may not offer much performance improvement for strong signals received in low levels of cochannel interference. On the other hand, comparison of Figures 5.7 and 5.9 show that significant performance improvements are possible for an eavesdropping receiver attempting to extract weak transmissions from high levels of cochannel interference.

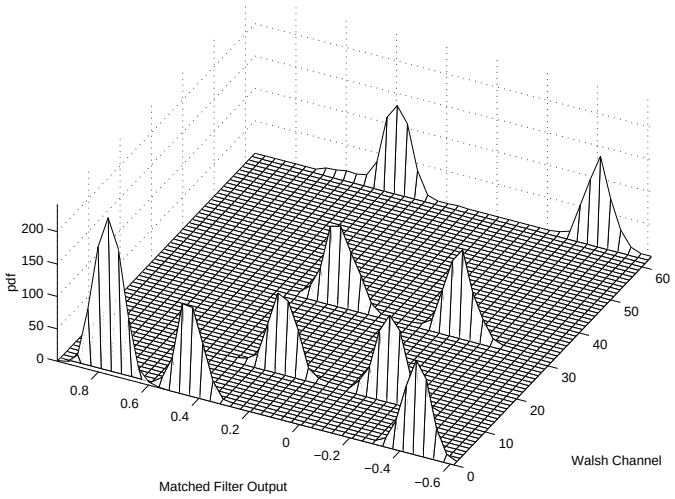

Figure 5.8: Histograms of GPIC outputs by Walsh channel for base station 1.

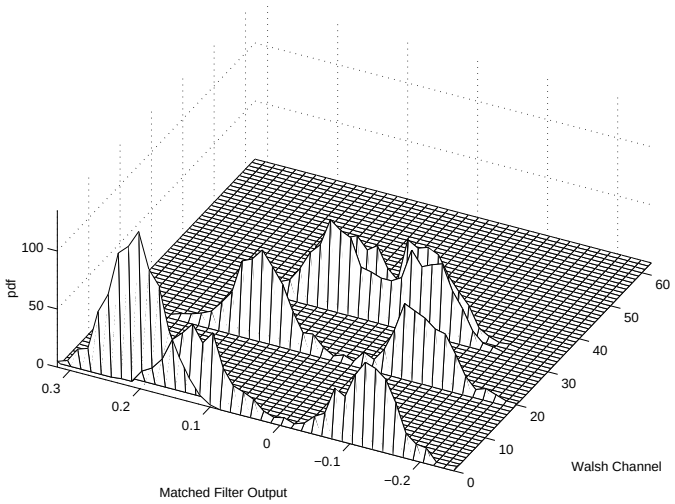

Figure 5.9: Histograms of GPIC outputs by Walsh channel for base station 2.

The performance adaptive techniques developed in Chapter 4 could also be applied here but little difference is anticipated in this case due to the widely disparate powers observed in the measured data. The performance adaptive PIC detectors all specify nearly full cancellation of base station one's signal and little or no cancellation of base station two's signal. The results here suggest that there is little or no tangible performance improvement observed in base station one's outputs regardless of whether we cancel base station two or not due to the fact the base station two's received power is very small in this snapshot. Full cancellation of base station one's transmissions does indeed yield large performance improvements in the detection of the users of base station two in this case.

5.8 Conclusions

In this chapter we considered the application of nonlinear multiuser detection techniques for improving the performance of IS–95 downlink reception. We used the orthogonality of the in-cell users of the IS–95 downlink to develop a reduced complexity optimum detector with exponentially lower complexity than the brute-force optimum detector under the assumption that propagation channels between the base stations and the receiver were all well modeled as single path channels. Examination of the properties of the reduced complexity optimum detector led to the development of the suboptimum GPIC detector. The GPIC detector has very low complexity and does not require any form of subspace tracking, matrix inversions, or exhaustive searches for global maxima. Simulations and experiments with on-air IS–95 downlink data suggest that the GPIC detector offers the greatest performance improvements in severe cochannel interference environments but

may also offer near-optimum performance for IS–95 downlink eavesdropping over a wide range of cochannel interference powers.

5.9 Appendix: IS-95 Received Power Distribution

In this appendix, we derive the received user power distribution for transmissions to users in the b^{th} cell observed by a receiver (eavesdropping or authorized) positioned at a deterministic distance $d^{(b,*)} \in (0, \infty)$ from the b^{th} base station. We assume:

- Each base station is located in the center of its circular cell of radius R.
- Each user's position is uniformly distributed in the cell and is independent of other user positions. The k^{th} user's distance from base station b is denoted by $d^{(b,k)} \in (0, R]$.
- Each base station maintains perfect power control with its users such that the power received by each user from its base station is identical for all users within the cell.
- The ratio of received to transmitted power may be approximated with a simple path loss model $1/d^{2\lambda}$ where d is the distance separating the transmitter and receiver, and λ is the path loss exponent.

The circular shape of each cell and the users' uniformly random positions imply that the cumulative distribution function of the $(b,k)^{th}$ user's distance from base

station b, denoted as $d^{(b,k)}$, is equal to the ratio of the area of 2 circles,

$$F_{d^{(b,k)}}(x) = P(d^{(b,k)} \leq x) = \begin{cases} (x/R)^2 & x \in [0, R], \\ 0 & \text{otherwise.} \end{cases}$$

The pdf of $d^{(b,k)}$ follows directly as

$$f_{d^{(b,k)}}(x) = \frac{\partial}{\partial x} F_{d^{(b,k)}}(x) = \begin{cases} 2x/R^2 & x \in [0, R], \\ 0 & \text{otherwise.} \end{cases}$$

IS–95 downlink power control leads to random realizations for the user amplitudes observed at the deterministically positioned receiver. The received power ratio (deterministically positioned receiver to randomly positioned user) may be expressed as

$$\Psi = \frac{P^{(b,*)}}{P^{(b,k)}} = \frac{P^{(b,*)}/P_t}{P^{(b,k)}/P_t} = \frac{(d^{(b,k)})^{2\lambda}}{(d^{(b,*)})^{2\lambda}}$$

where $P^{(b,*)}$, $P^{(b,k)}$, and P_t denote the power observed at the receiver, the power received at the user, and the power transmitted, respectively. To find the cumulative distribution of Ψ, we note that $F_\Psi(x) = P(\Psi \leq x) = P((d^{(b,k)})^{2\lambda}/(d^{(b,*)})^{2\lambda} \leq x) = F_{d^{(b,k)}}(d^{(b,*)} x^{1/2\lambda})$ hence

$$F_\Psi(x) = \begin{cases} (d^{(b,*)}/R)^2 x^{1/\lambda} & x \in [0, (d^{(b,*)}/R)^{-2\lambda}], \\ 0 & \text{otherwise} \end{cases}$$

and the pdf of Ψ follows directly as

$$f_\Psi(x) = \begin{cases} \lambda^{-1}(d^{(b,*)}/R)^2 x^{(1-\lambda)/\lambda} & x \in [0, (d^{(b,*)}/R)^{-2\lambda}], \\ 0 & \text{otherwise.} \end{cases}$$

This pdf is used to generate the random amplitude realizations used for the simulation results in Section 5.6.

CHAPTER 6

APPLICATIONS OF MULTIUSER DETECTION: CROSSTALK MITIGATION FOR DIGITAL SUBSCRIBER LOOPS

This chapter of the dissertation considers the application of multiuser detection techniques for crosstalk mitigation in digital subscriber loops (DSLs). Good introductions to this topic can be found in [CKB+99] where the crosstalk environment is discussed for ADSL and VDSL systems and [GHW99] where crosstalk mitigation is considered. In general, DSLs are subject to two forms of crosstalk interference that result from electromagnetic coupling between twisted pairs of unshielded copper wires in close proximity – near-end crosstalk (NEXT) and far-end crosstalk (FEXT). Figure 6.1 illustrates these forms of crosstalk observed by a DSL modem at the customer premises. Although not shown in the figure, NEXT and FEXT may also be observed by the data switch (ATU-C) as well.

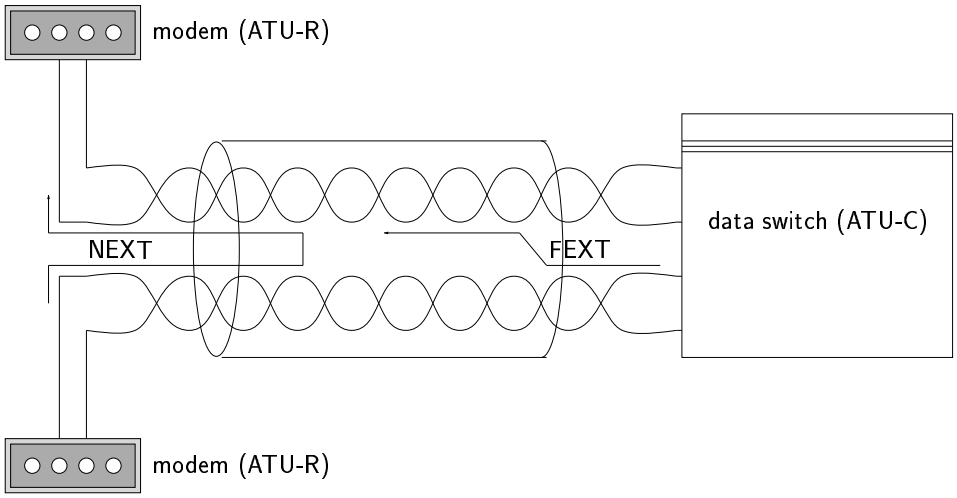

Figure 6.1: Near-end crosstalk (NEXT) and far-end crosstalk (FEXT).

Typically, NEXT and FEXT are modeled as colored Gaussian noise. This is a worst-case assumption that prevents the use of known structure inherent to the

interference. This section discards the Gaussian assumption and exploits the structure of the crosstalk in order to cancel it from the received signal. The techniques developed in this section could lead to more sophisticated DSL receivers that are resistant to crosstalk or could be used for DSL eavesdropping.

In general, the twisted pair cables from several customers are bundled in a single multi-pair cable called a "binder group". The twisted pair cable of a user subscribing to one particular broadband access service is bundled with twisted pair cables of other users also subscribing to broadband access services. The term crosstalk is general and includes interference from disparate services (e.g., an ADSL modem observing crosstalk from another line using ISDN modulation) and identical services (e.g., an ADSL modem observing crosstalk from another line using ADSL modulation). In the latter case, this form of crosstalk has a special name – self-NEXT or self-FEXT. It is this form of crosstalk that is considered in this chapter.

The balance of this chapter considers crosstalk mitigation at the ATU-R modem. Crosstalk cancellation at the ATU-C data switch was considered in [IW95] and [IS98] where the input data sequences generating the NEXT interference are known and canceled via a cross-channel data-driven echo canceler. The problem of crosstalk mitigation at the ATU-R modem is more difficult since the ATU-R modem does not know the input data sequences generating the NEXT. Moreover, unlike the CDMA problem where it is commonly assumed that the receiver has access to a *bank* of matched filter outputs generating a *vector* observation, the ATU-R modem in a DSL system has access to only a *single* matched filter (matched to the transmitter pulse shape in this case) output generating a *scalar* observation. Hence, crosstalk mitigation at the ATU-R modem will in general be more difficult than interference cancellation in a CDMA receiver since the ATU-R modem does

not have access to the sources of diversity available in CDMA systems enabling improved estimation of the interfering input sequences.

6.1 Near-End Crosstalk Power

To study the feasibility of crosstalk mitigation for DSL loops, this section examines the power of NEXT interference using empirical models from the literature and standards body. This analysis is important since, if the NEXT interference power is typically much smaller than the received signal power, crosstalk mitigation would likely yield only modest improvements in performance. On the other hand, if NEXT interference power is large then there is at least hope that a clever crosstalk mitigation scheme could dramatically improve performance.

This section focuses on the echo-canceled discrete multitone asymmetric DSL (EC-DMT-ADSL) as described in [Rau99] and [Int99a, Annex B]. EC-DMT-ADSL is sometimes called "overlapped spectrum operation" DMT-ADSL where "overlapped spectrum" specifies that the upstream and downstream data are sent in overlapping frequency bands. Classic echo cancellation (not the cross-channel echo cancellation described in [IW95]) is necessary to demodulate the received data. Moreover, EC-DMT-ADSL exhibits self-NEXT since upstream transmissions from neighboring ATU-R transceivers interfere with the desired downstream downstream transmission through near end cross talk coupling in the binder group. The literature clearly states that self-NEXT is the most deleterious form of crosstalk and is often several orders of magnitude stronger than self-FEXT. Most manufactures of DSL equipment prefer a version of ADSL called frequency division multiplexed (FDM) DMT-DSL which uses a non-overlapping spectrum to avoid

self-NEXT [Rau99, pp. 225]. In the following, the we present an analysis of the relative powers of the received signal and self-NEXT under some nominal assumptions.

According to the specifications in [Int99a, Annex B], the nominal ATU-C downstream transmit power is given as -40dBm/Hz over the overlapping frequency range. The nominal ATU-R upstream transmit power is specified as -38dBm/Hz. Each tone in DMT-ADSL uses a 4.3125MHz frequency interval, hence the nominal power in each tone is -3.65dBm for the downstream and -1.65dBm for the upstream.

Picking a standard test loop of 13.5k feet of 26AWG wire (denoted as "T Loop # 7" in [Int99b]) the insertion loss data provided in [Int99b, Table 2] leads to an empirically determined expression for insertion loss in this loop as

$$L(f) = 25\log_{10}(f) - 75.5\text{dB} \qquad 25.875\text{kHz} \leq f \leq 138\text{kHz}$$

where insertion loss is a function of frequency f. The NEXT insertion loss is also a function of frequency and is modeled with the expression from [Int99b, Section 7.1] as

$$L_{\mathsf{NEXT}}(f) = -15\log_{10}(f) - 6\log_{10}(n) + 140.7\text{dB} \qquad 0 \leq f < \infty,\ n < 50$$

where n is the number of crosstalkers. Note that this expression differs slightly from the expression for NEXT given in [Ung85] where $n = 49$ and

$$L_{\mathsf{NEXT}}(f) = -14\log_{10}(f) + 126.2\text{dB} \qquad f > 20\text{kHz}$$

but both expressions are similar and the remainder of this analysis will use the former since it allows specification of the number of crosstalkers. The ratio of

desired signal power to NEXT power then follows directly as

$$\begin{aligned} \text{SIR(dB)} &= (-3.64\text{dBm} - 25\log_{10}(f) + 75.5) \\ &\quad - (-1.65\text{dBm} + 15\log_{10}(f) + 6\log_{10}(n) - 140.7) \\ &= -40\log_{10}(f) - 6\log_{10}(n) + 214.2\text{dB} \end{aligned} \tag{6.1}$$

and is plotted in Figure 6.2.

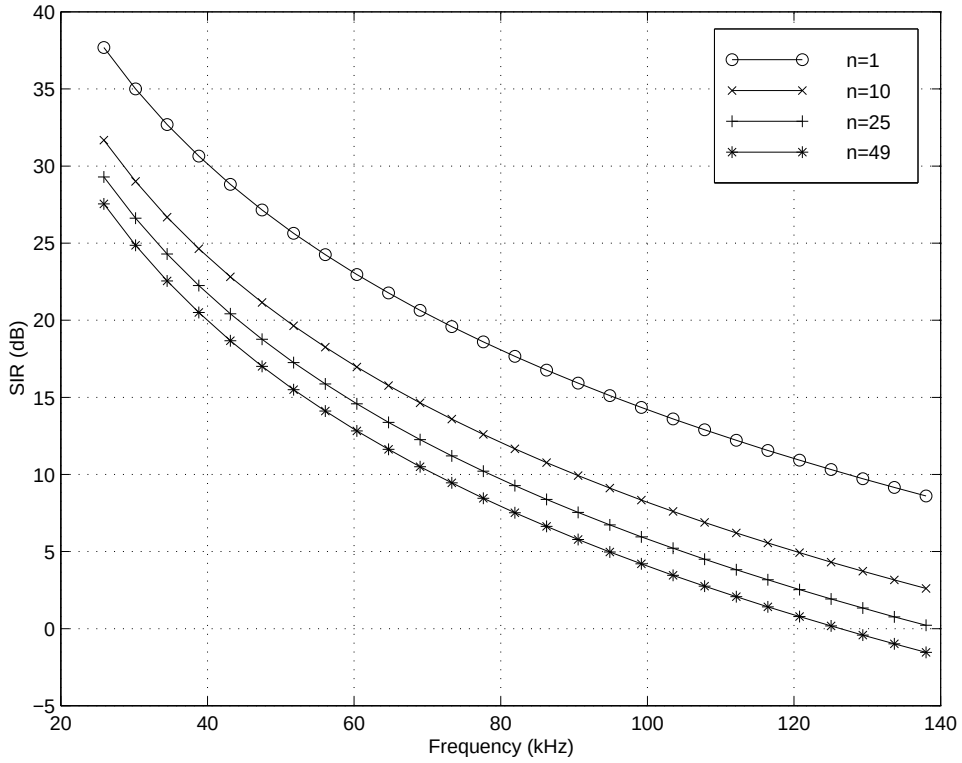

Figure 6.2: Signal to NEXT power ratio from (6.1) for n near-end crosstalkers.

These results show that:

1. NEXT is more severe at the higher frequencies in the upstream transmission band and is less severe at the lower frequencies. This is intuitively satisfying since attenuation in the desired signal increases with frequency and NEXT attenuation (the inverse of NEXT coupling) decreases with frequency.

2. Each additional user adds less interference than the prior user.

3. A single NEXT interferer could be received with power equal to approximately one eighth of the desired signal's power.

The conclusion suggested by this rough analysis is that there exist tones in the upstream frequency band where the observed NEXT power can be on the same order of magnitude as the desired signal. This implies that NEXT cancellation, if successful, might significantly improve the fidelity of EC-DMT-ADSL communications.

6.2 Analytical Model and Assumptions

Consider the simplified DMT-ADSL model shown in Figure 6.3. This model ignores the details of scrambling, encoding, and interleaving present in actual DMT-ADSL transceivers and focuses on a single DMT-ADSL transmitter-receiver pair "inside the coders". This model also assumes that the cyclic prefix and time domain equalizer operations (see [Rau99, pp. 208] for descriptions of these elements) found in actual DMT-ADSL systems are ideal and can be ignored. This last assumption, although not valid in the case when the the time-domain equalizer (TEQ) is unable to remove all of the intersymbol interference, is imposed in this case in order to isolate and understand the crosstalk cancellation problem more clearly.

Assuming that the IDFT and DFT blocks are ideal, Figure 6.3 leads to an expression for the N-vector output of the DFT block as

$$\boldsymbol{r}(n) \;=\; \boldsymbol{C}\boldsymbol{s}(n) + \sigma \boldsymbol{F}\boldsymbol{w}(n) \tag{6.2}$$

where $\boldsymbol{C}$ represents an N-dimensional diagonal matrix of channel gains for each

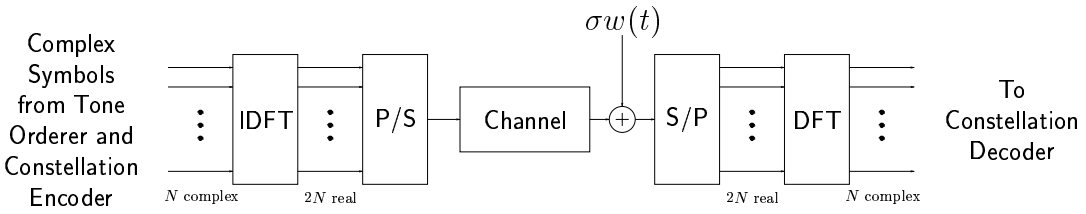

Figure 6.3: Simplified single transmitter-receiver pair for DMT-ADSL where $\sigma w(t)$ represents the additive white Gaussian channel noise, P/S denotes parallel to serial conversion, and S/P denotes serial to parallel conversion.

tone, $\boldsymbol{s}(n)$ represents the N-vector of complex symbols[1] from the constellation encoder with each symbol corresponding to a distinct tone, $\boldsymbol{F} \in \mathbb{C}^{N\times 2N}$ is the upper half of the standard $2N$-dimensional DFT matrix, and $\sigma\boldsymbol{w}(n)$ represents the $2N$-vector of real valued AWGN channel noise with variance σ^2. The assumption that $\boldsymbol{C}$ is diagonal implies that there is no intermodulation noise in the sense that each DMT tone is received free of interference from other DMT tones. We have also used the assumption that all DMT tones are received uncorrupted by intersymbol interference. The following proposition further simplifies (6.2).

Proposition 10. *If $\boldsymbol{w}$ is real, white, and Gaussian with variance σ^2 then the elements of $\boldsymbol{y} = \boldsymbol{F}\boldsymbol{w}$, except for the first element corresponding to the DC term, are complex, white, and Gaussian with real and imaginary variances equal to $\sigma^2/2$ and independent real and imaginary terms.*

Proof. It is clear that $\boldsymbol{y}$ is Gaussian since linear transformations of joint Gaussian random variables result in joint Gaussian random variables and $\boldsymbol{F}$ is linear. Let $\boldsymbol{f}_t^H$

[1]In contrast to Chapters 2-4 where the symbol b was used to represent binary user symbols, the DSL systems considered in this chapter do not use binary signaling in general. As a consequence, we use the symbol s to denote the user symbols in this chapter.

represent the t^{th} row of $\boldsymbol{F}$ for $t \in \{1, \ldots, N\}$ such that $y_t = \boldsymbol{f}_t^H \boldsymbol{w}$ and $\boldsymbol{f}_t^H \boldsymbol{f}_t = 1$. Note that t denotes a "tone" in the DMT system. Then

$$\begin{aligned}
E[\mathrm{Re}(y_t)\mathrm{Re}(y_{t'})] &= \mathrm{Re}(\boldsymbol{f}_t^H) E[\boldsymbol{w}\boldsymbol{w}^\top] \mathrm{Re}(\boldsymbol{f}_{t'}) \\
&= \frac{\sigma^2}{2N} \sum_{\ell=0}^{2N-1} \cos\left(\frac{2\pi\ell(t-1)}{2N}\right) \cos\left(\frac{2\pi\ell(t'-1)}{2N}\right) \\
&= \frac{\sigma^2}{2N} \sum_{\ell=0}^{2N-1} \frac{1}{2}\left[\cos\left(\frac{2\pi\ell(t-t')}{2N}\right) + \cos\left(\frac{2\pi\ell(t+t'-2)}{2N}\right)\right] \\
&= \begin{cases} 0 & t \neq t' \\ \sigma^2/2 & t = t' \neq 1 \\ \sigma^2 & t = t' = 1 \end{cases}
\end{aligned}$$

since $\sum_{\ell=0}^{2N-1} \cos(\frac{2\pi\ell t}{2N}) = 0$ when t is an integer not evenly divisible by $2N$ and $\sum_{\ell=0}^{2N-1} \cos(\frac{2\pi\ell t}{2N}) = 2N$ when t is evenly divisible by $2N$ (including $t = 0$). In both cosine terms, since t and t' are both constrained to the set $\{1, \ldots, N\}$, $t = 0$ is the only admissible value of t evenly divisible by $2N$. Similarly,

$$\begin{aligned}
E[\mathrm{Im}(y_t)\mathrm{Im}(y_{t'})] &= \mathrm{Im}(\boldsymbol{f}_t^H) E[\boldsymbol{w}\boldsymbol{w}^\top] \mathrm{Im}(\boldsymbol{f}_{t'}) \\
&= \frac{\sigma^2}{2N} \sum_{\ell=0}^{2N-1} \sin\left(\frac{2\pi\ell(t-1)}{2N}\right) \sin\left(\frac{2\pi\ell(t'-1)}{2N}\right) \\
&= \frac{\sigma^2}{2N} \sum_{\ell=0}^{2N-1} \frac{1}{2}\left[\cos\left(\frac{2\pi\ell(t-t')}{2N}\right) - \cos\left(\frac{2\pi\ell(t+t'-2)}{2N}\right)\right] \\
&= \begin{cases} 0 & t \neq t' \\ \sigma^2/2 & t = t' \neq 1 \\ 0 & t = t' = 1 \end{cases}
\end{aligned}$$

and finally

$$\begin{aligned} E[\mathrm{Re}(y_t)\mathrm{Im}(y_{t'})] &= \mathrm{Re}(\boldsymbol{f}_t^H)E[\boldsymbol{w}\boldsymbol{w}^\top]\mathrm{Im}(\boldsymbol{f}_{t'}) \\ &= \frac{\sigma^2}{2N}\sum_{\ell=0}^{2N-1}\cos\left(\frac{2\pi\ell(t-1)}{2N}\right)\sin\left(\frac{2\pi\ell(t'-1)}{2N}\right) \\ &= \frac{\sigma^2}{2N}\sum_{\ell=0}^{2N-1}\frac{1}{2}\left[\sin\left(\frac{2\pi\ell(t+t'-2)}{2N}\right)-\sin\left(\frac{2\pi\ell(t-t')}{2N}\right)\right] \\ &= 0. \end{aligned}$$

These expressions show that y_t is complex, white, and Gaussian with real and imaginary variances equal to $\sigma^2/2$ and independent real and imaginary terms in the case when $t \neq 1$. □

Assuming that the first tone is not used (this is the case in all DSLs since they must not interfere with voice service), this last result implies that (6.2) can be rewritten as

$$\boldsymbol{r}(n) = \boldsymbol{C}\boldsymbol{s}(n) + \sigma\tilde{\boldsymbol{w}}(n)$$

where $\tilde{\boldsymbol{w}}(n)$ is an N-vector with independent complex Gaussian elements, where each element has independent real and imaginary parts each with variance 1/2. This expression implies that crosstalk cancellation can be considered on a *tone-by-tone* basis where

$$r_t(n) = c_t s_t(n) + \sigma\tilde{w}_t(n) + \underbrace{x_t(n)}_{\text{NEXT in the } t^{th} \text{ tone}} \tag{6.3}$$

Under the assumption that $s_t(n)$ is independent of $s_{t'}(n)$ for all $t \neq t'$ then this formulation shows that there is no benefit to performing crosstalk cancellation jointly on all of the tones and that crosstalk cancellation can be considered on a tone-by-tone basis. The crosstalk cancellation schemes we will consider in the

sequel will perform cancellation on a single tone hence we will suppress the tone index t. Assuming for clarity in the analytical development that carrier and phase recovery are ideal for the desired user and that the NEXT term is synchronous, the symbol index n can also be eliminated and an expression for the crosstalk corrupted scalar observation can be written as

$$r = s^{(1)} + \sum_{k=2}^{K} \rho^{(k)} s^{(k)} + \sigma\tilde{w} \tag{6.4}$$

where $s^{(1)}$ is the desired user's symbol scaled such that $E[|s^{(1)}|^2] = 1$, $s^{(k)}$, $k = 2, \ldots, K$ are the symbols from the interfering NEXT transmissions also scaled to unit power, and $\rho^{(k)}$ is the (possibly complex) NEXT coupling factor from the k^{th} user's transmission into the desired user's signal. The noise standard deviation σ has been scaled from (6.3) without loss of generality in order to retain the correct ratio with the unit power desired signal.

6.3 Multiuser Detection for DMT-ADSL

6.3.1 Single-User Detector

Assuming that all elements of the desired user's symbol alphabet are equiprobable then the single-user detector simply takes the sampled matched filter output r from (6.3) and finds the constellation element of the desired user closest to it. The single-user detector does not exploit any of the known information about the crosstalk environment and forms symbol estimates by the expression

$$\hat{s}^{(1)}_{\mathsf{SU}} \;=\; \arg\min_{s \in \mathcal{S}^{(1)}} |r - s|^2.$$

where $\mathcal{S}^{(1)}$ is the desired user's symbol alphabet. Single-user detection can be shown to be optimum when the desired signal is corrupted by zero-mean AWGN

but is, in general, suboptimum when the interference is non-Gaussian.

6.3.2 Joint Maximum Likelihood

Under the assumptions that the desired and interfering symbol alphabets are equiprobable (but not necessarily identical) and that the symbols are independent, and that the receiver has perfect knowledge of the NEXT coupling factors $\rho^{(k)}$ and interfering user alphabets $\mathcal{S}^{(k)},\ k = 2, \ldots, K$ for $k = 1, \ldots, K$, then the joint maximum likelihood detector is defined as

$$\begin{aligned} \hat{\boldsymbol{s}}_{\mathsf{JML}} &= \left(\arg \max_{\boldsymbol{s} \in \mathcal{S}} \exp \left(-\frac{1}{\sigma^2} |r - \boldsymbol{\rho}^\top \boldsymbol{s}|^2 \right) \right) \\ &= \left(\arg \min_{\boldsymbol{s} \in \mathcal{S}} |r - \boldsymbol{\rho}^\top \boldsymbol{s}|^2 \right) \end{aligned}$$

where $\rho = [1, \rho^{(2)}, \ldots, \rho^{(K)}]^\top$ and $\mathcal{S} = [\mathcal{S}^{(1)}, \ldots, \mathcal{S}^{(K)}]^\top$. Note that $\hat{\boldsymbol{s}}_{\mathsf{JML}}$ is an estimate of *all* users' symbols. We denote the first element of $\hat{\boldsymbol{s}}_{\mathsf{JML}}$ corresponding to the JML estimate of the desired user as $\hat{s}^{(1)}$. The JML detector for DMT-ADSL is similar to the JML detector for CDMA with one critical difference: the DMT-ADSL observation is *scalar* as opposed to the *vector* observation available in CDMA. This is a consequence of the assumption that the DMT-ADSL receiver (the ATU-R modem) generally does not have access to the observations of other receivers in the system.

6.3.3 Linear Detection

Under the assumptions imposed, the DSL receiver's observation is assumed scalar which implies that all linear detectors would only consist of a scalar (possibly complex) gain. We have assumed that the DMT-DSL receiver has already corrected the phase and gain of the received signal prior to the multiuser detection opera-

tion, hence linear detection does not provide any benefit in this scenario. Linear detection will not be considered further in this chapter.

6.3.4 Parallel Interference Cancellation

The parallel interference cancellation (PIC) detector is defined as

$$\hat{s}^{(1)}_{\mathsf{HPIC}} \;=\; \arg\min_{s\in\mathcal{S}^{(1)}} |(r-\hat{x})-s|^2.$$

where $\hat{x}$ is the estimated aggregate NEXT interference. LPIC detection, as described in Chapter 3 where it was shown that the LPIC detector is a linear detector, is not examined here for reasons discussed in the prior section. A two-stage HPIC detector with single-user detector first stage forms the NEXT interference estimate as

$$\hat{x} \;=\; \sum_{k=2}^{K} \rho^{(k)}\hat{s}^{(k)}_{\mathsf{SU}}$$

where

$$\hat{s}^{(k)}_{\mathsf{SU}} = \arg\min_{s\in\mathcal{S}^{(k)}} |r-s|^2.$$

In the context of a scalar observable, PIC is not an intuitively satisfying technique for crosstalk mitigation in DSL systems. To see why, consider the case of a desired user transmitting 4-QAM with a single NEXT interferer also transmitting 4-QAM with coupling factor $\rho^{(2)} = 0.6$ and no noise. The single user decision for the desired user $\hat{s}^{(1)}_{\mathsf{SU}}$ will always be correct in this scenario since the interference is not large enough to cause the received signal to cross a decision boundary and there is no noise. On the other hand, the single user decision for the NEXT interferer

will be correct only with probability 1/4 since

$$\begin{aligned}
\hat{s}_{\mathsf{SU}}^{(2)} &= \arg\min_{s\in\mathcal{S}^{(2)}} |r-s|^2 \\
&= \arg\min_{s\in\mathcal{S}^{(1)}} |r-s|^2 \\
&= \hat{s}_{\mathsf{SU}}^{(1)} \\
&= s^{(1)}
\end{aligned}$$

assuming that the desired and NEXT users symbols are independent and equiprobable. In this case, this means that the hard PIC symbol estimate for the desired user can be written as

$$\begin{aligned}
\hat{s}_{\mathsf{HPIC}}^{(1)} &= \arg\min_{s\in\mathcal{S}^{(1)}} |(r-\hat{x})-s|^2 \\
&= \arg\min_{s\in\mathcal{S}^{(1)}} |(r-0.6s^{(1)})-s|^2 \\
&= \arg\min_{s\in\mathcal{S}^{(1)}} |0.4s^{(1)}+0.6s^{(2)}-s|^2 \\
&= s^{(2)}
\end{aligned}$$

which is correct with probability 1/4. Hence, because the NEXT interference estimates are unreliable in this case, attempting to cancel them causes the performance to be worse than the single user detector in this example. It can be shown that additional stages do not rectify this problem. In CDMA systems, the matched filter bank provides a vector observable that often allows reasonably accurate estimation of the interference. In DSL crosstalk mitigation, the scalar observable does not provide any means for accurate interference estimation and leads to poor interference estimates in many cases. These poor interference estimates often lead to reduced performance with respect to the single user detector. The reasoning behind the example presented here suggests that PIC may not be directly applicable to the crosstalk mitigation problem but, on the other hand, this example suggests that PIC may have potential in a DSL eavesdropping scenario.

6.3.5 Successive Interference Cancellation

The successive interference cancellation (SIC) detector for user k is defined as

$$\hat{s}_{\mathsf{SIC}}^{(k)} = \arg\min_{s\in\mathcal{S}^{(k)}} |(r-\hat{x}_{k-1})-s|^2.$$

where $\hat{x}_{k-1}$ is the estimated aggregate interference of users $1,\ldots,k-1$ defined as

$$\hat{x}_{k-1} = \sum_{\ell=1}^{k-1} \rho^{(\ell)}\hat{s}_{\mathsf{SIC}}^{(\ell)}.$$

It is common (although not always optimal [Ver98, pp. 387]) to order the users in terms of decreasing amplitude so that the most powerful user is canceled first and the least powerful user is canceled last. Since the desired user is typically the most powerful user in the received signal, the desired user's performance is equivalent to the single user detector since no interference cancellation has occurred prior to their decision. The more interesting case is a two-stage SIC detector where

$$\hat{s}_{\mathsf{SIC2}}^{(k)} = \arg\min_{s\in\mathcal{S}^{(k)}} |(r-\tilde{x}_{k-1})-s|^2.$$

where $\tilde{x}_{k-1}$ is the estimated aggregate interference of all interfering users defined as

$$\tilde{x}_{k-1} = \sum_{\ell=1}^{k-1} \rho^{(\ell)}\hat{s}_{\mathsf{SIC2}}^{(\ell)} + \sum_{\ell=k+1}^{K} \rho^{(\ell)}\hat{s}_{\mathsf{SIC}}^{(\ell)}.$$

In this case, the desired user's symbol estimate can be written as

$$\hat{s}_{\mathsf{SIC2}}^{(1)} = \arg\min_{s\in\mathcal{S}^{(k)}} \left| \left(r - \sum_{k=2}^{K} \rho^{(k)}\hat{s}_{\mathsf{SIC}}^{(k)} \right) - s \right|^2.$$

The two-stage SIC detector is justified intuitively under the same noiseless, 2-user scenario described in Section 6.3.4. As was seen for the PIC detector, $\hat{s}_{\mathsf{SIC}}^{(1)} = s^{(1)}$

since $\hat{s}^{(1)}_{\mathsf{SIC}} = \hat{s}^{(1)}_{\mathsf{SU}}$. The second user's symbol estimate is then

$$\begin{aligned}
\hat{s}^{(2)}_{\mathsf{SIC}} &= \arg\min_{s\in\mathcal{S}^{(2)}} |(r - \hat{s}^{(1)}_{\mathsf{SIC}}) - s|^2. \\
&= \arg\min_{s\in\mathcal{S}^{(2)}} |s^{(2)} - s|^2. \\
&= s^{(2)}
\end{aligned}$$

which differs from the results seen for the hard PIC detector. Finally,

$$\begin{aligned}
\hat{s}^{(1)}_{\mathsf{SIC2}} &= \arg\min_{s\in\mathcal{S}^{(1)}} |(r - \hat{s}^{(2)}_{\mathsf{SIC}}) - s|^2. \\
&= \arg\min_{s\in\mathcal{S}^{(1)}} |s^{(1)} - s|^2. \\
&= s^{(1)}
\end{aligned}$$

which shows that the two-stage SIC detector does not experience the same difficulties as the hard PIC detector in this example. However, although the SIC and two-stage SIC detectors yield a symbol error rate of zero for the NEXT user in this example, the desired user's symbol error rate has not been improved with respect to single user detection (an impossibility in this case). The question then is, "Does SIC outperform the single-user detector in terms of bit error rate for the desired user in the presence of AWGN?" A somewhat surprising result developed in Section 6.4 states that, even in the presence of AWGN, there is no benefit in using any method of crosstalk mitigation to estimate the desired user's symbol in a class of operating conditions that includes this particular example. In other words, in this class of operating conditions, the best detectors perform equivalently to the single-user detector. Hence, in this example, even in the presence of noise, the two-stage SIC detector can not outperform the single-user detector and may in fact perform worse. Examples of crosstalk mitigation for operating scenarios outside of this class are presented in Section 6.5.

6.4 Analytical Results

An implication of the scalar observable inherent to the crosstalk mitigation problem at the ATU-R modem is that there exists a class of operating conditions where the single-user and JML detectors yield exactly the same symbol estimates. This claim is made more precise in the following proposition.

Proposition 11. *Suppose that the desired user's signal constellation is 2^M-QAM, with M even, placed on a square grid with spacing $2d$, with equiprobable elements in the set $\mathcal{A}$. Under the following assumptions:*

(A1) The set $\mathcal{A}'$ denotes the set of all possible NEXT interference terms generated by all equiprobable possibilities of the expression $\sum_{k=2}^{K} \rho^{(k)} s^{(k)}$. The set $\mathcal{A}'$ is symmetric in the sense that if $z \in \mathcal{A}'$ then so is $-z$, z^*, and $-z^*$.

(A2) The NEXT interference is bounded in the sense that $|Re(z)| < d$ and $|Im(z)| < d$ for all $z \in \mathcal{A}'$.

Then $\hat{s}^{(1)}_{\mathsf{SU}} = \hat{s}^{(1)}_{\mathsf{JML}}$.

Proof. Consider the scenario posed in Figure 6.4.

The single-user decision boundary between desired user constellation points a_1 and a_2 is denoted as $L_{\mathsf{SU}}(a_1, a_2)$ and defined as

$$L_{\mathsf{SU}}(a_1, a_2) \triangleq \{x \in \mathbb{C} \ : \ |x - a_1|^2 = |x - a_2|^2\}$$

for $a_1, a_2 \in \mathcal{A}$. The JML decision boundary between any two JML constellation points $a_1 + z_1$ and $a_2 + z_2$ is defined similarly as

$$L_{\mathsf{JML}}(a_1 + z_1, a_2 + z_2) = \{x \in \mathbb{C} \ : \ |x - (a_1 + z_1)|^2 = |x - (a_2 + z_2)|^2\}$$

for $a_1, a_2 \in \mathcal{A}$ and $z_1, z_2 \in \mathcal{A}'$.

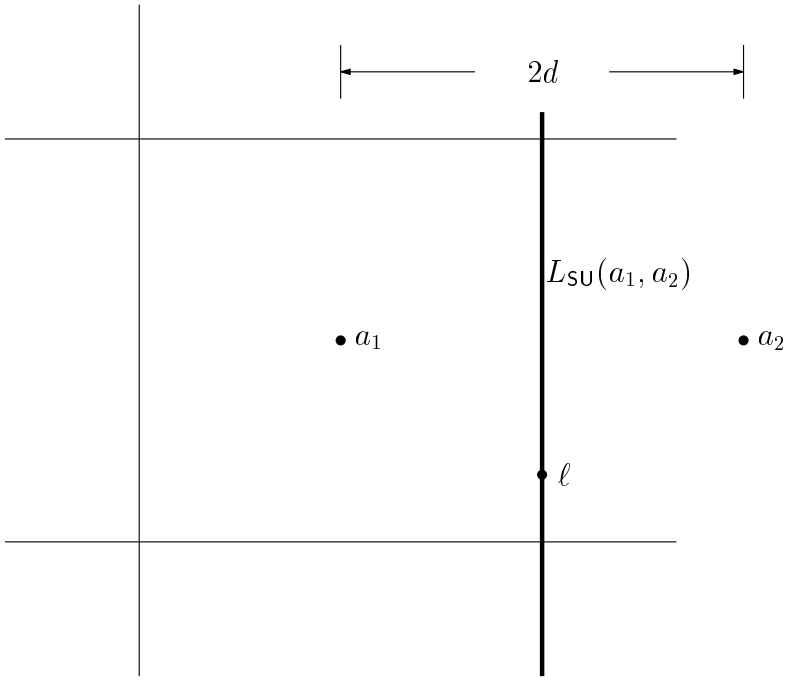

Figure 6.4: Desired user constellation elements $a_1, a_2 \in \mathcal{A}$ separated by $2d$, single-user decision boundary denoted by $L_{\mathsf{SU}}(a_1, a_2)$ and a point on the decision boundary denoted by ℓ.

Suppose that $\hat{s}_{\mathsf{SU}}^{(1)} = a_1$ which implies that the received sample r is in the single-user decision region of constellation point a_1. Set

$$z_2 = \arg\min_{z \in \mathcal{A}'} |r - (a_2 + z)|^2.$$

By assumption (A1), if $z_2 \in \mathcal{A}'$ then so is $-z_2^*$ hence the point $a_1 - z_2^*$ is a valid point in the JML constellation. The JML decision boundary between $a_1 - z_2^*$ and $a_2 + z_2$ can be written as

$$L_{\mathsf{JML}}(a_1 - z_2^*, a_2 + z_2) = \{x \in \mathbb{C} \ : \ |x - a_1 + z_2^*|^2 = |x - a_2 - z_2|^2\}. \tag{6.5}$$

Choose any point $\ell \in L_{\mathsf{SU}}(a_1, a_2)$. Then

$$\begin{aligned}
|\ell - a_2 - z_2|^2 &= [\mathrm{Re}(\ell - a_2 - z_2)]^2 + [\mathrm{Im}(\ell - a_2 - z_2)]^2 \\
&= [\mathrm{Re}(-d - z_2^*)]^2 + [\mathrm{Im}(\ell - a_1 + z_2^*)]^2 \\
&= [\mathrm{Re}(d + z_2^*)]^2 + [\mathrm{Im}(\ell - a_1 + z_2^*)]^2 \\
&= [\mathrm{Re}(\ell - a_1 + z_2^*)]^2 + [\mathrm{Im}(\ell - a_1 + z_2^*)]^2 \\
&= |\ell - a_1 + z_2^*|^2
\end{aligned}$$

using the facts that $\mathrm{Re}(\ell - a_2) = -d$, $\mathrm{Re}(\ell - a_1) = d$, $\mathrm{Re}(z_2) = \mathrm{Re}(z_2^*)$, $\mathrm{Im}(a_2) = \mathrm{Im}(a_1)$, and $\mathrm{Im}(z_2) = -\mathrm{Im}(z_2^*)$. This last equality combined with (6.5) implies that $L_{\mathsf{SU}}(a_1, a_2) \subset L_{\mathsf{JML}}(a_1 - z_2^*, a_2 + z_2)$. The opposite containment can be shown similarly which implies that

$$L_{\mathsf{JML}}(a_1 - z_2^*, a_2 + z_2) = L_{\mathsf{SU}}(a_2, a_2). \tag{6.6}$$

Since $\hat{s}_{\mathsf{SU}}^{(1)} = a_1$ then r is left of the $L(a_1, a_2)$ decision boundary in Figure 6.4. This fact combined with assumption (A2) and (6.6) then implies that r is left of the $L_{\mathsf{JML}}(a_1, -z_2^*, a_2 + z_2)$ decision boundary and closer to the JML constellation element $a_1 - z_2^*$ than $a_2 + z_2$. Finally, since $a_2 + z_2$ is the closest JML constellation

element to r under the constraint that the desired user's symbol is set to a_2 then this implies that $\hat{s}^{(1)}_{\mathsf{JML}} \neq a_2$.

The remaining desired user constellation points in $\mathcal{A}$ are eliminated as follows. Let $\bar{\mathcal{A}} \subset \mathcal{A}$ be the subset of all desired user constellation points a_i satisfying $|a_i - a_1| = 2d$ or $|a_i - a_1| = 2\sqrt{2}d$. Using the implied symmetry of the desired user's square QAM constellation, the same argument developed in this proof can be applied to eliminate any JML constellation point $a_i + z_i$ where $a_i \in \bar{\mathcal{A}}$ and $z_i \in \mathcal{A}'$ since there exists $z \in \mathcal{A}'$ such that $L_{\mathsf{JML}}(a_1+z, a_i+z_i) = L_{\mathsf{SU}}(a_1, a_i)$. The remaining desired user constellation points in $\mathcal{A} \setminus \bar{\mathcal{A}} \setminus a_1$ are eliminated by considering that r is in the decision region for a_1 and that, given any JML constellation point $a_o + z_o$ with $a_o \in \mathcal{A} \setminus \bar{\mathcal{A}} \setminus a_1$ and $z_o \in \mathcal{A}'$, there must exist at least one JML constellation point $a_i + z_i$ with $a_i \in \bar{\mathcal{A}}$ and $z_i \in \mathcal{A}'$ such that $|r - a_i - z_i|^2 < |r - a_o - z_o|^2$. This implies that $\hat{s}^{(1)}_{\mathsf{JML}} \neq a_i$ for all $i \neq 1$. Hence $\hat{s}^{(1)}_{\mathsf{JML}} = a_1$ and since $\hat{s}^{(1)}_{\mathsf{SU}} = a_1$ and a_1 was chosen arbitrarily then $\hat{s}^{(1)}_{\mathsf{JML}} = \hat{s}^{(1)}_{\mathsf{SU}}$. □

It turns out that the converse of Proposition 11 is not true and this is due to the fact that assumption (A1) is stronger than necessary. To prove the converse, assumption (A1) would have to be relaxed slightly to (A1)' and state that

(A1)' ... is symmetric in the sense that if $z \in \tilde{\mathcal{A}}'$ then so is $-z$, z^*, and $-z^*$.

where $\tilde{\mathcal{A}}' \triangleq \{z \in \mathcal{A}' : |a_1 - z - \ell| < |a_1 - z' - \ell| \ \forall z' \in \mathcal{A}' \text{ and at least one } \ell \in L(a_1)\}$ where $L(a_1)$ is the union of the (at most) four decision boundaries that enclose the single-user decision region for a_1. In words, this relaxed assumption (A1)' only requires that the points on the "perimeter" of the NEXT constellation have the symmetry property and that points on the "interior" of the next constellation do not need to have any such symmetry. This is intuitive since the symmetry of

only the "perimeter" points of the NEXT constellation is necessary in order to establish the result in (6.6) and it can be shown conversely that if (6.6) then the "perimeter" points of the NEXT constellation must have the required symmetry (assuming that $\mathcal{A}'$ has a finite number of elements).

Assumption (A2) can be viewed as an implicit bound on the maximum constellation order of the desired user given $\max_{z\in\mathcal{A}'} \mathrm{Re}(z)$ and $\max_{z\in\mathcal{A}'} \mathrm{Im}(z)$ since increasing the desired user's constellation order decreases d to a threshold where d becomes too small to satisfy assumption (A2). Figure 6.5 plots this maximum constellation order versus the real amplitude (i.e., no phase rotation) of a single NEXT interferer transmitting 4-QAM or 256-QAM. All points to the "southwest" of the appropriate line satisfy assumption (A2) and all points to the "northeast" of the appropriate line violate assumption (A2).

This proposition implies, somewhat surprisingly, that in cases where the assumptions of Proposition 11 are valid, crosstalk mitigation is *not* beneficial and standard single-user detection is optimum. Hence, it can be inferred that knowledge of the NEXT interference structure including coupling factors and interference alphabets, both of which may be quite difficult to estimate in practice, as well as the additional computation burden of crosstalk mitigation is not beneficial to the receiver in these cases. It can also be inferred that crosstalk mitigation might be beneficial in the cases where the assumptions of Proposition 11 are violated. These cases are considered in the following section.

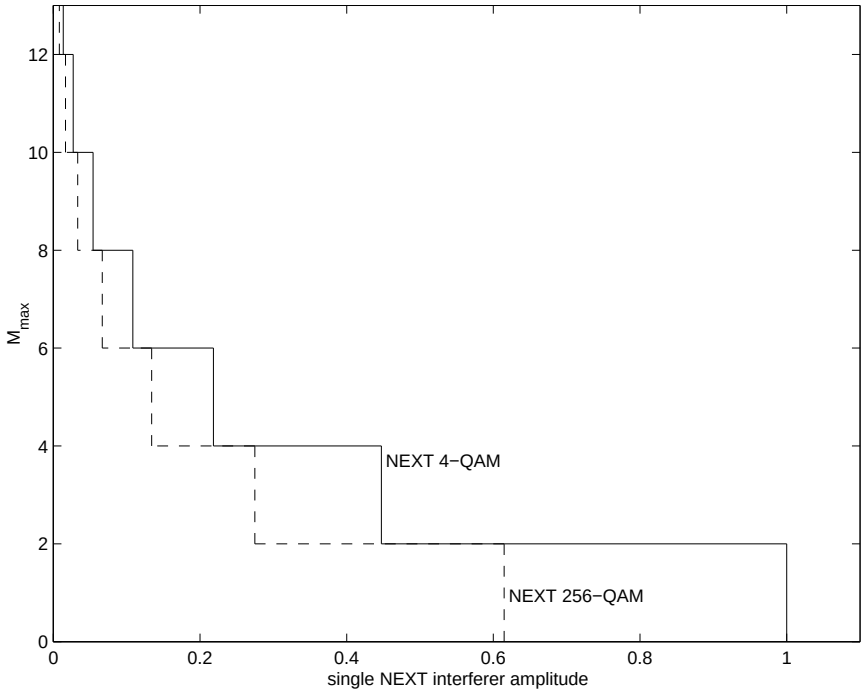

Figure 6.5: Maximum constellation order ($2^{M_{max}}$-QAM) for the desired user to satisfy assumption (A2) of Proposition 11 for a single NEXT interferer with 4-QAM constellation (solid line) and 256-QAM constellation (dashed line).

6.5 Numerical Examples

As a first step towards understanding the performance of multiuser detection for DSL crosstalk mitigation, this section considers the scenario where the desired user is observed at the receiver corrupted by a single, synchronous NEXT interferer and AWGN. Two cases are shown that satisfy the assumptions of Proposition 11 and two cases are shown that violate these assumptions. In the latter two cases, it is shown via simulation that NEXT interference mitigation can improve the symbol error rate of the desired user.

Figures 6.6 and 6.7 show the constellation diagrams and decision boundaries of two cases where the assumptions of Proposition 11 are satisfied in a system with one NEXT interferer. In each plot, the JML decision region for the desired user's symbol $+1/\sqrt{2} + j/\sqrt{2}$ is the union of the regions labeled A, B, C, and D. These figures show that the JML and single-user decision regions are identical and that sophisticated crosstalk cancellation schemes provide no benefit to the detection of the symbols the desired user.

Figure 6.8 shows a constellation diagram and decision boundaries of a case where Assumption (A1) of Proposition 11 is violated. In this case the JML decision region for the desired user's symbol $+1/\sqrt{2} + j/\sqrt{2}$ clearly differs from the corresponding single-user decision region implying that JML detection will improve the performance of symbol detection for the desired user in this case. Figure 6.9 verifies this claim and shows that JML detection does indeed outperform the single-user detector in this case. Unfortunately, the two-stage SIC detector yields performance identical to the single-user detector and two-stage hard PIC detection performs dramatically worse than single-user detection, as predicted in the prior analysis.

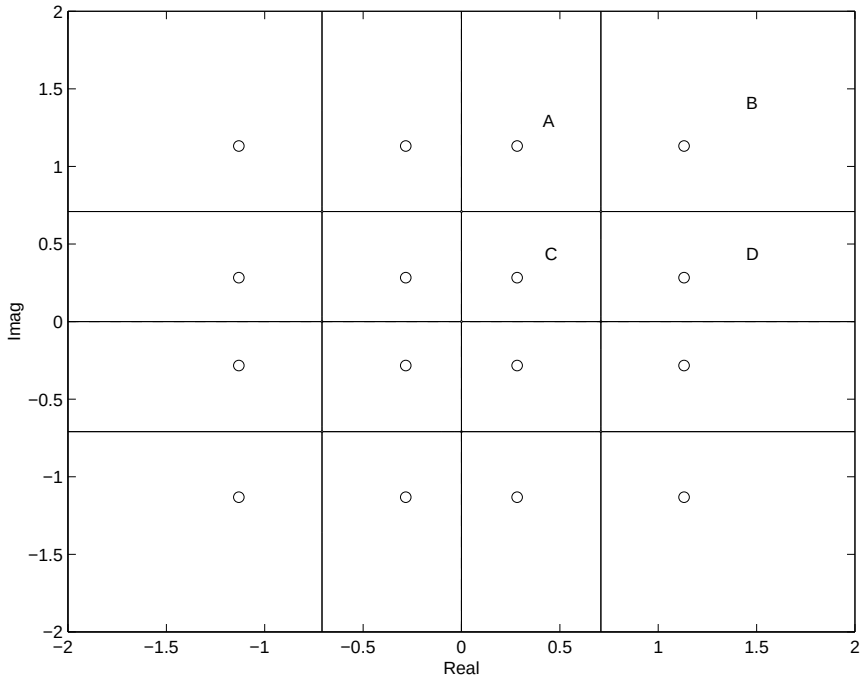

Figure 6.6: JML decision boundaries for a signal with a 4-QAM desired user and one 4-QAM NEXT interfering user with coupling factor $\rho^{(2)} = 0.6$.

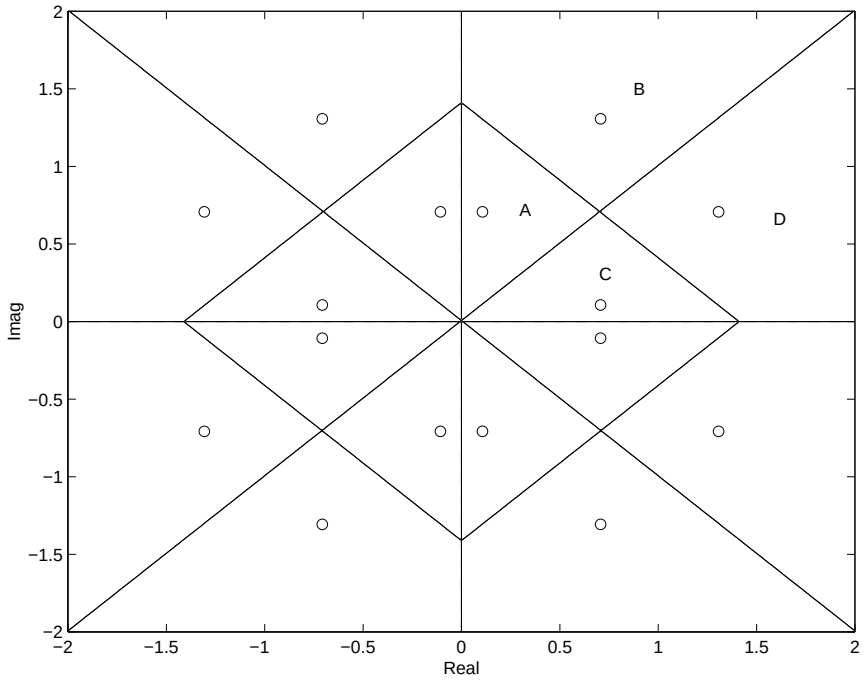

Figure 6.7: JML decision boundaries for a signal with a 4-QAM desired user and one 4-QAM NEXT interfering user with coupling factor $\rho^{(2)} = 0.6e^{j\pi/4}$.

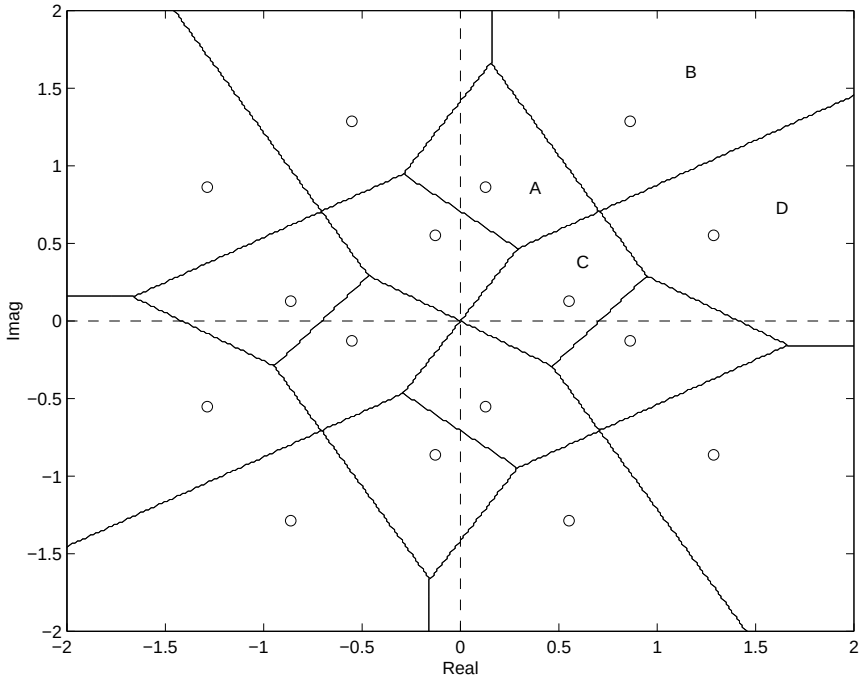

Figure 6.8: JML (solid) and single-user (dashed) decision boundaries for a signal with a 4-QAM desired user and one 4-QAM NEXT interfering user with coupling factor $\rho^{(2)} = 0.6e^{j\pi/6}$.

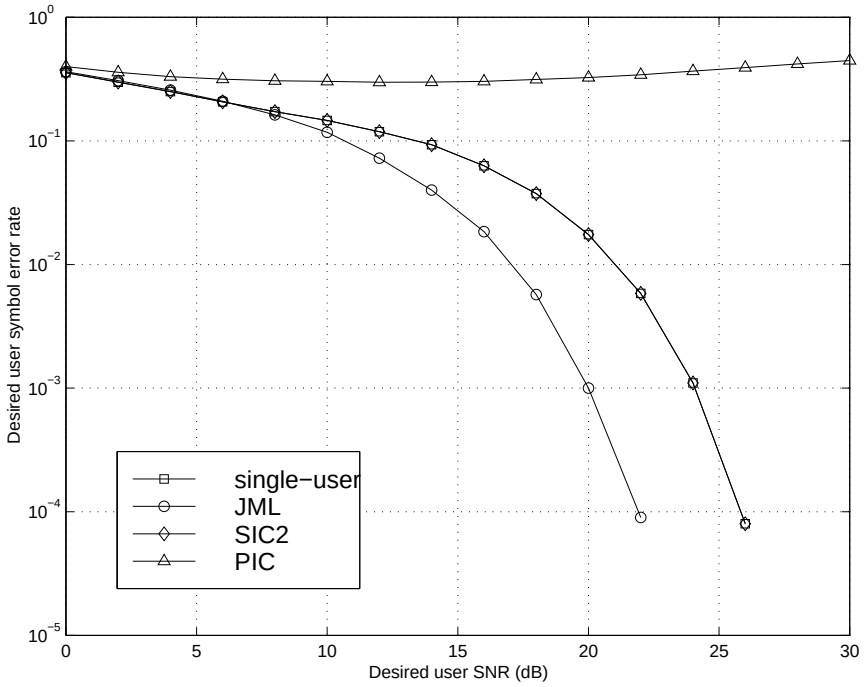

Figure 6.9: Symbol error rate for desired user for various NEXT mitigation schemes under scenario shown in Figure 6.8.

Figure 6.10 shows a constellation diagram and decision boundaries of a case where Assumption (A2) of Proposition 11 is violated. Again, the JML decision region for $+1/\sqrt{2}+j/\sqrt{2}$ clearly differs from the corresponding single-user decision region which implies that JML detection will improve the performance of symbol detection for the desired user in this case. Figure 6.11 shows the symbol error rate performance of the detectors considered in this case.

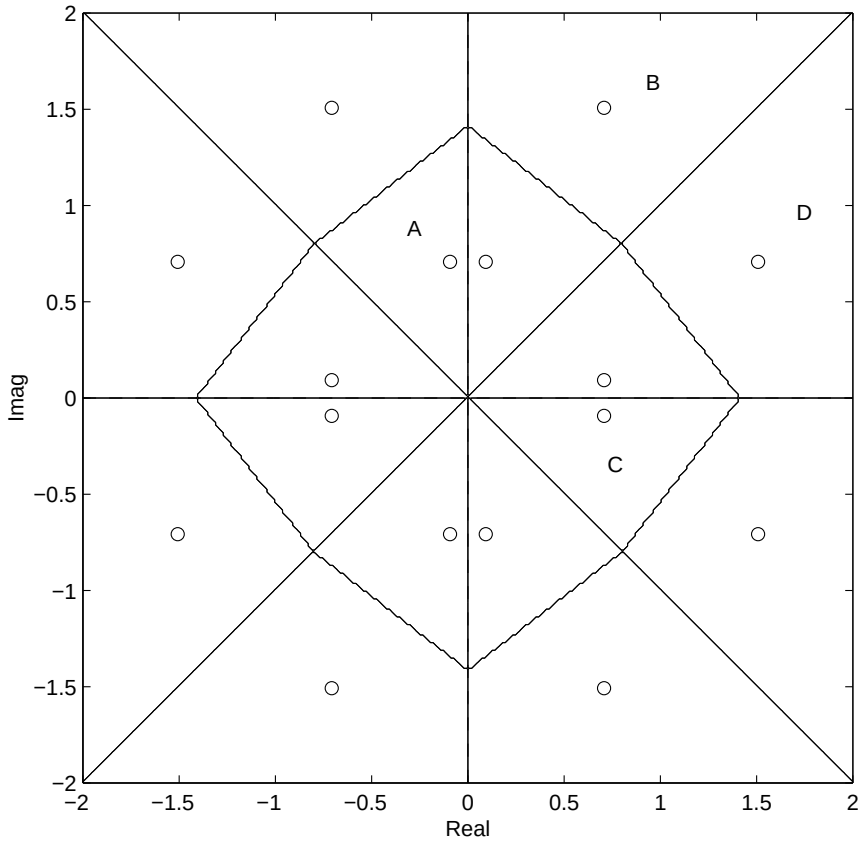

Figure 6.10: JML (solid) and single-user (dashed) decision boundaries for a signal with a 4-QAM desired user and one 4-QAM NEXT interfering user with coupling factor $\rho^{(2)} = 0.8e^{j\pi/4}$.

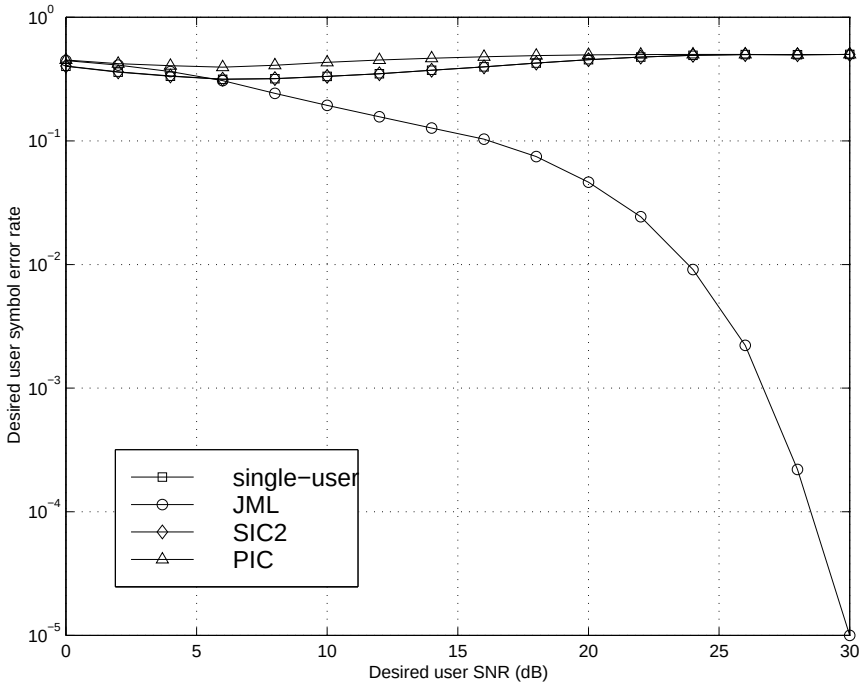

Figure 6.11: Symbol error rates for desired user for various NEXT mitigation schemes under scenario shown in Figure 6.10.

6.6 Conclusions

In this chapter we considered the application of multiuser detection for crosstalk mitigation at the ATU-R (customer premises) modem. We presented a first order analysis of the near-end crosstalk powers received in an ADSL scenario and showed that these powers can be significant. This result implied that crosstalk mitigation, if successful, could yield significant performance benefits including increased transmission rates and improved fidelity of reception. We considered several different multiuser detectors for crosstalk mitigation and showed that, as a consequence of the scalar observable at the ATU-R modem, there exist a class of operating conditions where the single user detector is in fact the optimum detector. We also showed that via simulations that, when operating outside of this class, crosstalk mitigation via optimum multiuser detection may provide significant performance improvements. The problem of canceling crosstalk in a computationally efficient manner remains open for this application.

CHAPTER 7

CONCLUSIONS AND FUTURE RESEARCH

7.1 Summary

Multiuser detection shows promise as one of the core technologies that will enable cellular service providers to meet the future demands of their rapidly growing and increasingly sophisticated subscriber base. Parallel interference cancellation multiuser detectors have been shown to possess a unique combination of desirable properties including near optimum performance, very low computational complexity, and low decision latency. In this dissertation, we presented new analytical results on the performance of two different types of PIC detection, we developed and tested new approaches to improve the performance of PIC detection, and we investigated two distinct applications for PIC detection.

The contributions of Chapters 2-3 of this dissertation present new analytical results regarding the BER and SINR performance of HPIC and LPIC detection. In Chapter 4, we proposed and tested the performance adaptive PC-HPIC and SC-PIC detectors and showed that they improved the performance of PIC detection. In Chapters 5-6 we considered application of PIC detection for eavesdropping in digital cellular systems and for crosstalk cancellation in digital subscriber loops. We summarize our results by chapter below.

Chapter 2. In this chapter, we presented an analysis of two performance measures for HPIC detection: bit error rate and SINR. The bit error rate analysis showed that exact computation of the bit error rate for the HPIC detector required evaluation of several K-dimensional integrals of the joint Gaussian pdf over rectangular regions, where K is the number of users in the system.

An approximate expression for the bit error rate of the HPIC detector was posed that does not require integration. We also presented an exact SINR analysis for the HPIC detector and showed that its computation, although not as difficult as bit error rate, does require the evaluation of several two-dimensional integrals. We suggested an approximation that holds when the BER of the matched filter detector is reasonably low and presented an analytical comparison to the SIC and MF detectors suggesting that HPIC detection offers superior performance under a large class of operating conditions.

Chapter 3. Unlike the majority of recent literature that suggests techniques to improve the performance of the LPIC detector, this chapter analyzed the performance of the unmodified LPIC detector. The results showed that the two-stage HPIC detector tends to be a better estimator of multiuser interference than the two-stage LPIC detector and that there exists several nontrivial cases where the multistage LPIC detector's BER is worse than the conventional matched filter. We showed the somewhat surprising result that, in the large-system CDMA case, the two-stage LPIC detector exhibits worse asymptotic output SINR performance than the matched filter detector when the number of users K exceeds $1/3$ of the spreading gain N. We also showed the asymptotic result that application of the multistage LPIC detector to a CDMA system with $K/N > 0.17$ does not converge to the decorrelating detector as the number of stages of interference cancellation $M \to \infty$ and that at least one user will exhibit an error probability worse than 0.5 in each bit interval.

Chapter 4. In this chapter, we considered two different approaches to improve the

performance of the two-stage HPIC detector. In the first approach, we suggested that, when the multiuser interference estimates are unreliable, the interference estimates should be scaled to avoid performance degradation from interference doubling due to incorrect binary estimates. Since each user's interference estimate may have different levels of reliability, we proposed a PC-HPIC detector that assigns an individual partial cancellation factor to each user. We investigated optimum values for these partial cancellation factors under three different criteria including a maximum-SINR criterion that can be computed with reasonable complexity in the K-user case. The second approach considered the replacement of the $\mathrm{sgn}(\cdot)$ nonlinearity with a nonlinearity that minimizes the Bayesian MSE of the interference estimates under the intuition that better multiuser interference estimates yield better output BER or SINR performance for the HPIC detector. Analytical and simulation results in this chapter showed that the proposed techniques did indeed, in most cases, yield improved bit error rate performance with respect to the HPIC, LPIC, and MF detectors.

Chapter 5. This chapter considered the application of nonlinear multiuser detection techniques for improving the performance of IS–95 downlink reception in an eavesdropping scenario. We developed a reduced complexity optimum detector that exploits the group-orthogonal structure of the IS–95 downlink and also developed the suboptimum GPIC detector that has the features of very low complexity and potentially near-optimum performance. Experiments with on-air IS–95 downlink data suggested that the GPIC detector offers the greatest performance improvement when demodulating weak signals in the presence of strong out-of-cell multiuser interference.

Chapter 6. Although the earlier chapters of this dissertation focused on multiuser detection for wireless communication systems, Chapter 6 considered the application of multiuser detection for crosstalk mitigation in wire-based digital subscriber loops. We presented an analysis of the crosstalker powers as a first step towards generating a mathematical system model that discards the prevailing Gaussian assumption on the multiuser interference. The analysis showed that near end crosstalker powers could be on the same order of magnitude as the desired signal implying that crosstalk mitigation, if successful, could yield significant performance benefits. We considered several different multiuser detectors for crosstalk mitigation and showed that, at the customer's modem, there exist a class of operating conditions where the single user detector is in fact the optimum detector. We also showed that, when operating outside of this class, crosstalk mitigation via optimum multiuser detection may provide significant performance improvements.

7.2 Future Research Directions

The results in Chapters 2-4 of this dissertation pertained to the synchronous K-user CDMA system model. Extensions to the asynchronous case or, even more generally, to the multipath channel case with fixed or random spreading codes would be valuable results. The evidence presented in Chapter 5 with on-air IS–95 downlink data suggests that PIC detection does offer the potential for significant performance improvements in real-world scenarios.

In Chapter 2, we showed that computation of the exact bit error rate of the two-stage HPIC detector was quite difficult, even in the two-user case. Although

we posed one approximation in Chapter 2 and the literature also contains several papers with bit error rate approximations, accurate bounds on the bit error rate performance of the two-stage (or multistage) HPIC detector are currently unknown and may be a more valuable tool. A bit error rate expression for the HPIC detector in a large CDMA system with random spreading sequences is also an important result that is currently unknown. Also in Chapter 2, we note that SINR in actually not well defined for nonlinear detectors and that there are several definitions that lead to identical results for linear detectors but lead to different results for nonlinear detectors such as the HPIC detector. One such definition was posed in [Sme00, Appendix D] where SINR was defined as "the ratio of output power when the noise and interference are set to zero to the output power when the desired signal component is set to zero". In this case, it is easy to verify that this definition leads to significantly different expressions for SINR for the two-stage HPIC detector than those posed in Chapter 2. The definition used in Chapter 2 appears to be the most intuitive definition of SINR and is consistent with the other definitions for linear detectors but the matter of defining SINR consistently for nonlinear detectors remains open. A SINR expression for the HPIC detector in a large CDMA system with random spreading sequences is also an important result that is currently unknown.

In Chapter 3, we showed that if $\rho(\boldsymbol{R}) > 2$, there exists at least one user whose probability of error will exceed 0.5 at the output of the multistage LPIC detector when the number of stages of interference cancellation (M) is sufficiently large and odd. We also showed by example that there exist a class of signature cross-correlation matrices such that this proposition can not be extended to imply that *all* users will have an error probability of greater than 0.5. Simulations suggest

that this class of signature crosscorrelation matrices is very small and that this proposition does extend to all users over a large class of signature crosscorrelation matrices, including those covered by Perron's Theorem and its extensions. Rigorous characterization of these classes of signature crosscorrelation matrices remains and open problem. Also in Chapter 3, we observed in a numerical example that the LPIC detector's error probabilities at odd and even stages appeared to converge to respective fixed points symmetric around 0.5 as $M \to \infty$. Additional numerical evidence suggests that this may be true in general at least for the class equicorrelated signature crosscorrelation matrices. A rigorous proof of this conjecture would be useful in order to further our understanding of LPIC detection behavior for even numbers of stages. Finally, in Chapter 3, we described several open problems in the case where an multistage LPIC detector is operating in large CDMA system with random spreading sequences. A proof that the multistage detector's output decision statistic is a Gaussian random variable in the large-system, random spreading sequences scenario appears to be difficult and remains an open problem. A proof of this property would be valuable since it would imply that the bit error rate of the multistage LPIC detector could be expressed as a single $Q(\cdot)$ function in this case and it would facilitate comparisons to other detectors for which this result is known. A key element that appears to be necessary for this proof is an expression for the random eigenvalues (and eigenvectors) of $\boldsymbol{R}^M$ for arbitrary M. This result would also then immediately yield expressions for the multistage LPIC detector's SINR in the large-system, random spreading sequences scenario.

In Chapter 4, we showed that bit error rate optimum partial cancellation factors could yield significant performance improvements to the HPIC detector in the two user case but that computation of these partial cancellation factors was quite dif-

ficult in the two-user case and practically impossible in the K-user case. Although we developed simple expressions for SINR maximizing partial cancellation factors in this chapter, they were shown to only provide modest performance gains when the user powers were equal and that the ad-hoc techniques developed in [DSR98] could actually outperform the PC-HPIC detector in terms of bit error rate. The matter of finding low complexity expressions for partial cancellation factors that yield good performance over a range of typical operating conditions remains open.

Perhaps an even more important result that would supersede the PC-HPIC approach would be determination of optimum nonlinearities to replace the $\mathrm{sgn}(\cdot)$ nonlinearity in the HPIC detector. In Chapter 4, we showed that replacing the $\mathrm{sgn}(\cdot)$ nonlinearity with a $\tanh(\cdot)$ function to propose the SC-PIC detector, under the argument that the interference estimates would minimize the Bayesian MSE, could yield large performance improvements. Derivation of a nonlinearity that minimizes the output bit error rate or SINR would be an important result.

In Chapter 5 we developed the GPIC detector for eavesdropping in the IS–95 downlink. We did not investigate application of the performance adaptive techniques of Chapter 4 for GPIC detection but we postulate that these may yield even greater performance gains in some cases.

In Chapter 6 we showed that for a particular DSL model, the single user detector was optimum under a particular class of operating conditions. We also showed via simulation that conventional interference cancellation techniques such as HPIC and SIC do not yield improved performance in many typical cases and that optimum detection is required in order to realize any performance improvement. The problem of developing algorithms for canceling crosstalk in a computationally efficient manner for DSL communication systems remains open.

BIBLIOGRAPHY

[AS72] M. Abramowitz and I.A. Stegun. *Handbook of Mathematical Functions*. Dover, New York, NY, 1972.

[AZJ95] B.S. Abrams, A.E. Zeger, and T.E. Jones. Efficiently structured CDMA receiver with near-far immunity. *IEEE Transactions on Vehicular Technology*, 44(1):1–13, February 1995.

[BC94] D. Brady and J.A. Catipovic. Adaptive multiuser detection for underwater acoustical channels. *IEEE Journal of Oceanic Engineering*, 19(2):158–165, April 1994.

[BCW96] R.M. Buehrer, N.S. Correal, and B.D. Woerner. A comparison of multiuser receivers for cellular CDMA. In *Proceedings of GLOBECOM '96. 1996 Global Telecommunications Conference*, volume 3, pages 1571–7, London, UK, November 18-22, 1996.

[Bil95] P. Billingsly. *Probability and Measure*. Wiley, New York, NY, third edition, 1995.

[BJP99] D.R. Brown, C.R. Johnson Jr., and H.V. Poor. Eavesdropping on the IS–95 downlink: Reduced complexity optimum and suboptimum multiuser detectors. In *Proceedings of the IEEE Wireless Communications and Networking Conference*, volume 2, pages 819–23, New Orleans, LA, September 21-24, 1999.

[BN99] R.M. Buehrer and S.P. Nicoloso. Comments on 'Partial Parallel Interference Cancellation for CDMA'. *IEEE Transactions on Communications*, 47(5):658–61, May 1999.

[BW96] R.M. Buehrer and B.D. Woerner. Analysis of adaptive multistage interference cancellation for CDMA using an improved gaussian approximation. *IEEE Transactions on Communications*, 44(10):1308–21, October 1996.

[BW97] R.M. Buehrer and B.D. Woerner. The asymptotic multiuser efficiency of m-stage interference cancellation receivers. In *Proceedings of the 8th International Symposium on Personal, Indoor, and Mobile Radio Communications*, volume 2, pages 570–4, Helsinki, Finland, September 1-4, 1997.

[BY93] Z.D. Bai and Y.Q. Yin. Limit of the smallest eigenvalue of a large dimensional sample covariance matrix. *The Annals of Probability*, 21(3):1275–1293, 1993.

[CBW97] N.S. Correal, R.M. Buehrer, and B.D. Woerner. Improved CDMA performance through bias reduction for parallel interference cancellation. In *Proceedings of the 8th International Symposium on Personal, Indoor, and Mobile Radio Communications*, volume 2, pages 565–9, Helsinki, Finland, September 1-4, 1997.

[CBW98] N.S. Correal, R.M. Buehrer, and B.D. Woerner. Real-time DSP implementation of a coherent partial interference cancellation multiuser receiver for DS-CDMA. In *1998 IEEE International Conference on Communications Conference Record*, volume 3, pages 1536–40, Atlanta, GA, June 7-11, 1998.

[CBW99] N.S. Correal, R.M. Buehrer, and B.D. Woerner. A DSP-based DS-CDMA multiuser receiver employing partial parallel interference cancellation. *IEEE Journal on Selected Areas in Communications*, 17(4):613–30, April 1999.

[CC99] K. Cheong and J.M. Cioffi. Coexistence of 1 mbps hpna and dmt vdsl via multiuser detection and code division multiplexing. *ANSI Standards Contribution T1E1.4/99-120*, March 8, 1999.

[CCLS98] J.M. Cioffi, K. Cheong, J. Lauer, and A. Salvekar. Mitigation of DSL crosstalk via multiuser detection and code-division multiple access. *ANSI Standards Contribution T1E1.4/98-253*, August 31, 1998.

[CKB+99] J.W. Cook, R.H. Kirkby, M.G. Booth, K.T. Foster, D.E.A. Clark, and G. Young. The noise and crosstalk environment for ADSL and VDSL systems. *IEEE Communications Magazine*, 37(5):73–78, May 1999.

[DS94] D. Divsalar and M.K. Simon. Improved CDMA performance using parallel interference cancellation. In *Proceedings of the 1994 Military Communications Conference*, volume 3, pages 911–7, Fort Monmouth, NJ, October 2-5, 1994.

[DSR98] D. Divsalar, M.K. Simon, and D. Raphaeli. Improved parallel interference cancellation for CDMA. *IEEE Transactions on Communications*, 46(2):258–68, February 1998.

[FA95] U. Fawer and B. Aazhang. A multiuser receiver for code division multiple access communications over multipath channels. *IEEE Transactions on Communications*, 43(2/3/4):1556–65, February/March/April 1995.

[FR97] T. Frey and M. Reinhardt. Signal estimation for interference cancellation and decision feedback equalization. In *Proceedings of 47th*

Vehicular Technology Conference, pages 155–9, Phoenix, AZ, May 4-7, 1997.

[GF99] M. Gollanbari and G.E. Ford. Signal monitoring on the downlink of cellular CDMA communications with interference cancellation. In *1999 IEEE Wireless Communications and Networking Conference*, volume 1, pages 80–84, New Orleans, LA, September 21-24, 1999.

[GHW99] L.M. Garth, G. Huang, and J.J. Werner. Crosstalk mitigation for xDSL channels. *IEEE Circuits and Systems Newsletter*, 10(1):3,8–9,32, March 1999.

[GMNK95] V. Ghazi-Moghadam, L.B. Nelson, and M. Kaveh. Parallel interference cancellation for CDMA systems. In *Proceedings of the 33rd Annual Allerton Conference on Communications, Control and Computing*, pages 216–24, Monticello, IL, October 4-6, 1995.

[GNHB98] S. Gollamudi, S. Nagaraj, Y.-F. Huang, and R.M. Buehrer. Optimal multistage interference cancellation for CDMA systems using the nonlinear MMSE criterion. In *Conference Record of the Thirty-Second Asilomar Conference on Signals, Systems, and Computers*, volume 1, pages 665–9, Pacific Grove, CA, November 1-4, 1998.

[GRL99] D. Guo, L.K. Rasmussen, and T. Lim. Linear parallel interference cancellation in long-code CDMA multiuser detection. *IEEE Journal on Selected Areas in Communications*, 17(12):2074–81, December 1999.

[GRS+98] D. Guo, L.K. Rasmussen, S. Sun, T. Lim, and C. Cheah. MMSE-based linear parallel interference cancellation in CDMA. In *Proceedings of the IEEE 5th International Symposium on Spread Spectrum Techniques and Applications*, volume 1, pages 917–21, Sun City, South Africa, September 2-4, 1998.

[GRSL00] D. Guo, L.K. Rasmussen, S. Sun, and T. Lim. A matrix algebraic approach to linear parallel interference cancellation in CDMA. *IEEE Transactions on Communications*, 48(1):152–61, January 2000.

[HD98] Y.-F. Huang and P.S.R. Diniz. Interference suppression in CDMA wireless communications. *IEEE Circuits and Systems Society Newsletter*, 9(3):1,8–9,14, September 1998.

[HHT95] A. Hottinen, H. Holma, and A. Toskala. Performance of multistage multiuser detection in a fading multipath channel. In *Proceedings of the 6th International Symposium on Personal, Indoor, and Mobile Radio Communications*, volume 3, pages 960–4, Toronto, Ontario, Canada, September 27-29, 1995.

[HJ94] R.A. Horn and C.R. Johnson. *Matrix Analysis*. Cambridge University Press, New York, NY, 1994.

[Int99a] International Telecommunication Union, Telecommunication Standardization Sector. *Recommendation G.992.2 – Splitterless Asymmetric Digital Subscriber Line (ADSL) Transceivers*. ITU, Geneva, 1999.

[Int99b] International Telecommunication Union, Telecommunication Standardization Sector. *Recommendation G.996.1 – Test Procedures for Digital Subscriber Line (DSL) Transceivers*. ITU, Geneva, 1999.

[IS98] G.H. Im and N.R. Shanbhag. A pipelined adaptive NEXT canceller. *IEEE Transactions on Signal Processing*, 46(8):2252–8, December 1998.

[IW95] G.H. Im and J.J. Werner. Bandwidth efficient digital transmission over unshielded twisted-pair wiring. *IEEE Journal on Selected Areas in Communications*, 13(12):1643–55, December 1995.

[Kay93] S.M. Kay. *Fundamentals of Statistical Signal Processing, Estimation Theory*. Prentice Hall, Upper Saddle River, NJ, 1993.

[KIHP90] R. Kohno, N. Imai, M. Hatori, and S. Pasupathy. An adaptive canceller of cochannel interference for spread-spectrum multiple-acess communication networks in a power line. *IEEE Journal on Selected Areas in Communications*, 8(4):691–9, April 1990.

[KKKF93] M. Kawabe, T. Kato, A. Kawahashi, and A. Fukasawa. Advanced CDMA scheme based on interference cancellation. In *43rd Annual IEEE Vehicular Techology Conference*, pages 448–51, May 18-20, 1993.

[KW94] A. Kaul and B.D. Woerner. Analytic limits on the performance of adaptive multistage interference cancellation. *Electronics Letters*, 30(25):2093–4, December 1994.

[LE99] W. Luo and A. Ephremides. Energy efficiency of multiuser detection. In *Proceedings of the IEEE Wireless Communications and Networking Conference*, volume 2, pages 852–6, New Orleans, LA, September 21-24, 1999.

[MP99] G.V. Moustakides and H.V. Poor. On the relative error probabilities of linear multiuser detectors. *Submitted to IEEE Transactions on Information Theory*, tbd(tbd):tbd, tbd 1999.

[MV98a] N.B. Mandayam and S. Verdu. Analysis of an approximate decorrelating detector. *Wireless Personal Communications*, 6(1-2):97–111, January 1998.

[MV98b] A. McKellips and S. Verdú. Eavesdropper performance in cellular CDMA. *European Transactions on Telecommunications*, 9(4):379–89, July/August 1998.

[MV98c] A. McKellips and S. Verdú. Eavesdropping syndicates in cellular communications. In *1998 IEEE 48th Vehicular Technology Conference*, volume 1, pages 318–22, Ottowa, Canada, May 18-21, 1998.

[PH94] P. Patel and J. Holtzman. Performance comparison of a DS/CDMA system using a successive interference cancellation (ic) scheme and a parallel ic scheme under fading. In *Proceedings of the ICC/SUPERCOMM '94 - 1994 International Conference on Communications*, volume 1, pages 510–4, New Orleans, LA, May 1-5, 1994.

[Pro95] J.G. Proakis. *Digital Communications*. McGraw-Hill, New York, NY, third ed. edition, 1995.

[Pur77] M.B. Pursley. Performance evaluation for phase-coded spread-spectrum multiple-access communication - Part I: System analysis. *IEEE Transactions on Communications*, 25(8):795–9, August 1977.

[PV97] H.V. Poor and S. Verdu. Probability of error in MMSE multiuser detection. *IEEE Transactions on Information Theory*, 43(3):858–71, May 1997.

[Rau99] D.J. Rauschmayer. *ADSL/VDSL Principles*. Macmillan Technology Publishing, Indianapolis, IN, 1999.

[Ren98] P.G. Renucci. *Masters Thesis: Optimization of Soft Interference Cancellation in DS-CDMA Receivers*. Virginia Polytechnic Institute and State University, 1998.

[RGLM98] L.K. Rasmussen, D. Guo, T.J. Lim, and Y. Ma. Aspects on linear parallel interference cancellation in CDMA. In *Proceedings of the 1998 IEEE International Symposium on Information Theory*, page 37, Cambridge, MA, August 16-21, 1998.

[RW98a] P.G. Renucci and B.D. Woerner. Analysis of soft cancellation to minimize BER in DS-CDMA interference cancellation. In *ICT 1998 (International Conference on Telecommunications)*, volume 4, pages 106–14, Chalkidiki, Greece, June 21-25, 1998.

[RW98b] P.G. Renucci and B.D. Woerner. Optimisation of soft interference cancellation for DS-CDMA. *Electronics Letters*, 34(8):731–3, April 16, 1998.

[SCS99] T. Starr, J.M. Cioffi, and P.J. Silvermann. *Understanding Digital Subscriber Line Technology.* Prentice-Hall, Upper Saddle River, NJ, 1999.

[Sme00] J.E. Smee. *PhD Dissertation: Adaptive Feedforward Feedback Detection for High Data Rate Communications.* Princeton University, 2000.

[Str95] R.S. Strichartz. *The way of analysis.* Jones and Bartlett, Boston, MA, 1995.

[Tel95] Telecommunications Industry Association. *Mobile Station – Base Station Compatibility Standard for Dual-Mode Wideband Spread Spectrum Cellular Systems IS–95A.* TIA/EIA, Washington, DC, 1995.

[Ung85] J.H.W. Unger. Near-end crosstalk model for line code studies. *ECSA Contribution, T1D1.3/85-244*, November 12, 1985.

[VA88] M. Varanasi and B. Aazhang. Near-optimum demodulation for coherent communications in asynchronous gaussian CDMA channels. In *Proceedings of the 22nd Conference on Information Sciences and Systems*, pages 832–9, Princeton, NJ, March 1988.

[VA90] M. Varanasi and B. Aazhang. Multistage detection in asynchronous code-division multiple-access communications. *IEEE Transactions on Communications*, 38(4):509–19, April 1990.

[VA91] M. Varanasi and B. Aazhang. Near-optimum detection in synchronous code-division multiple-access systems. *IEEE Transactions on Communications*, 39(5):725–36, May 1991.

[Ver86] S. Verdu. Minimum probability of error for asynchronous Gaussian multiple-access channels. *IEEE Transactions on Information Theory*, 32(1):85–96, January 1986.

[Ver98] Sergio Verdú. *Multiuser Detection.* Cambridge University Press, New York, NY, 1998.

[Vit95] A.J. Viterbi. *CDMA: Principles of Spread Spectrum Communications.* Addison-Wesley, Reading, MA, 1995.

[VS99] S. Verdu and S. Shamai. Specral efficiency of CDMA with random spreading. *IEEE Transactions on Information Theory*, 45(2):622–40, March 1999.

[XWLNT99] G. Xue, J. Weng, T. Le-Ngoc, and S. Tahar. Adaptive multistage parallel interference cancellation for CDMA. *IEEE Journal on Selected Areas in Communications*, 17(10):1815–27, October 1999.

[YKI92] Y.C. Yoon, R. Kohno, and H. Imai. Cascaded co-channel interference cancelling and diversity combining for spread-spectrum multi-access over multipath fading channels. In *SITA '92 (Symposium on Information Theory and its Applications)*, Minakami, Japan, September 8-11, 1992.

[YKI93] Y.C. Yoon, R. Kohno, and H. Imai. Cascaded co-channel interference cancelling and diversity combining for spread-spectrum multi-access over multipath fading channels. *IEICE Transactions on Communications*, E76-B(2):163–8, 1993.

[ZB93] X. Zhang and D. Brady. Soft-decision multistage detection for asynchronous AWGN channels. In *Proceedings of the 31st Allerton Conference on Communications, Control, and Computing*, pages 54–63, Monticello, IL, September 1993.

[ZB98] X. Zhang and D. Brady. Asymptotic multiuser efficiencies for decision-directed multiuser detection. *IEEE Transactions on Information Theory*, 44(3):502–15, March 1998.